

Methods in Molecular Biology™

VOLUME 196

Oxidants and Antioxidants

*Ultrastructure and
Molecular Biology
Protocols*

Edited by

Donald Armstrong



HUMANA PRESS

Cytochemical Localization of H_2O_2 in Biological Tissues

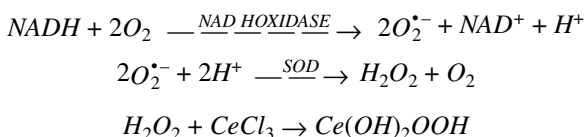
E. Ann Ellis and Maria B. Grant

1. Introduction

Free radicals and free radical-derived oxidants play important roles in biological systems and have been implicated in the pathology of many diseases. The major problem in determining the role of reactive oxygen species (ROS) has been that these short-lived species are difficult to measure *in vivo* (**1**). ROS in cells and tissues have been demonstrated by a number of methods. Effects of free radical scavengers such as superoxide dismutase (SOD), catalase, glutathione peroxidase, and antioxidants such as vitamin E have been detected indirectly (**2,3**). Many of the approaches used in free radical studies provide an aggregate assessment of oxidative stress but do not show specific information about the *in situ* subcellular sites of distribution of specific free radicals such as can be revealed by cytochemical approaches.

At the light microscopical level, nitroblue tetrazolium has been used for histochemical demonstration of superoxide ($\text{O}_2^{\bullet-}$) in retina (**4**). Briggs et al. (**5**) introduced the principles of cerium capture cytochemistry based on the observations that cerium and H_2O_2 react to produce a water-insoluble precipitate cerium perhydroxide ($\text{Ce}[\text{OH}]_2\text{OOH}$) (**6**). The first application of cerium cytochemistry was the demonstration of NADH oxidase on the plasmalemma of polymorphonuclear leukocytes. Variations of the basic reaction with cerium chloride as the capture agent have been used to localize a number of oxidases and sites of H_2O_2 generation (**7**). Cerium derived cytochemistry has played an important role in detecting *in situ* generation of H_2O_2 in studies of oxidative stress (**8–11**).

Oxidase activity can be detected as shown in the example of NADH oxidase. NADH oxidase, in the presence of oxygen, reacts with the substrate, NADH, to produce $O_2^{\bullet-}$ which dismutates, either spontaneously or catalyzed by SOD, to yield H_2O_2 . Sodium azide or aminotriazole, inhibitors of catalase and glutathione peroxidase, are included in the incubation medium to prevent removal of H_2O_2 by catalase or glutathione peroxidase. H_2O_2 reacts with cerium chloride to produce $Ce(OH)_2OOH$, a fine electron-dense precipitate, which is easily viewed by transmission electron microscopy (TEM) (**Fig. 1**). In addition, the reaction can be viewed by confocal microscopy (**12,13**) and conventional LM after amplification with diaminobenzidine (DAB) and cobalt or nickel chloride (**14**).



2. Materials

2.1. Equipment

1. Fume hood (minimum flow rate of 100 ft/min).
2. Shaking water bath at 37°C.
3. Transmission electron microscope (Hitachi H-7000).
4. Ultramicrotome (Reichert Ultracut S).
5. Vibratome® or similar apparatus (optional).

2.2. Reagents

All reagents for the localization procedures can be purchased from Sigma Chemical Co. (St. Louis, MO) and/or Ted Pella, Inc. (Redding, CA).

1. Acrolein (fixative) (Sigma cat. # A 2773).
2. Allopurinol (inhibitor of xanthine oxidase) (Sigma cat. # A 8003).
3. 3-Amino-1, 2, 4-triazole (inhibitor of catalase) (Sigma cat. # A 8056).
4. Cerium chloride (chromagen) (Sigma cat. # C 8016).
5. Cobalt chloride (for amplification for LM) (Sigma cat. # C 2644).
6. 3, 3'-Diaminobenzidine tetrahydrochloride (DAB) (Sigma cat. # D 5673).
7. Dimethyl sulfoxide (DMSO) (Sigma cat. # D 8779).
8. Diphenyleneiodonium (inhibitor of NADH oxidase) (Sigma cat. # D 2926).
9. HEPES buffer, free acid (Sigma cat. # H 3375).
10. Hypoxanthine (substrate for xanthine oxidase) (Sigma cat. # H 9377).
11. β -nicotinamide adenine nucleotide, reduced form (β -NADH) (substrate for NADH oxidase and/or xanthine oxidase) (Sigma cat. # N 6005).
12. Osmium tetroxide (Ted Pella, Inc. cat. # 18459).

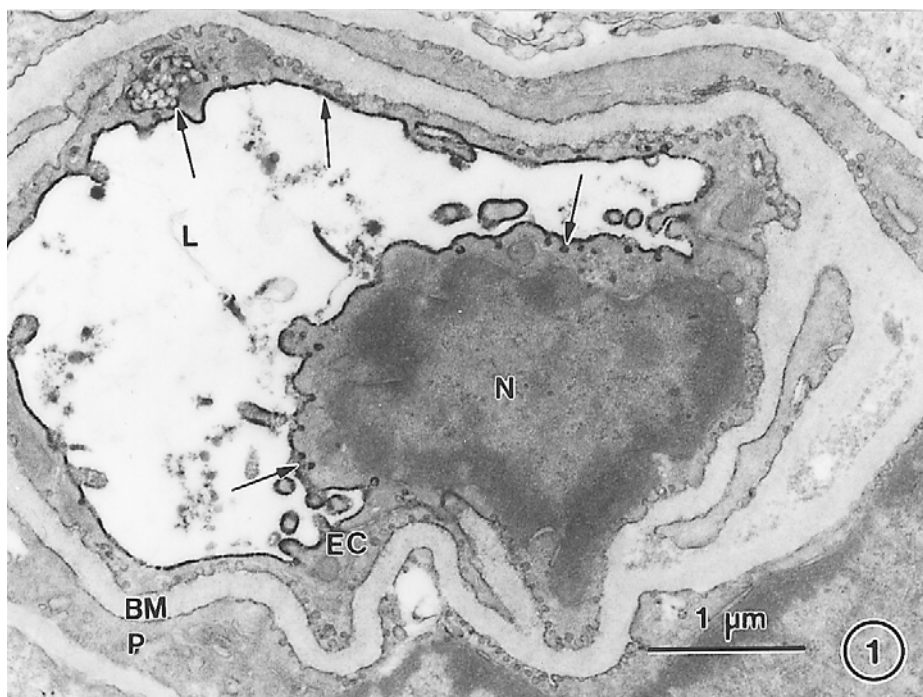


Fig. 1. Localization of H_2O_2 (arrows) produced by NADH oxidase in vessel lumen (L), plasmalemma, and cytoplasmic vesicles of endothelial cell (EC) in a capillary in the retina of a BBZ/Wor rat after 5 mo of diabetes. Basement membrane (BM); nucleus (N); pericyte (P). $\times 20,000$.

13. Paraformaldehyde powder (Sigma cat. # P 6148).
14. Sodium azide (inhibitor of catalase and glutathione peroxidase that can be substituted for aminotriazole) (Sigma cat. # S 8032).
15. Sodium cacodylate (buffer for fixation) (Ted Pella, Inc. cat. # 18851).
16. Triton X-100 (Sigma cat. # T 9284).

3. Methods

The protocols given here have been used extensively to identify sites of H_2O_2 production by NADH oxidase and xanthine oxidase in fixed ocular and cardiovascular tissues. The protocols can be broken down into the following steps:

1. tissue procurement and fixation;
2. buffer washes to stop fixation, to remove any unreacted aldehydes, and to protect enzyme (oxidase) activity;

3. preincubation in a reaction medium at 37°C in a shaking water bath that contains all reaction components except the substrate;
4. incubation in complete reaction medium at 37°C in a shaking water bath that contains all reaction components including the substrate;
5. stopping the localization reaction and postfixation in osmium tetroxide (OsO_4) for TEM or amplification with DAB and cobalt chloride for LM;
6. dehydration, infiltration, and embedding the tissue; and
7. sectioning and examining sections by TEM, confocal, or conventional LM (*see Note 1*).

3.1. Tissue Procurement and Fixation

1. Some investigators have perfused a reaction mixture containing CeCl_3 through the organ or tissue of interest (*8,15,16*) followed by fixation with 2%paraformaldehyde-2.5% glutaraldehyde or other standard aldehyde combinations in sodium cacodylate, PIPES, or HEPES buffers. In cardiovascular studies specimens were perfused for 3–5 min with a low concentration of fixative followed by perfusion with CeCl_3 medium (*15,16*).
2. Other investigators find it more practical to fix the tissue in cold buffered 4% paraformaldehyde or 5% acrolein for 1 h (*see Note 2*). **Phosphate buffers should not be used in any of the stages, including fixation and buffer washes, of cerium-based localization procedures** (*see Note 3*).
3. The initial buffer wash contains sucrose and DMSO (0.5–1% v/v), which aids in rapid removal of the aldehyde fixative and protects enzyme and antigenic activity. Specimens can be held in cold buffer wash (refrigerator temperatures, 0–4°C) overnight or up to several weeks.
4. For some tissues it may be better to cut 100 μm sections with the vibratome or similar instruments at this stage before starting the incubations for localization.
5. Add 0.1 M glycine to the last two buffer washes as the specimen is brought to room temperature just prior to the localization procedure. The glycine in the final buffer washes aids in removing any unbound aldehydes from the tissue.
6. Preincubation steps (done at 37°C in a shaking water bath for 30 min) are critical to successful localizations. Buffers for the preincubation and complete reaction incubation can be made the day before; however, **all preincubation and incubation mixtures should be made fresh and filtered immediately before use through a 0.45 μm filter**. Buffers for all incubation steps should be kept at room temperature. Preincubations with the chromagen (CeCl_3) and appropriate inhibitors are essential to insure adequate penetration of these reagents into subcellular sites of enzymes. Cerium has slow penetration into cells and tissues and penetration can be enhanced by addition of 0.0001–0.0002% Triton X-100 to the reaction medium (*17*).
7. Sodium azide (100 mM) or 3-amino-1,2,4-triazole (10 mM), inhibitors of catalase and glutathione peroxidase which can scavenge any H_2O_2 generated in the reaction, are included in the preincubation medium. Controls for the

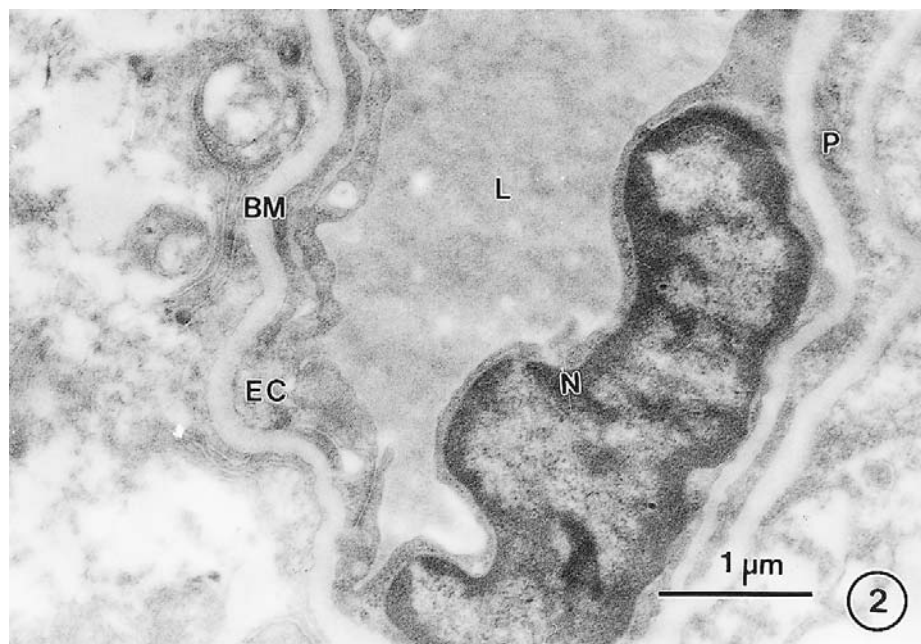


Fig. 2. Control for specificity of localization of H_2O_2 in the same retina as shown in Fig. 1 in which the substrate, NADH, was omitted. There is no cerium precipitate. $\times 20,000$.

specificity of the reaction are initiated during the preincubation step. These controls include samples in which:

- a. all substrate is omitted (**Fig. 2**);
 - b. specific inhibitors are included (diphenyleneiodonium [DPI] for NADH oxidase and allopurinol for xanthine oxidase); and
 - c. inhibitors of other enzymes are included such as using allopurinol in NADH oxidase medium and DPI in xanthine oxidase medium. Appropriate inhibition cannot be obtained unless the inhibitors are included in the preincubation medium as well as in the complete reaction medium.
8. The second stage in the localization procedure involves inclusion of substrate, NADH, hypoxanthine, or both substrates for xanthine oxidase localization, in a new batch of incubation medium that contains all the components that were used in the preincubation step. Incubation is done in at 37°C in a shaking water bath for 30 min to 1 h. For optimal results, the complete reaction mixture is changed after 30 min and incubation is continued for an additional 30 min.
 9. Reactions are stopped by placing the vials of tissue in an ice bath and washing immediately with **cold** buffer (the same buffer that was used for making preincubation and incubation medium) followed by a quick rinse in **cold** 0.1 *M*

sodium cacodylate, pH 7.4 (*see Note 4*). Tissues can then be postfixed overnight in the cold in 1% OsO₄ followed by dehydration, infiltration, and embedment in epoxy resins for TEM. Gold sections (100 nm) are cut and examined without poststaining in the TEM at standard accelerating voltages.

10. If specimens are to be examined by LM, the osmication step is skipped and sections can be examined directly using scanning laser reflectance microscopy (*12,13*), which lends itself to reconstruction and quantification of the final reaction product. If conventional LM is done the reaction product is amplified using a DAB and nickel or cobalt chloride procedure (*14*), which results in a blue reaction product. Tissue is then embedded and sectioned using standard paraffin methods.

3.1.1. Procedure

Prepare fresh fixative (5% acrolein in 0.1 *M* sodium cacodylate-HCl buffer, pH 7.4 [4% paraformaldehyde can be substituted for acrolein with some enzymes]) immediately before use (*see Note 5*). The buffer wash (0.15 *M* sodium cacodylate-HCl, pH 7.4, 5% sucrose, 1% DMSO) can be prepared ahead of time and kept in the refrigerator.

1. Sacrifice animal with overdose of euthanasia solution and immediately dissect out tissue. Once the tissue of interest is exposed, drip fixative onto the tissue. Quickly remove the tissue and cut it into smaller pieces while the tissue is submerged in fixative. Place tissue into a prelabeled scintillation vial.
2. Fix tissue in cold fixative (ice bath) for 1 h.
3. Wash 4 × 15 min with cold buffer wash. Continue to wash overnight. Bring to room temperature in final two buffer washes containing 0.1 *M* glycine.
4. Incubate tissue in preincubation medium for 30 min in a shaking water bath at 37°C.
5. Incubate tissue in complete reaction medium for 1 h in shaking water bath at 37°C. Change reaction medium at 30-min intervals.
6. Stop reaction by washing once in cold 0.1 *M* reaction medium buffer, 7% sucrose followed by one wash in cold 0.1 *M* sodium cacodylate-HCl buffer, pH 7.4, 7% sucrose.
7. Postfix overnight in the refrigerator in 1% osmium tetroxide in 0.1 *M* sodium cacodylate-HCl buffer, pH 7.4, 7% sucrose.
8. Dehydrate with a cold ethanol series (20, 40, 60, 80, 90, 2 × 95, 2 × 100%) to propylene oxide (3 × 5 min.).
9. Infiltrate and embed in epoxy resin.
10. Cut gold sections and examine in TEM without poststaining.

Figure 1 shows intracellular localization of NADH oxidase. **Figure 2** shows no reaction product for NADH oxidase when the substrate is omitted.

3.2. NADH Oxidase Localization

3.2.1. Preincubation Medium

Same as the complete incubation medium listed below except that NADH is **omitted**. Some protocols reduce the aminotriazole to 1.0 mM; but it is safer to leave the concentration at 10 mM to insure complete inhibition of catalase and glutathione peroxidase. Control specimens to demonstrate the specificity of the reaction (omission of substrate and inclusion of specific inhibitors such as 1.0 mM DPI [3.15 mg/10 mL] or 1.0 mM allopurinol [1.36 mg/10 mL]) should be initiated during preincubation. Appropriate inhibition cannot be demonstrated if the inhibitors are not included in the preincubation step.

Complete Incubation Medium: 7.45 mg/10 mL 2.0 mM cerium chloride, 5.68 mg/10 mL 0.8 mM NADH, 8.41 mg/10 mL 10 mM aminotriazole (*see Note 6*). (100 mM sodium azide [65 mg/10 mL] can be substituted for aminotriazole), 0.1 M Tris-maleate buffer, pH 7.5, 7% sucrose, 0.0002% Triton X-100. (Make a 1% (v/v) stock solution in deionized water and add 1–2 drops with a Pasteur pipet to each 10 mL of incubation medium)

3.3. Xanthine Oxidase Localization

3.3.1. Preincubation Medium

Same as the complete incubation medium listed below except that hypoxanthine and/or NADH are **omitted**. Under certain metabolic conditions, xanthine oxidase can use NADH as a substrate (**18**). Use of three different substrate combinations ([1] hypoxanthine alone; [2] NADH alone; [3] hypoxanthine and NADH together) can be used to probe this shift in substrate requirements.

Complete Incubation Medium: 37.25 mg/10 mL 10.0 mM cerium chloride, 1.40 mg/10 mL 1.0 mM hypoxanthine, 5.68 mg/10 mL 0.8 mM NADH (optional substrate), 8.41 mg/10 mL 10 mM aminotriazole (*see Note 6*). (100 mM sodium azide can be substituted for aminotriazole), 0.1 M HEPES-NaOH buffer, pH 8.0, 7% sucrose, 0.0002% Triton X-100.

3.4. Amplification for LM Visualization

This amplification protocol has been modified from that of Gossrau et al. (**13**). Amplification Medium: 0.05 M Tris-HCl buffer, pH 7.6, 0.05% (w/v) DAB, 0.02% (v/v) H_2O_2 , 1.0% (w/v) cobalt chloride.

1. Prepare the amplification medium fresh, immediately before use.
2. Incubate the tissue in a shaking water bath for 10–15 min at 40°C. Longer incubation times may be required based on the thickness and size of the specimen used.

3. A positive reaction appears as cobalt blue color in the tissue. Color intensity can be checked by LM. Stop the reaction by rinsing the tissue in cold Tris-HCl buffer.
4. This protocol can be used also on frozen sections, which were reacted for NADH oxidase, xanthine oxidase, or any other cerium-based histochemical procedure.

3.5. Quantitation

Cerium enzyme oxidase techniques show actual sites of peroxide generation, not merely the presence or absence of hydrogen peroxide. The cerium perhydroxide reaction product, a direct indication of oxidase activity, lends itself to a number of quantitative and semiquantitative methods. Briggs et al. (19) used a semiquantitative method to determine amounts of cerium perhydroxide in chronic granulomatous PMNs vs normal, control cells. Cells that contained cerium perhydroxide were scored positive (+) and the results were expressed as a percentage of positive cells divided by the total number of cells examined. In studies of diabetic retinopathy, blood vessels positive for NADH oxidase activity were expressed as a percentage of the total number of blood vessels examined for each eye (11,20). Computer morphometric analysis can also be used to quantitate the cerium perhydroxide precipitate (10) (see Note 7).

4. Notes

1. A positive (complete reaction mixture) and negative (omission of substrate and inclusion of specific enzyme inhibitors in the complete reaction mixture) control is essential for determining specificity of the reaction.
2. Prolonged fixation is not recommended and **glutaraldehyde should be avoided** since it cross-links tissue components and may denature the oxidase that one is trying to localize.
3. Phosphates can react with cerium ions to produce nonspecific precipitates.
4. Buffers to stop the reaction should be kept in an ice bath (4°C). Sample vials should be placed in the ice bath as soon as removal from the 37°C water bath to prevent diffusion of the reaction product.
5. **ACROLEIN AND PARAFORMALDEHYDE SHOULD BE HANDLED ONLY IN A PROPERLY FUNCTIONING FUME HOOD. KEEP BISULFITE AVAILABLE TO NEUTRALIZE ACROLEIN.**
6. Aminotriazole is toxic to thyroid function. Use gloves when handling this compound and do not inhale the powder.
7. The protocols presented here can be modified and applied to any enzyme system that generates O_2^- and H_2O_2 by using appropriate substrates and inhibitors. Although the first studies used Tris-maleate buffer for localization of NADH oxidase in PMNs (5), this buffer system is not applicable to all enzymes. Amino acid oxidase appears to be inhibited by maleate and therefore Tris-HCl or HEPES buffer should be substituted (21).

Acknowledgments

This work was supported in part by NIH Grant EY07739 and EY12601; the American Heart Association; and the Department of Health and Rehabilitative Services of the State of Florida for the University of Florida Diabetes Research, Education and Treatment Center.

References

1. Halliwell, B. and Gutteridge, J. (1999) *Free Radicals in Biology and Medicine*. Oxford University Press, New York, p. 936.
2. Bravenboer, B., Kappelle, A. C., Hamers, F. P. T., van Buren, T., Erkelens, D. W., and Gispen, W. H. (1992) Potential use of glutathione for the prevention and treatment of diabetic neuropathy in the streptozotocin-induced diabetic rat. *Diabetologia* **3**, 813–817.
3. Cameron, N. E., Cotter, M. A., and Maxfield, E. K. (1993) Anti-oxidant treatment prevents the development of peripheral nerve dysfunction in streptozotocin-diabetic rats. *Diabetologia* **36**, 299–304.
4. Zhang, H., Agardh, E., and Agardh, C-D. (1993) Nitro blue tetrazolium staining: a morphological demonstration of superoxide in the rat retina. *Graefe's Arch. Clin. Exp. Ophthalmol.* **231**, 178–183.
5. Briggs, R. T., Karnovsky, M. L., and Karnovsky, M. J. (1975) Localization of NADH oxidase on the surface of human polymorphonuclear leukocytes by a new cytochemical method. *J. Cell Biol.* **67**, 566–586.
6. Feigl, F. (1958) *Spot Tests in Inorganic Analysis*. Elsevier, New York.
7. Van Noorden, C. J. F. and Frederiks, W. M. (1993) Cerium methods for light and electron microscopical histochemistry. *J. Microsc.* **171**, 3–16.
8. Warren, J. S., Kunkel, R. G., Simon, R. H., Johnson, K. J., and Ward, P. A. (1989) Ultrastructural cytochemical analysis of oxygen radical-mediated immunoglobulin A immune complex induced lung injury in the rat. *Lab. Invest.* **60**, 641–658.
9. Schlafer, M., Brosamer, K., Forder, J. R., Simon, R. H., Ward, P. A., Grum, C. M. (1990) Cerium chloride as a histochemical marker of hydrogen peroxide in reperfused ischemic hearts. *J. Mol. Cardiol.* **22**, 83–97.
10. Guy, J., Ellis, E. A., Mames, R., and Rao, N. A. (1993) Role of hydrogen peroxide in experimental optic neuritis: a serial quantitative ultrastructural study. *Ophthalmic Res.* **25**, 253–264.
11. Ellis, E. A., Grant, M. B., Murray, F. T., Wachowski, M. B., Guberski, D. L., Kubalis, P. S., and Lutty, G. A. (1998) Increased NADH oxidase activity in the retina of the BBZ/Wor diabetic rat. *Free Rad. Biol. Med.* **24**, 111–120.
12. Robinson, J. M. and Batten, B. E. (1990) Localization of cerium-based reaction products by scanning laser reflectance confocal microscopy. *J. Histochem. Cytochem.* **38**, 315–318.
13. Telek, G., Scoazec, J-Y., Chariot, J., Cucroc, R., Feldmann, G., and Rozé, C. (1999) Cerium-based histochemical demonstration of oxidative stress in taurocholate-

- induced acute pancreatitis in rats: a confocal laser scanning microscopic study. *J. Histochem. Cytochem.* **47**, 1201–1212.
14. Gossrau, R., van Noorden, C. J. F., and Frederiks, W. M. (1989) Enhanced light microscopic visualization of oxidase activity with the cerium capture method. *Histochemistry* **92**, 349–353.
 15. Slezak, J. T., Tribulova, N., Pristacova, J., Uhrik, B., Thomas, T., Khaper, N., et al. (1995) Hydrogen peroxide changes in ischemic and reperfused heart: cytochemistry and biochemical and x-ray microanalysis. *Am. J. Pathol.* **147**, 772–781.
 16. Skepper, J. N., Pierson III, R. N., Younk, V. K., Rees, J. A., Powell, J. M., Navaratnam, V., et al. (1998) Cytochemical demonstration of sites of hydrogen peroxide generation and increased vascular permeability in isolated pig hearts after ischemia and reperfusion. *Microsc. Res. Tech.* **42**, 369–385.
 17. Robinson, J. M. (1985) Improved localization of intracellular sites of phosphatases using cerium and cell permeabilization. *J. Histochem. Cytochem.* **33**, 749–754.
 18. Zhang, A., Blake, D. R., Stevens, C. R., Kanczler, J. M., Winyard, P. G., Symons, M. C. R., et al. (1998) A reappraisal of xanthine dehydrogenase and oxidase in hypoxic reperfusion injury: the role of NADH as an electron donor. *Free Rad. Res.* **28**, 151–164.
 19. Briggs, R. T., Karnovsky, M. L., and Karnovsky, M. J. (1977) Hydrogen peroxide in chronic granulomatous disease: a cytochemical study of reduced pyridine nucleotide oxidases. *J. Clin. Invest.* **59**, 1088–1098.
 20. Ellis, E. A., Guberski, D. L., Somogyi-Mann, M., and Grant, M. B. (2000) Increased H₂O₂, vascular endothelial growth factor and receptors in the retina of the BBZ/Wor diabetic rat. *Free Rad. Biol. Med.* **28**, 91–101.
 21. Fahimi, H. D. and Baumgart, E. (1999) Current cytochemical techniques for the investigation of peroxisomes: a review. *J. Histochem. Cytochem.* **47**, 1219–1232.

Localization of Intracellular Lipid Hydroperoxides Using the Tetramethylbenzidine Reaction for Transmission Electron Microscopy

E. Ann Ellis, Shigehiro Iwabuchi, Don Samuelson,
and Donald Armstrong

1. Introduction

Histochemical reactions for lipid hydroperoxides (LHP) using indophenol, benzidine, or phenylendiamine as the electron donor have been described previously for auto-oxidized adipose (1) and neuronal (2) tissue. More recently, tetramethylbenzidine (TMB) has been proposed as another chromagen (3). The usefulness of the TMB reaction for ultrastructural studies of lipid peroxidation was demonstrated in retina where LPH was generated by incubation with exogenous lipoxigenase. The glutaraldehyde fixed tissue, which was reacted with TMB and then postfixed in osmium tetroxide, showed an electron-dense product (4). This technique allows intra- and extracellular localization, as well as a comparison of relative intensity among various cell types and subcellular organelles (5). In light-induced lipid peroxidation, discs of the outer segments, which are rich in oxidizable long-chain polyunsaturated fatty acids, stain strongly and appear as bubble-like structures (6). These are however, quite similar to fingerprint profiles seen acutely in outer segments and chronically in neurons, which are visualized without TMB following exogenous exposure to LHP (7,8). A possible caveat to the reported method is that peroxidized protein and carbohydrates may also react and so the TMB method has not been proven to be specific for LHP only.

The present method uses *in vivo* exposure of tissue to pure 18:2 linoleic acid LHP and tissue from obese, diabetic rats with known elevation of endogenous LHP as a definitive marker of lipid peroxidative processes occurring *in vivo*.

From: *Methods in Molecular Biology*, vol. 196: *Oxidants and Antioxidants: Ultrastructure and Molecular Biology Protocols*
Edited by: D. Armstrong © Humana Press Inc., Totowa, NJ

2. Materials

2.1. Equipment

This protocol is for ultrastructural demonstration of LHP and is done best by technical staff who are experienced in processing tissue for transmission electron microscopy.

1. Fume hood for osmication and embedding tissue.
2. Shaking water bath for TMB reaction and osmication.
3. Ultramicrotome (Reichert Ultracut S).
4. Transmission electron microscope (Hitachi H-7000).

2.2. Reagents

1. 0.1 *M* citric acid.
2. 0.2 *M* Na₂HPO₄.
3. Osmium tetroxide (Ted Pella, Inc., Redding, CA) (*see Note 1*).
4. Sodium cacodylate (Ted Pella, Inc.) (*see Note 2*).
5. 3, 3', 5, 5'-tetramethylbenzidine dichloride (Sigma Chemical Co., St. Louis, MO) (*see Note 3*).

3. Methods

3.1. Tissue Fixation

1. Fix tissue in a cold, freshly prepared, buffered aldehyde fixative for 1 h. Any standard aldehyde fixative for electron microscopy such as 2–3% glutaraldehyde, 4% paraformaldehyde, or 2.5–5% acrolein can be used (*see Note 4*).
2. Wash the tissue in several changes (4 × 15 min) of cold, buffer wash to removed unreacted fixative.

3.2. Reaction with TMB and Post Fixation with Osmium Tetroxide

1. TMB reaction: 0.5 mg/mL TMB dichloride in 0.1 *M* Na₂HPO₄/citric acid buffer, pH 3.0. Dissolve 0.5 mg/mL of TMB in 4 parts of 0.1 *M* citric acid first and then add 1 part 0.2 *M* Na₂HPO₄ to adjust pH to 3.0. It is not necessary to check the pH with a pH meter.
2. Incubate tissue at 4°C overnight in TMB solution. Cover the vial that contains the tissue with aluminum foil and place this in a an insulated container with cold packs to keep the temperature at approx 4°C. Place the insulated container on the shaker, which is set at a low speed, and **agitate over night**. Rinse in cold citrate/phosphate buffer. Rinse in 0.1 *M* sodium cacodylate buffer, pH 7.0.
3. Osmicate in 1% OsO₄ in 0.1 *M* sodium cacodylate buffer, pH 7.2 in shaking water bath at 37°C for 1 h. Rinse one time in 0.1 *M* cacodylate buffer, pH 7.2 (*see Note 5*).
4. Dehydrate in 80, 90, 95, 100% × 2 ETOH for 15 min at each step. 2 × 10 min in acetone to propylene oxide (*see Note 6*).

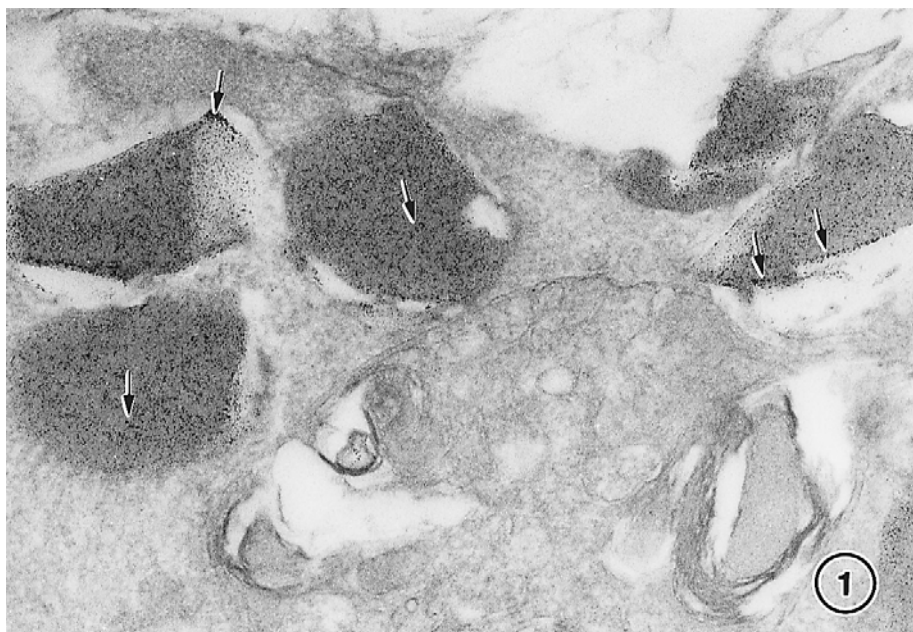


Fig. 1. Localization of LHP by the TMB reaction (arrows) in a retinal pigment epithelial cell macrophage. The retina was injected 2 wk earlier with 50 μ g of authentic 18:2 linoleic LHP. $\times 50,000$.

5. Infiltrate and embed in epoxy resin. Cut gold sections (90–100 nm) and examine in the TEM without poststaining (*see Note 7*).

3.3. Results

Figure 1 shows LHP localized with TMB in the retina of a New Zealand albino rabbit, which was injected with authentic 18:2 linoleic acid LHP. There are areas of electron dense TMB reaction product in the outer segments of the retina of a diabetic rat (**Fig. 2**).

4. Notes

1. Osmium tetroxide is extremely reactive and should be handled only in a properly functioning hood (flow rate of 100 ft/min). Osmium is also an expensive reagent and can be purchased from electron microscopy vendors as crystals or as 4% aqueous solution under an inert gas. Glassware and utensils should be cleaned in ethanol and then acetone before use with osmium tetroxide solutions. Plastic containers should not be used with osmium.
2. Sodium cacodylate contains arsenic and should be handled in an appropriate manner. Gloves should be worn when working with this buffer. If one chooses to

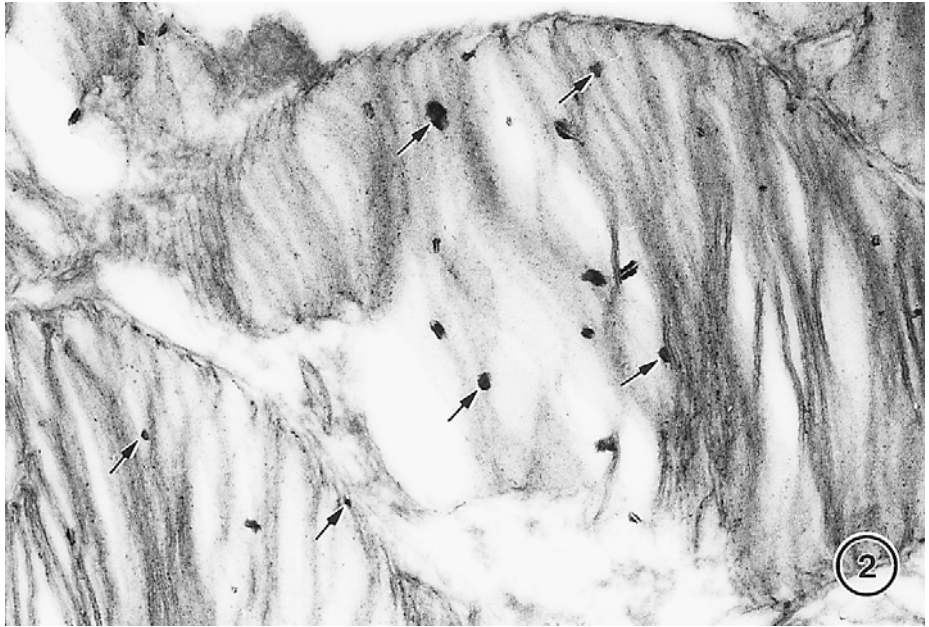


Fig. 2. Localization of LHP by the TMB reaction (arrows) in the outer segments of a diabetic rat with uncontrolled hyperglycemia for 6 mo. $\times 50,000$.

substitute another buffer, HEPES or PIPES are good choices. Phosphate buffers should be **avoided** since these buffers often result in nonspecific precipitates. Cacodylate can be purchased from any chemical supply company; however, it is cheaper to buy this compound from electron microscopy vendors.

3. Tetramethylbenzidine is available in several forms. Do not substitute the free base for the dichloride form recommended in this protocol. The free base is not soluble in aqueous solution without lowering the pH. The dichloride form is soluble in the buffers used in this protocol.
4. Paraformaldehyde and acrolein are extreme irritants and must be worked with in a properly functioning fume hood.
5. Osmication at room temperature or higher at neutral pH is necessary for preservation of the TMB reaction product through dehydration and embedding in epoxy resins. Optimal conditions for conversion of the TMB reaction product into the osmicated insoluble product occur at 37–45°C and pH 7.2. Use of osmium tetroxide with 1.5% potassium ferricyanide should **not** be done since this results in complete loss of the reaction product (9).
6. The TMB reaction product is soluble in lower concentrations of alcohol. Do **not** start dehydration below 80% ethanol. Do **not en bloc** stain with uranyl acetate.
7. Do **not** poststain sections with uranyl acetate and lead stains. Weak reactions can be overshadowed by uranyl acetate or removed. Staining with lead citrate

alone for 3 min can be used if necessary to improve the visibility of weak areas of TMB reaction product (10).

References

1. Mlarid, J., Hianadoe, H., Hartmann, S. and Dam, H. (1949) A histochemical method for the demonstration of fat peroxides. *Experientia* **5**, 84–85.
2. Armstrong, D. and Koppang, N. (1982) Histochemical evidence of lipid peroxidation in canine ceroid lipofuscinosis, in *Ceroid-Lipofuscinosis (Batten's Disease)* (Armstrong, D., Koppang, N., and Rider, J. A., eds.), Elsevier Biomedical Press, Amsterdam, pp. 159–165.
3. Thomas, P. D., and Poznansky, M. J. (1990) A modified tetramethylbenzidine method for measuring lipid hydroperoxides. *Anal. Biochem.* **188**, 228–232.
4. Schraermeyer, U., Kayatz, P., and Heimann, K. (1998) New method for ultrastructural localization of lipid peroxides in the eye. *Ophthalmologie* **95**, 291–295.
5. Kayatz, P., Heimann, K., Esser, P., Peters, S., and Schraermeyer, U. (1999) Ultrastructural localization of lipid peroxides as benzidine-reactive substances in the albino mouse eye. *Graefes Arch. Clin. Exp. Ophthalmol.* **237**, 685–690.
6. Kayatz, P., Heimann, K., and Schraermeyer, U. (1999) Ultrastructural localization of light-induced lipid peroxides in the rat retina. *Invest. Ophthalmol. Vis. Sci.* **40**, 2314–2321.
7. Armstrong, D. and Hiramitsu, T. (1982) Studies on experimentally induced retinal degeneration. 1. Effect of lipid peroxides on electroretinographic activity in albino rabbit. *Exp. Eye. Res.* **35**, 157–172.
8. Armstrong, D., Ueda, T., Ueda, T., Hiramitsu, T., Stockton, R., Brown, R., et al. (1998) Dose dependent mechanisms of lipid hydroperoxide induced retinal pathology, in *Pathophysiology of Lipid Peroxides and Related Free Radicals* (Yagi, K., ed.), Japan Sci. Soc. Press, Tokyo and S. Karger, Basel, pp. 57–76.
9. Carson, K. A. and Mesulam, M.-M. (1982) Electron microscopic demonstration of neural connections using horseradish peroxidase: a comparison of the tetramethylbenzidine procedure with seven other histochemical methods. *J. Histochem. Cytochem.* **30**, 425–435.
10. Stürmer, C., Bielenberg, K., and Spatz, W. B. (1981) Electron microscopical identification of 3, 3', 5, 5'-tetramethylbenzidine-reacted horseradish peroxidase after retrograde axoplasmic transport. *Neurosci. Lett.* **23**, 1–5.

The Immunohistochemical Localization of Glutathione Peroxidase

Kiyoshi Akeo, Tadahisa Hiramitsu, and Keiichi Watanabe

1. Introduction

Glutathione peroxidase (GSH-PO), a selenium-dependent and lipid peroxide-scavenging enzyme that effectively reduces lipid peroxides with the concomitant oxidation of glutathione is distributed in mitochondria (*1,2*). Utsunomiya et al. (*3*) confirmed the dual localization of GSH-PO in the cytosol and mitochondria of normal rat hepatocytes. We have shown that short-term incubation with linoleic acids (LA) increased the thiobarbituric acid- reactive substance (TBARS) in the RPE cells, which indicated the level of lipid peroxides (*4*). Mitochondria in the RPE cells were swollen by the incubation with LA or linoleic acid hydroperoxide (LHP) (*5*). We speculate that exposure of RPE cells to LA or LHP may cause damage to the mitochondria by lipid peroxidation, resulting in the cytotoxicity of RPE cells. We also found loss of mitochondria of bovine RPE cells cultured in hypoxia as low as 1% oxygen, induced malfunction of phagocytosis and a decrease in antioxidants such as glutathione containing sulfur (*6*).

Photoreceptor outer segments are susceptible to lipid peroxidation because of their high content of polyunsaturated fatty acids (PUFA) (*7–9*). If the degenerating photoreceptor outer segments not phagocytized by RPE cells were to undergo peroxidation in the retina of the Royal College of Surgeons (RCS) rats (*10*), the distribution of GSH-PO of mitochondria or cytoplasm in the retina and choroid could be altered. We evaluated the immunocytochemical localization of GSH-PO using laser scanning microscopy (LSM) and transmission electron microscopy (TEM) as well as conventional electron microscopy

(CLM) in an effort to identify subcellular organelles and to observe any pathological changes evident in sections of the retinas of RCS rats.

2. Materials

2.1. Equipment

1. DuPont Sorvall MT 6000 ultramicrotome (Newtown, CT).
2. Carl Zeiss LSM 410 laser scanning microscope (Jena, Germany).
3. Jeol JEM-1010 transmission electron microscope (Tokyo, Japan).

2.2. Animals

Pregnant strains of Wistar and RCS rats homozygous for the inherited retinal dystrophy gene (*rdy/rdy*) (CLEA Inc., Tokyo, Japan).

2.3. Reagents

2.3.1. Immunoblot Analysis

Chemicals used included tris-HCl, glycerol, sodium dodecyl sulfate (SDS), and mercapto-ethanol (for sample buffer), tris base, glycine, and methanol (for blotting buffer), and bovine serum albumin (BSA), gelatin, NaN_3 , and $\text{MgCl}_2 \cdot 6\text{H}_2\text{O}$ (for buffer G) were from Wako Inc. (Wako, Tokyo, Japan).

2.3.2. Immunohistochemical Localization

1. Phosphate-buffered saline (PBS), glutaraldehyde, formalin, periodate, lysine hydrochloride, paraformaldehyde, and sucrose were obtained from Wako.
2. OCT compound (10.24% polyvinyl alcohol, 4.26% polyethylene glycol, 85.5% nonreactive ingredients) was the embedding medium for frozen tissue specimens (Miles Inc. Diagnostics Division Elkhart, IN).
3. Osmium tetroxide, uranyl acetate, and lead acetate were obtained from TAAB Laboratories Ltd (Berks, UK).
4. Horseradish peroxidase (HRP)-labeled F(ab) fragments of rabbit IgG against rat liver GSH-PO (HRP-conjugated anti-GSH-PO) (3).
5. Epon 812 (Polysciences Inc., Warrington, PA).

3. Methods

3.1. Immunoblot Analysis (see Note 1)

1. Ten eyes were obtained from 5 animals in each group of rats 3 wk after birth. Anterior segments were removed, the retinas dissected, and homogenized separately with 50 mM tris-HCl, pH 6.5, to achieve a 10% homogenate (w/v). The SDS buffer contained 125 mM tris-HCl, pH 6.5, 5% SDS, 5% 2-mercaptoethanol, and 25% glycerol. Homogenized retinas were added to the same volume of SDS, heated at 95°C for 5 min, and centrifuged at 10,000 rpm for 10 min. The SDS sample buffer was put on a cooling plate for SDS-PAGE and the homogenates

subjected to electrophoresis (150 mA) on 12.5% polyacrylamide gels, and electrotransferred to polyvinylidene difluoride (PVDF) (Millipore).

2. The PVDF membrane was then washed with 0.05% Tween 20 in 0.01 M PBS. For Western blotting, the membrane was blocked for 30 min at 37°C with 3% BSA, 0.1% NaN₃, in 0.01 M PBS, washed with 0.05% Tween 20 in 0.01 M PBS, and incubated for 30 min at room temperature with 2% normal goat serum.
3. The membrane was reacted with affinity-purified anti-rat GSH-PO, 10 µg/mL, diluted with buffer G, washed with 0.05% Tween 20 in 0.01 M PBS, reacted for 1 h at room temperature with anti-rabbit IgG, HRP-F(ab) fragment from goat diluted 5,000 times with 0.05% Tween 20 in 0.01 M PBS, then washed with 0.05% Tween 20 in 0.01 M PBS.
4. The membrane was incubated with ECL Western blotting reagent (Amersham, Tokyo, Japan) for 1 min at room temperature, and exposed to X-ray film.

3.2. Conventional Light Microscopy (CLM) (see Note 2)

1. Eyes from RCS rats and Wistar rats were obtained 3 wk after birth. The eyes were fixed in 5% formalin and 2.5% glutaraldehyde, and embedded in paraffin. Embedded tissue blocks were sectioned on a microtome.
2. After the sections had been deparaffinated with xylene and ethanol, endogenous peroxidase activity was blocked by application of 3% hydrogen peroxide in methanol for 30 min and of 2% normal goat serum for 30 min.
3. The sections were reacted for 1 h with HRP-conjugated anti-GSH-PO. 100 mL of 50 mM Tris-HCl buffer, pH 7.6, containing hydrogen peroxide (17 µL) as the substrate and DAB (20 mg) as the hydrogen donor were used. Specimens were stained with methylene green, dehydrated in a graded series of ethanol and xylene solutions, and mounted.

3.3. Laser Scanning Microscopy (LSM) (see Note 3)

After reacting with DAB, the sections were postfixed with 2% OsO₄ for 10 min preparatory to LSM. The wavelength of excitation was 488 nm for electronic signals (contrast, 329; brightness, 9,921; pinhole, 20; zoom, 5) that enhance positive reaction signals by processing methods. A planapochromat (×63) objective lens was used. A 0.3-µm slice of the specimen was observed by LSM (LSM410) (excitation 488 nm, emission free).

3.4. Immuno Histochemical Transmission Electron Microscopy (TEM) (see Note 4)

1. Eyes from RCS rats and Wistar rats were obtained 3 wk after birth. The eyes were fixed for 12 h at 4°C in PLP (periodate-lysine-paraformaldehyde) solution (4% paraformaldehyde, 0.075 M lysine, 0.0375 M phosphate buffer, 0.01 M NaIO₄, pH 6.2), incubated in a graded series of sucrose solutions at 4°C, and embedded in OCT compound in dry ice and acetone. Such embedded tissue blocks were sectioned on a cryostat.

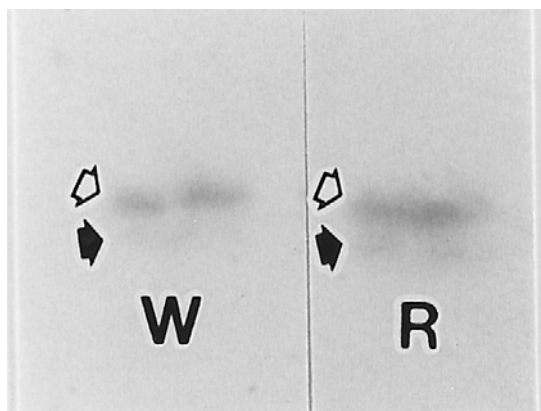


Fig. 1. Immunoblot analysis of GSH-PO molecules in retinas of Wistar rats (W) and RCS rats (R). (Open arrows: GSH-PO of cytosol, closed arrows: GSH-PO of mitochondria.)

2. Endogenous peroxidase activity was blocked by application of 3% hydrogen peroxide in methanol for 30 min and of 2% normal goat serum for 30 min. The sections were reacted for 1 h with HRP-conjugated anti-GSH-PO and fixed in 1% glutaraldehyde for 5 min. 100 mL of 50 mM Tris-HCl buffer, pH 7.6, containing hydrogen peroxide (17 μ L) as the substrate and DAB (4 mg) as the hydrogen donor were used.
3. The sections were rinsed with PBS and then postfixated for 2 h in 2% osmium tetroxide solution. Specimens were dehydrated in a graded series of ethanol solutions and embedded in Epon 812, with absolute ethanol used as an infiltrating agent. Ultrathin sections (70 nm) were cut with a diamond knife on an ultramicrotome. These ultrathin sections were examined by TEM at an accelerating voltage of 80 kV.

3.5. Results

3.5.1. Immunoblot Analysis

Immunoblot analysis confirmed the presence of GSH-PO molecules in the cytosol and the mitochondria of the retinas of the Wistar rats and RCS rats (**Fig. 1**). The size of the GSH-PO molecule was slightly smaller in the mitochondria (about 21KD) than in the cytosol (about 23KD).

3.5.2. Conventional Light Microscopy of Specimens Reacted with HRP-Conjugated Anti-GSH-PO, DAB, and OsO₄ (Methylene-Green Staining)

Photoreceptor outer segments of Wistar rats were well-developed, and negative-stained with anti-GSH-PO, DAB, and OsO₄ (**Fig. 2A**). In the RCS

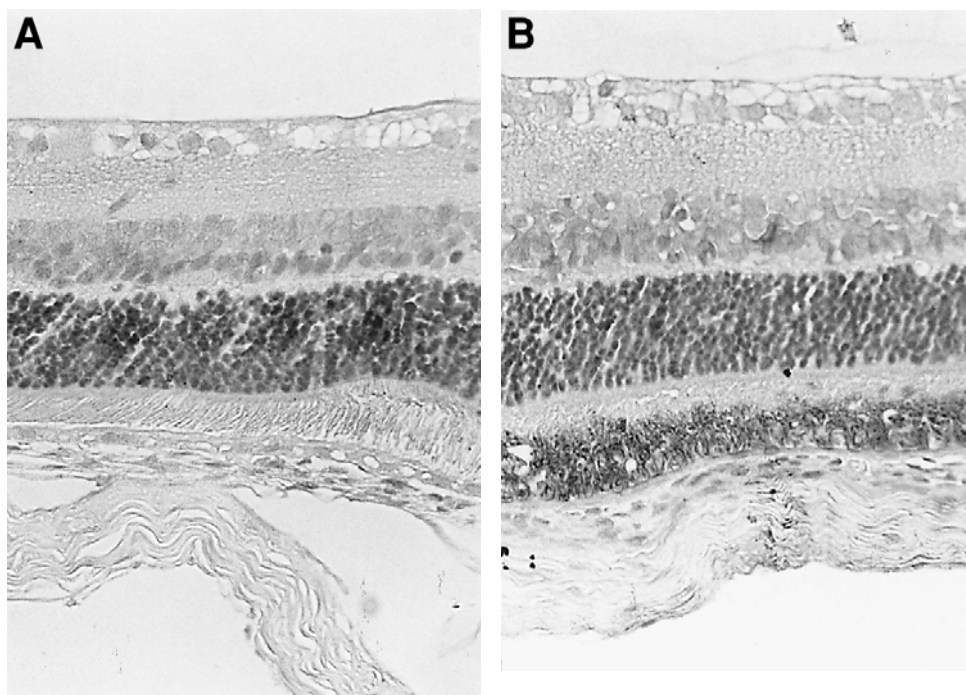


Fig. 2. Retina of (A) Wistar and (B) RCS rats reacted with anti-rat α GSH-PO. (Methylene-green staining, 400 \times).

rats, we can see strong positive-staining with anti-rat α GSH-PO, DAB, and OsO_4 in the degenerating photoreceptor outer segments (**Fig. 2B**).

3.5.3. Laser Scanning Microscopy of Specimens Reacted with HRP-Conjugated Anti-GSH-PO, DAB, and OsO_4

In the Wistar rats fluorescent granules that stained positively for F(ab) fragment of anti-rat α GSH-PO, DAB, and OsO_4 were detected in the photoreceptor inner segments and around the nuclei of the outer nuclear layer (**Fig. 3A**). In the RCS rats, the degenerating photoreceptor outer segments showed strong positive staining with anti-rat α GSH-PO, DAB, and OsO_4 , and fluorescent granules were visible around the nuclei of the photoreceptor cells. However, the photoreceptor inner segments were not stained (**Fig. 3B**).

*3.5.4. Transmission Electron Microscopy of Specimens Reacted with HRP-Conjugated Anti-GSH-PO, DAB, and OsO_4 (see **Note 4**)*

In the Wistar rats GSH-PO was localized in the mitochondria of the photoreceptor inner segments (**Fig. 4A**). In the RCS rats, no mitochondria stained

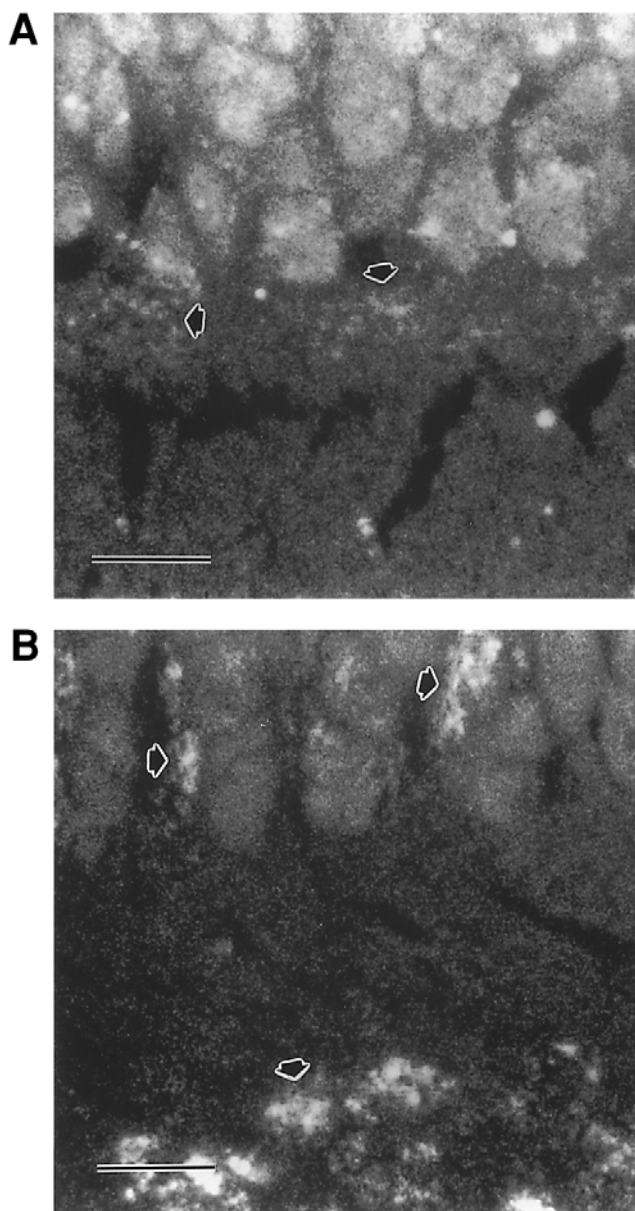


Fig. 3. Laser scanning microscopic (LSM) graphs of photoreceptor cells of (A) Wistar and (B) RCS rats reacted with anti-rat α GSH-PO. (Closed arrows: fluorescent granules, a bar = 5 μ m).

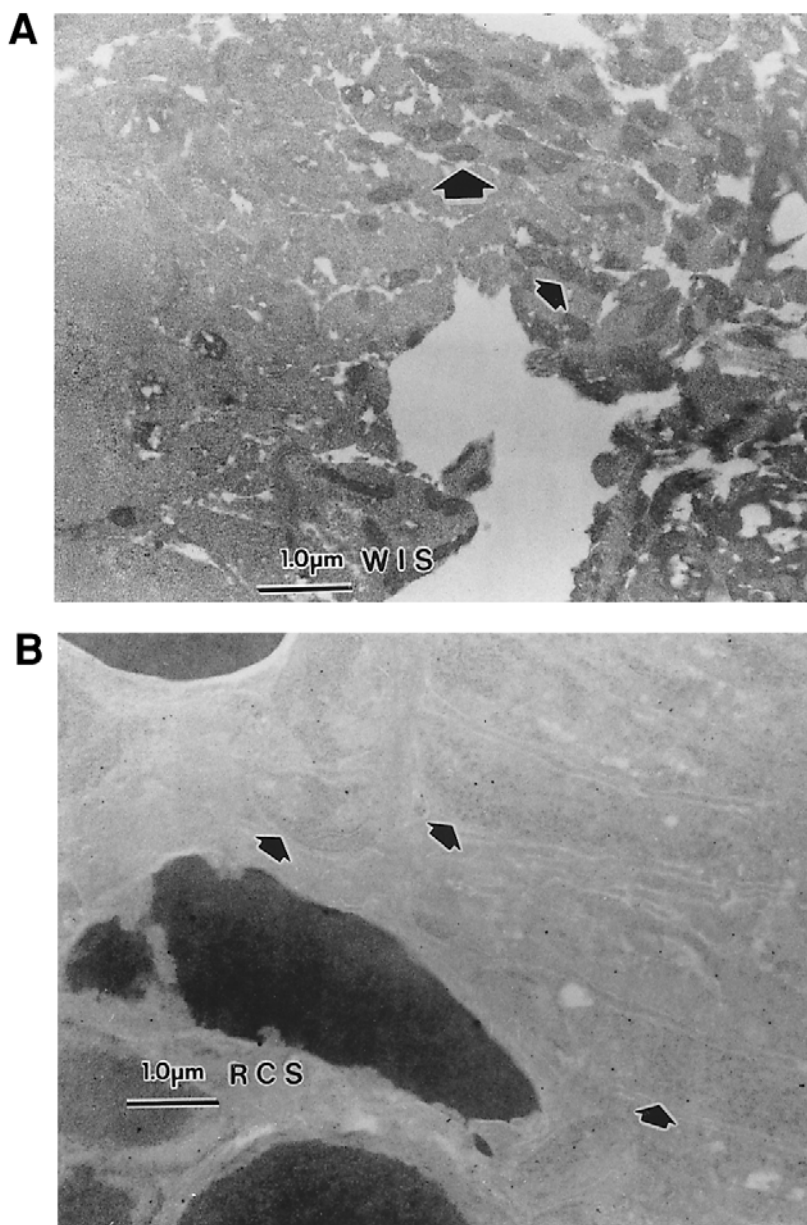


Fig. 4. TEM graphs of photoreceptor cells of Wistar rat (A) (WIS) and (B) RCS rat (RCS) reacted with anti-rat α GSH-PO. (Closed arrows: mitochondria).

with anti-rat α GSH-PO, DAB, and OsO_4 could be detected in the photoreceptor outer segments. Diffuse, fine high-electron-density granules showed HRP-labeled IgG Fab fragments, the smallest bioactive antibody molecules, in the cytoplasm of the photoreceptor inner segments (**Fig. 4B**).

4. Notes

1. We confirmed the presence of GSH-PO in the retina, and attempted to perform immunoblot analysis of homogenized retinas of the Wistar rats and RCS rats. This is the first study to detect two types of GSH-PO molecules, that is, the mitochondrial (21 KD) and the cytosolic (23 KD), in the retina. We detected GSH-PO in the retina of both strains, with the molecules being the same as those of GSH-PO in the liver of Wistar rats (**3**). The difference of the GSH-PO molecules between the mitochondrial and the cytosolic is consistent with the general biological rule for the importation of mitochondrial proteins from the cytosol (**11**).
2. In specimens of retinas of the two groups of rats stained with methylene green and observed by CLM, the photoreceptor outer segments of RCS rats had degenerated by 3 wk after birth and the debris layer showed strong positive staining with HRP-conjugated anti-GSH-PO, DAB, and OsO_4 . The comparable structures in the Wistar rats had not degenerated, and remained unstained by these reagents. GSH-PO in RCS rats may be released or leaked from the photoreceptor inner segments that ordinarily contain many mitochondria. Hyperoxia and irradiation are known to induce lipid peroxidation by free radicals in most microsomes and the membranes of some mitochondria, and to enhance the leakage of lipid hydroperoxides from membrane phospholipids. These lipid hydroperoxides or free radicals lead to a fragility of the membranes, an accumulation of hydroperoxides in the cytosol, with a disturbance of lipoprotein synthesis and transport (**12**).
3. LSM revealed subcellular organelles of retinal specimens from Wistar and RCS rats that had reacted with HRP-conjugated anti-GSH-PO, DAB, and OsO_4 and we assessed the relationship between degeneration of the photoreceptor cells and localization of GSH-PO, the enzyme that scavenges lipid hydroperoxides. Immuno- and/or enzyme histochemical staining of the marker substances or enzymes of subcellular organelles is usually employed to identify the organelles or to observe pathological changes in the sections prepared for light microscopy, it is usual to apply (**13**). Three weeks after birth, numerous fluorescent granules were detected in photoreceptor inner segments of Wistar rats, but fluorescent granules only accumulated in the degenerating outer segments of RCS rats. These fluorescent granules reacted with HRP-conjugated anti-GSH-PO, DAB, and OsO_4 and represent the aggregated GSH-PO observed by light microscopy. The disappearance of the granules, i.e., GSH-PO, from the photoreceptor inner segments of RCS rats indicated impairment of the protective function against

peroxidation. The granules accumulated in the degenerating outer segments might be antioxidative enzymes, i.e., scavengers, against the peroxidation of residual PUFA in the outer segments unphagocytized by the RPE cells of RCS rats. RCS rats exhibited distinct fluorescent granules around the nuclei of photoreceptor cells or fine granules in the nuclei themselves. One investigator considered such granules to be the result of artifactual diffusion (mobilization) of cytosolic GSH-PO into the nuclei, and urged application of microwave fixation to prevent it (3).

4. We used immuno-TEM to observe the morphology of mitochondria and GSH-PO on the membranes of the mitochondria in the retina and observed a large number of mitochondria in the photoreceptor inner segments of Wistar rats. Immuno-TEM enabled us to localize of GSH-PO in the mitochondrial membranes of the photoreceptor inner segments of Wistar rats. Utsunomiya et al. (3) showed that HRP-labeled IgG Fab fragments, the smallest bioactive antibody molecules, were required for consistent localization of mitochondrial antigens by pre-embedding immuno-TEM, which impaired antigenicity much less than the postembedding immuno-gold technique. The uncertainty of the presence of GSH-PO by immuno-electron microscopy in RCS rats may be related to the fact that we utilized HRP to localize reaction products. We could not detect any GSH-PO in the mitochondria of the photoreceptor inner segments of RCS rats by immuno-TEM. However, we carried out the immunohistochemical studies of GSH-PO in RCS rats in the same way as in Wistar rats, and the differences in staining with HRP-conjugated anti-GSH-PO, DAB, and OsO_4 in the mitochondria of the photoreceptor cells between Wistar and RCS rats were evident. The results of our study indicated that the pathogenesis of retinal degeneration in RCS rats may be related to this loss of GSH-PO in mitochondria of the photoreceptor inner segments. Utsunomiya et al. (3) observed that a majority of mitochondria in periportal hepatocytes showed GSH-PO immunoreactivity, whereas cytosolic staining was relatively weak. GSH-PO probably enters the mitochondria through the membranes in normal tissue according to the general biological rule for the importation of mitochondrial proteins from the cytosol (11); that is, members of the Hsp70 chaperones have been implicated in protein folding, the assembly and disassembly of oligomeric complexes, protein synthesis and degradation, and the dislocation of polypeptides across cellular membranes (14). However, the mitochondria in the photoreceptor inner segments of RCS rats were not detected by immuno-TEM of GSH-PO. We hypothesize that antioxidative enzymes against phototoxicity, such as GSH-PO, could not be transported into the mitochondria because of a malfunction of the molecular chaperones. Clarke et al. (15) reported that the Hsp70 level in the retinas of 12-wk-old RCS rats was more than fivefold that animals aged 6 wk. An understanding of GSH-PO fractionation in mitochondria and cytosol requires not only quantification by enzyme immunoassay or detection by immunoblot analysis, but studies of heat-shock proteins, molecular chaperones, that maintain the transport of proteins, such as antioxidative enzymes, i.e., GSH-PO (16).

References

1. Watanabe, K. (1986) Lipid peroxidation and cell injury. Roles of glutathione peroxidase as a scavenger of lipid peroxidase. *Trans. Soc. Pathol. Jpn.* **76**, 39–74.
2. Zarowski, J. and Tappel, A. L. (1978) Purification and properties of rat liver mitochondrial glutathione peroxidase. *Biochem. Biophys. Acta* **526**, 65–76.
3. Utsunomiya, H., Komatsu, N., Yoshimura, S., Tsutsumi, Y., and Watanabe, K. (1991) Extra ultrastructural localization of glutathione peroxidase in normal rat hepatocytes: advantages of microwave fixation. *J. Histochem. Cytochem.* **39**, 1167–1174.
4. Akeo, K. and Hiramitsu, T. (1998) Changes in lipid peroxide level in retinal pigment epithelial cells in vitro upon addition of linoleic acids or linoleic acid hydroperoxides under varying concentrations of oxygen. *Pigment Cell Res.* **11**, 320–326.
5. Akeo, K., Hiramitsu, T., Kanda, T., Yorifuji, H., and Okisaka, S. (1996) Comparative effects of linoleic acid and linoleic acid hydroperoxide on growth and morphology of bovine retinal pigment epithelial cells in vitro. *Curr. Eye Res.* **5**, 467–476.
6. Akeo, K., Fujiwara, T., Yorifuji, H., and Okisaka, S. (1997) X-ray microanalysis and phagocytotic activity of cultured retinal pigment epithelial cells in hypoxia. *Pigment Cell Res.* **10**, 257–264.
7. Poincelot, R. P. and Abrahamson, E. W. (1970) Fatty acid composition of bovine rod outer segments and rhodopsin. *Biochim. Biophys. Acta* **202**, 382–385.
8. Hendricks, T. K., Klompmakers, A. A., Daemen, F. J. M., and Bonting, S. L. (1976) Biochemical aspects of the visual process. XXII. Movement of sodium ions through bilayers composed of retinal and rod outer segment lipids. *Biochim. Biophys. Acta* **443**, 271–281.
9. Stone, W. L., Farnsworth, C. C., and Dratz, E. A. (1979) A reinvestigation of fatty acid content of bovine, rat and frog retinal rod outer segments. *Exp. Eye Res.* **28**, 387–397.
10. Zigler, J. S. Jr. and Hess, H. H. (1985) Cataracts in the Royal College of Surgeons rat: Evidence for initiation by lipid peroxidation products. *Exp. Eye Res.* **41**, 67–76.
11. Doonan, S., Marra E., Passarella S., Saccone C., and Quagliariello, E. (1984) Transport of proteins to mitochondria. *Int. Rev. Cytol.* **91**, 141–186.
12. Savanian, A., Mukkassah-Kely, S. F., and Montestruque, S. (1983) The influence of phospholipase A₂ and glutathione peroxidase on the elimination of membrane lipid peroxides. *Arch. Biochem. Biophys.* **223**, 441–452.
13. Itoh, J., Osamura, Y., and Watanabe, K. (1992) Subcellular visualization of light microscopic specimens by laser scanning microscopy and computer analysis: a new application of image analysis. *J. Histochem. Cytochem.* **40**, 955–967.
14. Glick, B. S. (1995) Can Hsp70 proteins act as force-generating motors? *Cell* **80**, 11–14.
15. Clarke, I. S., Dzialoszynski, T., Sanford, S. E., and Trevithick, J. R. (1991) A possible relationship between cataract, increased levels of the major heat shock

protein Hsp70 and decreased levels of S-antigen in the retina of the RCS rat. *Exp. Eye Res.* **53**, 545–548.

16. Yoshimura, S., Komatsu, N., and Watanabe, K. (1980) Purification and immuno-histochemical localization of rat liver glutathione peroxidase. *Biochem. Biophys. Acta* **621**, 130–137.

4-Hydroxy-2-Nonenal (4-HNE) Staining by Anti-HNE Antibody

Hideyuki J. Majima, Takako Nakanishi-Ueda, and Toshihiko Ozawa

1. Introduction

In almost all aerobic cells, the oxygen metabolism generates reactive oxygen species (ROS), such as superoxide, hydroxyl radicals, and hydrogen peroxide. These ROS can peroxidize membrane lipids of a cell and its organelles, and can also attack DNA or protein (**1**). During the process of lipid peroxidation, polyunsaturated fatty acids (PUFA), especially linoleic acid, arachidonic acid, and docosahexaenoic acid, in biomembranes are degraded to a great variety of water-soluble, short-chain carbonyl compounds (**2**). Malonaldehyde and other aldehydes, such as alkaneals, 2-alkenals, hydroxyalkenals (**3**), and phospholipid-bound aldehydes (**4**) are generated in the lipid peroxidation process. The major representative of 4-hydroxyalkenals, 4-hydroxynonenal (4-HNE), is the main product formed from omega 6-PUFA (**5**). 4-HNE, a highly toxic aldehyde product of lipid peroxidation (**5**), is a sensitive marker of oxidative damage and lipid peroxidation and can be evaluated by immunohistochemical staining using an anti-4-HNE monoclonal antibody (MAb) (**6–8**) and labeled goat anti-mouse IgG antibody (**9**).

This chapter describes a simple method for evaluating 4-HNE in tissues.

2. Materials

2.1. Instrumentation

1. Laser confocal unit (Yokogawa Electric Corp, CSU10, Tokyo, Japan).
 - a. Confocal light microscope (Olympus Tokyo, Japan).
 - b. 3CCD Camera (Hamamatsu Photonics, Hamamatsu, Japan).
 - c. Monitor.

From: *Methods in Molecular Biology*, vol. 196: *Oxidants and Antioxidants: Ultrastructure and Molecular Biology Protocols*
Edited by: D. Armstrong © Humana Press Inc., Totowa, NJ

- d. Laser system (Yokogawa).
- e. Macintosh computer.

2.2. Reagents and Supplies

1. 35-mm culture dish with glass bottom (Glass Bottom No.0 poly-d-lysine coated, MatTek Corporation, MA).
2. 4% buffered paraformaldehyde.
3. Phosphate-buffered saline (PBS).
4. Ethanol/acetic acid (95/5, v/v).
5. Anti-4-hydroxy-2-nonenal monoclonal antibody, 100 $\mu\text{g/mL}$, (anti-4-HNE antibody, 100 $\mu\text{g/mL}$, Nippon Yushi Co. Ltd., Tokyo, Japan).
6. Labeled goat anti-mouse IgG antibody 2 mg/mL (Alexa, Molecular Probes, OR).
7. 0.1% bovine serum albumin (BSA) contained PBS.

3. Methods

3.1. Preparation of Monolayer Culture

1. Bovine RPE cells are cultured in 35 mm culture dish with glass bottom (*see Notes 1 and 2*), fixed with 4% buffered formaldehyde at room temperature for 30 min, rinsed twice with PBS, and postfixed with ethanol/acetic acid solution for 2 min.
2. After the postfixation, cells are rinsed twice with PBS.

3.2. HNE Stain

1. Nonspecific antigenic sites are blocked with 0.1% BSA in PBS for 2 min. Add 1 mL with 0.1% BSA containing PBS to the cells, incubate with 5 μL anti-4-HNE antibody for 60 min at room temperature, and rinse twice for 2 min with 0.1% BSA containing PBS. Add 0.1% BSA containing PBS (1 mL), and reincubate with 5 μL Alexa for 60 min at room temperature (*see Note 3*).
2. The cells are rinsed twice with PBS, and examined with the laser con-focal unit (Yokogawa Electric Corp.) coupled to an inverted microscope (Olympus). The dye is excited at 488 nm and emission is filtered using a 515 nm barrier filter. The intensity of the laser beam and the sensitivity of the photo detector are held constant to allow quantitative comparisons of relative fluorescent intensity of the cells between experimental groups (*see Note 4*).
3. Images of microscopic fields are taken using a color chilled 3CCD camera (Hamamatsu Photonics). Cells were chosen for analysis on a random basis. Values for average staining intensity/% of area are obtained using "IPLab" software programmed by the author (HJM).

3.3. Results

1. **Figure 1** illustrates the fine HNE stain in cultured RPE cells. The green fluorescence indicates intracellular and membrane locations. This is contrasted

HNE stain

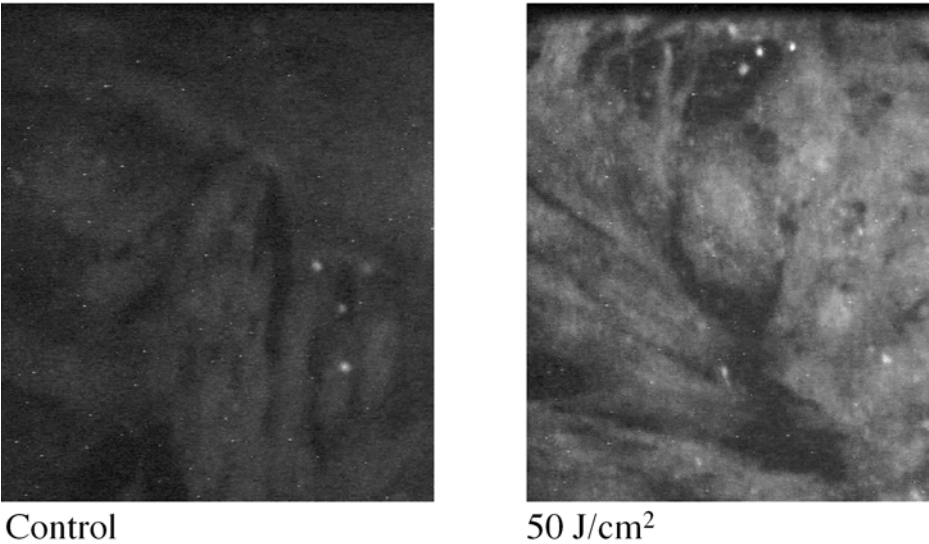


Fig. 1.

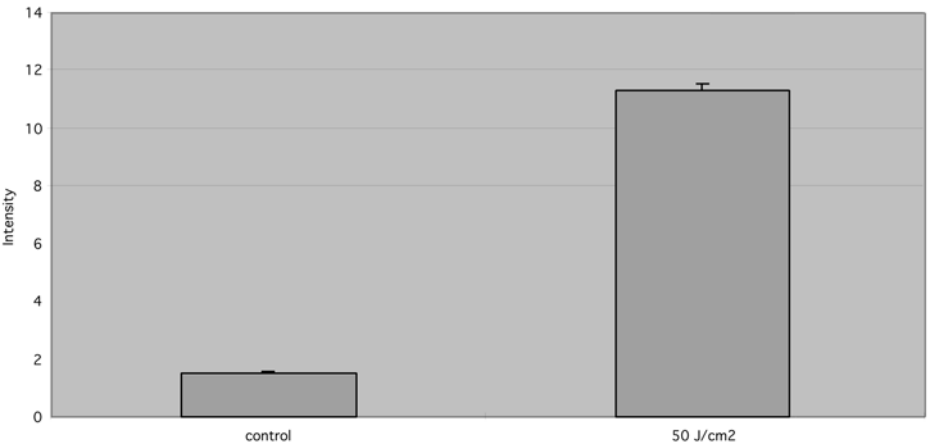


Fig. 2.

with cells expressed to conditions of oxidative stress. Control RPE cell (**Fig. 1**) show weak staining for HNE, however strong staining is observed in **Fig. 1** after cells received 50 J/cm² of blue light (470 nm LED) exposure.

- 2. HNE can be quantified by appropriate densitometry. **Figure 2** shows the effect of blue light after 50 J/cm² exposure.

4. Notes

1. Maintain cultured cell in healthy condition. 4-HNE stain in damaged cell is stronger than in healthy cells.
2. Keep constant physiological pH (pH 7.2–7.4) and osmotic pressure in medium of sample throughout experiments including fixation procedure.
3. Keep in the dark after loading with Alexa. Alexa is a fluorescent probe, so it loses its fluorescence by light exposure.
4. Laser intensity must be kept constant. The relative fluorescent intensity of the cells are easily changed by the laser intensity.

References

1. Halliwell, B. and Gutteridge, J. M. C. (eds.) Oxidative stress: adaptation, damage, repair and death, in *Free Radicals in Biology and Medicine*, 3rd ed. Oxford University Press, Oxford, 1999, pp. 246–350.
2. Dillard, C. J. and Tappel, A. L. (1979) Volatile hydrocarbon and carbonyl products of lipid peroxidation: a comparison of pentane, ethane, hexanal, and acetone as in vivo indices. *Lipids* **14**, 989–995.
3. Esterbauer H., Cheeseman K. H., Dianzani M. U., Poli G., and Slater T. F. (1982) Separation and characterization of the aldehydic products of lipid peroxidation stimulated by ADP-Fe²⁺ in rat liver microsomes. *Biochem. J.* **15**, 129–140.
4. Tam, B. K. and McCay, P. B. (1970) Reduced triphosphopyridine nucleotide oxidase-catalyzed alterations of membrane phospholipids. 3. Transient formation of phospholipid peroxides. *J. Biol. Chem.* **245**, 2295–2300.
5. Esterbauer, H., Zollner, H., and Lang, J. (1985) Metabolism of the lipid peroxidation product 4-hydroxynonenal by isolated hepatocytes and by liver cytosolic fractions. *Biochem. J.* **228**, 363–373.
6. Majima, J. H., Oberley, T. D., Furukawa, K., Mattson, M. P., Yen, H.-C., Szveda, L. I., and St. Clair, D. K. (1998) Prevention of mitochondrial injury by manganese superoxide dismutase reveals a primary mechanism for alkaline-induced cell death. *J. Biol. Chem.* **273**, 8217–8224.
7. Uchida, K., Itakura, K., Kawakishi, S., Hiai, H., Toyokuni, S., and Stadman, E. R. (1995) Characterization of epitopes recognized by 4-hydroxy-2-nonenal specific antibodies. *Arch. Biochem. Biophys.* **324**, 241–248.
8. Uchida, K., Szveda, L. I., Chae, H.-Z., and Stadman, E. R. (1993) Immunochemical detection of 4-hydroxynonenal protein adducts in oxidized hepatocytes. *Proc. Natl. Acad. Sci. USA* **90**, 8742–8746.
9. Ueda, T. N., Fukuda, S., Ueda, T., Ozawa, T., Koide, R., and Majima, H. J. (1999) Effect of light-emitting diode (LED) light exposure on retinal pigment epithelial cells, in vitro, 1999 International Laser Safety Conference, Proceedings, Laser Institute of America, pp. 57–62.

Immunohistochemical Detection of Protein Oxidation

Jürgen Frank, Alfonso Pompella, and Hans K. Biesalski

1. Introduction

The oxidative modification of proteins by reactive oxygen species (ROS) and other reactive compounds is associated with a number of disease and pathophysiological processes as well as aging (*1*). Under physiological conditions, almost all oxidative modifications of proteins are resulting in an increase of carbonylated proteins. The three major pathways leading to carbonyl group formation (protein oxidation) are shown in **Fig. 1**. Carbonyl groups are introduced into proteins as a result of: 1) metal catalyzed oxidation of amino acid residues; 2) lipid peroxidation (the Michael addition of protein amino, sulfhydryl, and imidazole groups to the double bond of α,β unsaturated aldehydes, which are produced during the oxidation of polyunsaturated fatty acids); and 3) protein glycation and glycoxidation reactions. The carbonyl content of proteins is therefore an index of the amount of oxidative protein damage attributable to either direct attack of free radicals or the modification of proteins by oxidation products of carbohydrates or polyunsaturated fatty acids (PUFAs).

The histochemical visualization of protein-bound carbonyl groups can provide valuable information concerning the distribution of oxidative processes in vivo. For the specific detection of protein-associated carbonyl functions (oxidized proteins) (*2*), the method originally developed by Levine et al. (*3*) has been modified. As demonstrated in **Fig. 2**, the procedure consists of a first step, in which protein carbonyls are derivativized by 2,4-DNPH to yield the corresponding 2,4-dinitrophenyl hydrazones. In a second step, the dinitrophenyl (DNP) groups, which become associated with proteins

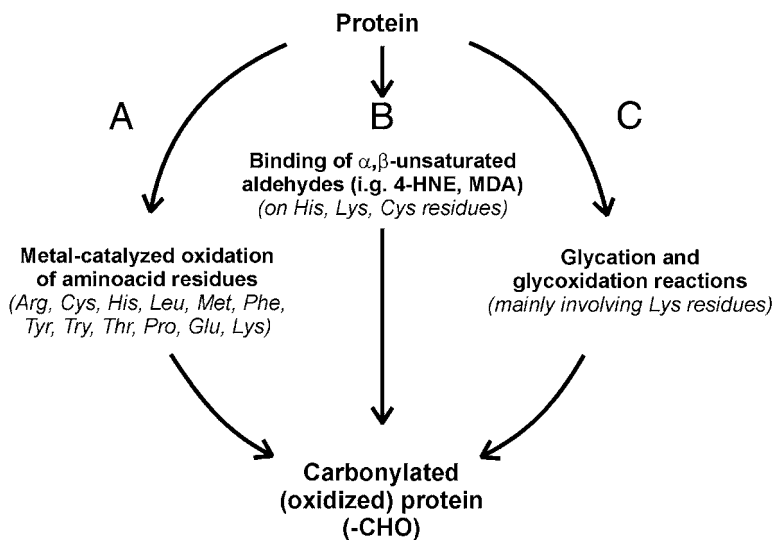


Fig. 1. Mechanisms of increase of carbonyl groups in proteins. Carbonyl groups are introduced into proteins (**A**) as a result of direct oxidant attack to protein, through the metal-catalyzed oxidation of side chains of several amino acids; (**B**) following a process of lipid peroxidation, by the reaction of the double bond of α,β -unsaturated aldehydes with amino, sulfhydryl, and imidazole groups in protein; and (**C**) by reaction of protein amino groups with carbohydrates, through glycation and glycoxidation reactions.

in this way are detected immunochemically by means of a commercial anti-DNP antiserum; finally, antibodies bound to specimens are identified with a conventional peroxidase staining system, or equivalent. In principle, the 2,4-DNPH/anti-DNP procedure should reveal all kinds of carbonyls becoming associated with protein, irrespective of their origin. With this method, oxidized proteins have been visualized in several interesting studies, e.g., in activated neutrophil phagocytes (4,5), in brain tissue from Alzheimer patients (6), and in sarcoma cells exposed to prooxidant treatments (7).

2. Materials

2.1. Equipment

1. Isopentane bath refrigerated with dry ice plus acetone, or liquid nitrogen bath.
2. Cryostat.
3. Humidified chambers for processing of microscope slides.
4. Coplin Jars.
5. Light microscope.

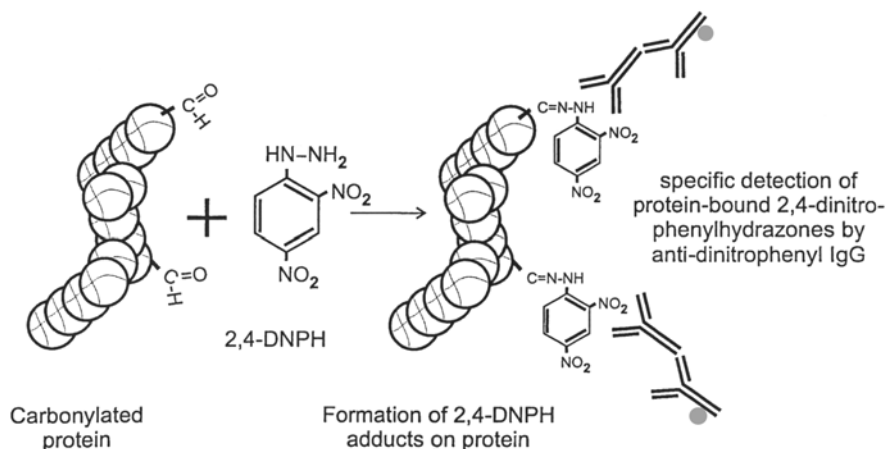


Fig. 2. The two-step procedure for the histochemical detection of protein carbonyl groups (oxidized proteins).

2.2. Reagents

1. Phosphate-buffered saline (PBS), pH 7.4.
2. 2,4-dinitrophenyl-hydrazine (2,4-DNPH) (Merck, Cat. # 103081) (*see Note 1*).
3. 3-amino-9-ethylcarbazole (AEC) (Sigma, Cat. # A6926) (*see Note 2*).
4. Tissue freezing medium, (4853[®] O.C.T. Compound, Electron Microscopy Science, Cat. # 62550-01).
5. Serial dilutions of ethanol: 100, 95, 70, 50, 30% in distilled water.
6. Rabbit anti-dinitrophenyl IgG (Dako Cat. # V0401).
7. Peroxidase-labeled sheep anti-rabbit IgG (Roche Diagnostic, Cat. # 1238850).
8. Mayer's hemalum solution (Merck, Cat. # 109249).

3. Methods

3.1. Preparation of Tissue and Staining Procedure

1. Small tissue blocks should be embedded in suitable freezing medium, and immediately frozen in liquid nitrogen or an isopentane bath refrigerated with dry ice plus acetone.
2. Frozen blocks were transferred into a cryostat chamber and were allowed to equilibrate temperature (-15° to -20°C) for 30–45 min before cutting.
3. Cut 5–10 μm thick tissue sections and allow to air-dry tissue for at least 1 h at room temperature (*see Note 3*).
4. Fix samples by immersing the slides in ethanol: diethylether (1:1 v/v) for 15 min in a Coplin jar at room temperature.
5. Allow the carbonyls to react with 2,4-DNPH by immersing the slides in acid 2,4-DNPH reagent (15 mM 2,4-DNPH dissolved in absolute ethanol containing

1.5% concentrated sulfuric acid) over night at room temperature in a Coplin jar.

6. Wash the samples by immersing the slides in absolute ethanol containing 1.5% (v/v) concentrated sulfuric acid for 5 min at room temperature.
7. Rehydrate the samples by sequentially immersing the slides through graded ethanol washes (95, 70, 50, 30%) for 3 min each at room temperature.
8. Wash the samples by immersing the slides in PBS for 5 min at room temperature. Repeat one time for a total of two washes.
9. Specific detection of the 2,4-dinitrophenyl hydrazones formed in proteins can be done by indirect peroxidase staining (*see Note 4*).
10. Remove excess liquid from around the specimen and place the slide on a flat surface in a humid chamber.
11. Cover the tissue with 50–100 μL rabbit anti-dinitrophenyl polyclonal antiserum (diluted 1:200). Incubate slides for 1 h at 4°C in a humid chamber (*see Note 5*).
12. To avoid unspecific binding of secondary antibody (peroxidase-labeled sheep anti-rabbit IgG), apply 4–6 drops of normal sheep serum (diluted 1:5–1:20) to each slide to cover the tissue section. Incubate for 30 min at 4°C in a humid chamber.
13. Wash the samples by immersing the slides in PBS for 5 min in a Coplin jar.
14. Remove excess liquid by tapping the slides. Cover the tissue with 50–100 μL peroxidase-labeled sheep anti-rabbit IgG (diluted 1:200). Incubate slides for 1 h at room temperature in a humid chamber.
15. Gently wash the samples by immersing the slides in PBS for 5 min in a Coplin jar.
16. Remove excess liquid from around the specimen. Apply AEC-solution to give colored endproduct and incubate until desired color intensity has developed (10–15 min).
17. Gently wash the samples by immersing the slides in PBS for 5 min in a Coplin jar.
18. Rinse gently with distilled water from a wash bottle. Counterstain with Mayer's hemalum and coverslip.

3.2. Results

A representative immunohistochemical detection of protein-associated carbonyls (“oxidized proteins”) in tumor after pro-oxidant treatment (7) is shown in **Fig. 3**. Protein oxidation was found largely to involve plasma membrane proteins of tumor cells. Areas of increased protein oxidation often correspond, on adjacent sections, to sites of accumulation of protein bound 4-HNE, an indicator of lipid peroxidation (*see Chapter 6*).

The possibility should be mentioned that aspecific reactions with 2,4-DNPH can be given under some circumstances by nucleic acids (8). To date however such phenomenon has not been observed in histochemical studies.

4. Notes

1. 2,4-DNPH should be recrystallized. Therefore, dissolve 2,4-DNPH in hot 2-butanol until the solution is saturated. Cool down the solution over night in

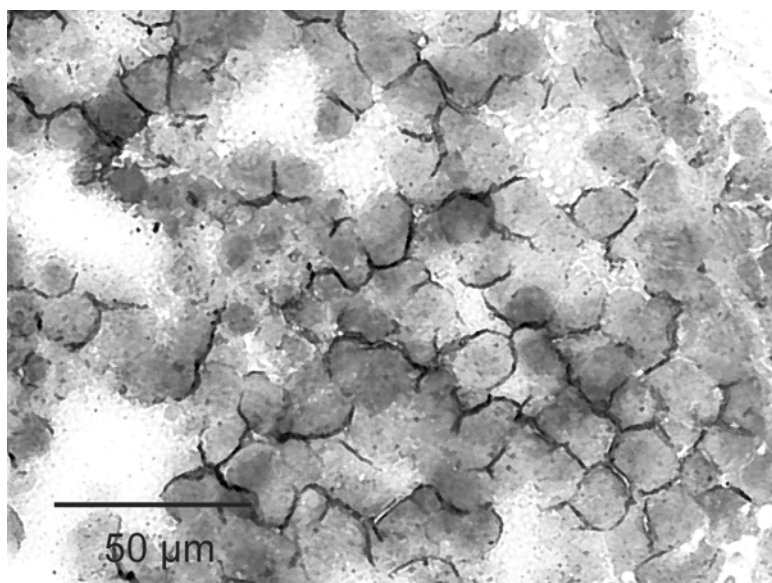


Fig. 3. Localization of protein oxidation (rose-red precipitate) at sites of cellular injury.

a refrigerator. Filter the solution and wash the formed crystals once in hexane. Air-dry the crystals and store in the dark at room temperature.

2. AEC-substrate solution. Dissolve 1 mg AEC in 1 mL N,N-dimethylformamide. Add 14 mL 0.1 M acetate buffer, pH 5.2, and 0.15 mL 3% hydrogen peroxide. Mix and filter if precipitate forms. Add solution to tissue and incubate for 5–15 min at room temperature.
3. Microscope slides should be cleaned with ether:ethanol (1:1 v/v) for 5 min in an ultrasonic bath.
4. Other substrates (alkaline phosphatase, fluorescence-labeled secondary antibodies) and chromogens (DAB, new fuchsin) can be used depending on the expression of endogene phosphatases or peroxidases in the tissue (for more details see *Handbook of Immunochemical Staining Methods*, DAKO Corporation, Carpinteria, CA).
5. When required, adequate spreading of antisera over tissue sections can be ensured by applying a piece of plastic sheet (the kind used for transparencies) to the drop of reagent.

Acknowledgment

The financial support of the Associazione Italiana Ricerca sul Cancro (AIRC), the Association for International Cancer Research (UK), and of the

Italian Ministry for Education and Scientific Research (Cofinanziamento 98) is gratefully acknowledged.

References

1. Davies, M. J. and Dean, R. T. (eds.) (1997) *Radical-Mediated Protein Oxidation—From Chemistry to Medicine*. Oxford University Press Inc., New York.
2. Frank, J., Biesalski, H. K., Dominici, S., and Pompella, A. (2000) Histochemical visualization of oxidant stress in tissues and isolated cells. *Histol. Histopathol.* **15**, 173–184.
3. Levine, R. L., Williams, J. A., Stadtman, E. R., and Schacter, E. (1994) Carbonyl assays for determination of oxidatively modified proteins. *Methods Enzymol.* **233**, 346–357.
4. Pompella, A., Cambiaggi, C., Dominici, S., Paolicchi, A., Tongiani, R., and Comporti, M. (1996) Single-cell investigation by laser scanning confocal microscopy of cytochemical alterations resulting from extracellular oxidant challenge. *Histochem. Cell Biol.* **105**, 173–178.
5. Cambiaggi, C., Dominici, S., Comporti, M., and Pompella, A. (1997) Modulation of human T lymphocyte proliferation by 4-hydroxynonenal, the bioactive product of neutrophil-dependent lipid peroxidation. *Life Sci.* **61**, 777–785.
6. Smith, M. A., Perry, G., Richey, P. L., Sayre, L. M., Anderson, V. E., Beal, M. F., and Kowall, N. (1996) Oxidative damage in Alzheimer's. *Nature* **382**, 120–121.
7. Frank, J., Kelleher, D. K., Pompella, A., Thews, O., Biesalski, H. K., and Vaupel, P. (1998) Enhancement of the antitumour effect of localized 44°C hyperthermia upon combination with xanthine oxidase and respiratory hyperoxia. *Cancer Res.* **58**, 2693–2698.
8. Cao, G. and Cutler, R. G. (1995) Protein oxidation and aging. I. Difficulties in measuring reactive protein carbonyls in tissues using 2,4-dinitrophenylhydrazine. *Arch. Biochem. Biophys.* **320**, 106–114.

Indirect Immunofluorescence Detection of Protein-Bound 4-Hydroxynonenal in Tissue Sections and Isolated Cells

Alfonso Pompella, Silvia Dominici, Jürgen Frank,
and Hans K. Biesalski

1. Introduction

4-Hydroxynonenal (4-hydroxy-2,3-*trans*-nonenal; 4-HNE) is the best known and thoroughly studied aldehydic product originating in biological samples during the process of lipid peroxidation (**Fig. 1**) (*1*). The latter is an autocatalytic, self-propagating sequence of free radical reactions, ultimately resulting in the fragmentation of the carbon atom chains of unsaturated fatty acids esterified in phospholipids of cellular membranes, which can be set into motion in conditions of severe oxidative stress within the cell (*2*). Many of the lipid fragments thus originated are aldehydes and other carbonyl products, provided with variable reactivity towards cellular macromolecules. 4-HNE was originally identified *in vitro* as a specific, dialyzable, cytotoxic product of peroxidation of microsomal phospholipids (*3*), but subsequent studies have consistently detected it in a number of experimental conditions, in which it has been shown to exert a variety of biological actions (*4*), as well as in important human diseases such as atherosclerosis, neurodegeneration, and cancer (*5–7*). Like other α,β -unsaturated aldehydes, 4-HNE is capable of binding covalently to side chains of cysteine, histidine, lysine, and other amino acids in proteins (*8*), thus originating new epitopes that can be detected by suitable antibodies (**Fig. 2**). Here a convenient procedure is described using polyclonal antibodies (PABs) and fluorescent revelation.

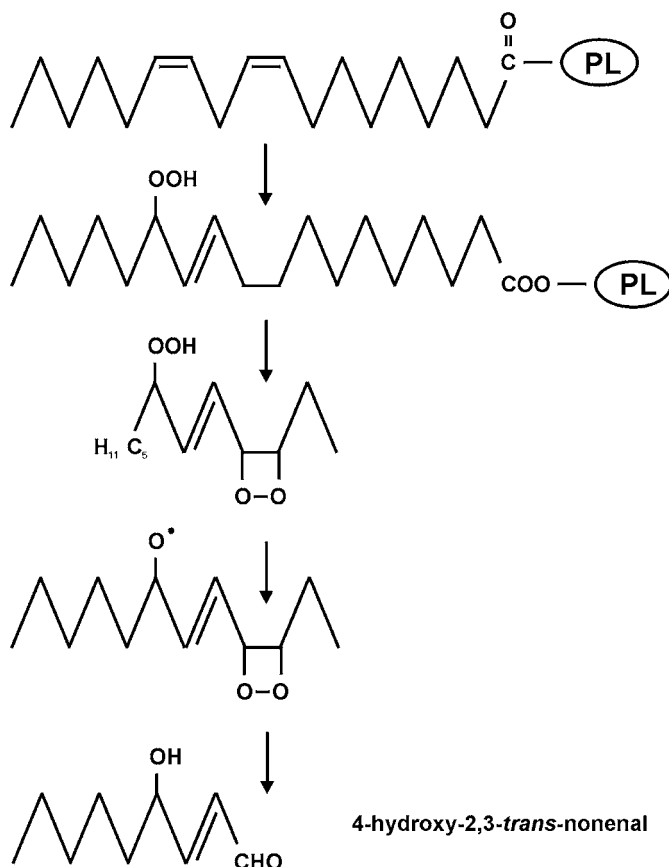


Fig. 1. Proposed mechanism for the formation of 4-hydroxy-2,3-trans-nonenal (4-HNE) from peroxidation of a phospholipid (PL) containing linoleic acid.

2. Materials

2.1. Equipment

1. Isopentane bath refrigerated with dry ice plus acetone, or liquid nitrogen bath.
2. Cryostat.
3. Polylysine-coated glass slides (Polysine™ microslides, Menzel-Gläser, Cat. # 041400).
4. Humid chambers for processing of slides (e.g., petri dishes with a piece of wet filter paper).
5. Coplin jars.
6. Fluorescence microscope with fluorescein filter set.

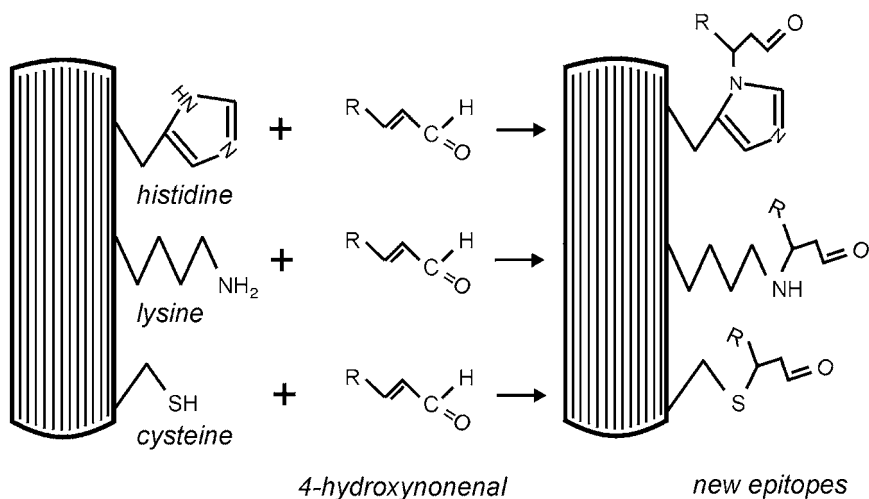


Fig. 2. The formation of new epitopes in protein following the binding of 4-HNE to representative amino acid residues.

2.2. Reagents

1. Phosphate-buffered saline (PBS), pH 7.4.
2. Serial dilutions of acetone: 100, 95, 70, 50, 30% in distilled water.
3. Fetal calf serum (FCS), 1% in PBS.
4. Anti-4-HNE-protein rabbit PAb (*see Note 1*).
5. Anti-rabbit immunoglobulin antibody, biotinylated (Dako, Cat. # E 0432 or E 0353).
6. Fluorescein-isothiocyanate (FITC)-extravidin (Sigma, Cat. # 104H-4804).
7. SlowFade Light™ Antifade kit (Molecular Probes, Cat. # S7461).

3. Methods

3.1. Preparation of Tissue or Cells

1. Small tissue blocks embedded in freezing medium (4583 O.C.T. Compound, Electron Microscopy Science, Cat. # 62550-01) are immediately frozen in an isopentane bath refrigerated with dry ice plus acetone, or in a liquid nitrogen bath.
2. Frozen blocks are allowed to equilibrate their temperature in the cryostat chamber (-15° to -20°C) for 30–45 min prior to cutting.
3. Cut sections 5–10 μm thick and allow to air-dry tissue for 1 h at room temperature.
4. Alternatively, cell smears are obtained from isolated cells in suspension and are allowed to air-dry as above.

5. Fix sections or cell smears by immersing slides in 100% cold acetone in a Coplin jar for 20 min at -20°C .
6. In the case of smears of isolated cells, fixation with methanol (15 min) can be preferred, if analysis has to be extended to cellular subcompartments (nucleus).

3.2. Processing of Samples for Immunohistochemistry

1. Rehydrate samples by sequentially immersing slides through serial dilutions of acetone (95, 70, 50, 30%) for 3 min each at room temperature.
2. Wash the samples 5 min in PBS at room temperature. Repeat once, for a total of two washes.
3. Remove excess liquid from slides by gently tapping them, and place slides on a flat surface in a humid chamber.
4. To prevent unspecific binding of primary antibody (rabbit anti-4-HNE-protein polyclonal antiserum), aspecific binding sites should be blocked. Cover sections or cell smears with 100 μL 1% FCS in PBS, or 10 μL normal rabbit serum and incubate for 30 min (*see Note 2*).
5. Wash the samples by immersing slides in PBS at room temperature for 5 min.
6. Remove excess liquid and cover the sections or cell smears with 50–100 μL of a 1:100 dilution in PBS of anti-4-HNE-protein antiserum and incubate for 60 min.
7. Wash the samples in three changes of PBS at room temperature.
8. Remove excess liquid and cover the sections with 50–100 μL of a 1:50 dilution of anti-rabbit immunoglobulin antibody, biotinylated. Incubate for 60 min at room temperature (*see Note 3*).
9. Wash the samples in three changes of PBS (5 min each) at room temperature.
10. Remove excess liquid. Add 50–100 μL of a 1:100 dilution of FITC-extravidin and incubate for 30 min at room temperature.
11. Wash the samples in deionized water for 5 min at room temperature. Repeat washing for a total of three washes.
12. Incubate the samples in SlowFade equilibration buffer for 10 min. Remove excess liquid and mount slides with glass coverslips using 1–2 drops of Anti-fade solution.
13. Analyze samples with a fluorescence microscope, using a green fluorescence filter set (520 ± 20 nm). Slides can be stored at 4°C in the dark up to several days.

3.3. Results

An example of detection of protein-bound 4-HNE in isolated cells with the procedure described earlier is reported in **Fig. 3**. The procedure proved sensitive enough to detect epitopes generated in cells after exposure to as low as 1 μM 4-HNE, i.e., concentrations likely to be found in vivo at tissue sites involved in lipid peroxidation processes (**1**). A recent study has documented by immunohistochemical means the translocation of 4-HNE bound to transcription factor proteins to the nuclear compartment of living cells (**10**).

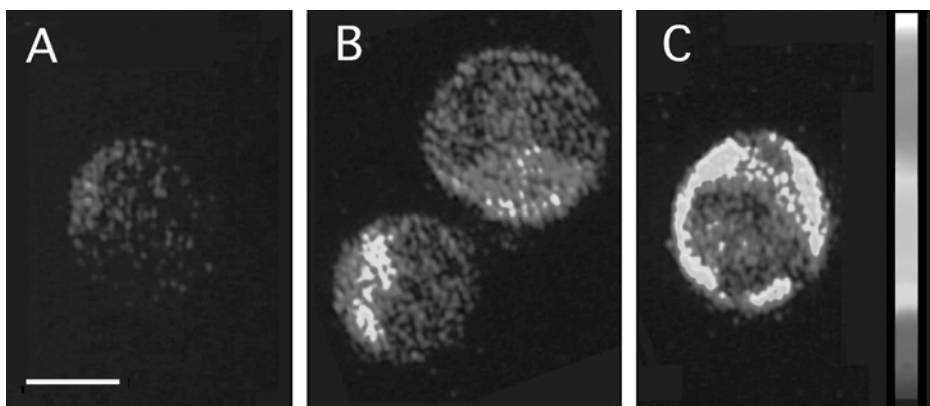


Fig. 3. Indirect immunofluorescence detection of protein-bound 4-HNE in acetone-fixed human peripheral blood lymphocytes. Cells had been pre-incubated with increasing concentrations of the free aldehyde. False-colour, confocal fluorescence microscopy imaging obtained as described (see **ref. 9**). (A) Control; (B) incubated with 1 μM 4-HNE (20 min); (C) incubated with 10 μM 4-HNE (20 min). Binding of 4-HNE to cell surface and cytoplasmic proteins is apparent. Bar in panel A corresponds to 5 μm .

4. Notes

1. Production of anti-4-HNE-protein polyclonal antiserum was described elsewhere (**9**). Anti-4-HNE rabbit polyclonal antiserum can be purchased by request from: FEP (Research Center for Nutrition in Prevention and Therapy) Hohenheim gGmbH, Postfach 720168, D-70577 Stuttgart, E-mail: FEPEsslingen@compuserve.com Phone: +49-711-459 4195. Fax: +49-711-4593822.
2. When required, adequate spreading of antisera over tissue sections or cell smears can be ensured by applying a piece of plastic sheet (of the kind of that used for transparencies) to the drop of reagent.
3. As an alternative, a fluorescent anti-rabbit immunoglobulin antibody can be directly used, instead of the biotinylated. The latter is usually preferred for its versatility of employment with other avidin-conjugated revelation systems (e.g., extravidin-peroxidase).

References

1. Esterbauer, H., Shaur, R. J., and Zollner, H. (1991) Chemistry and biochemistry of 4-hydroxynonenal, malonaldehyde and related aldehydes. *Free Rad. Biol. Med.* **11**, 81–128.
2. Halliwell, B. (1990) The measurement and mechanism of lipid peroxidation in biological samples. *Trends Biochem. Sci.* **15**, 129–135.
3. Benedetti, A., Comporti, M., and Esterbauer, H. (1980) Identification of 4-hydroxynonenal as a cytotoxic product originating from the peroxidation of liver microsomal lipids. *Biochim. Biophys. Acta* **620**, 281–296.

4. Dianzani, M. U. (1998) 4-Hydroxynonenal and cell signaling. *Free Rad. Res.* **28**, 553–560.
5. Palinski, W., Rosenfeld, M. E., Ylä-Herttuala, S., Gurtner, G. C., Socher, S. S., Butler, S. W., et al. (1989) Low density lipoprotein undergoes oxidative modification in vivo. *Proc. Natl. Acad. Sci. USA* **86**, 1372–1376.
6. Yoritaka, A., Hattori, N., Uchida, K., Tanaka, M., Stadtman, E. R., and Mizuno, Y. (1996) Immunohistochemical detection of 4-hydroxynonenal protein adducts in Parkinson disease. *Proc. Natl. Acad. Sci. USA* **93**, 2696–2701.
7. Okamoto, K., Toyokuni, S., Uchida, K., Ogawa, O., Takenawa, J., Kakehi, Y., et al. (1994) Formation of 8-hydroxy-2'-deoxyguanosine and 4-hydroxy-2-nonenal-modified proteins in human renal-cell carcinoma. *Int. J. Cancer* **58**, 825–829.
8. Uchida, K., Szweda, L. I., Chae, H.-Z., and Stadtman, E. R. (1993) Immunochemical detection of 4-hydroxynonenal protein adducts in oxidized hepatocytes. *Proc. Natl. Acad. Sci. USA* **90**, 8742–8746.
9. Pompella, A., Cambiaggi, C., Dominici, S., Paolicchi, A., Tongiani, R., and Comporti, M. (1996) Single-cell investigation by laser scanning confocal microscopy of cytochemical alterations resulting from extracellular oxidant challenge. *Histochem. Cell Biol.* **105**, 173–178.
10. Parola, M., Robino, G., Marra, F., Pinzani, M., Bellomo, G., Leonarduzzi, G., et al. (1998) HNE interacts directly with JNK isoforms in human hepatic stellate cells. *J. Clin. Invest.* **102**, 1942–1950.

Methods for Studying the Binding of Advanced Glycated Proteins to Receptors for Advanced Glycation Endproducts (AGE Receptors)

Paul J. Thornalley

1. Introduction: Cell Surface Receptors for Advanced Glycation Endproducts

Advanced glycation endproducts (AGEs) are stable end-stage adducts formed by the nonenzymatic reaction of saccharide derivatives with proteins, nucleotides, and phospholipids. They are formed in physiological systems by glycation reactions of glucose and physiological α -oxoaldehydes, particularly glyoxal, methylglyoxal, and 3-deoxyglucosone (3-DG) with amino and guanidino groups. The concentration of intracellular AGEs is kept at a low level by protein, nucleotide, and phospholipid turnover and repair but AGEs formed on extracellular proteins may accumulate with age. Clearance of extracellular AGEs is achieved by binding of AGE-modified proteins to specific cell surface receptors—AGE receptors. AGE-ligand binding to AGE receptors is associated with internalization of the AGE ligand-receptor complex and proteolytic processing of the AGE-modified proteins. AGE-modified proteins are also stimuli for cell activation. AGE ligand binding is associated with increased expression of extracellular matrix (ECM) proteins, vascular adhesion molecules, cytokines, and growth factors. Depending on the cell type and concurrent signaling, this is associated with chemotaxis, angiogenesis, oxidative stress, and cell proliferation or apoptosis. These processes are thought to contribute to disease mechanisms associated with the chronic clinical complications of diabetes mellitus—retinopathy, neuropathy and nephropathy, cataract, macrovascular disease, Alzheimer's disease (AD), and renal insufficiency. Several candidate AGE receptor proteins have been identified: the receptor for advanced glycation

*From: Methods in Molecular Biology, vol. 196: Oxidants and Antioxidants:
Ultrastructure and Molecular Biology Protocols
Edited by: D. Armstrong © Humana Press Inc., Totowa, NJ*

endproducts (RAGE), oligosaccharyl transferase 48 kDa subunit, 80H-K protein, galectin-3, and scavenger receptors (1,2).

The molecular characteristics and functions of these candidate AGE receptor proteins are now described. Thereafter, experimental methods used in characterization of ligand binding to AGE receptors are discussed.

1.1. Receptor for Advanced Glycation Endproducts (RAGE)

RAGE is a protein of sequence mass 42 kDa, which with oligosaccharide glycosylation had a mass of 45 kDa. It is a member of the immunoglobulin superfamily of proteins (3). Human RAGE has an extracellular V-shaped domain of 320 amino acids with two N-linked oligosaccharides, a membrane spanning domain of 21 amino acids, and a short cytoplasmic domain of 41 amino acids. RAGE protein is expressed in endothelial cells, vascular smooth muscle cells, cardiac myocytes, monocytes, microglia, and neurons. Two forms of RAGE of mass 35 kDa and 45 kDa were detected by immunoblotting in most tissues; in brain tissue, two forms of mass 23 kDa and 48 kDa were found. These different isoforms are thought to arise from distinctive post-translational processing (4). The proteolytic 35 kDa fragment of the extracellular domain was termed soluble-RAGE, which has been used as an affinity ligand for AGE-modified proteins (5) and a pharmacological agent to prevent the vascular effects of advanced glycation in experimental diabetes in vivo (6).

RAGE is thought to exist in a complex with lactoferrin-like protein (LF-L). The binding site for RAGE in lactoferrin is in the C-terminal half of the protein, amino acids 357-708. The dissociation constant K_D for LF-L binding to RAGE was 100 pM. The binding affinities of AGE-modified protein to RAGE, LFL-L, and RAGE-LF-L complex were remarkably similar (7). AGE-BSA is polyanionic and therefore expected to bind to lactoferrin (see below). AGE-BSA binding to RAGE had a K_D value of *ca.* 100 nM (3). RAGE also binds amphoterin (8) and β -amyloid protein (9) (*see Note 1*).

The gene of human RAGE was localized to chromosome 6p 21.3, in the HLA class III region (10,11). Four polymorphisms in the amino acid coding region have been found but their functional significance is unknown (12). RAGE transcription was regulated by interactions at two NF- κ B binding sites in the promoter sequence through which lipopolysaccharide induced an increase in RAGE expression in vascular endothelial and smooth muscle cells (13). Signal transduction associated with AGE-modified protein binding to RAGE involved activation of p21^{ras} and mitogen activated kinases (MAPK), ERK1, and ERK2 (14). RAGE-mediated neurite outgrowth stimulated by amphoterin involved the small GTPases Rac and Cdc42 rather than the Ras-MAPK pathway (15). AGE-modified proteins binding to RAGE-induced activation of NF- κ B. Antibodies to RAGE and LF-L, and deletion of the

cytosolic domain of RAGE inhibited activation of NF- κ B by AGE-modified protein. RAGE bound the highly modified AGE-proteins prepared in vitro and the minimally modified AGE-proteins found in vivo (5).

1.2. Oligosaccharyl Transferase-48 (AGE-Receptor 1; AGE-R1)

Oligosaccharyl transferase 48 kDa subunit (OST-48) or dolichyl-diphospho-oligosaccharide-protein glycosyltransferase (DDOST; EC 2.4.1.119) has been designated an AGE receptor (16). OST-48 is present in the endoplasmic reticulum as a complex with ribophorin I, ribophorin II, and defender against apoptosis protein-1. It is a type I membrane protein that is essential for oligosaccharyl transferase activity (17). It catalyses the transfer of high mannose oligosaccharide (GlcNac₂Man₉Glc₃) from dolichol-linked oligosaccharide donor to the asparagine acceptor site within an Asn-X-Ser/Thr motif consensus motif in nascent polypeptide chains in the endoplasmic reticulum. The DDOST gene is on chromosome 1p36.1. OST-48 is widely distributed in physiological systems as a component of the oligosaccharyl complex catalyses and controls essential protein glycosylation (18). AGE-HSA bound OST-48 with a K_D value of 40 nM (19) (see Note 2).

1.3. Phosphoprotein 80K-H (AGE-Receptor 2; AGE-R2)

The protein 80K-H is a cytosolic docking protein for fibroblast growth factor receptor-3 (FGFR3) linking cell stimulation by acidic or basic fibroblast growth factor (aFGF/bFGF) to the Ras/MAPK pathway. On cell activation, it is phosphorylated and binds to the cytosolic domain of FGFR3 in a complex with Grb2-Sos and a further protein pp66. FGFR3 may also use another but minor signaling pathway where Shc interacts with activated FGFR3 and the Grb2-Sos complex. Human 80K-H protein is an acidic protein (pI = 4.4) of mass 59 kDa. Although designated an AGE receptor, 80K-H did not bind AGE-protein in ligand blotting studies but rather was retained by an AGE-protein affinity column and antibodies to 80K-H partially prevented AGE-protein binding to membrane extracts (16) (see Note 2).

1.4. Galectin-3 or AGE-R3

Galectin-3 (is also known as Mac-2, carbohydrate-binding protein 35, IgE-binding protein, RL-29, HL-29, and L-34) is a 30-35 kDa β -galactoside-binding S-lectin. It has an important regulatory role in the immune response. It binds laminin and thereby facilitates the adhesion of monocytes and neutrophils to basement membrane and endothelium. The expression of galectin-3 increases during monocyte maturation to macrophages and was increased in macrophages and foam cells of atherosclerotic plaques. It stimulates the respiratory burst of monocytes and neutrophils by a priming response. It is not an intrinsic

membrane protein but is rather anchored to the membrane through interaction with membrane proteins: one such galectin-3 binding protein is Mac-2 binding protein, a member of the macrophage scavenger receptor cysteine-rich domain protein super family (2). AGE-BSA was bound by galectin-3 (and to a lesser extent, also by galectin-4, but not by galectin-1 and galectin-2). Galectin-3 was identified as an AGE binding protein by screening an expression library with antibodies to AGE-R2, now recognized as 80K-H phosphoprotein (20). The physiological function of galectin-3 as a physiological AGE receptor has not yet been established.

1.5. Scavenger Receptors

Macrophage scavenger receptors (MSRs) bind and internalize proteins highly modified by AGEs (21,22). They are expressed in macrophages of the lung, liver, kidney, spleen, sinus, skin, and perivascular region of the brain. Two types of MSR have been isolated and cloned: type I and type II, expressed by the alternate splicing of a single gene at the human 8P22 locus. Both types are homotrimeric glycoproteins consisting of 6 domains: (1) a 50 amino acid N-terminal cytoplasmic domain; (2) a 26 amino acid transmembrane domain; (3) a 32 amino acid spacer domain of 2-N linked sites; (4) a helical coiled coil domain of 163 amino acid consisting of 5-N-linked sites; (5) a 72 amino acid collagen-like triple-helix domain (not previously observed in an integral membrane protein); and (6) a C-terminal type-specific that participates in ligand binding—a cysteine-rich domain of 110 amino acid residues in type I, and 17 amino acid residues in type II (23). Proteins highly-modified by AGEs were bound by scavenger receptors I and II of macrophages (21,22). Scavenger receptors have very unusual binding properties, exhibiting a wide range of ligand specificity for a diverse array of polyanionic compounds (24). Scavenger receptors promote the endocytic uptake of oxidized low-density lipoprotein (LDL) and have a role in atherosclerosis and susceptibility to infection (22,25).

1.6. Nonreceptor AGE Binding Proteins

Bovine serum albumin (BSA) highly modified by glucose-derived AGE (AGE-BSA) was found to bind lysozyme and lactoferrin. Binding of AGE-BSA to lysozyme inhibited the enzymatic and bacteriocidal activity of lysozyme, and binding of AGE-BSA to lactoferrin inhibited the bacterial agglutination and bacteriocidal activity of lactoferrin. The binding of AGE-BSA to both proteins was inhibited by heparin and polyanions (26). A lysozyme-linked affinity matrix bound and removed AGE-modified proteins from sera of diabetic patients with end-stage renal disease, indicating that lysozyme attached to an affinity matrix can bind physiologically AGE-modified proteins (27).

2. Materials

2.1. Advanced Glycated Proteins

1. Advanced glycated proteins have typically been prepared by incubating proteins with glucose or glucose-6-phosphate (28,29). Recently, as the importance of α -oxoaldehydes in the formation of AGE-modified proteins in vivo proteins has emerged, AGE-modified proteins have also been prepared from methylglyoxal and 3-deoxyglucosone (22,30,31). The protein substrates most often used are BSA and human serum albumin (HSA) but others have also been used. In some instances, glucose concentrations typical of those found in hyperglycaemia associated with diabetes mellitus (20–50 mM) have been employed (32,33). Very high concentrations of glucose or glucose-6-phosphate (250 mM–1.7 M) (28,29,34,35) have also been used. For α -oxoaldehydes, 0.1–100 mM modifying agent has been used (22,30,31).
2. Incubation periods are usually short (3–24 h) for α -oxoaldehydes, because of their high reactivity with proteins, whereas incubations with glucose or glucose-6-phosphate are usually 3–8 wk or longer. These methods produce either minimally modified proteins (proteins with 1–2 modified amino acids per protein molecule) (31), or highly-modified proteins (proteins with much higher extents of modification) (see **Note 3**). Proteins highly modified with AGEs have markedly increased net negative charge and molecular mass (36). In some instances, the peptide backbone of the protein was cleaved and the resulting fragments formed dimers with disulphide linkage (37).
3. Ligand binding to receptors or non-receptor proteins is measured using a [125 I]-radiolabeled protein. A mild iodinating reagent that avoids direct contact of the protein and the oxidizing agent, such as IODO-BEADSTM (38), is preferable since the glycated protein substrate is particularly susceptible to autoxidation.

2.2. Isolation and Culture of Cells Expressing AGE Receptors

1. Receptors that bind AGE-modified proteins have been found on a variety of cell types including monocytes, macrophages, Kupffer cells, T-lymphocytes, endothelial cells, kidney mesangial cells, and retinal pericytes.
2. Monocytes may be isolated from venous blood by density gradient centrifugation (39). They may be cultured for 9 d to differentiate to macrophages. Differentiation leads to expression of the scavenger receptor and increased expression of galectin-3: scavenger receptor expression was detectable after day 3 (23), whereas galectin-3 expression was present initially, increased in day 1 of culture and thereafter (40).
2. AGE receptor binding of AGE-HSA also increased during differentiation of human monocytic THP-1 cells (41).
3. Rat liver Kupffer cells and sinusoidal endothelial cells may be isolated by the exemplary method of Berry and Friend (42), or by recent modifications of this, which can be applied to small amounts of human tissue (43,44).
4. T-lymphocytes may be isolated from peripheral mononuclear lymphocytes of venous blood (45).

5. Endothelial cells have been isolated and cultured from retinal (46), aorta (47), and umbilical cord (48).
6. Pericytes have been isolated and cultured from retinal capillaries (46) and renal glomeruli (49).

3. Methods

3.1. Binding of AGE-Modified Protein by AGE Receptors

1. AGE-modified protein binding to AGE receptors is investigated by incubation of cells expressing AGE receptors with AGE-protein ligand. The amount of AGE-protein bound specifically as a function of incubation time and total AGE protein concentration is determined. Experiments are performed at 4°C (the low temperature prevents receptor internalization). Cell suspensions or monolayers of adherent cells on the walls of multiwell plates (1–2 million) are used in culture medium containing 3% (w/v) albumin to suppress nonspecific binding; total volume is typically 100–250 μL .
2. After incubation, suspended cells are sedimented by centrifugation. The cell pellet is washed three times with ice-cold culture medium with 3% albumin, twice with ice-cold phosphate-buffered saline (PBS), and then counted. The cell pellet can be dissolved in 0.1 M sodium hydroxide solution overnight and then total cell protein determined by the Bradford method. After the incubation time required to maximise ligand binding is found, a dose-response relationship is investigated, usually in the AGE-protein concentration range of 1–1000 nM, depending on the affinity of the ligand. This is repeated with a 20–50 fold excess of nonradiolabeled AGE-modified protein (20–50 μM) to correct for nonspecific binding.
3. Data of the dependence of AGE-protein receptor binding on the AGE-protein concentration [AGE-protein] are fitted by nonlinear regression to the binding equation:

$$[\text{AGE-protein}]_{\text{Bound}} = R_{\text{T}} \times \frac{[\text{AGE-protein}]_{\text{Free}}}{[\text{AGE-protein}]_{\text{Free}} + K_{\text{D}}}$$

where $[\text{AGE-protein}]_{\text{Free}}$ and $[\text{AGE-protein}]_{\text{Bound}}$ are the concentrations of free and bound AGE-modified protein, R_{T} is the receptor concentration, and K_{D} the dissociation constant of the AGE-protein/receptor complex. Data are fitted by nonlinear regression to determine the values of R_{T} and K_{D} . Linear transformations (such as the Scatchard plot) may be produced for presentation, if required (*see Note 4*).

4. AGE receptor binding experiments using proteins highly modified by AGEs may show significant binding of the AGE-protein to the walls of plastic tubes, wells, and pipet tips. To avoid this, the internal surface of tubes, wells and pipet tips are coated with a thin layer of SIGMACOAT™ (chlorinated organopolysiloxane in heptane), drained, and dried overnight (50) (*see Note 4*).

3.2. Probing Receptor Binding Specificity: AGEs Implicated in AGE Receptor Recognition

1. Very little is known of the binding specificity of AGE receptors for different AGEs. Proteins highly modified by AGEs have anionic character (36). Polyanionic compounds such as heparin and polyglutamate compete for binding at some AGE receptors (31,51,52). This indicated that ligand anionic character of the AGE-protein ligand may be critical for receptor recognition. Yet proteins minimally modified by AGEs prepared *in vitro* or present *in vivo* bind AGE receptors. There may be other explanations for polyanions competing for AGE receptor binding. For example, lactoferrin is part of the RAGE complex and this binds heparin and other polyanions. In so-doing, it may block the AGE-protein binding properties of RAGE.
2. Two approaches to identify AGE receptor recognition are available: (1) synthetic AGE ligands of known molecular structure can be used in competitive binding experiments to displace AGE-protein from the AGE receptor, and (2) immobilized AGE receptors may be used in affinity chromatography to isolate AGE-modified proteins from physiological glycated proteins and the AGE content characterized. For experiment (1) to be valid, the competing ligand should have an extent of modification similar to that found of proteins *in vivo*; and for experiment (2), the AGE recognition factor and other AGEs are both expected to be present. To date, there is evidence to suggest that hydroimidazolones (31) and N_ε-carboxymethyl-lysine (CML) are AGE recognition factors (53). As yet, only competitive ligand displacement experiments have been performed. The evidence in support of hydroimidazolone recognition was based on a synthetic hydroimidazolone derived from N-acetylarginine and no protein-linked hydroimidazolone studies have yet been reported, although MG_{min}-HSA approximates to this (31). The evidence in support of CML used a protein derivative of CML, ovalbumin-CML. This had, however, CML modification 10–20-fold higher than those found in glycated proteins *in vivo* (53).
3. It is possible that recognition factors are different for each AGE receptor. Ligand recognition by the scavenger receptor, for example, is dependent on modification of critical lysine residues in LDL. Modification of critical lysine groups in AGE-modified LDL and other proteins may be key to AGE-protein recognition by scavenger receptors. It has been claimed also that proteins modified by fructosamines may be recognized by cell surface receptors (54,55). The ligand affinity of the receptors was such however, that the receptors would be expected to always be saturated *in vivo*. It has recently emerged that AGEs may be formed in parallel to fructosamine in glucose glycation reactions (56). Proteins modified by fructosamine, therefore, also contain AGEs and this may contribute to the receptor binding activities of early glycated proteins.

3.3. Results

1. Specimen Binding Data—THP-1 Monocytic Cells. Experimental data of the binding of HSA highly modified by glucose-derived AGEs (AGE-HSA) and

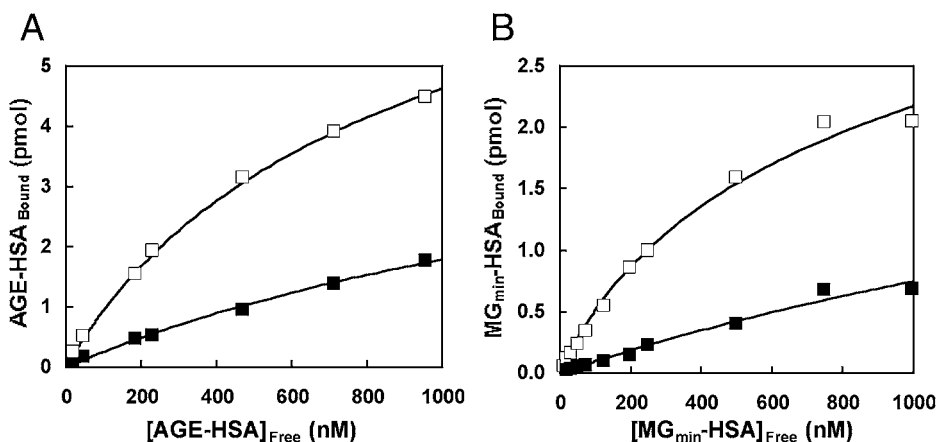


Fig. 1. Binding of AGE-HSA (A) and MG_{min}-HSA (B) to human monocytic THP-1 cells in vitro. THP-1 cells (2×10^6 , 100 μ L) were incubated with 5–1000 nM AGE-HSA (A) or MG_{min}-HSA (B) in the absence (□) and presence (■) of 30 μ M cold modified protein in RPMI 1640 with 3% (w/v) HSA for 2 h at 4°C. The amount of AGE-protein ligand bound to cell surface AGE receptors was then determined (31).

HSA minimally modified by methylglyoxal (MG_{min}-HSA) are given in **Fig. 1**. AGE-HSA had 21 modified lysine residues, 16 modified arginine residues and a molecular mass by MALDI mass spectrometry of $73,226 \pm 122$ Da ($n = 5$). MG_{min}-HSA had predominantly arginine modification with a molecular mass by MALDI mass spectrometry of $66,519 \pm 121$ Da ($n = 5$) (36).

- Summary of AGE-modified protein/AGE receptor binding data. Binding data from studies of the binding of AGE-proteins to cells are summarized in **Table 1**. Estimates of K_D vary from 2–850 nM and R_T from 0.1 – 8.5×10^6 receptors per cell. It is not known if AGE receptor docking proteins affect AGE-protein affinity for AGE receptors but they may do and thereby influence K_D values *in situ*. The concentration of AGEs in plasma proteins is in the range 0.01–0.1% of lysine or arginine residues (1). AGE receptor binding affinities, therefore, are appropriate for significant binding of AGE-modified proteins in vivo. This is expected to contribute to protein turnover. The metabolic flux of AGE internalization by AGE receptors in physiological systems has not yet been reported.

4. Notes

The AGE/AGE receptor hypothesis has its critics and investigators planning to enter this field should be aware of them. Only by understanding the weaknesses of this hypothesis will we eventually be able to recognize its true worth.

Table 1
Summary of the Characteristics of the Binding of AGE-Modified Proteins to Cell Surface AGE Receptors

Cell	Source	Ligand	Apparent K_D (nM)	Receptor number, R_T (receptors/cell)	Reference
Monocytes	Human (normal control)	AGE-HSA	700	139,000	(61)
	Human (IDDM)	AGE-HSA	546	183,000	(61)
Macrophage	Murine peritoneum	AGE-HSA	57	106,000	(32)
	"	3-DG-BSA	8.5, 950 ^a	—	(22)
Kupffer cells	Rat peritoneum	AGE-HSA	240	—	(28)
	Rat liver	AGE-HSA	210	—	(28)
Monocytic cells	Human leukaemia THP-1	AGE-HSA	377	590,000	(31)
Endothelial cells	Bovine aorta	MG _{min} -HSA	449	120,000	(31)
		AGE-HSA	99	260,000	(33)
Mesangial cell	Human kidney/rat kidney	AGE-HSA	500	300,000	(62)
T-Lymphocytes	Human/rat (resting)	AGE-HSA	13	1,220,000	(45)
	(activated)	AGE-HSA	1.7	8,460,000	(45)

^aTwo binding affinities were quantified: high- and low-affinity sites.

1. There has been dispute on the presence or absence of specific AGE receptors, particularly relating to the role of RAGE in Alzheimer's disease (9,57).
2. The physiological locus and functions of OST-48 and 80K-H are not consistent with that of cell surface AGE receptors. It is uncertain if a physiological role for OST-48 and 80K-H as AGE receptors can be sustained since they have intracellular localization and have other cell functions (58).
3. Many experiments have used AGE-protein ligands that are much more highly modified by AGEs than found in vivo and, generally, the AGE epitopes in the AGE-protein ligand have not been characterized (2).
4. In some instances, it has not been possible to observe specific binding for AGE-proteins (59).

Contrary to this are the observations that RAGE has been used to affinity purify AGE-modified proteins from blood plasma of diabetic subjects and the cytosolic domain has been shown to be important for AGE-protein mediated cell activation (5,15). Moreover, the clearance of AGE-BSA from circulation by liver sinusoidal endothelial cells and Kupffer cells in vivo has been demonstrated, albeit highly-modified AGE-BSA (60). The physiological importance and regulation of AGE-protein/AGE receptor interactions is not yet fully understood. This presents current problems and future opportunities.

References

1. Thornalley, P. J. (1999) Clinical significance of glycation. *Clin. Lab.* **5-6**, 263-273.
2. Thornalley, P. J. (1998) Cell activation by glycated proteins. AGE receptors, receptor recognition factors and functional classification of AGEs. *Cell. Mol. Biol.* **44**, 1013-1023.
3. Neeper, M., Schmidt, A.-M., Brett, J., Yan, S. D., Wang, F., Pan, Y.-C. E., et al. (1992) Cloning and expression of a cell surface receptor for advanced glycosylation endproducts of proteins. *J. Biol. Chem.* **267**, 14998-15004.
4. Brett, J., Schmidt, A.-M., Yan, S. D., Zou, S., Weidman, E., Pinsky, D., et al. (1993) Survey of the distribution of a newly characterized receptor for advanced glycation end-products in tissues. *Am. J. Pathol.* **143**, 1699-1712.
5. Yan, S. D., Schmidt, A.-M., Anderson, G. M., Zhang, J., Brett, J., Zou, Y. S., et al. (1994) Enhanced cellular oxidant stress by the interaction of the advanced glycation end products with their receptors/binding proteins. *J. Biol. Chem.* **269**, 9889-9897.
6. Renard, C., Chappey, O., Wautier, M. P., Nagashima, M., Lundh, E. R., Morser, J., et al. (1997) Recombinant advanced glycation endproduct receptor pharmacokinetics in normal and diabetic rats. *Mol. Pharmacol.* **52**, 54-62.
7. Schmidt, A.-M., Mora, R., Cao, R., Yan, S.-D., Brett, J., Ramakrishnan, R., et al. (1994) The endothelial cell binding site for advanced glycation endproducts consists of a complex: An integral membrane protein and a lactoferrin-like polypeptide. *J. Biol. Chem.* **269**, 9882-9888.

8. Merenmies, J., Pihlaskari, R., Laitinen, J., Wartiovaara, J., and Rauvala, H. (1991) 3-kDa Heparin-binding protein of brain (Amphoterin) involved in neurite outgrowth. *J. Biol. Chem.* **266**, 16722–16729.
9. Yan, S. D., Chen, X., Fu, J., Chen, M., Zhu, H., Roher, A., et al. (1996) RAGE and amyloid-beta peptide neurotoxicity in Alzheimer's disease. *Nature* **382**, 685–691.
10. Vissing, H., Aagaard, L., Tommerup, N., and Boel, E. (1994) Localization of the human gene for advanced glycosylation end product-specific receptor (AGER) to chromosome 6p 21.3. *Genomics* **24**, 606–608.
11. Ursini, F., Maiorino, M., Brigeliusflohe, R., Aumann, K. D., Roveri, A., Schomburg, D., and Flohe, L. (1995) Diversity of glutathione peroxidases. *Methods Enzymol.* **252**, 38–53.
12. Hudson, B. I., Stickland, M. H., and Grant, P. J. (1998) Identification of polymorphisms in the receptor for advanced glycation end products (RAGE) gene. Prevalence in type 2 diabetes and ethnic groups. *Diabetes* **47**, 1155–1157.
13. Li, J. and Schmidt, A.-M. (1997) Characterization and functional analysis of the promoter of RAGE, the receptor for advanced glycation end products. *J. Biol. Chem.* **272**, 16498–16506.
14. Lander, H. M., Tauras, J. M., Ogiste, J. S., Hori, O., Moss, R. A., and Schmidt, A.-M. (1997) Activation of the receptor for advanced glycation endproducts triggers p21^{ras}-dependent mitogen-activated protein kinase pathway regulated oxidative stress. *J. Biol. Chem.* **272**, 17810–17814.
15. Huttunen, H. J., Fages, C., and Rauvala, H. (1999) Receptor for advanced glycation end products (RAGE)-mediated neurite outgrowth and activation of NF- κ B require the cytoplasmic domain of the receptor but different downstream signaling pathways. *J. Biol. Chem.* **274**, 19919–19924.
16. Li, Y. M., Mitsuhashi, T., Wojciechowicz, D., Shimizu, N., Li, J., Stitt, A., et al. (1996) Molecular identity and cellular distribution of advanced glycation end-product receptors: relationship of p60 to OST-48 and p90 to 80K-H membrane proteins. *Proc. Natl. Acad. Sci. USA* **93**, 11047–11052.
17. Kumar, V., Korza, G., Heinemann, F. S., and Ozols, J. (1995) Human oligosaccharyl transferase: isolation, characterization, and the complete amino acid sequence of 50 kDa subunit. *Arch. Biochem. Biophys.* **320**, 217–223.
18. Yamagata, T., Tsuru, T., Momoi, M. Y., Suwa, K., Nozaki, Y., Mukasa, T., et al. (1997) Genome organization of human 48-kDa oligosaccharyltransferase (DDOST). *Genomics* **45**, 535–540.
19. Yang, Z., Makita, Z., Horii, Y., Brunelle, S., Cerami, A., Sehajpal, P., et al. (1991) Two novel rat liver membrane proteins that bind advanced glycosylation endproducts: relationship to macrophage receptor for glucose-modified proteins. *J. Exp. Med.* **174**, 515–524.
20. Vlassara, H., Li, Y. M., Imani, F., Wojciechowicz, D., Yang, Z., Liu, F.-T., and Cerami, A. (1995) Identification of galectin-3 as a high-affinity binding protein for advanced glycation end products (AGE): a new member of the AGE-receptor family. *Mol. Med.* **1**, 634–646.

21. Araki, N., Higashi, T., Mori, T., Shibayama, R., Kawabe, Y., Kodama, T., et al. (1995) Macrophage scavenger receptor mediates the endocytic uptake and degradation of advanced glycation end-products of the Maillard reaction. *Eur. J. Biochem.* **230**, 408–415.
22. Shinoda, T., Hayase, F., Van Chuyen, N., and Kato, H. (1993) Uptake of proteins modified with 3-deoxyglucosone, a Maillard reaction intermediate, by the type I macrophage scavenger receptor. *Biosci. Biotech. Biochem.* **57**, 1826–1831.
23. Takeya, M., Tomokiyo, R., Jinnouchi, K., Sakaguchi, H., Hagiwara, S., Honda, M., et al. (1999) Macrophage scavenger receptors: structure, function and tissue distribution. *Acta Histochem. Cytochem.* **32**, 47–51.
24. Krieger, M., Acton, S., Ashkenas, J., Pearson, A., Penman, M., and Resnick, D. (1993) Molecular flypaper, host defense, and atherosclerosis: structure, binding-properties, and functions of macrophage scavenger receptors. *J. Biol. Chem.* **268**, 4569–4572.
25. Suzuki, H., Kurihara, Y., Takeya, M., Kadama, N., Kataoka, M., Jishage, K., et al. (1997) A role for macrophage scavenger receptors in atherosclerosis and susceptibility of risk to infection. *Nature* **386**, 292–296.
26. Li, M. Y., Tan, A. X., and Vlassara, H. (1995) Antibacterial activity of lysozyme and lactoferrin is inhibited by binding of advanced glycation-modified proteins to a conserved motif. *Nature Med.* **1**, 1057–1061.
27. Mitsuhashi, T., Li, Y. M., Fishbane, S., and Vlassara, H. (1997) Depletion of reactive advanced glycation endproducts from diabetic uremic sera using a lysozyme-linked matrix. *J. Clin. Invest.* **100**, 847–854.
28. Takata, K., Horiuchi, S., Araki, N., Shiga, M., Saitoh, M., and Morino, Y. (1988) Endocytic uptake of non-enzymatically glycosylated proteins is mediated by a scavenger receptor for aldehyde modified proteins. *J. Biol. Chem.* **268**, 14189–14825.
29. Yang, Z., Makita, Z., Horii, Y., Brunelle, S., Cerami, A., Sepajpal, P., Suthanthiran, M., and Vlassara, H. (1991) Two novel rat liver membrane proteins that bind advanced glycosylation endproducts: relationship to macrophage receptor for glucose-modified proteins. *J. Exp. Med.* **174**, 515–524.
30. Westwood, M. E., McLellan, A. C., and Thornalley, P. J. (1994) Receptor-mediated endocytic uptake of methylglyoxal-modified proteins. *J. Biol. Chem.* **269**, 32293–32298.
31. Westwood, M. E., Argirov, O. K., Abordo, E. A., and Thornalley, P. J. (1997) Methylglyoxal-modified arginine residues: a signal for receptor-mediated endocytosis and degradation of proteins by monocytic THP-1 cells. *Biochim. Biophys. Acta* **1356**, 84–94.
32. Vlassara, H., Brownlee, M., and Cerami, A. (1985) High-affinity-receptor-mediated uptake and degradation of glucose-modified proteins: A potential mechanism for the removal of senescent macromolecules. *Proc. Natl. Acad. Sci. USA* **82**, 5588–5592.
33. Esposito, C., Gerlach, H., Brett, J., Stern, D., and Vlassara, H. (1989) Endothelial receptor-mediated binding of glucose-modified albumin is associated with increased

- monolayer permeability and modulation of cell surface coagulant properties. *J. Exp. Med.* **170**, 1387–1407.
34. Makita, Z., Vlassara, H., Cerami, A., and Bucala, R. (1992) Immunochemical detection of advanced glycosylation end products *in vivo*. *J. Biol. Chem.* **267**, 5133–5138.
35. Schmidt, A.-M., Vianna, M., Gerlach, M., Brett, J., Ryan, J., Kao, J., et al. (1992) Isolation and characterization of two binding proteins for advanced glycosylation endproducts from bovine lung which are present on the endothelial cell surface. *J. Biol. Chem.* **267**, 14987–14997.
36. Westwood, M. E. and Thornalley, P. J. (1995) Molecular characteristics of methylglyoxal-modified bovine and human serum albumins. Comparison with glucose-derived advanced glycation endproduct-modified serum albumins. *J. Prot. Chem.* **14**, 359–372.
37. Finotti, P. and Pagetta, A. (1997) Heparin-induced structural modifications and oxidative cleavage of human serum albumin in the absence and presence of glucose—implications for transcapillary leakage of albumin in hyperglycaemia. *Eur. J. Biochem.* **247**, 1000–1008.
38. Markwell, M. A. K. (1982) A new solid state reagent to iodinate proteins: conditions for the efficient labelling of antiserum. *Anal. Biochem.* **125**, 427–432.
39. Boyum, A. (1984) Separation of lymphocytes, granulocytes, and monocytes from human blood using iodinated density gradient media. *Methods Enzymol.* **108**, 88–109.
40. Liu, F.-T., Hsu, D. K., Zuberi, R. I., Kuwabara, I., Chi, E. Y., and Henderson, W. R. Jr. (1995) Expression and function of galectin-3, a beta-galactoside-binding lectin, in human monocytes and macrophages. *Am. J. Pathol.* **147**, 1016–1028.
41. Takata, K., Horiuchi, S., Araki, N., Shiga, M., Saitoh, M., and Morino, Y. (1989) Scavenger receptor of human monocytic leukemia cell line (THP-1) and murine macrophages for nonenzymatically glycosylated proteins. *Biochim. Biophys. Acta* **986**, 18–26.
42. Berry, M. N. and Friend, D. S. (1969) High-yield preparation of isolated rat liver parenchymal cells. *J. Cell Biol.* **43**, 506–520.
43. Heuff, G., Meyer, S., and Beelen, R. H. J. (1994) Isolation of rat and human kupffer cells by a modified enzymatic method. *J. Immunol. Methods* **174**, 61–65.
44. Braet, F., Dezanger, R., Sasoaki, T., Baekeland, M., Jannsens, P., Smedsrod, B., and Wisse, E. (1994) Methods in laboratory investigation: assessment of a method of isolation, purification, and cultivation of rat liver sinusoidal cells. *Lab. Invest.* **70**, 944–952.
45. Imani, F., Horii, Y., Suthanthiran, M., Skolnik, E. Y., Makita, Z., Sharma, V., et al. (1993) Advanced glycosylation end product-specific receptors on human and rat T-lymphocytes mediate synthesis of interferon γ : role in tissue remodeling. *J. Exp. Med.* **178**, 2165–2172.
46. Chibber, R., Molinatti, P. A., Rosatto, N., Lambourne, B., and Kohner, E. M. (1997) Toxic action of advanced glycation end products on cultured retinal capillary pericytes and endothelial cells: relevance to diabetic retinopathy. *Diabetologia* **40**, 156–164.

47. Schwartz, S. (1978) Selection and characterization of bovine aortic endothelial cells. *In Vitro* **14**, 966–972.
48. Jaffe, E. A., Nachman, R. L., Becker, C. G., and Minick, C. R. (1973) Culture of human endothelial cells derived from umbilical veins. *J. Clin. Invest.* **52**, 2745–2756.
49. Striker, G. E. and Striker, L. J. (1985) Glomerular cell culture. *Lab. Invest.* **53**, 131.
50. Shaw, S. M. and Crabbe, M. J. C. (1994) Minimizing spurious receptor binding kinetics with modified proteins. *Anal. Biochem.* **219**, 161–163.
51. Vlassara, H., Brownlee, M., and Cerami, A. (1986) Novel macrophage receptor for glucose-modified proteins is distinct from previously described scavenger receptors. *J. Exp. Med.* **164**, 1301–1309.
52. Maccioni, R. B., Vera, J. C., and Slebe, J. C. (1981) Arginyl residues involvement in the microtubule assembly. *Arch. Biochem. Biophys.* **207**, 248–255.
53. Kislinger, T., Fu, C., Huber, B., Qu, W., Taguchi, A., Yan, S. D., et al. (1999) N^ε-(Carboxymethyl)lysine adducts of proteins are ligands for receptor for advanced glycation end products that activate cell signaling pathways and modulate gene expression. *J. Biol. Chem.* **274**, 31740–31749.
54. Salazar, R., Brandt, R., and Krantz, S. (1995) Expression of fructosyllysine receptors on human monocytes and monocyte-like cell lines. *Biochim. Biophys. Acta* **1266**, 57–63.
55. Wu, V.-Y. and Cohen, M. P. (1993) Identification of aortic endothelial cell binding proteins for Amadori adducts in glycated albumin. *Biochem. Biophys. Res. Com.* **193**, 1131–1136.
56. Thornalley, P. J., Langborg, A., and Minhas, H. S. (1999) Formation of glyoxal, methylglyoxal and 3-deoxyglucosone in the glycation of proteins by glucose. *Biochem. J.* **344**, 109–116.
57. Liu, Y., Dargusch, R., and Schubert, D. (1997) Beta amyloid toxicity does not require RAGE protein. *Biochem. Biophys. Res. Com.* **237**, 37–40.
58. Stitt, A. W., Li, Y. M., Gardiner, T. A., Bucala, R., Archer, D. B., and Vlassara, H. (1999) Advanced glycation end products (AGEs) colocalize with AGE receptors in the retinal vasculature of diabetic and AGE-infused rats. *Am. J. Pathol.* **150**, 523–531.
59. Shaw, S. M. and Crabbe, M. J. C. (1994) Non-specific binding of advanced glycosylation endproducts to macrophages outweighs specific receptor-mediated interactions. *Biochem. J.* **304**, 121–129.
60. Smedsrod, B., Melkko, J., Araki, N., Sano, H., and Horiuchi, S. (1997) Advanced glycation end products are eliminated by scavenger-receptor-mediated endocytosis in hepatic sinusoidal Kupffer and endothelial cells. *Biochem. J.* **322**, 567–573.
61. Festa, A., Schmolzer, B., Scherthaner, G., and Menzel, E. J. (1998) Differential expression of receptors for advanced glycation end products on monocytes in patients with IDDM. *Diabetologia* **41**, 674–680.
62. Skolnik, E. Y., Yang, Z., Makita, Z., Radoff, S., Kirstein, M., and Vlassara, H. (1991) Human and rat mesangial cell receptors for glucose-modified proteins: potential role in kidney tissue remodelling and diabetic nephropathy. *J. Exp. Med.* **174**, 931–939.

Measurement of Blue Fluorescence as a Protein Marker for Oxidized Membranes

Kiyomi Kikugawa

1. Introduction

Fluorescence generated in living cells has been referred to as an age-related lipofuscin-like substances and also an index of aging (1,2). Cells and tissues contain three kinds of fluorescence: yellow, green, and blue. Among them, yellow fluorescence that fluoresced at around 620 nm is regarded as an age-related lipofuscin observed histochemically under microscope. Although yellow fluorescent pigment was regarded in the past as the products between proteins and lipid peroxidation products, it is not likely that the pigment is derived from lipid peroxidation (3). Green fluorescence that fluoresced at around 520 nm is due to flavin-containing components. Blue fluorescence that fluoresced at around 450 nm is believed to be derived from the reaction of proteins with lipid peroxidation products in living cells *in situ* (4).

In earlier studies, lipid-soluble blue fluorescence has been extracted with chloroform-methanol (5), and many reports using this organic solvent extraction method have appeared. However, it is shown that the organic solvent extraction produces an artificial blue fluorescence and the amount of blue fluorescence generated in tissues may be overestimated in the method (6). Several studies have claimed that water-soluble blue fluorescence is a better protein marker for lipid peroxidation than lipid-soluble blue fluorescence (7–9). It is important to remove or separate disturbing green fluorescence for accurate determination of blue fluorescence generated by lipid peroxidation.

Structures of the fluorophores generated in the reaction of proteins and lipid peroxidation products are not known. Malonaldehyde, one of the lipid peroxidation products, has received attention in the production of blue fluorescence (1),

but the aldehyde generates blue fluorescence whose fluorescence maximum is rather longer than that of blue fluorescence generated in oxidized biological samples (4,10).

A methodology is described here for accurate determination of blue fluorescence generated in lipid peroxidation of microsomes (10). This method can measure water-soluble blue fluorescence after removal of disturbing green fluorescent, flavin-containing components.

2. Materials

2.1. Equipment

1. Centrifuge.
2. Fraction collector.
3. Hitachi 650-60 fluorescence spectrophotometer with a xenon-lamp with excitation and fluorescence slit width set at 10 nm.

2.2. Reagents

1. Sephadex G-10 (Pharmacia Company, Upsala, Sweden).
2. Adenosine-5'-diphosphate monopotassium salt (ADP • K) (Oriental Yeast Company, Tokyo, Japan).

3. Methods

3.1. Standardization

The instrument is standardized with a solution of 0.1 μ M quinine sulfate in 0.1 M sulfuric acid to give a fluorescence intensity of 1.00 at 450 nm when excited at 350 nm. Relative fluorescence intensity of the sample solution against that of the quinine sulfate solution is then determined.

3.2. Preparation of Rat Liver Microsomes

1. Wistar male rats are fed a normal solid diet CE-2 type for 10–20 wk. and sacrificed by bleeding from common carotid arteries after anesthesia with chloroform.
2. Quickly isolate liver and wash well with cold physiological saline.
3. Microsomes are obtained from 12.0 g wet weight of liver according to the method of Albro et al. (11). A microsomal suspension in 30 mL of 25 mM 3-(N-morpholino)-propanesulfonic acid buffer, pH 7.4, containing 0.25 M mannitol is obtained.

3.2. Oxidation of Microsomes

1. Mix the 30 mL microsomal suspension with 30 mL of 0.05 M Tris-0.15 M KCl buffer, pH 7.5, containing 2.0 mM ADP • K, 2.0 mM sodium ascorbate, 24 μ M FeCl_2 , and incubate the mixture at 37°C for 6 h.

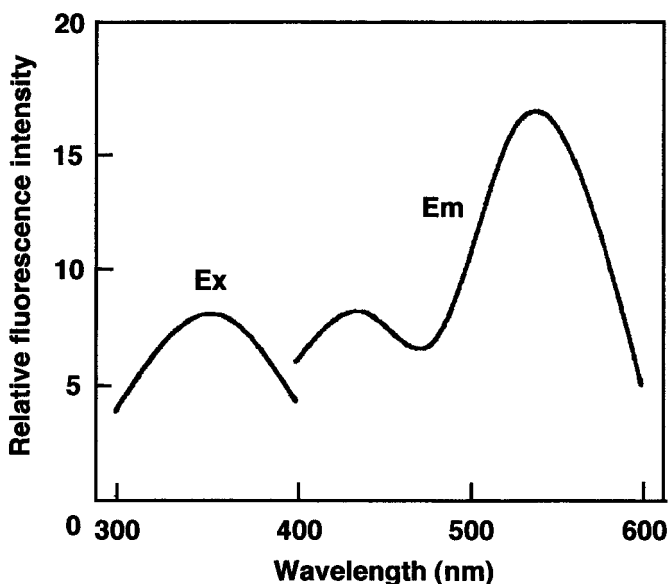


Fig. 1. Fluorescence spectrum of the supernatant of the microsomal suspension oxidized at 37°C for 6 h with ADP • K-ascorbate-FeCl₂.

2. Centrifuge the suspension at 4,300 rpm for 10 min, and measure fluorescence spectrum of the supernatant with excitation at 360 nm.

3.3. Separation of Blue Fluorescence

1. Lyophilize the whole supernatant of the oxidized microsomes and subject the lyophilized sample to a column (0.9 × 100 cm) of Sephadex G-10 equilibrated with 0.01 M NaCl containing 0.02% NaN₃. Elute the column with the same solvent. Monitor the fractions by fluorescence at 450 nm with excitation at 360 nm (for blue fluorescence), and by fluorescence at 520 nm with excitation at 380 nm (for green fluorescence).

3.4. Characterization of Blue Fluorescence

1. Collect the blue-fluorescent peak fractions composed of multiple fluorescent components, and measure fluorescence spectrum and intensity of the fractions.

3.5. Results

1. The supernatant of the oxidized microsomal suspensions shows blue fluorescence at 450 nm together with strong green fluorescence at 520 nm when excited at 360 nm (Fig. 1). Green fluorescence may be due to flavin-containing substances because the fluorescence maximum is similar to that of flavins.

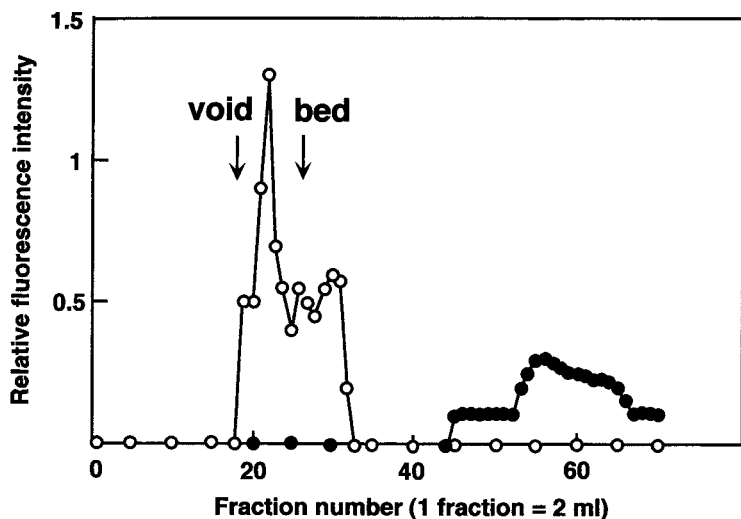


Fig. 2. Gel filtration of the supernatant of the oxidized microsomal suspension. The supernatant of the oxidized microsomal suspension is subjected to gel filtration through a column of Sephadex G-10 equilibrated with 0.01 *M* NaCl containing 0.2% NaN_3 . Blue fluorescence at 450 nm when excited at 360 nm (○) and green fluorescence at 520 nm when excited at 380 nm (●) are monitored.

- Blue fluorescence can be separated by passing through a column of Sephadex G-10 (Fig. 2). Blue fluorescence and green fluorescence in the fractions are monitored. Blue fluorescence is eluted between the void and the bed volumes of the column and green fluorescence is tightly adsorbed to the column.
- Blue fluorescent fractions show a single fluorescence maximum at 450 nm when excited at 360 nm. Relative fluorescence intensity of the fractions is 5 times as high as that of the blue fluorescent fractions obtained from the supernatant of the unoxidized microsomal suspension (Fig. 3).
- Blue fluorescence from the oxidized microsomes is resistant to treatment with 0.1 *M* sodium borohydride.
- Fluorescence spectra and intensities of the blue fluorescent fractions are only slightly affected by the pH values of the solution between pH 1.0 and 13.0.
- Blue fluorescence thus determined may be due to the reaction products of microsomal proteins and alkenals generated during lipid peroxidation. Treatment of the unoxidized microsomes or bovine serum albumin with phosphatidylcholine hydroperoxide, alkenals, 4-hydroxyalkenals or malonaldehyde gives blue fluorescence. Wavelengths of the maximum fluorescence of the products obtained by the reaction with phosphatidylcholine hydroperoxide and alkenals are similar to that of the products from the oxidized microsomes, whereas that of the products obtained by the reaction with 4-hydroxyalkenals is somewhat shorter, and that of the products obtained by the reaction with malonaldehyde is somewhat longer.

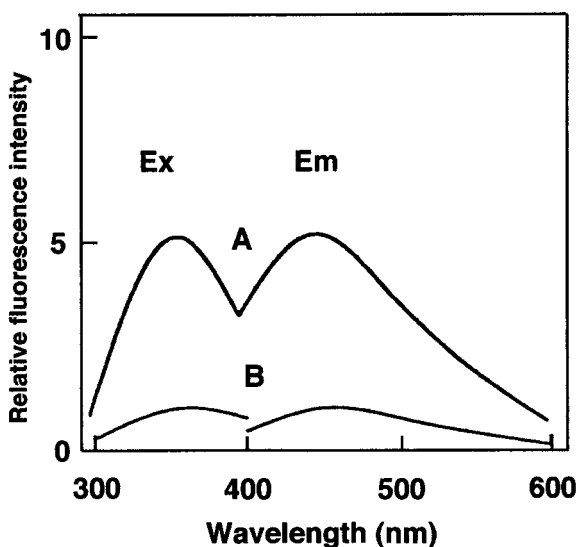


Fig. 3. Fluorescence spectra and intensities of blue fluorescence of the supernatants of the oxidized (A) and the unoxidized microsomal suspensions (B) after the gel filtration shown in Fig. 2.

References

1. Kikugawa, K. (1986) Fluorescent products derived from the reaction of primary amines and components in peroxidized lipids. *Adv. Free Rad. Biol. Med.* **2**, 389–417.
2. Hammer, C. and Braum, E. (1988) Quantification of age pigments (lipofuscin). *Comp. Biochem. Physiol.* **90B**, 7–17.
3. Kikugawa, K., Beppu, M., Sato, A., and Kasai, H. (1997) Separation of multiple yellow fluorescent lipofuscin components in rat kidney and their characterization. *Mech. Age. Dev.* **97**, 93–107.
4. Kikugawa, K. (1991) Involvement of lipid oxidation products in the formation of fluorescent and cross-linked membrane proteins, in *Membrane Lipid Oxidation II* (Vigo-Pelfrey, C., ed.), CRC Press, Boca Raton, FL, pp. 171–189.
5. Dillard, C. J. and Tappel, A. L. (1984) Fluorescent damage products of lipid peroxidation, in *Oxygen Radicals in Biological Systems, Methods in Enzymology*, vol. 105 (Packer, L., ed.), Academic Press, New York, pp. 337–341.
6. Kikugawa, K., Kato, T., Yamaki, S., and Kasai, H. (1994) Examination of the extraction methods and re-evaluation of blue fluorescence generated in rat tissues in situ. *Biol. Pharm. Bull.* **17**, 9–15.
7. Desai, I. D., Fletcher, B. L., and Tappel, A. L. (1981) Fluorescent pigments from uterus of vitamin E-deficient rats. *Lipids* **10**, 307–309.
8. Csallany, A.S., Ayaz, K.L., and Menken, B.Z. (1984) Effect of dietary vitamin E upon fluorescent compounds of the rat uterus. *Lipids* **19**, 911–915.

9. Tsuchida, M., Miura, T., and Aibara, K. (1987) Lipofuscin and lipofuscin-like substances. *Chem. Phys. Lipids* **44**, 297–325.
10. Inoue, T. and Kikugawa, K. (1998) Blue fluorescence generated during lipid oxidation of rat liver microsomes cannot be derived from malonaldehyde but can be from other aldehyde species. *Biol. Pharm. Bull.* **21**, 319–325.
11. Albro, P. W., Corbett, J. T., and Schroeder, J. L. (1987) Rapid isolation of microsomes for studies of lipid peroxidation. *Lipids* **22**, 751–756.

X-Ray Diffraction Analysis of Membrane Structure Changes with Oxidative Stress

R. Preston Mason and Robert F. Jacob

1. Introduction

Lipid peroxidation alters membrane structure-function relationships by disrupting chemical bonds associated with phospholipid acyl chains (1). Fluorescence polarization techniques have been used previously to demonstrate changes in membrane fluidity, one of the consequences of peroxidative modification (2). However, these previous studies do not provide direct insights into the molecular structure of the lipid bilayer. Small-angle X-ray diffraction is one technique that has been used successfully to measure the effects of oxidative stress on the molecular parameters of the membrane lipid bilayer. Molecules in the “liquid-crystalline” membrane bilayer have an amphipathic chemical structure consisting of a hydrophilic headgroup that associates with the water phase and hydrophobic acyl chains that interact strongly with neighboring acyl chains. As a result of this biomolecular orientation, the membrane is highly amenable to X-ray diffraction analysis, especially when layered or stacked in a periodic fashion. In this article, we review the protocol for the use of X-ray diffraction analysis to directly characterize structural changes associated with oxidative modification. The results of these analyses provide important insights into mechanisms of cellular injury and death associated with free radical damage at the biomembrane level.

2. Materials

2.1. Equipment

1. Glass (Hamilton) syringes.
2. Vortex/mixer.

From: *Methods in Molecular Biology*, vol. 196: *Oxidants and Antioxidants: Ultrastructure and Molecular Biology Protocols*
Edited by: D. Armstrong © Humana Press Inc., Totowa, NJ

3. Organic solvent evaporator.
4. Ultracentrifuge.
5. Sedimentation cells (*see Note 1*).
6. Small-angle X-ray diffraction system.
 - a. Rigaku Rotaflex RU-200 rotating anode microfocus X-ray diffractometer (Rigaku USA, Danvers, MA).
 - b. Franks single-mirror camera (Charles Supper Co., Natick, MA).
 - c. Temperature-controlled water baths (Neslab Inc., Portsmouth, NH).
 - d. Brass sample holders hermetically sealed with aluminum foil windows.
7. Position-sensitive, one-dimensional X-ray photon detector system (Innovative Technologies, Newburyport, MA).
8. Spectrophotometer.

2.2. Reagents

1. The following reagents are HPLC-grade and obtained from Fisher Scientific (Pittsburgh, PA) or Sigma Chemical Co. (St. Louis, MO): chloroform (CHCl_3), ethylenediaminetetraacetic acid (EDTA), N-(2-Hydroxyethyl) piperazine-N'-(2-ethanesulfonic acid) (HEPES), sodium chloride (NaCl), sodium hydroxide (NaOH), hydrochloric acid (HCl), potassium phosphate, monobasic (K_2HPO_4), potassium iodide (KI), sodium azide (NaN_3), benzlkonium chloride, ammonium molybdate, butylated hydroxytoluene (BHT), Triton X-100.
2. Saturated salt solutions (followed by associated relative humidities). Tartaric acid ($\text{C}_4\text{H}_4\text{O}_6\text{K}_2$), 74% RH; potassium sodium tartrate ($\text{C}_4\text{H}_4\text{O}_6\text{NaK}$), 87% RH; ammonium dihydrophosphate ($[\text{NH}_4]\text{H}_2\text{PO}_4$), for 93% RH. Tartaric acid is typically used to establish the relative humidity level for X-ray diffraction analyses of sample membranes, and all salt solutions are used for membrane swelling analyses (*see below*).
3. Diffraction buffer. Add 0.11915 g HEPES and 8.99976 g NaCl to 1 L double-deionized water (for 0.5 mM HEPES, 154 mM NaCl solution); mix well and adjust pH to 7.3. Buffer can be stored for approx 1 mo at 4°C.
4. CHOD Reagent stock. Combine 27.22 g K_2HPO_4 , 19.92 g PI, and 9.752 mg NaN_3 in ~500 mL double-deionized water while stirring. Add 0.1 g benzlkonium chloride followed by 12.359 mg ammonium molybdate. Add double-deionized water to 1 L total volume. Stir for 2–3 h until solution clears. Store at 4°C until use in active CHOD solution.
5. Active CHOD solution. Add following reagents to a volume of CHOD stock reagent to achieve the following concentrations (in parentheses): BHT (20 μM), EDTA (24 μM), Triton X-100 (0.2%). Stir gently for ~30 min and filter (using Whatman #1 filter paper). Use immediately (*see Note 2*).
6. Nitrogen (prepurified).
7. Synthetic lipids characterized by gas-liquid chromatographic analysis were obtained from Avanti Polar Lipids (Alabaster, AL). For these studies, use the

polyunsaturated fatty acid lipid, dilinoleoyl phosphatidylcholine (DLPC). DLPC is dissolved in CHCl_3 (25 mg/mL) and stored at -80°C until use.

3. Methods

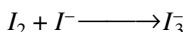
3.1. Preparation of Membrane Samples

1. Transfer aliquots of DLPC (in CHCl_3) to 13×100 mm test tubes using Hamilton glass syringes. For X-ray diffraction experiments, 250 μg of lipid is typically used for a single membrane sample; lipid peroxidation experiments generally employ multiple samples, each at 1 mg lipid per sample.
2. Shell-dry the lipid samples to the walls of the test tubes under a steady stream of nitrogen gas while vortex mixing (medium speed). Wrap samples in aluminum foil to minimize exposure to light and remove residual solvent by drying for at least 3 h under vacuum.
3. Add diffraction buffer to the dried lipid samples to yield a final phospholipid concentration of 1.0 mg/mL. Vortex the buffer and lipids at moderate speed for 3 min at ambient temperature to form multilamellar vesicle (MLV) samples (3).
4. For diffraction analysis, control and oxidized membrane samples are oriented by subjecting them to centrifugation, as previously described (4). Membrane multilamellar vesicles are loaded into sedimentation cells fitted with aluminum foil substrates upon which the samples are collected. The vesicles are sedimented in an ultracentrifuge at 35,000g for 1.5 h at 5°C . Following centrifugation, the supernatants are aspirated from the pellets and the samples are then mounted onto curved glass supports. The samples (0.5 cm in diameter and ~ 1.0 mm in height) are placed in sealed brass canisters in which relative humidity and temperature are controlled during the diffraction experiments (4,5). A saturated salt solution consisting of tartaric acid ($\text{C}_4\text{H}_4\text{O}_6\text{K}_2$) is used for defining a relative humidity level of 74%.

3.2. Lipid Peroxidation Analysis

1. For lipid peroxidation experiments, transfer MLV samples (still in 13×100 mm test tubes) to a shaking water bath preheated to 37°C . The samples holder should be set to gently oscillate so that the samples are kept well-suspended. Autooxidation of DLPC vesicles occurs as a function of time as the membrane samples are incubated under these conditions.
2. To measure the extent of lipid peroxidation, aliquots of membrane samples are removed at various time points (e.g., 24 h intervals) and combined with 1.0 mL of active CHOD reagent (per sample). Sufficient active CHOD reagent should be prepared from the CHOD stock solution (as previously described) so that one preparation can be used for all timepoint measurements. After adding the active CHOD reagent, cover the samples with foil and incubate for 2 h in the absence of light.

3. Read sample absorbances against a CHOD blank at 365 nm (6). The CHOD colorimetric assay is based on the spectrophotometric measurement of triiodide (I_3^-). The molar quantity of I_3^- is directly proportional to the quantity of lipid hydroperoxides (LOOH) that are formed in the process of lipid peroxidation. The following reactions demonstrate this relationship:



4. Determine the concentration of I_3^- (and LOOH) by applying a molar absorptivity value (ϵ) of $2.4 \times 10^4 M^{-1} cm^{-1}$ ($\epsilon_{365\text{ nm}}$) and a pathlength (b) of 1 cm to the Beer-Lambert law:

$$\text{Sample LOOH Conc. } [M] = \frac{Abs_{(365\text{ nm})}}{\epsilon b}$$

3.3. X-Ray Diffraction Analysis

3.3.1. Theoretical Considerations

1. The theoretical basis for the application of X-ray diffraction methodology to the study of membrane structure is well-understood. X-ray scattering from stacked, membrane systems has been shown to produce constructive interference at discrete angles, as defined geometrically by Bragg's law:

$$n\lambda = 2d \sin\theta$$

in which n is the diffraction order number, λ is the wavelength of the X-ray radiation (1.54 \AA), d is the membrane unit cell periodicity (the measured distance from the center of one membrane to the next, including surface hydration), and θ is the Bragg angle equal to one-half of the angle between the incident and scattered radiation.

2. The coordinate used to describe the position of the scattered X-ray data in the diffraction pattern is the vector S , known as the reciprocal space vector. In these experiments, diffraction analysis is conducted on membranes separated by well-defined aqueous layers of essentially constant width. The width of the water space is a function of relative humidity, which is maintained by saturated salt solutions. The time-averaged electron density in one dimension perpendicular to the membrane plane is calculated from the X-ray scattering data. The amplitude of the scattered wave from an arbitrary origin such as the center of the interbilayer water space is proportional to $\rho(x)$ and its phase relative to the origin is $2\pi iSx$. $F(S)$ is the structure factor and defines both the amplitude and phase of the scattered radiation. $F(S)$ is also the Fourier transform of $\rho(x)$ so that if $F(S)$ is known at every value of S , then the electron density distribution can be obtained by using the inverse relationship:

$$\rho x = \int_s F(S) \exp(-2\pi iSx) dS$$

3. During X-ray diffraction experiments, coherent scattering associated with areas of constructive interference are collected on various detector systems (in this case, a position-sensitive electronic detector). The resultant structure factor, $F(S)$, is generated from the square root of these intensities. An obstacle to overcome in the analysis of the diffraction analysis is the phase of the function $F(S)$. During diffraction experiments, only the intensity is observed, $I(S)$, and thus the phase (+ or -) remains to be solved as $I(S)$ is related to $F(S)$ by the following relationship, $I(S) = F(S)^2$. Determination of the phase of $F(S)$ can be ascertained by swelling analysis, as previously described (7). In swelling analysis of oriented membranes, diffraction data are collected at different relative humidity levels that correspond to unique unit cell repeat distances as a result of modulating interbilayer water content.

3.3.2. X-Ray Diffraction Experiments

X-ray diffraction analyses are conducted by aligning the stacked membrane samples (control and oxidized) at grazing incidence with respect to a collimated X-ray beam (**Fig. 1**). The radiation source is a nickel-filtered monochromatic X-ray ($\text{CuK}_{\alpha} = 1.54 \text{ \AA}$) produced by a high-brilliance rotating anode microfocus generator (Rigaku Rotaflex RU-200, Danvers, MA). The fixed geometry beam line consists of a single, nickel-coated Franks mirror to define a line source where $\text{K}_{\alpha 1}$ and $\text{K}_{\alpha 2}$ are unresolved. The diffraction data are collected on a one-dimensional, position-sensitive electronic detector placed at a distance of 150 mm from the sample. Each diffraction peak is Lorentz- and background-corrected, as previously described (5). The phases of the diffraction data are determined by swelling analysis (8), using the saturated solutions of the following salts (relative humidities in parentheses): tartaric acid (74%); potassium sodium tartrate (87%); and ammonium dihydrophosphate (93%). Fourier transformations of the data are generated using customized program modules written for Microcal Origin (Microcal Software, Northampton, MA).

3.4. Results

1. Representative X-ray diffraction patterns from control and test samples (following 24 and 48 h autooxidation at 5°C and 74% relative humidity) are shown in **Fig. 2**. X-ray diffraction analysis of oriented DLPC membranes produces a maximum of four reproducible orders in both the control and test samples. In this example, the unit cell periodicity or d -space (distance from the center of one membrane bilayer to the next) for the control DLPC sample was 49.2 Å while the intrabilayer headgroup separation was 35.4 Å. Following autooxidation of the membrane samples for 24 h and 48 h, the lipid bilayer d -space values were reduced to 46.7 Å and 46.1 Å, respectively. Intrabilayer headgroup separation was reduced to 34.0 and 32.6 following 24 h and 48 h autooxidation, respectively. These changes in membrane structure correlated with lipid peroxidation levels

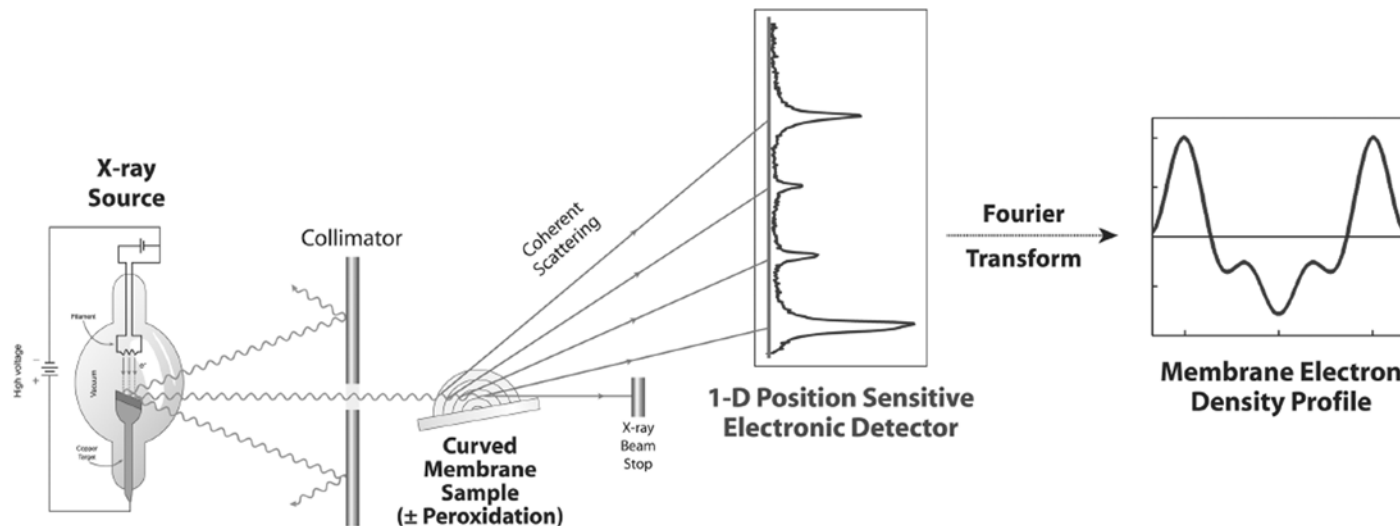


Fig. 1. Membrane diffraction experiments utilized monochromatic radiation ($\lambda = 1.54 \text{ \AA}$) from a high-brilliance rotating anode X-ray generator source. Oriented membrane samples at various stages of peroxidation were placed on a curved mounts at near-grazing incidence with respect to the focused X-ray beam. Coherent scattering data from the samples were collected on a one-dimensional position-sensitive detector. The diffraction order intensities were integrated and used to generate a one-dimensional electron density profile of the membrane.

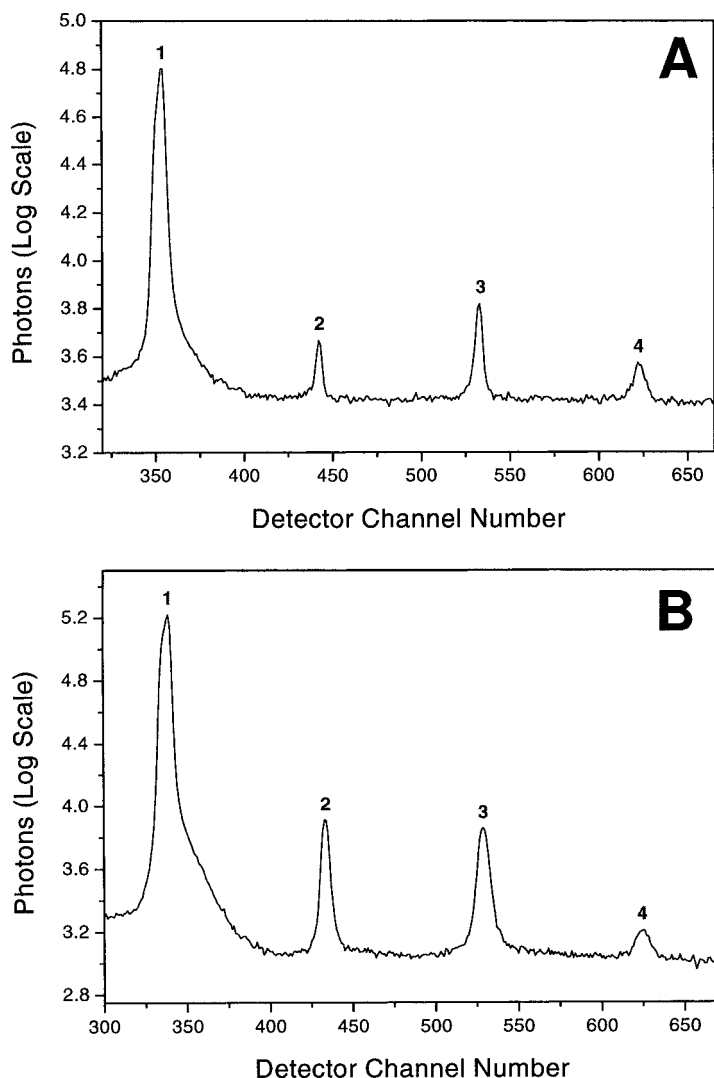


Fig. 2. Representative X-ray diffraction patterns obtained from control (A) and oxidized (B) DLPC membrane bilayer samples. Data were collected on a one-dimensional, position-sensitive electronic detector at 5°C and 74 % relative humidity. Diffraction peaks are labeled and correspond to unit cell periodicities of 49.2 Å and 46.1 Å for control and oxidized membrane samples, respectively.

of $175.57 \pm 10.51 \mu\text{M}$ and $228.12 \pm 27.07 \mu\text{M}$, respectively, following these incubation periods.

- Fourier transformation of the diffraction data produces centrosymmetric electron density profiles for the membrane samples (Fig. 3). The two peaks of electron

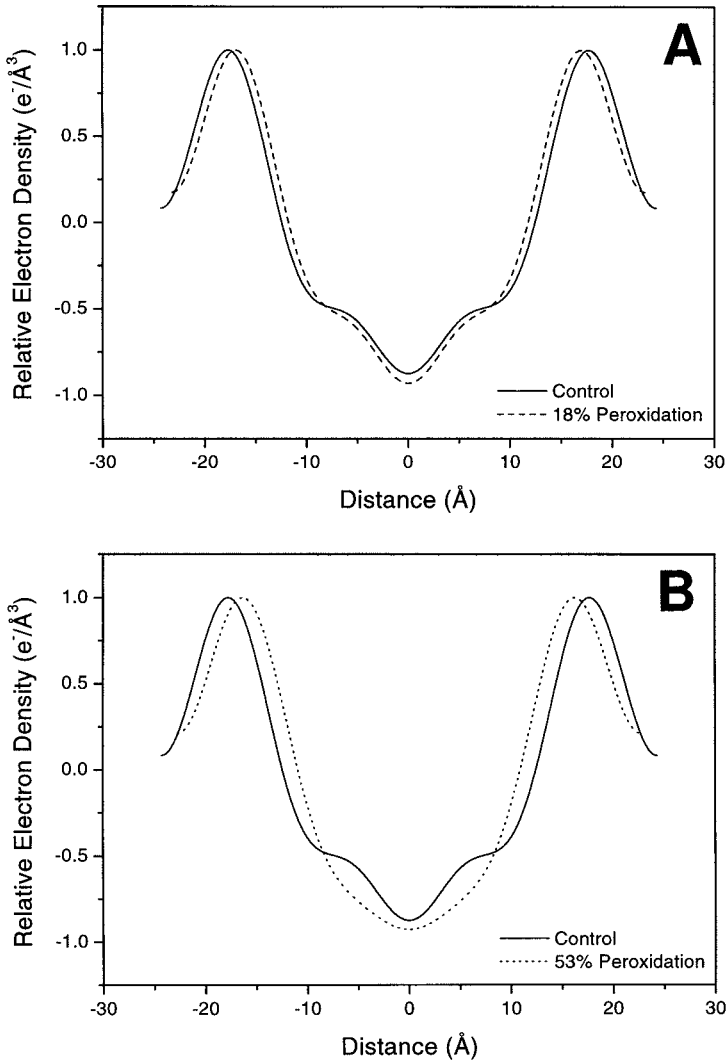


Fig. 3. Effect of lipid peroxidation on the molecular structure of DMPC membrane bilayer. Superimposed electron density profiles ($e/\text{\AA}^3$) of DLPC membrane bilayers before and after lipid peroxidation for 24 h (A, 18% lipid peroxidation) and 48 h (B, 53% lipid peroxidation). The two peaks of electron density on either side of the centrosymmetric profile correspond to phospholipid headgroups, while the minimum of electron density at the center of the membrane is associated with terminal methyl segments of the phospholipid acyl chains.

density on either side of the figure correspond to the electron-dense phospholipid headgroups, while the minimum of electron density at the center of the membrane correlates with the terminal methyl segments associated with the phospholipid acyl chains. Superimposition of the membrane electron density profiles reveals significant changes in structure following lipid peroxidation (48 h), including a marked inward displacement in the phospholipid headgroups by 2.8 Å. In addition, electron density (electrons/Å³) associated with the hydrocarbon core is reduced over a broad range, ± 8.2 Å from the center of the membrane. This observed decrease in relative electron density and change in the molecular dimensions of the phospholipids are direct evidence for disruptions in the intermolecular packing of the phospholipid acyl chains.

3. These data demonstrate the utility of X-ray diffraction analysis in characterizing changes in the molecular structure and organization of membrane lipid bilayers following oxidative modification (9). The observed changes in membrane structure, including a marked reduction in membrane hydrocarbon core width and increase in hydrocarbon core molecular volume, are indicative of alterations in the intermolecular packing and thermodynamic properties of the phospholipid bilayer (10). The observed changes in membrane structure also demonstrate that even modest levels of membrane free radical damage produce marked changes in the molecular organization of the lipid bilayer. These data are consistent with reports that establish that membrane lipid peroxidation can result in the breakage or loss of double bonds in the fatty acyl chain (1). Changes in membrane fluidity have also been attributed to loss of unsaturation in regions of the membrane bilayer that are susceptible to peroxidative damage (i.e., region of fatty acid double bonds) (2).
4. Alterations in membrane structure following oxidative stress have important implications for understanding the function of integral membrane proteins involved in transmembrane ion gradients and cellular metabolic processes (11). A common structural motif for the transmembrane protein is the repeating, α -helical domain in which the average distance between adjacent amino acids is 1.5 Å while a single, complete turn of the α -helix (3.6 amino acids per turn) is 5.4 Å in length. A reduction in membrane width by 3.1 Å and reorganization of phospholipid packing with lipid peroxidation, as observed in this study, would be expected to significantly alter the structure of transmembrane amino acids in register with the surrounding amphipathic phospholipid bilayer (12). These membrane biophysical changes may contribute to mechanisms by which oxidative stress produces a loss in cellular function in various diseases, such as atherosclerosis and ischemia-reperfusion injury. Indeed, previous X-ray diffraction studies have demonstrated in reconstituted membrane systems that protein function is highly influenced by the molecular organization and dimensions of the lipid bilayer (13).

4. Notes

1. For these X-ray diffraction analyses, the sedimentation cells are fitted with aluminum foil substrates upon which the membrane samples are collected.

2. Volume of CHOD stock to use depends on total number of samples and timepoint measurements; 1 mL of CHOD solution is required for each sample. We find that overestimating total volume by 30–40 mL prevents shortage of solution due to preparative losses.

References

1. Leibowitz, M. E. and Johnson, M. C. (1971) Relation of lipid peroxidation to loss of cations trapped in liposomes. *J. Lipid Res.* **12**, 662–670.
2. Kornbrust, D. J. and Mavis, R. D. (1980) Microsomal lipid peroxidation. I. Characterization of the role of iron and NADPH. *Mol. Pharmacol.* **17**, 400–407.
3. Bangham, A. D., Standish, M. M., and Watkins, J. C. (1965) Diffusion of univalent ions across the lamellae of swollen phospholipids. *J. Mol. Biol.* **13**, 238–252.
4. Chester, D. W., Herbet, L. G., Mason, R. P., Joslyn, A. F., Triggle, D. J., and Koppel, D. E. (1987) Diffusion of dihydropyridine calcium channel antagonists in cardiac sarcolemmal lipid multibilayers. *Biophys. J.* **52**, 1021–1030.
5. Mason, R. P., Gonye, G. E., Chester, D. W., and Herbet, L. G. (1989) Partitioning and location of Bay K 8644, 1,4-dihydropyridine calcium channel agonist, in model and biological membranes. *Biophys. J.* **55**, 769–778.
6. El-Saadani, M., Esterbauer, H., el-Sayed, M., Goher, M., Nassar, A. Y., and Jurgens, G. (1989) A spectrophotometric assay for lipid peroxides in serum lipoproteins using a commercially available reagent. *J. Lipid Res.* **30**, 627–630.
7. Mason, R. P., Shoemaker, W. J., Shajenko, L., Chambers, T. E., and Herbet, L. G. (1992) Evidence for changes in the Alzheimer's disease brain cortical membrane structure mediated by cholesterol. *Neurobiol. Aging* **13**, 413–419.
8. Moody, M. F. (1963) X-ray diffraction pattern of nerve myelin: a method for determining the phases. *Science* **142**, 1173–1174.
9. Mason, R. P., Walter, M. F., and Mason, P. E. (1997) Effect of oxidative stress on membrane structure: small angle x-ray diffraction analysis. *Free Radic. Biol. Med.* **23**, 419–425.
10. Mason, R. P., Trumbore, M. W., and Pettegrew, J. W. (1996) Molecular membrane interactions of a phospholipid metabolite. Implications for Alzheimer's disease pathophysiology. *Ann. NY Acad. Sci.* **777**, 368–373.
11. Dinis, T. C., Almeida, L. M., and Madeira, V. M. (1993) Lipid peroxidation in sarcoplasmic reticulum membranes: effect on functional and biophysical properties. *Arch. Biochem. Biophys.* **301**, 256–264.
12. Zhang, Y. P., Lewis, R. N., Hodges, R. S., and McElhaney, R. N. (1992) FTIR spectroscopic studies of the conformation and amide hydrogen exchange of a peptide model of the hydrophobic transmembrane alpha-helices of membrane proteins. *Biochemistry* **31**, 11572–11578.
13. Chang, H. M., Reitstetter, R., Mason, R. P., and Gruener, R. (1995) Attenuation of channel kinetics and conductance by cholesterol: an interpretation using structural stress as a unifying concept. *J. Membr. Biol.* **143**, 51–63.

Detection of Estrogen Receptor by *In Situ* Hybridization

Kaori Kobayashi and Hiroshi Kobayashi

1. Introduction

Neurons in widely disparate regions of the central nervous system (CNS), regions not intimately associated with reproductive behaviors, express the estrogen gene. Recent *in situ* hybridization (ISH) studies have documented the widespread distribution of estrogen receptor mRNA in the adult rat brain (1–3). Clearly labeled cells were found in regions with widespread connections throughout the brain, suggesting that estrogen receptor may modulate a wide variety of neural functions. Furthermore, we reported the expression of estrogen receptor mRNA in bovine retina (4).

ISH is an important method for tracing the regional and cellular sites of gene expression within a tissue (5,6). Because a high resolution is required to discriminate among different cell types that have close histological associations, this chapter describes a method of ISH for estrogen receptor using digoxigenin (DIG)-labeled oligonucleotides (oligo-DNAs) in which the signals are detected immunohistochemically with a horseradish peroxidase (HRP)-labeled anti-DIG antibody (7). The DIG molecule is a unique steroid isolated from the plant *Digitalis purpurea*. No binding of the anti-DIG antibody in other biological material occurs. It has recently been confirmed that, under appropriate conditions, there is no substantial difference in the sensitivity of detection between radioactive probes and nonradioactive probes. Koji and Brenner reported that, in monkey uterus, most of the glandular epithelial cells of the basalis as well as endometrial stromal cells were positive for estrogen receptor mRNA, while all vascular smooth muscle, endothelium, and

perivascular stromal cells were negative (7). However, the most appropriate conditions for specifically sensitive ISH must be established for each tissue.

We describe a protocol for ISH of estrogen receptor mRNA in frozen sections of bovine retina with a DIG-labeled estrogen receptor antisense oligo-DNA probe, that allows one to determine of expression of estrogen receptor mRNA in the central nervous system.

2. Materials

2.1. Equipment

1. Cryostat microtome (Reichert Histostat, Buffalo, NY).
2. Aminopropyltriethoxy-silane-coated slides (DAKO, Glostrup, Denmark).
3. Slide racks with wire handle.
4. Incubator.
5. Water bath.
6. Light microscope (Nikon, Tokyo, Japan).

2.2. Reagents

1. O.C.T. compound (Tissue-Tec, Miles Scientific, Naperville, IL).
2. 4% paraformaldehyde (PFA) in phosphate-buffered saline (PBS). Prepare this solution as follows. Transfer 4 gram of PFA (general-purpose reagent grade) (Wako, Japan) into 50 mL of sterile water (treat with diethylpyrocarbonate [DEPC] and autoclave) and add 2 *N* NaOH several dropwise. Warm up the suspension at 60–65°C. Do not heat above this temperature. Add 0.2 *M* phosphate buffer (treat with DEPC and autoclave), mix well and chill the solution in an ice/water bath (*see Note 1*).
3. 0.2 *N* HCl, Triton X-100, Tween 20 (Wako, Japan)
4. 10 *mM* Tris-HCl, pH 8.0, deionized H₂O (DNase- and RNase- free solutions are available from Nippon Gene.)
5. Proteinase K (Wako, Japan) in 10 *mM* Tris-HCl, pH 8.0, 1 *mM* EDTA
6. Hybridization buffer: 4X SSC, 0.01% SDS, 200 U/mL heparin, 40% deionized formamide (Wako, Japan). Hybridization buffer is also available from RNA color kit (Amersham, UK).
7. The following reagents are obtained from Boehringer Mannheim (Mannheim, Germany): blocking reagent, alkaline phosphatase-conjugated anti-DIG antibody, nitroblue tetrazodium (NBT)/5-bromo-4-chloro-3-indolyl-phosphate toluidium (BCIP) stock solution.
8. DIG buffer I: 0.1 *M* maleic acid, 0.15 *M* NaCl. Adjusted to pH 7.5 (20°C) with solid NaOH.
9. Blocking stock solution; 10% blocking reagent in buffer 1. Dissolve blocking reagent by constantly stirring on a heating block (65°C), autoclave and store at 4°C. The solution remains opaque.
10. DIG buffer II; 1% blocking buffer. Working solution is prepared by diluting the blocking stock solution 1:9 in DIG buffer I.

11. DIG buffer III; 100 mM Tris-HCl, 100 mM NaCl, 50 mM MgCl₂, pH 9.5 (20°C).

3. Methods

3.1. Synthesis of Oligo-DNAs and Labeling of Oligo-DNAs by Terminal Deoxynucleotidyl Transferase

1. The estrogen receptor antisense oligo-DNA, selected as described by Koji and Brenner (7), was complementary to the mRNA sequence coding for amino acids 13-27 of the human estrogen receptor protein as follows; 5'-GTT CAG GGG CTC CAG CTC GTT CCC TTG GAT CTG ATG CAG TAG GGC-3'. The estrogen receptor sense oligo-DNA selected corresponding to the mRNA sequence as follows; 5'-GCC CTA CTG CAT CAG ATC CAA GGG AAC GAG CTG GAG CCC CTG AAC-3' (see **Note 2**).
2. The oligo-DNAs were synthesized on an automatic DNA synthesizer (Applied Biosystems, Expedite 8900) and labeled at their 3'-end with DIG-11-dUTP or DIG-11-ddUTP by terminal deoxynucleotidyl transferase.

3.2. Preparation and Fixation of Sections

1. Embed fresh bovine retina in O.C.T. compound and freeze immediately in liquid nitrogen and store at -70°C (see **Note 3**).
2. Cut 8 µm sections by cryostat microtome at -20°C. Thaw mount the sections on to aminopropyltriethoxy-silane-coated slides. Allow sections to dry at room temperature for an hour.
3. Transfer dry sections into fresh 4% PFA for 15 min at room temperature.

3.3. Pretreatment of Sections

1. Rehydrate sections with PBS for 5 min (see **Note 4**).
2. Transfer sections into 0.2 N HCl for 20 min, 0.2% Triton X-100 for 10 min, and 1 µg/mL proteinase K for 15 min successively.
3. Postfix with 4% PFA for 10 min.
4. Transfer sections into PBS for 5 min.
5. Keep sections in 40% deionized formamide in 4X SSC until used for hybridization at 37°C.

3.4. Application and Hybridization of Probes to Sections

1. Warm up hybridization buffer at 85°C for 10 min. Prepare 1 µg/mL DIG-labeled oligonucleotide probe in the hybridization buffer. Vortex vigorously, incubate at 85°C for 3 min, vortex, and spin down.
2. Apply 100 µL of probe/hybridization buffer in the slides and cover parafilm as coverslips carefully. The parafilm must be flat and free of wrinkles. Remove any large air bubbles.
3. Incubate the slides in a humid chamber at 37°C for 15-17 h. To maintain humidity, tissue papers saturated with 50% formamide/4X SSC are placed in the humid chamber. Seal the lid of the dish by stretching layers of parafilm around it.

3.5. Washing and Detection

1. Remove the parafilm gently by immersion in prewarmed 2X SSC at 37°C Wash the slides four times with 2X SSC at 37°C for 30 min each time.
2. Transfer the sections into DIG buffer I for 15 min.
3. Incubate for 1 h with 1.5% blocking solution.
4. Incubate the sections overnight at 4°C with alkaline phosphatase-conjugated anti-DIG antibody (1:500) in DIG buffer II (1% blocking buffer) in a humid chamber. Do not allow the sections to dry out.
5. Then the sections were washed with DIG buffer I (maleic acid buffer) with 0.2% Tween 20 for 15 min four times.
6. Equilibrate the sections for 5 min in DIG buffer III.
7. Staining was visualized with nitroblue tetrazodium (NBT) and 5-bromo-4-chloro-3-indolyl-phosphate toluidium (BCIP) stock solution in DIG buffer III at room temperature in the dark. Color development may be occasionally controlled under the binocular microscope and stopped in 10 mM Tris-HCL, pH 7.6, 1 mM EDTA before background develops.

3.6. Results

ISH of bovine retina with estrogen receptor sense and antisense of oligo-DNAs was performed. Estrogen receptor mRNA was detected in some cell bodies in the ganglion cell layer (**Fig. 1B**). Intense staining was observed in the inner nuclear layer and outer portion of the outer nuclear layer. Estrogen receptor mRNA localized to the retinal pigment epithelium and endothelium of blood vessels in the choroid. No specific staining was seen in sections hybridized with the sense probe (**Fig. 1A**).

4. Notes

1. Older solutions may contain oxidation products that may damage nucleic acids.
2. To confirm the specificity of estrogen receptor mRNA signals, Koji and Brenner conducted various types of control experiments on sections adjacent to those used for test experiments (7). First, sense probe was used as a negative control in every run. Furthermore, some reactions were hybridized with ER antisense probe in the presence of an excess amount of either homologous or nonhomologous unlabeled oligo-DNA to provide definitive evidence for the sequence specificity of the signal. To eliminate possible involvement of proteins and DNA in signal formation, some sections were digested with RNase-A (100 µg/mL; 37°C; 1 h) before the postfixation step.
3. After freezing the tissue, one should not to thaw because this will allow RNase access to RNA and destroy the morphology. On the day of cutting, the frozen tissue in the O.C.T. compound is transferred from the -70°C freezer to the -20°C freezer or cryostat chamber to equilibrate for at least 1 h before cutting.

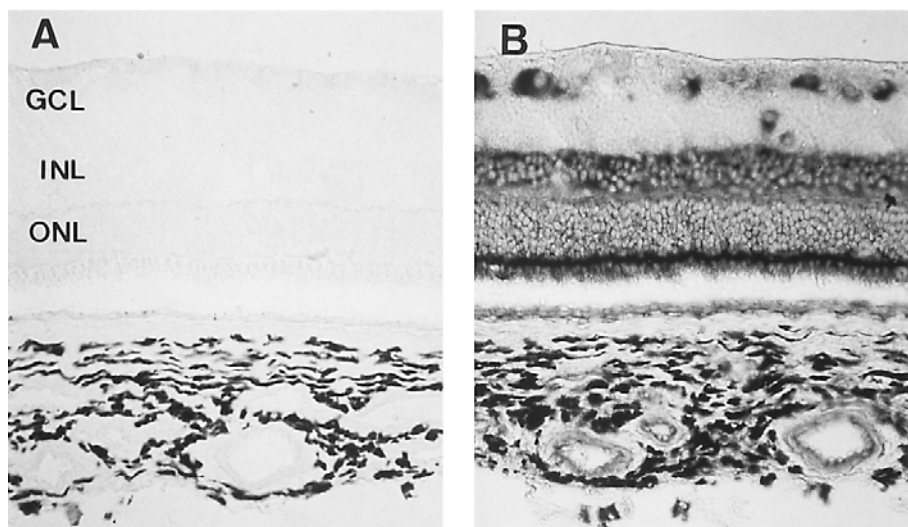


Fig. 1. *In situ* hybridization with DIG-labeled oligo-DNAs corresponding to the estrogen receptor sequence in bovine retina. (A) No hybridization is seen with the control probe. (B) The expression of the estrogen receptor mRNA is predominantly observed in ganglion cell layer, the inner nuclear layer, and outer portion of the outer nuclear layer. Original magnifications $\times 100$. Reprinted with permission (4).

4. Perform all pretreatment hybridization steps in Eppendorf tubes. Potential RNase contamination should be avoided. Use DEPC-treated and autoclaved water to prepare all the solutions used before hybridization step and for the hybridization buffers itself, and also wear gloves.

References

1. Pelletier, G., Liano, N., Follea, N., and Govindan, M. V. (1988) Mapping of estrogen receptor-producing cells in the rat brain by *in situ* hybridization. *Neurosci Lett.* **94**, 23–28.
2. Toran-Allerand, C. D., Miranda, R. C., Hochberg, R. B., and MacLusky, N. J. (1992) Cellular variations in estrogen receptor mRNA translation in the developing brain: evidence from combined [125 I] estrogen autoradiography and non-isotopic *in situ* hybridization histochemistry. *Brain Res.* **576**, 25–41.
3. Simerly, R. B., Chang, C., Muramatsu, M., and Swanson, L. W. (1990) Distribution of androgen and estrogen receptor mRNA-containing cells in the rat brain: an *in situ* hybridization study. *J. Comp. Neurol.* **294**, 76–95.
4. Kobayashi, K., Kobayashi, H., Ueda, M., and Honda, Y. (1998) Estrogen receptor expression in bovine and rat retinas. *Invest. Ophthalmol. Vis. Sci.* **39**, 2105–2110.

5. Gee, C. E., Chen, C. L., Roberts, J. L., Thompson, R., and Watson, S. J. (1983) Identification of proopiomelanocortin neurones in rat hypothalamus by in situ cDNA-mRNA hybridization. *Nature* **306**, 374–376.
6. Wisden, W. and Morris, B. J. (1994) *In Situ Hybridization Protocols for the Brain*. Academic Press, New York.
7. Koji, T. and Brenner, R. M. (1993) Localization estrogen receptor messenger ribonucleic acid in rhesus monkey uterus by nonradioactive in situ hybridization with digoxigenin-labeled oligodeoxynucleotides. *Endocrinology* **132**, 382–392.

Tumor Necrosis Factor- α Quantification and Expression by *In Situ* Hybridization

Tracey A. Ignatowski and Robert N. Spengler

1. Introduction

The pleiotropic cytokine, tumor necrosis factor- α (TNF- α), has been shown to affect not only pathological and inflammatory conditions, but also plays a seminal role in the maintenance of physiological homeostasis. Due to these diverse activities, TNF- α is widely studied using various assay methods. The WEHI 164 clone 13 (1) and WEHI-13VAR (2) bioassays are the method of choice for detection of biologically active TNF in biological fluids and tissue homogenates (3,4). However, data generated from these assays are limited, providing only bioactive levels of this cytokine in a whole tissue homogenate or in serum/plasma. In order to determine the cellular localization for production of this cytokine, the techniques of immunohistochemistry and *in situ* hybridization are invaluable. These methods allow for the successful identification of the cell types involved in the regulation and production of this cytokine.

We describe modification of both methodologies that allows for detection of TNF- α protein as well as the messenger RNA (5–7) for this protein in rat brain tissue preparations.

2. Materials

2.1. Equipment

1. Water bath.
2. Freezing bolts or Tissue embedding rings (VWR Scientific).
3. Cryo-cut Microtome Cryostat (American Optical Corp.).
4. Humidifier chamber consisting of a plastic box lined with wet paper towels, or with H₂O at the bottom to maintain moisture.

From: *Methods in Molecular Biology*, vol. 196: *Oxidants and Antioxidants: Ultrastructure and Molecular Biology Protocols*
Edited by: D. Armstrong © Humana Press Inc., Totowa, NJ

5. Leitz Orthoplan 2 Microscope.
6. Hotplate.
7. Fume hood.

2.2. Supplies

1. Whatman filter paper #2 and glass microfiber (GF/C) Whatman disks (Whatman LabSales).
2. Wooden sticks.
3. Plastic resealable (Tupperware) containers.
4. Slide mailers, slide boxes, and vertical slide drying rack.
5. Glassware: Coplin staining jars, staining dishes, glass slides, and cover slips.
6. P6 column (Bio-Spin 6 column) (Bio-Rad).
7. Scintillation fluid (Ultima Gold, Packard).

2.3. Reagents

1. Liquid N₂.
2. Histostick solution (Accurate).
3. OCT Tissue-Tek embedding compound (VWR).
4. The following reagents are obtained from Sigma Chemical Co.: Diaminobenzidine (DAB) tablet sets, H₂O₂ or periodic acid, Mayer's hematoxylin and Eosin-Y stains, poly-L-lysine, diethyl pyrocarbonate (DEPC), triethanolamine (TEA), paraformaldehyde, Ficoll Type 400, polyvinylpyrrolidone, tRNA type XX, imidazole, NaCl, dibasic sodium phosphate heptahydrate (Na₂HPO₄•7H₂O), potassium phosphate monobasic (KH₂PO₄), CaCl₂, Trizma Hydrochloride (Tris-HCl), RNase-A, formamide, dextran sulfate, SalSpDNA, monoclonal anti-neurofilament 200 antibody (NF-200 Ab), and BSA (fraction V).
5. Three types of normal serum (for blocking, use same species from which the secondary antibody is generated; for negative control staining, use same species from which the primary antibody is generated; for pre-absorption of secondary antibody, use same species as tissue sections being stained).
6. Antibodies: primary (polyclonal or monoclonal) and enzyme-linked secondary antibodies.
7. Dithiothreitol (DTT) (Boehringer Mannheim).
8. Proteinase K (Promega).
9. Terminal deoxynucleotidyl transferase (TdT) labeling kit (Gibco-BRL or Boehringer Mannheim).
10. AG-501-XA resin (Bio-Rad).
11. ³⁵S-dCTP (NEN).
12. NTB-2 emulsion, D-19 developer, Rapid Fix (Eastman Kodak).

3. Methods

3.1. Sample Collection and Freezing Procedure

1. Label identification tags and place on bolts.
2. Using tongs, place bolt in liquid N₂ for 10 s to get cold.

3. Put OCT embedding compound on bolt surface to prepare a base; submerge bolt in liquid N₂ only up to the OCT, leaving the top portion of the base as a liquid.
4. Mount/orient tissue section on the OCT base.
5. Pour OCT over and around the tissue specimen, covering completely.
6. Slowly submerge bolt into liquid N₂; OCT begins to freeze around tissue (*see Note 1*).
7. Place bolt containing frozen tissue specimen immediately in a -20°C freezer; leave for at least 4 h before preparing sections.
8. For long-term storage, place bolts containing tissue specimens into plastic storage bags, seal, and store at -20°C until ready to cut.

3.2. Sample Processing

1. Cut frozen tissue sections 4 μ m thick using a cryostat at temperature of -23°C; mount tissue sections onto pretreated (as below) glass slides.
 - a. Immunohistochemical staining. Coat alcohol (95%)-cleaned slides with histostick solution. Add 6 drops of histostick to 200 mL of distilled water, shake well, and store in brown (light-proof) bottle at 4°C (*see Note 2*).
 - b. *In situ* hybridization. Use slides coated with poly-L-lysine. Diamond-etch around each mounted tissue section to easily locate tissue section and to prevent fluid leakage off sections.
2. Immediately fix mounted tissue sections to preserve membrane antigens.
 - a. Immunohistochemical staining:
 - i. Air-dry slides for 30 min at room temperature (RT) to prevent sections from falling off slides during incubations.
 - ii. Fix mounted slides in acetone at RT for 10 min; dry slides thoroughly (at RT for 45 min or by fan for 10 min).
 - iii. Store fixed slides in slide boxes at -20°C or lower until ready to stain.
 - b. *In Situ* hybridization:
 - i. Place slides in ice cold 4% paraformaldehyde (make fresh every 2 d: In fume hood, heat 300 mL DEPC water + 16 mL 25X PBS to 80–84°C on a hot-plate (*see Note 3*); add 16 g paraformaldehyde while stirring; Qs to 400 mL; filter with Whatman #2 in a funnel and store at 4°C) for 15 min.
 - ii. Rinse slides 3 times in fresh, ice-cold 70% EtOH.
 - iii. Store slides in 70% EtOH at 4°C until use.

3.3. Two-Step Indirect Immunohistochemical Staining Procedure

1. Thoroughly dry frozen slides 45 min by fan.
2. Use water repellant marking stick or solution to label around each tissue section on slide.
3. Hydrate slides in PBS (add 6.8 g NaCl, 2.79 g Na₂HPO₄•7H₂O, and 0.43g KH₂PO₄, bring to 1 L with distilled water, pH 7.2), 2 times, 5 min each.
4. Start pre-absorption of secondary antibody, if necessary, in order to remove any potential cross-reactive antibodies to the tissue sections (rat brain tissue) that

are being stained. The secondary antibody is a peroxidase-conjugated swine-anti-rabbit antibody; it is pre-absorbed by preparing a 1:50 dilution using normal rat serum and incubating at 37°C for 45 min. Be sure to prepare a large enough volume to cover all tissue sections to be stained (need ~100 μ L per section).

5. Block slides for endogenous peroxidase in tissue sections using either 0.3% H_2O_2 for 20 min or 0.28% periodic acid for 50 s (prepare solutions right before use).
6. Rinse slides in fresh PBS, 2 times, 5 min each.
7. Block all slides against nonspecific binding of the secondary antibody using normal serum from the species in which the secondary antibody was generated (e.g., if the secondary antibody is swine-anti-rabbit antibody, the serum used for blocking would be normal pig serum). A 1:20 dilution in PBS for 10 min should effectively block nonspecific binding; cover tissue sections completely, and place slides in humidifier chamber for incubation at RT (*see Note 4*).
8. Do **not** rinse slides; tap normal serum off slides (turn slides sideways on paper towels) and wipe away excess. Place slides back into chamber.
9. Add primary antibody (polyclonal and monoclonal rabbit-anti-mouse TNF- α antibodies have been used, that cross-react with rat) to each section of the experimental slides as well as to each section of the positive control slides (*see Notes 5 and 6*). Add negative isotype-matched control antibody or normal serum from the species that the primary antibody was produced (normal rabbit serum in this case) to each section of the negative control slides. Incubate slides in humidifier chamber for 30 min at RT (*see Note 7*).
10. Rinse slides in fresh PBS, 2 times, 5 min each.
11. Wipe back of slides off and return to humidifier chamber. Add pre-absorbed secondary antibody to all sections of all slides. Incubate in chamber at RT for 45 min.
12. Rinse slides in fresh PBS, 2 times, 5 min each. Do not let slides dry before developing.
13. Prepare DAB for developing reaction: use 1 silver tablet (DAB) and 1 gold tablet (H_2O_2) per mL 0.05 M Tris-HCl buffer, pH 7.65. Vortex well.
14. Enhancement of DAB is routinely performed using 0.01 M imidazole (8,9). A 1 M imidazole solution (68.08 mg/mL 0.05 M Tris-HCl) is prepared, and a 1:100 dilution is prepared using the DAB solution described earlier.
15. Add DAB/imidazole solution to each section of all slides. Develop for 3–10 min, watching for appearance of brown color (monitor under a microscope).
16. Stop the development of color by rinsing slides in distilled H_2O , 3 times, 5 min each.
17. Counter stain slides with Mayer's hematoxylin for 2 min.
18. Rinse slides in distilled H_2O , changing until purple color is gone from H_2O .
19. Dehydrate slides through graded alcohol (70, 90, 90, 100, 100%), 2 min each, and through xylene, 3 times, 2 min each.
20. Wipe slides carefully and mount coverslips onto slides using permount. Tap coverslips lightly with forceps to remove any bubbles.

3.4. In Situ Hybridization Procedure

3.4.1. Pretreatment of Mounted Sections

1. Post-fix: Fix sections again in 4% paraformaldehyde, RT, 10 min.
2. Wash slides in 0.5X SSC (prepare 1/40 dilution of 20X SSC consisting of 3 M NaCl, 0.3 M sodium citrate, pH 7.0, w/HCl. Filtered, DEPC-treated, and autoclaved), RT, 10 min.
3. Flood sections with 37°C proteinase K (250 µg/mL in 50 mM Tris-HCl, pH 8.0, 10 mM CaCl₂; store at -20°C; good for 3 mo as stock solution) at 5 µg/mL in 2X SSC, and incubate for 15 min at 37°C.
4. Rinse with 2X SSC at RT.
5. Sections to be treated with RNase-A as a negative control should be performed at this step (see **Note 8**). Keep all glassware separate. Working RNase-A solution of 200 µg/mL: 1000 µL RNase stock (10 mg/mL) + 50 mL RNase buffer (10 mM Tris-HCl, pH 8.0; 1 mM EDTA; 500 mM NaCl) (7).
6. Acetylate sections with freshly prepared 0.5% acetic anhydride in 0.1 M TEA (1.87 g TEA in 100 mL DEPC H₂O), pH 7.2, for 5 min. (Add 500 µL acetic anhydride to TEA and immediately pour onto slides).
7. Rinse slides in 0.5X SSC at RT.

3.4.2. Prehybridization

1. Flood sections with 42°C hybridization solution which is kept in water bath while in use:

	Stock	10 mL	30 mL	[working]
a. Deionized formamide		2.0 mL	6.0 mL	20%
Deionize in AG-501-XA resin, 30 min, RT; pH to 7.0 w/0.1 N HCl. Store in 50 mL aliquots at -20°C.				
b. 20X SSC		2.5 mL	7.5 mL	5X
3 M NaCl, 0.3 M sodium citrate, pH 7.0 w/HCl. Filter, DEPC-treat, and autoclave.				
c. 50% Dextran sulfate		1.0 mL	3.0 mL	5%
Add 10 g in 20 mL DEPC H ₂ O. Stir several hours at 37°C to dissolve.				
d. 10 mg/mL tRNA		1000 µL	3000 µL	100 µg/mL
The amount in each bottle is different and is labeled as mg of solid (e.g., 108 mg solid; add 10.8 mL sterile double-distilled H ₂ O to bottle and triturate). Aliquot (4 mL) and store at -20°C.				
e. 10 mg/mL SalSpDNA		1000 µL	3000 µL	100 µg/mL
(see Note 9)				

Shear DNA by passing it 12 times rapidly through a 17-gauge needle. Boil 10 min, adjust concentration to 10 mg/mL, and store in 1 mL aliquots at -20°C. Boil greater than the amount needed 5 min prior to use.

(continued)

(continued)

	Stock	10 mL	30 mL	[working]
f.	50X Denhardt's 1 g Ficoll Type 400, 1 g polyvinylpyrrolidone, 1 g BSA fraction V. Add DEPC H ₂ O to 100 mL while slowly stirring on a stir plate. Filter-sterilize (0.22 filter), aliquot (4 mL), and store at -20°C.	200 µL	600 µL	1X
g.	1 M DTT Dissolve 3.09 g DTT in 20 mL 0.01 M sodium acetate, pH 5.2. Filter-sterilize. Prepare 1 mL aliquots and store at -20°C. Freeze-thaw as needed, but store on ice. Good for 6 mo at 1 M.	100 µL	300 µL	10 mM
h.	DEPC H ₂ O (Bring to)	10 mL	30 mL	—

2. Place slides in a humidified container containing filter paper, wooden sticks, and 42°C box buffer (4X SSC containing 50% formamide: for 50 mL or 2 boxes worth, use 10 mL 20X SSC, 25 mL deionized formamide, and 15 mL DEPC H₂O). To maintain humidity, use a Tupperware container with 2 sheets of Whatman filter paper at the bottom and wooden sticks directly on top of the paper; flood sticks and paper with box buffer, and place slides on top of sticks.
3. Incubate slides at 42°C for 2 h.

3.4.3. ³⁵S Oligonucleotide Labeling

1. An antisense 30-mer cDNA oligonucleotide probe (5'-GTC-CCC-CTT-CTC-CAG-CTG-GAA-GAC-TCC-TCC-3') that is complementary to mRNA specific for rat TNF-α is 3'-labeled with ³⁵S-dCTP.
2. Add reagents, as listed below, to microfuge tube *in sequence* (see **Note 10**).

<u>TDT Reaction</u>	or	<u>Boehringer Mannheim labeling kit</u> (better kit, but more expensive)
a. oligonucleotide probe	1 µL (400 ng)	1 µL (400 ng)
b. ³⁵ S dCTP 0.125 mCi total final activity	10 µL	10 µL
c. DEPC H ₂ O	14.7 µL	16.8 µL
d. TdT (Gibco-BRL; 75 units/40 µL rxn vol)	6.3 µL (75 units/40 µL rxn vol)	3 µL (75 units/40 µL rxn vol)
e. 5X buffer	8 µL	6 µL
f. CoCl ₂ 25 mM, 2 mM in solution	—	3.2 µL

3. Incubate at 37°C for 1 h.
4. Stop reaction with the addition of 1X buffer (prepared from 5X buffer) to bring reaction volume to 100 µL (should add 60 µL of 1X buffer).
5. Run probe through a P6 column (Bio-Spin 6 column). Gravity drain the P6 column, never letting the column dry. Do **not** centrifuge as stated in the directions. Prime the column with 5X SSC containing 10 mM DTT, 3 times. With the 5X

SSC containing 10 mM DTT 200 μ L above the resin, add the total volume of the labeled oligo. Collect 12–200 μ L fractions in microfuge tubes while maintaining the liquid level of the column about 200 μ L above the resin.

6. Spot 1 μ L from each fraction collected onto 2 separate GF/C Whatman disks and completely dry. Place 1 of each pair of the disks in 4 mL scintillation fluid; this is considered Total radioactivity.
7. Check the % incorporation by washing the other disk of each pair with 5% TCA wash (made fresh), 3 times, 20 mL each (swirl disks 3 times in TCA and decant), to remove unbound radioactivity; follow with 1 wash in 100% EtOH to speed the drying process. Completely dry disks and place in 4 mL scintillation fluid. This is Bound radioactivity.
8. Count vials for 1 min each in liquid scintillation counter.
9. Calculations:

% Incorporation = bound cpm/total cpm

Specific Activity = bound cpm/ng probe

Add enough labeled probe to the hybridization solution to give between $0.3\text{--}0.175 \times 10^6$ bound cpm/ μ L. If count is $>300,000$ cpm, background will be too high; if count is $<175,000$, signal will be too weak (*see Note 11*).

3.4.4. Hybridization

1. Dilute probe in hybridization solution, mix thoroughly, and place at 42°C. Each section/slide should have 1×10^6 bound cpm/100 μ L solution.
2. Decant prehybridization solution from sections and pipet 100 μ L of hybridization solution containing the probe onto each section. Tissue sections should receive 100 μ L per section. Cover with baked, autoclaved coverslips, and remove any air bubbles.
3. Place slides back into the container and incubate at 42°C for 15–18 h.

3.4.5. Posthybridization

1. Wash slides 2 times with 2X SSC, RT, 10 min each to remove nonadherent radioactivity. Dispose of radioactive aqueous waste properly.
2. Wash slides once with 1X SSC, 42°C, 60 min.
3. Dehydrate sections in ascending series of ethanol (50%, 70%, and 95%) containing 0.3 M NH_4Ace , 3–5 min each. For a 0.3 M solution in EtOH, add 23.12 g NH_4Ace (FWt = 77.08) and bring to 1 L.
4. Air-dry slides.

3.4.6. Autoradiogram

Use dark room safe light with #1 red filter only, *see Note 12*.

1. Remove NTB-2 emulsion from refrigerator and place in 42°C bath to dissolve emulsion.
2. Warm 10 ml DEPC H_2O to 42°C.
3. Using a slide mailer, mix the 10 mL H_2O with about 10 mL of melted emulsion.

4. Dip 2 blank slides into the emulsion mixture to remove any air bubbles.
5. Dip completely dry section-mounted slides into emulsion for 3–5 s, wipe back of slides to remove excess emulsion, and place vertically in a drying rack.
6. Air dry slides for **minimum** of 1 h in a vertical position. It is critical that the emulsion is *completely* dry. Otherwise, background will be too grainy and samples will form mold.
7. Place slides in slide boxes with a blank slide separating the experimental slides from a packet of desiccant. Tape box shut (all slides must be “safe” prior to this step) and place slide boxes inside another box. Wrap *this* box with foil and place box in 4°C. Let slides expose emulsion for 1–10 wk (for ³⁵S). If exposure extends longer than 2 wk, replace desiccant.

3.4.7. Slide Development

1. Remove slides, D-19 developer, and Rapid Fix from 4°C at least 1 h before use. Developer should be about 16°C.
2. Develop slides for 3 min in D-19 developer, diluted 1:1 with H₂O. Prepare developer with distilled H₂O, and then dilute.
3. Stop reaction for 20 s in H₂O.
4. Fix for 3 min in Kodak Rapid Fix (solution A only).
5. Rinse slides 3 times, 5 min each in H₂O.
6. Counterstain slides for 1 min in Mayer’s hematoxylin stain.
7. Rinse slides in distilled H₂O, 2 times, 10 dips each.
8. Counterstain slides for 1 min in Eosin-Y (alcoholic) stain.
9. Rinse slides in distilled H₂O, 2 times, 10 dips each.
10. Dehydrate slides in 100% alcohol, 2 times, 10 dips each; also through xylene, 2 times, 10 dips each.
11. Wipe slides carefully and mount coverslips onto slides using permount. Tap coverslips lightly with forceps to remove any bubbles.

3.5. Results

3.5.1. Immunolocalization of TNF- α Staining

Representative TNF- α stained sections of the locus coeruleus and the hippocampus from the rat brain is shown in **Fig. 1**. Immunohistochemical staining for TNF- α is detected in both the neuron cell body and the neuron processes. Serial tissue sections stained with normal rabbit serum were negative for TNF- α (data not shown).

3.5.2. Localization of mRNA Specific for TNF- α

Figure 2A depicts constitutive expression of accumulated mRNA specific for TNF- α in a region of the rat brain containing the locus coeruleus by *in situ* hybridization. The accumulation of TNF- α mRNA is localized to neurons; the co-localization of silver grains with immunoreactivity for the neuron-specific antigen neurofilament (NF)-200 is depicted in the serial section (**Fig. 2B**).

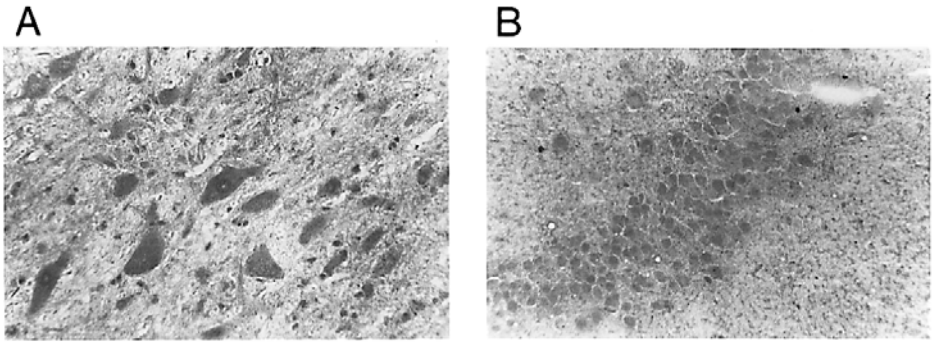


Fig. 1. Immunoperoxidase stained rat (A) locus coeruleus and (B) hippocampal brain slices. TNF- α -stained neuron cell bodies and neuronal processes are evident throughout both sections. Note: Same magnification (25 \times) and light intensity (70%) used for both pictures.

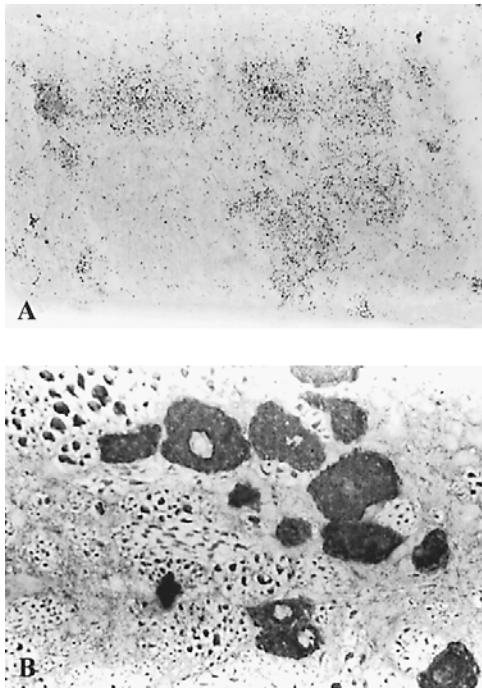


Fig. 2. Rat tissue sections obtained from a region of the brainstem containing the locus coeruleus probed for mRNA specific for rat TNF- α using *in situ* hybridization (A). The serial tissue section immunoperoxidase stained for the neuron-specific antigen, neurofilament 200 (B).

This technique is applicable to other tissues and/or cells, such as macrophage (5,7), human corneal tissue (6), and human retinal pigment epithelium (10).

4. Notes

- 1. If a crackling sound is audible, only submerge bolt with OCT-covered tissue specimen approximately 10–20 s longer and remove from liquid N₂. Repeat “dipping” process until OCT is frozen around tissue. Prolonged submersion in liquid N₂ may cause OCT base to break away from bolt.
- 2. Immerse slides into staining dish containing histostick solution for 20 s (10–15 dips). Remove slides and allow to completely dry. Store coated slides in dust-free slide boxes.
- 3. Do **not** heat paraformaldehyde above 84°C; it may become unstable and volatile.
- 4. Although a 1 : 20 dilution of normal serum in PBS for 10 min blocked nonspecific binding well, the dilution and incubation time may need to be adjusted depending on the serum used. Normal serum purchased from different companies varied in the ability to block effectively (eg., 1 : 20 dilution for 10 min vs a 20% solution for 30 min). This will have to be adjusted depending on the serum used. Also, if background staining is high, the normal serum (used for the first blocking step, **Subheading 3.3., step 7**) +/- 0.1% BSA in PBS may be included in the primary antibody incubation step to further aid in blocking non-specific staining.
- 5. The proper dilution (if using an anti-serum) or concentration of antibodies (primary and secondary) to be used for effective staining of tissue sections needs to be determined by performing checkerboard titrations. Various dilutions of the antibodies, as suggested by the manufacturer, should be run in combination to determine the optimal staining of experimental and control tissue sections. An example of a checkerboard titration using 9 slides is shown below:

1° Ab	1 : 25	1	2	3
	1 : 50	4	5	6
	1 : 10	7	8	9
		1 : 50	1 : 100	1 : 200
		2° Ab		

- 6. Positive control slides should consist of a preparation known to contain TNF- α protein. Cultured mononuclear cells or peritoneal macrophage harvested, fixed, and permeabilized at the peak of cytokine production after in vitro stimulation with LPS could be used as a positive control for TNF- α staining.
- 7. Negative control slides should consist of one or more of the following: Tissue sections stained with 1) a primary isotype-matched immunoglobulin of irrelevant antigen specificity at the same concentration as the cytokine-specific antibody; 2) a preincubation of the cytokine-specific antibody with its target cytokine at a 1 : 10 molar ratio for 30 min prior to addition to the tissue in order to abolish immunoreactivity; and 3) the secondary antibody staining alone.

8. Control samples may include: RNase-pretreated sections (200 $\mu\text{g/mL}$ for 20 min); hybridization of tissue sections with unlabeled oligonucleotide; and/or hybridization with the sense-TNF oligonucleotide probe, all of which lack specific signal detection.
9. The working concentration of both tRNA and SalSpDNA in the prehybridization and hybridization solutions is routinely 100 $\mu\text{g/mL}$. Our laboratory has also used a working concentration of 10 $\mu\text{g/mL}$ for each, resulting in successful labeling.
10. The volumes of ^{35}S , TDT, probe, and H_2O change as the concentrations are sometimes changed by the company. Adjust the concentrations to meet the aforementioned reaction protocol for a final volume of 40 μL .
11. It is critical to purchase the ^{35}S from New England Nuclear, because this has a sufficiently low amount of DTT, allowing the added enzyme to work. Other sources contain too high an amount of DTT, such that the enzyme does not work as efficiently.
12. This step must be performed in a darkroom, using only safe lights with #1 red filters for illumination.

References

1. Eskandari, M. K., Nguyen, D. T., Kunkel, S. L., and Remick, D. G. (1990) WEHI 164 subclone 13 assay for TNF: sensitivity, specificity, and reliability. *Immunol. Invest.* **19**, 69–79.
2. Khabar, K. S. A., Siddiqui, S., and Armstrong, J. A. (1995) WEHI-13VAR: a stable and sensitive variant of WEHI 164 clone 13 fibrosarcoma for tumor necrosis factor bioassay. *Immunol. Lett.* **46**, 107–110.
3. Ignatowski, T. A. and Spengler, R. N. (1994) Tumor necrosis factor- α : presynaptic sensitivity is modified after antidepressant drug administration. *Brain Res.* **665**, 293–299.
4. Chou, R. C., Dong, X. L., Noble, B. K., Knight, P. R., and Spengler, R. N. (1998) Adrenergic regulation of macrophage-derived tumor necrosis factor- α generation during a chronic polyarthritis pain model. *J. Neuroimmunol.* **82**, 140–148.
5. Kunkel, S. L., Spengler, M., May, M. A., Spengler, R., Larrick, J., and Remick, D. G. (1988) Prostaglandin E2 regulates macrophage-derived tumor necrosis factor gene expression. *J. Biol. Chem.* **263**, 5380–5384.
6. Elner, V. M., Strieter, R. M., Pavilack, M. A., Elner, S. G., Remick, D. G., Danforth, J. M., and Kunkel, S. L. (1991) Human corneal interleukin-8. IL-1 and TNF-induced gene expression and secretion. *Am. J. Pathol.* **139**, 977–988.
7. Remick, D. G., Scales, W. E., May, M. A., Spengler, M., Nguyen, D., and Kunkel, S. L. (1988) In situ hybridization analysis of macrophage-derived tumor necrosis factor and interleukin-1 mRNA. *Lab. Invest.* **59**, 809–816.
8. Straus, W. (1982) Imidazole increases the sensitivity of the cytochemical reaction for peroxidase with diaminobenzidine at a neutral pH. *J. Histochem. Cytochem.* **30**, 491–493.
9. Trojanowski, J. Q., Obrocka, M. A., and Lee, V. M.-Y. (1983) A comparison of eight different chromogen protocols for the demonstration of immunoreactive neurofila-

- ments or glial filaments in rat cerebellum using the peroxidase-antiperoxidase method and monoclonal antibodies. *J. Histochem. Cytochem.* **31**, 1217–1223.
10. Elner, V. M., Burnstine, M. A., Strieter, R. M., Kunkel, S. L., and Elner, S. G. (1997) Cell-associated human retinal pigment epithelium interleukin-8 and monocyte chemotactic protein-1: immunochemical and in situ hybridization analyses. *Exp. Eye Res.* **65**, 781–789.

Translocation of p47^{phox} and Activation of NADPH Oxidase in Mononuclear Cells

Ahmad Aljada, Husam Ghanim, and Paresh Dandona

1. Introduction

Diabetes mellitus is associated with increased reactive oxygen species (ROS) generation by mononuclear cells (MNC) and an increased oxidative load, which causes oxidative damage to proteins, lipids and DNA (1–3). Recently, we have demonstrated that glucose challenge causes an increase in ROS generation by MNC and polymorphonuclear cells (PMNL). We have also demonstrated that the suppression of ROS generation by MNC by diphenylene iodonium (DPI), a specific inhibitor of NADPH oxidase and the membrane enzyme that generates the superoxide ($O_2^{\bullet -}$) radical, is significantly diminished in the obese and diabetics when compared with normal subjects (4). The assay system used in our ROS generation studies largely detects the superoxide radical, which is produced by the conversion of molecular O_2 by NADPH oxidase (5,6). Thus, it would appear that NADPH oxidase activity increases following glucose challenge and that it is relatively non-suppressible in the obese. NADPH oxidase consists of multiple subunits. Equimolar amounts of p47^{phox} and p67^{phox} in the cytosol combine to form a highly basic 250 kDa protein. During activation, this complex migrates from the cytosol to the membrane where this complex combines with cytochrome b_{558} , which in turn, consists of gp91^{phox} and p22^{phox}. Rac 2, the fifth component of the enzyme migrates to the membrane in association with p47^{phox}, which without it, is unable to reach the membrane (7–10). Thus, p47^{phox} is cardinal to the functional integrity of NADPH oxidase. The translocation of p47^{phox} subunit from the cytosol to the membrane can be used as an index of NADPH oxidase activation. In this study, MNC were

isolated from normal subjects prior to and following glucose challenge (75 g) at 1, 2, and 3 h. Plasma membranes were then isolated from MNC lysates by differential centrifugation. The effect of glucose on p47^{phox} subunit levels in MNC total lysate, the cytosol fraction, and the membrane fraction were then measured by Western blotting technique.

2. Materials

1. PMN isolation medium (Robbins Scientific Corp., Sunnyvale, CA).
2. Monoclonal anti-p47^{phox} antibody (Transduction Labs, Lexington, KY).
3. Peroxidase-conjugated goat anti-mouse immunoglobulin (BioRad, Hercules, CA).
4. Electrophoresis apparatus and gel transfer system (BioRad).
5. Super signal chemiluminescence reagent (Pierce, Rockland, IL).

3. Methods

3.1. MNC Isolation

1. Collect blood samples in EDTA containing tubes. The blood must be separated within 1 h (*see Note 1*).
2. Carefully layer 3.5 mL of the anticoagulated whole blood over 3.5 mL of the PMN medium in 15 mL centrifuge tube (*see Note 2*).
3. Centrifuge the whole blood layered over the PMN medium for 450g for 30 min in a swing out rotor at 18–22°C.
4. After centrifugation, two bands will separate out. The top band will consist of MNC while the bottom will consist of PMNL; the RBC are pelleted.
5. Harvest the MNC band with a Pasteur pipette and wash the cells twice with Hank's Balanced Salt Solution (HBSS).

3.2. Preparation of Subcellular Monocytic Fractions

MNC subcellular fractions can be prepared by either Percoll density centrifugation (*II*) or differential centrifugation. The method of choice is optional. However, differential centrifugation is easier and more convenient since it can be carried out in an Eppendorf microcentrifuge.

3.2.1. Differential Centrifugation

1. Resuspend the MNC in 1 mL ice-cold HEPES Buffer (10 mM HEPES, 100 mM KCl, 3 mM NaCl, 3.5 mM MgCl₂, 1 mM ATP (Na₂) and 0.1% Triton X-100, pH 7.3, 1 mM phenylmethylsulfonylfluoride, 100 U/mL aprotinin).
2. Disrupt the cells with a Potter homogenizer.
3. Remove the nuclei and unbroken cells by centrifugation (15 min, 500g).
4. Centrifuge the supernatant (15 min at 17,000g) to obtain the plasma membranes and mitochondria containing fraction. The pellet and the crude cytosol can be stored at –70°C.

3.3. p47^{phox} Western Blot

1. Plasma membranes are solubilized by the addition of 100 μ L of 1X lysis buffer (1% sodium dodecyl sulfate [SDS], 1 mM sodium ortho-vanadate, 10 mM Tris, pH 7.4).
2. Add equal volume of 2X lysis buffer (2% SDS, 2 mM sodium ortho-vanadate, 20 mM Tris, pH 7.4) to the crude cytosol fraction.
3. Boil for 5 min, sonicate for 10 s and centrifuge at 14,000g for 5 min.
4. Collect the supernatants and determine total protein concentrations using BCA protein assay (Pierce, Rockland, IL).
5. Dilute the samples with an equal volume of 2X gel loading buffer (100 mM Tris-HCl, pH 6.8, 20 mM dithiothreitol, 4% SDS, 0.2% bromophenol blue, and 20% glycerol).
6. Load 15 μ g of lysate into 10% SDS-PAGE.
7. Transfer the gels to polyvinylidene difluoride (PVDF) membrane.
8. Incubate the membrane for 1 h in 5% nonfat dry milk in 0.1% Tween-TBS buffer (20 mM Tris-HCl, pH 7.4, 0.5 mM NaCl) to block protein non-specific binding.
9. Incubate the membrane for 1 h with monoclonal anti-p47^{phox} antibody (diluted 1:250) in 5% milk in 0.1% TTBS.
10. Wash the membrane four times for 15 min each with Tween-TBS (TTBS) and incubate with peroxidase conjugated goat anti-mouse immunoglobulin (diluted 1:3000) for 1 h.
11. Wash the membrane again four times for 15 min each.
12. Finally, incubate the membrane in Pierce super signal chemiluminescence reagent, blot dry, and expose the membrane to X-ray films.

3.4. Results

The levels of p47^{phox} subunit, the key protein component of NADPH oxidase, in total MNC lysates did not increase at 1 h and increased significantly at 2 and 3 h following glucose intake (**Fig. 1**). However, MNC plasma membranes homogenates increased at 1 and 2 h after glucose intake. Levels of p47^{phox} started to decrease thereafter and returned to basal levels at 3 h (**Fig. 2**). On the other hand, p47^{phox} protein level decreased in MNC crude cytosol fraction at 1 h indicating that p47^{phox} subunit translocated from the cytosol to the plasma membrane. p47^{phox} protein level in the cytosol fraction then increased at 2 and 3 h (**Fig. 2**). This may be the result of increased biosynthesis of p47^{phox} in MNC. No increase was observed following the intake of 300 mL of water containing saccharine. Our data demonstrate clearly that glucose challenge in normal subjects results constantly in p47^{phox} subunit translocation from the cytosol to the membrane and an increase in the expression of p47^{phox}. This is consistent with the fact that hyperglycemia increases oxidative stress and may explain the mechanism causing the oxidative stress.

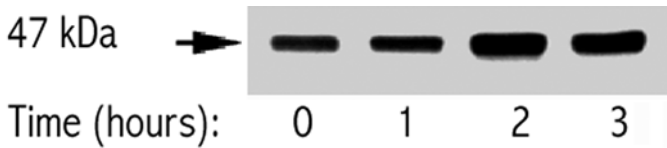


Fig. 1. A representative Western blot of MNC total cell lysates showing the relative expression of p47^{phox} in MNC following glucose challenge. Note that p47^{phox} expression is induced at 2 and 3 h after glucose intake. There was no significant change in p47^{phox} levels at 1 h. Maximum induction is observed at 2 h. p47^{phox} began to decline by 3 h.

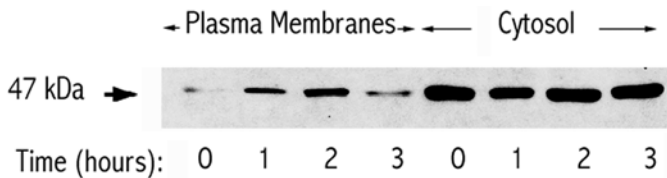


Fig. 2. A representative Western blot showing the relative expression of p47^{phox} in plasma membranes and crude cytosolic fractions of MNC following glucose intake. Note that there was an increase of p47^{phox} in the membrane fraction at 1 and 2 h; membrane p47^{phox} fraction declined at 3 h. On the other hand, p47^{phox} levels declined at 1 h and then increased at 2 and 3 h.

4. Notes

1. Macrophages in culture generally show progressive loss of the capability to produce microbicidal oxidants. Similarly, blood monocytes placed in culture lose the capacity to produce superoxide. Thus, in vivo glucose challenge is the best model to study acute hyperglycemia effect on MNC. We have also used similar in vivo models where we have shown that p47^{phox} levels in MNC and ROS generation by MNC decrease following vitamin E and glucocorticoids therapy (12,13). In addition, we have demonstrated that p47^{phox} levels increase following triiodothyronine administration, an agent which causes an increase in ROS generation by MNC.
2. When layering the whole blood over the PMN medium, take care to avoid mixing the blood with the media. Centrifugation conditions will be different if either the size or the tube or the amount of blood or medium is changed.

References

1. Hiramatsu, K. and Arimori, S. (1988) Increased superoxide production by mononuclear cells of patients with hypertriglyceridemia and diabetes. *Diabetes* **37**, 832–837.
2. Jain, S. K. (1989) Hyperglycemia can cause membrane lipid peroxidation and osmotic fragility in human red blood cells. *J. Biol. Chem.* **264**, 340–345.

3. Dandona, P., Thusu, K., Snyder, B., Makowski, J., Armstrong, D., and Nicotera, T. (1996) Oxidative damage to DNA in diabetes mellitus. *Lancet* **347**, 444–445.
4. Thusu, K., Dandona, P., Khurana, U., Aljada, A., Love, A., and Nicotera, T. (1995) Relative non-suppressibility of NADPH oxidase in diabetes mellitus. 55th Annual meeting and Scientific Sessions of the American Diabetes Association in Atlanta, GA, 1995.
5. Tosi, M. F. and Hamedani, A. (1992) A rapid specific assay for superoxide release from phagocytes in small volumes of whole blood. *Am. J. Clin. Pathol.* **97**, 566–573.
6. Hancock, J. T. and Jones, O. T. (1987) The inhibition of diphenylene iodonium and its analogues of superoxide generation by macrophages. *Biochem. J.* **242**, 103–107.
7. Park, J. W., Ma, M., Ruedi, J. M., Smith, R. M., and Babior, B. M. (1992) The cytosolic components of the respiratory burst oxidase exist as a M(r) approximately 240,000 complex that acquires a membrane-binding site during activation of the oxidase in a cell-free system. *J. Biol. Chem.* **267**(24), 17,327–17,332.
8. Park, J. W., Benna, J. E., Scott, K. E., Christensen, B. L., Chanock, S. J., and Babior, B. M. (1994) Isolation of a complex of respiratory burst oxidase components from resting neutrophil cytosol. *Biochemistry* **33**(10), 2907–2911.
9. el Benna, J., Ruedi, J. M., and Babior, B. M. (1994) Cytosolic guanine nucleotide-binding protein Rac2 operates in vivo as a component of the neutrophil respiratory burst oxidase. Transfer of Rac2 and the cytosolic oxidase components p47^{phox} and p67^{phox} to the submembranous actin cytoskeleton during oxidase activation. *J. Biol. Chem.* **269**(9), 6729–6734.
10. Heyworth, P. G., Curnutte, J. T., Nauseef, W. M., Volpp, B. D., Pearson, D. W., Rosen, H., and Clark, R. A. (1991) Neutrophil nicotinamide adenine dinucleotide phosphate oxidase assembly. Translocation of p47-phox and p67-phox requires interaction between p47-phox and cytochrome b558. *J. Clin. Invest.* **87**(1), 352–356.
11. Berregard, N., Heiple, J. M., Simons, E. R., and Clark, R. A. (1983) Subcellular localization of the b-cytochrome component of the human neutrophil microbicidal oxidase: translocation during activation. *J. Cell. Biol.* **97**, 52–60.
12. Dandona, P., Suri, M., Hamouda, W., Aljada, A., Kumbkarni, Y., and Thusu, K. (1999) Hydrocortisone induced inhibition of ROS by PMN leucocytes. *Crit. Care Med.* **27**(11), 2442–2444.
13. Dandona, P., Thusu, K., Hafeez, R., Abdel-Rahman, and Chaudhuri, A. (1998) Effect of hydrocortisone on oxygen free radical generation by mononuclear cells. *Metabolism* **47**(7), 788–791.

Activation of Nuclear Factor- κ B (NF- κ B) in Mononuclear Cells (MNC)

Ahmad Aljada, Husam Ghanim, and Paresh Dandona

1. Introduction

The transcription factor NF- κ B was first identified as a regulator of the expression of the kappa light-chain gene in murine B lymphocytes (1). It has a central role in the immunological processes and regulates a wide range of genes in a rapid fashion (2). NF- κ B interacts with its inhibitor protein I κ B and activation of NF- κ B causes it to move into the nucleus and this is controlled by the phosphorylation and subsequent degradation of I κ B (3,4). The activated form of NF- κ B is a heterodimer, which usually consists of two proteins, a p65 (relA) subunit and a p50 subunit. Other subunits (rel, relB, v-rel, and p52) can also bind to the activated NF- κ B and thus can activate different sets of genes.

NF- κ B regulates the expression of many genes involved in the immune and inflammatory responses (5–7). We have recently demonstrated that glucose challenge causes an increase in reactive oxygen species (ROS) generation by MNC and polymorphonuclear cells (PMNL). We have also shown that glucose intake results in NADPH oxidase activation as demonstrated by p47^{phox} subunit translocation from the cytosol to the membrane and an increase in the expression of p47^{phox} subunit. The activation of NADPH oxidase, the membrane enzyme that generates the superoxide ($O_2^{\bullet -}$) radical (8), is consistent with the fact that hyperglycemia increases oxidative stress (9,10). The increase in p47^{phox} subunit may be modulated through an increase in the transcription of pro-inflammatory genes modulated by NF- κ B. To test whether glucose intake causes NF- κ B activation, MNC were isolated from normal subjects prior to and following glucose challenge (75 g) at 1, 2, and 3 h. Nuclear protein extracts

were then prepared from MNC and the intranuclear NF- κ B levels were then measured by electrophoretic mobility-shift assay (EMSA).

2. Materials

1. PMN isolation medium (Robbins Scientific Corp., Sunnyvale, CA).
2. BCA protein assay (Pierce, Rockland, IL).
3. NF- κ B binding protein detection kit (Life Technologies, Long Island, NY).
4. Probe Quant G-50 micro columns (Amersham Pharmacia Biotech, Piscataway, NJ).

3. Methods

3.1. MNC Isolation

1. Collect blood samples in EDTA containing tubes. The blood must be separated within 1 h (*see Note 1*).
2. Carefully layer 3.5 mL of the anticoagulated whole blood over 3.5 mL of the PMN medium in 15 mL centrifuge tube (*see Note 2*).
3. Centrifuge the whole blood layered over the PMN medium for 450g for 30 min in a swing out rotor at 22°C.
4. After centrifugation, two bands will separate out. The top band will consist of MNC while the bottom will consist of PMNL; the RBC are pelleted.
5. Harvest the MNC band with a Pasteur pipet and wash the cells twice with Hank's Balanced Salt Solution (HBSS).

3.2. DNA-Binding Protein Extracts Preparation

DNA-binding protein extracts are prepared from MNC by the method described by Andrews et al. (*II*).

1. Resuspend MNC pellets in 400 μ L cold buffer A (10 mM HEPES-KOH, pH 7.9, 1.5 mM $MgCl_2$, 10 mM KCl, 0.5 mM dithiothreitol [DTT], 0.2 mM PMSF).
2. Allow cells to swell on ice for 10 min, and then vortex for 10 s.
3. Centrifuge the sample for 10 s at 14,000g and discard the supernatant fraction.
4. Resuspend the pellet in 100 μ L of cold buffer B (20 mM HEPES-KOH, pH 7.9, 25% glycerol, 420 mM NaCl, 1.5 mM $MgCl_2$, 0.2 mM EDTA, 0.5 mM DTT, 0.2 mM PMSF).
5. Incubates the sample on ice for 20 min for high-salt extraction, centrifuge for 2 min at 14,000g and then collect the supernatant fraction.
6. Determine the total protein concentrations using BCA protein assay (Pierce) or any available protein assay.

3.3. EMSA

NF- κ B gel retardation assay can be performed using NF- κ B binding protein detection kits that are commercially available. NF- κ B binding protein detection kit (Life Technologies, Long Island, NY) is described in this chapter.

3.3.1. Labeling the Double-Stranded Oligonucleotide

1. Label the double-stranded oligonucleotide containing a tandem repeat of the consensus sequence for the NF- κ B binding site with γ - 32 P by T4 kinase. The NF- κ B oligonucleotide comprises the sequences:
5'-GATCCAAGGGGACTTTCCATGGATCCAAGGGGACTTTCCATG-3'
3' - GTTCCCCTGAAAGGTACCTAGGTTCCCCTGAAAGGTACCTAG-5'
2. Add in a 1.5 mL microcentrifuge tube the following reagents: 1 μ L double-stranded oligonucleotide (5 ng); 5 μ L 5X polynucleotide kinase buffer (5X = 300 mM Tris, pH 7.5, 50 mM MgCl_2 , 75 mM β -mercaptoethanol and 1.65 μ M ATP); 100 μ Ci [γ - 32 P]ATP; x μ L H_2O to give a final volume of 25 μ L; add 1 μ L T4 kinase (5 units).
3. Incubate 45 min at 37°C.
4. Remove the unincorporated [32 P]ATP using Probe Quant G-50 micro columns (see **Note 3**) by applying the reaction to the micro column and spinning the tube in a microcentrifuge at 3,000 rpm for 2 min.
5. Determine the percentage of radioactive incorporation of [32 P]ATP by counting a 1 μ L aliquot in a scintillation counter (see **Note 4**).

3.3.2. Gel Retardation Assay

1. Preincubate the following mixture at 4°C for 15 min: 5–10 μ g Sample protein; 5 μ L 5X Incubation buffer; (5X = 50 mM Tris, pH 7.5; 500 mM NaCl; 5 mM DTT; 5 mM EDTA; 20% (v/v) glycerol and 0.4 mg/mL sonicated salmon sperm DNA); H_2O to a final volume of 25 μ L including the 32 P-labeled oligonucleotide volume (see **Note 5**).
2. Add labeled oligonucleotide (40,000–100,000 cpm) to the mixture and incubate at room temperature for 20 min (see **Note 6**).
3. Add 2 μ L 0.1% (w/v) bromophenol blue dye to each sample and load the samples onto 6% nondenaturing polyacrylamide gel. A 15 \times 17 cm gel, 0.8 mm thick with a 10–12 well comb is recommended. Avoid overloading the gel.
4. Dry the gel under vacuum and expose to X-ray film. Analyze gels by densitometry.

3.4. Results

The mean plasma glucose concentration increased from 83.3 ± 7.5 mg/dl at baseline to 108.5 ± 9.4 mg/dl at 1 h. It fell to 107.0 ± 8.8 mg/dl at 2 h and to 70 ± 3.4 mg/dl at 3 h. NF- κ B levels increased in all 6 subjects. However, there were some variations among the subjects. NF- κ B levels in 4 subjects started to increase at 1 h and continued to rise at 2 and 3 h after glucose intake (**Fig. 1**). Two subjects showed an increase at 1 h and continued to increase up to 2 h following glucose intake. NF- κ B levels decreased thereafter (**Fig. 1**). The mean basal intranuclear NF- κ B levels (100%) in the 6 subjects following glucose challenge increased significantly at 1 h ($215 \pm 90\%$) and stayed high at 2 h ($206 \pm 59\%$) and 3 h (245 ± 161) (**Fig. 2**). Kruskal-wallis one-way ANOVA

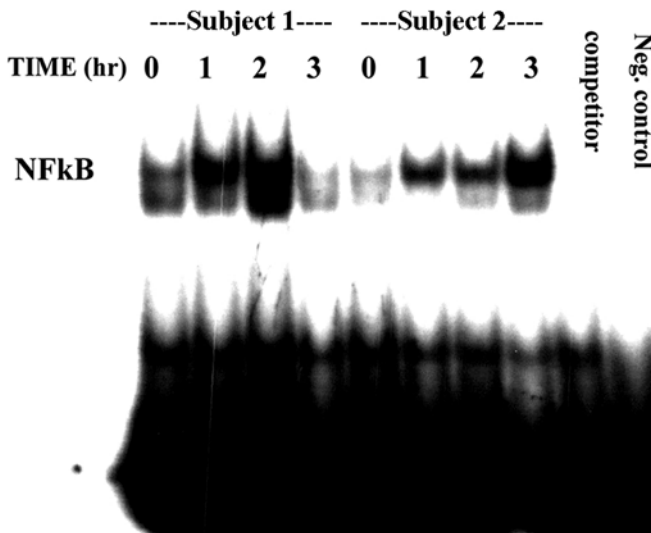


Fig. 1. A representative EMSA gel showing NF- κ B levels in MNC nuclear protein extracts for 2 subjects. The first subject showed an increase in NF- κ B level at 1 h, continued to increase at 2 h and levels declined thereafter at 3 h. The second subject showed a gradual increase in intranuclear NF- κ B levels at 1, 2, and 3 h following glucose challenge. The sequence-specificity of the protein-DNA interactions was determined using a specific unlabeled competitor oligonucleotide for NF- κ B binding site. Lane (competitor) shows the inhibition of NF- κ B binding using 2 μ L of competitor oligonucleotide in subject 1 baseline sample nuclear protein extract. Lane (Neg. control) is radiolabeled NF- κ B double stranded oligonucleotide binding site without any nuclear extract.

statistical analysis was significant at 1, 2, and 3 h ($p < 0.05$). There was no increase in NF- κ B concentrations following the intake of 300 mL of water or saccharine containing water. Our data demonstrate clearly that a challenge with glucose results in an increase in intranuclear NF- κ B in normal subjects. This effect may contribute to hyperglycemia associated increase in superoxide radical and oxidative stress and may lead to diabetic complications. In addition, this simple model is the best model to study the effect of acute hyperglycemia effect on MNC; blood monocytes placed in culture lose the capacity to produce superoxide.

4. Notes

1. Macrophages in culture generally show progressive loss of the capability to produce microbicidal oxidants. Similarly, blood monocytes placed in culture

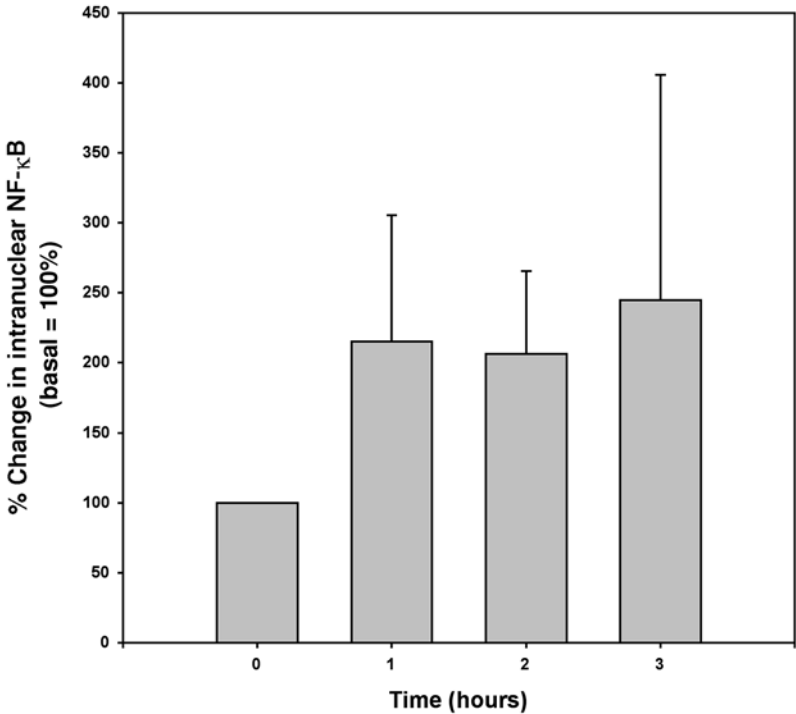


Fig. 2. Relative NF-κB binding to double stranded oligonucleotide containing NF-κB DNA binding site. All values were normalized to 100% for baseline time point and the following values were expressed as percent of basal. The results are presented as mean ± S.D.

lose the capacity to produce superoxide. Thus, in vivo glucose challenge is the best model to study acute hyperglycemia effect on MNC.

2. When layering the whole blood over the PMN medium, take care to avoid mixing the blood with the media. Centrifugation conditions will be different if either the size or the tube or the amount of blood or medium is changed.
3. The unincorporated [P^{32}]ATP can also be removed by NACS.52 PREPAC column (Life Technologies, Long Island, NY) or by ethanol precipitation (12).
4. Typically, the radioactive labeling should yield $>10^5$ cpm/ng.
5. Aspecific competitor oligonucleotide may be added to this reaction to observe competition with the sample. The kit provides an unlabeled double-stranded oligonucleotide (400 ng/ μ L). Competition assays may be performed in parallel with binding assays using 2, 1 and 0.5 μ L of the specific competitor oligonucleotide.
6. The sequence-specificity of the protein-DNA interactions can be determined using a specific competitor oligonucleotide for NF-κB binding site, a negative

control containing labeled oligonucleotide only and a positive control containing 5 µg of HeLa nuclear extract.

References

1. Sen, R. and Baltimore, D. (1986) Multiple nuclear factors interact with the immunoglobulin enhancer sequences. *Cell* **46**, 70S–16.
2. Baldwin, A. S., Jr. (1996) The NF-κB and IκB proteins: new discoveries and insights. *Annu. Rev. Immunol.* **14**, 649–681.
3. Baeuerle, P. E. and Baltimore, D. (1996) NF-κB: ten years after. *Cell* **87**, 13–20.
4. Didonato, J., Mercurio, F., Rosette, C., et al. (1996) Mapping of the inducible IκB phosphorylation sites that signal its ubiquitination and degradation. *Mol. Cell, Biol.* **16**, 1295–1304.
5. Baeuerle, P. and Henkel, T. (1994) Function and activation of NF-κB in the immune system. *Annu. Rev. Immunol.* **12**, 141–179.
6. Grilli, M., Jason, J. S., and Lenardo, M. (1993) NF-κB and rel-participants in a multiform transcriptional regulatory system. *Int. Rev. Cytol.* **143**, 1–62.
7. Liou, H. C. and Baltimore, D. (1993) Regulation of the NF-κB/Rel transcription factor and IκB inhibitor system. *Cell Biol.* **5**, 477–877.
8. Tosi, M. F. and Hamedani, A. (1992) A rapid specific assay for superoxide release from phagocytes in small volumes of whole blood. *Am. J. Clin. Pathol.* **97**, 566–573.
9. Jain, S. K. (1989) Hyperglycemia can cause membrane lipid peroxidation and osmotic fragility in human red blood cells. *J. Biol. Chem.* **264**, 340–345.
10. Marfella, R., Giovanni, V., Acampora, R., La Marca, C., Giunta, R., Lucarelli, C., et al. (1995) Glutathione reverses systemic hemodynamic changes induced by acute hyperglycemia in healthy subjects. *Am. J. Physiol.* **268**, E11 67–73.
11. Andrews, N. C. and Faller, D. V. (1991) A rapid microprep preparation technique for extraction of DNA-binding proteins from limiting numbers of mammalian cells. *Nucleic Acids Res.* **19**, 2499.
12. Ausubel, F., Brent, R., Kingston, R., Moore, D., Seldman, J., Smith, J., and Struhl, H. (1987) *Current Protocols in Molecular Biology*, vol. 1. Green Publishing Associates and Wiley-Interscience, New York, NY, p. 846.

Assay of Intracellular Hydrogen Peroxide Generation in Activated Individual Neutrophils by Flow Cytometry

Yoshikazu Ito and David A. Lipschitz

1. Introduction

Stimulation of neutrophils induces oxidative burst. The generations of oxygen radicals play a central role in host defense against bacteria. Once neutrophils are stimulated by inflammatory or bacterial stimuli, they produce superoxide anion in order to kill phagocytosed microorganisms. In the process, superoxide anion is converted to hydrogen peroxide (H_2O_2) by superoxide dismutase (EC 1.15.1.1) and can then be metabolized through the Fenton reaction to produce highly energetic hydroxyl radicals. Reactive oxygen species (ROS) are released into the phagosome and into the extracellular environment. Superoxide anion released outside cytoplasmic membrane determined by measuring reduction of cytochrome c (*1*). Although it provides the most specific assay to superoxide, it includes purification of neutrophils, needs at least 10^5 neutrophils per assay, and can only measure superoxide released outside neutrophils. A sensitive and simple method to measure ROS produced inside neutrophils is of particular interest. Flow cytometric assay may solve these problems. It provides a sensitive assay to measure intracellular ROS in individual neutrophils (*2,3*).

Dihydrorhodamine 123 (DHR 123) is a nonfluorescent, cell membrane-permeable compound. When the intracellular DHR 123 is oxidized, it is converted to the green fluorescent compound rhodamine 123 (R 123) by ROS (*4*). Then, membrane-impermeable R 123 accumulates in the cells. ROS are generated from superoxide through H_2O_2 during oxidative burst. Fluorescent intensity of R 123 is measured as a function of cellular oxidative

From: *Methods in Molecular Biology*, vol. 196: *Oxidants and Antioxidants: Ultrastructure and Molecular Biology Protocols*
Edited by: D. Armstrong © Humana Press Inc., Totowa, NJ

burst. Intracellular production of oxidants can also be measured using 2', 7'-dichlorofluorescein diacetate (DCFH-DA) and hydroethidine (HE). DHR 123 is more sensitive than the other two dyes that are also a common dye to measure reactive oxygen species (5). It is only possible with DHR 123 to measure the heterogeneous response of weak physiological stimuli such as formyl peptide-induced oxidative burst (6). DHR 123 is more specific to ROS metabolized from superoxide, while DCFH-DA is also sensitive to nitric oxide (7). In this chapter, we describe a method for generation and accumulation of intracellular hydrogen peroxide using DHR 123.

2. Materials

2.1. Instruments

1. FACScan (Becton Dickinson, San Jose, CA).
2. Low-speed centrifuge.
3. Hemocytometer and cover slip.
4. Light microscope.

2.2. Reagents

1. Acid-citrate-dextrose (ACD): Dissolve the following reagents in distilled water (0.14 M citric acid, 0.20 M trisodium citrate and 0.22 M dextrose).
2. Lysing solution: Dissolve 0.8% ammonium chloride (NH_4Cl), 0.08% sodium bicarbonate (NaHCO_3), and 0.08% EDTA in distilled water, pH 6.8.
3. Dihydrorhodamine 123 (DHR 123) (Molecular Probes Inc., Eugene, OR) dissolved in dimethylsulfoxide (DMSO) at 30 mM.
4. Fetal calf serum (FCS).
5. Glucose.
6. Dulbecco's Phosphate-buffered saline (PBS): Make three types of PBS.
 - PBS (-): PBS without anything.
 - PBS-FCS: PBS (-) containing 5 mM glucose and 2% FCS.
 - PBS-FCS-Ca: PBS-FCS containing 0.9 mM calcium chloride and 0.33 mM magnesium chloride.
7. N-formyl-methionyl-leucyl-phenylalanine (FMLP) (Sigma, St. Louis, MO) dissolved in DMSO at 10^{-2} M.
8. 3% acetic acid or Trypan Blue Stain (Life Technologies, Inc., Rockville, MD).

3. Methods

3.1. Preparation of Leukocytes

1. Venous blood is drawn by in ACD solution (approx 5 vol of blood in 1 volume of ACD) (see Note 1).
2. The red cells are lysed by diluting the blood 1:10 with the lysing solution at 15°C.
3. The leukocytes are centrifuged at 160g for 5 min.

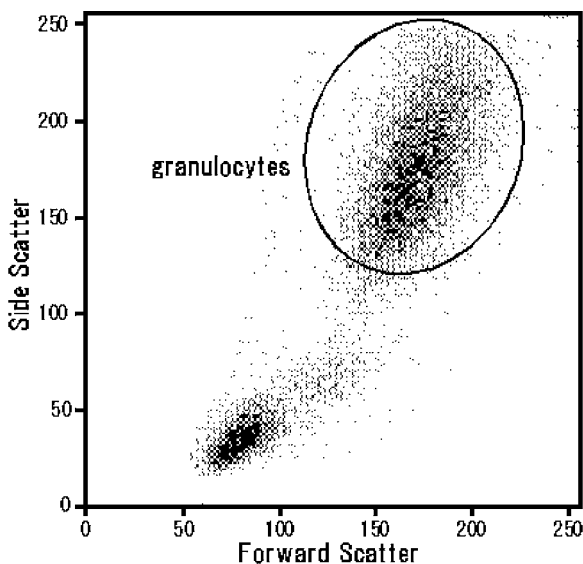


Fig. 1. Before measurements, granulocytes are discriminated from mononuclear cells such as lymphocytes and monocytes by a cytogram of forward angle and 90° light (side) scatter. Green fluorescence intensity of gated cells inside the circle should be measured as neutrophils oxidative burst, since most of granulocytes are neutrophils in human blood.

4. The pellet is resuspended in the same volume of the lysing solution.
5. After the second lysis of red cells, the cells are centrifuged again and finally washed once with approx 20 mL PBS (–) (*see Note 2*).
6. The cells are resuspended in 1 mL PBS-FCS until measurements (*see Note 3*).
7. Cells are counted using hemocytometer (*see Note 4*).
8. The concentration is adjusted at $5\text{--}10 \times 10^6$ cells/mL (*see Note 5*).

3.2. Neutrophil Intracellular Hydrogen Peroxide Generation

1. To minimize spontaneous oxidation of DHR 123 to R 123 over time, the indicator solution is kept refrigerated during the experiment and prewarmed to 37°C less than 60 min before use.
2. Leukocyte suspension is transferred to PBS-FCS-Ca at $1\text{--}5 \times 10^6$ cells/mL and preincubated for 10 min at 37°C (*see Note 6*).
3. The cells are suspended in 800 μL of prewarmed PBS-FCS-Ca containing 30 μM DHR 123 less than 1 min before running the samples (*see Note 7*).
4. Discrimination of granulocytes should be done prior to the measurements by flow cytometric technique of cellular forward angle and 90° light scatter (**Fig. 1**).
5. After the nonstimulated cells are measured, they are then treated with $10^{-5}\text{--}10^{-7}$ M FMLP (*see Note 8*).

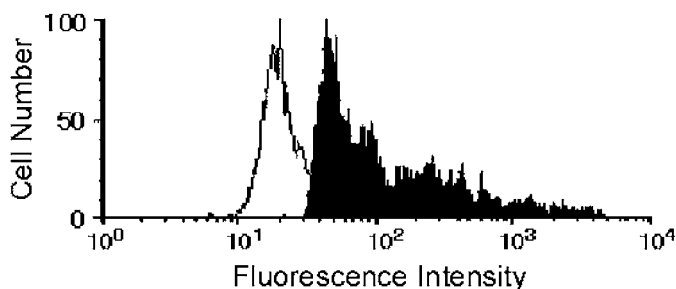


Fig. 2. H_2O_2 generation is measured. Histograms of granulocytes with (shaded histogram) and without (solid line) FMLP are demonstrated. An example of the histograms 10 min after stimulation is shown.

6. The emitted fluorescence which is excited at 488 nm is monitored every 5 min till 20 min after stimulation using a FACScan with the 530/30 nm band pass filter.
7. In order to discriminate the time dependent increase of fluorescence, samples without stimuli are also measured separately as controls.
8. The H_2O_2 generation is quantified as a ratio of fluorescence intensity to control. The ratio of fluorescence intensity (RFI) is calculated by setting a window around the peak and determining the mean channel numbers of the peaks for stimulated samples (MCNS) and controls (MCNC) (8).

$$\text{RFI} = \text{antilog}((\text{MCNS}-\text{MCNC})/256)$$

3.3. Results

1. Flow cytometric assay with DHR 123 offers a sensitive detection of H_2O_2 in activated neutrophils (**Fig. 2**). Higher concentrations such as 10^{-6} or 10^{-5} M of FMLP induces larger response of H_2O_2 generation, while 10^{-7} M is an optimal dose to measure superoxide by cytochrome c reduction (*1*), which is used commonly. As shown in **Fig. 2**, the heterogeneous response is also demonstrated using DHR 123. Generation of H_2O_2 by FMLP continues till about 20 min after stimulation (**Fig. 3**), while superoxide generation by cytochrome c reduction is over within 5 min after the stimulation. The reasons of these discrepancies are unclear.
2. Neutrophils generate superoxide anion from oxygen during oxidative burst. It is sometime controversial what kind of ROS reacts with DHR123. Most of them in neutrophils during oxidative burst should be superoxide itself or other species converted from superoxide. DHR123 has to be oxidized to R123 to be fluorescent, while superoxide anion usually reduces something. Superoxide generated by neutrophils must be converted to H_2O_2 by superoxide dismutase during oxidative burst. Other reactive oxygen species should be generated from the H_2O_2 . Thus, We consider that this method detects H_2O_2 mostly during oxidative burst in

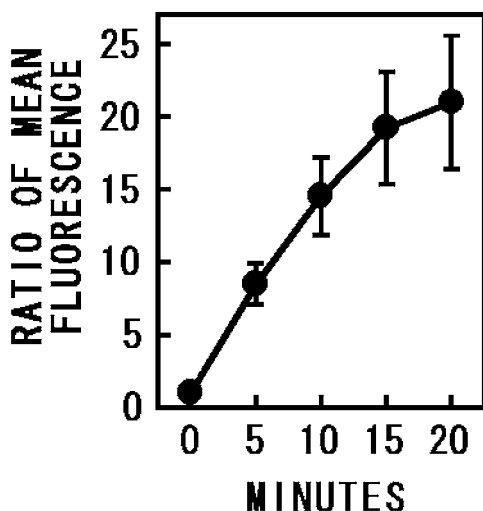


Fig. 3. Time-dependent increase of mean fluorescence intensity is demonstrated. RFI is calculated at every 5 min. Mean \pm standard error of mean for independent samples from 10 healthy donors is shown.

neutrophils. The discrepancies of reaction time and optimal dose of the stimulant may be due the difference of location where ROS are measured. We can measure superoxide released outside neutrophils by reduction of cytochrome c, while intracellular production of H_2O_2 are measured by using DHR123.

4. Notes

1. Plastic ware should be used to treat neutrophils. Glassware activates neutrophils.
2. After lysis of red cells, leukocytes should be kept on ice to avoid activation of neutrophils and to keep cell viability.
3. All measurements should be finished as quickly as possible not to lose viabilities of neutrophils.
4. Counting cells can be performed using a light microscope, hemocytometer and a proper cover slip. After diluting cell suspension with either 3% acetic acid or Trypan Blue Stain, place drops at the edge of cover slip on a hemocytometer. Count them under low power.
5. It is not necessary to count cells accurately. Approximate count should be enough. Flow cytometry performs the single cell analysis on intact cells. This range of the concentration for single-cell suspension allows them to flow single file in a suitable liquid stream (usually 200–300 cells/s).
6. Cell should be transferred to solution containing calcium and magnesium shortly before incubation. Otherwise neutrophils are easily activated in the presence of calcium and magnesium.

7. Measurement should be started immediately after mixing DHR 123 and leukocytes. Time dependent increase of fluorescence intensity will easily alter the results.
8. Each analysis is performed on approx 5000 cells.

References

1. Ito, Y., Ponnappan, U., and Lipschitz, D. A. (1996) Excess formation of lysophosphatidic acid with age inhibits myristic acid-induced superoxide anion generation in intact human neutrophils. *FEBS Lett.* **394**, 149–152.
2. Ito, Y., Kajkenova, O., Feuers, R. J., Udupa, K. B., Desai, V. G., Epstein, J., et al. (1998) Impaired glutathione peroxidase activity accounts for the age-related accumulation of hydrogen peroxide in activated human neutrophils. *J. Gerontol. A Biol. Sci. Med. Sci.* **53**, M169–M175.
3. Lund-Johansen, F. and Olweus, J. (1992) Signal transduction in monocytes and granulocytes measured by multiparameter flow cytometry. *Cytometry* **13**, 693–702.
4. Kinsey, B. M., Kassis, A. I., Fayad, F., Layne, W. W., and Adelstein, S. J. (1987) Synthesis and biological studies of iodinated ($^{127/125}\text{I}$) derivatives of rhodamine 123. *J. Med. Chem.* **30**, 1757–1761.
5. Rothe, G., Oser, A., and Valet, G. (1988) Dihydrorhodamine 123: a new flow cytometric indicator for respiratory burst activity in neutrophil granulocytes. *Naturwissenschaften* **75**, 354–355.
6. Rothe, G., Emmendörffer, A., Oser, A., Roesler, J., and Valet, G. (1991) Flow cytometric measurement of the respiratory burst activity of phagocytes using dihydrorhodamine 123. *J. Immunol. Methods* **138**, 133–135.
7. Rao, K. M. K., Padmanabhan, J., Kilby, D. L., Cohen, H. J., Currie, M. S., and Weinberg, J. B. (1992) Flow cytometric analysis of nitric oxide production in human neutrophils using dichlorofluorescein diacetate in the presence of a calmodulin inhibitor. *J. Leukoc. Biol.* **51**, 496–500.
8. Emmendörffer, A., Hecht, M., Lohmann-Matthes, M., and Roesler, J. (1990) A fast and easy method to determine the production of reactive oxygen intermediates by human and murine phagocytes using dihydrorhodamine 123. *J. Immunol. Methods* **131**, 269–275.

DNA-Binding Activity of Hypoxia-Inducible Factors (HIFs)

Gieri Camenisch, Roland H. Wenger, and Max Gassmann

1. Introduction

Electrophoretic mobility shift assay (EMSA) provides a fast and sensitive method for detecting sequence-specific DNA-binding proteins (*see Fig. 1*). Using an end-labeled DNA oligonucleotide as probe, proteins that specifically bind to these DNA sequence retard the mobility of the fragment during nondenaturing polyacrylamide gel electrophoresis (PAGE). This results in discrete band shifts corresponding to the individual protein-DNA complexes. This method can be used to investigate DNA-binding properties of purified proteins or of uncharacterized factors present in nuclear extracts. This assays also allows determination of affinity, sequence specificity, association and dissociation constants. Using specific antibodies that result in a supershift, individual proteins or protein complexes in DNA-binding activities can be identified. There is no single protocol that works equally for all proteins. We describe here a protocol designed to investigate DNA-binding properties of hypoxia-inducible factors (HIFs).

Molecular oxygen is the most important substrate to generate metabolic energy in a cell. Equalization of oxygen supply and demand represents a fundamental physiological challenge that is approached in different ways by different organisms (reviewed in *ref. 1*). Its ability to accept electrons enables oxygen to participate in oxidation-reduction reactions required to breakdown pyruvate, thereby yielding metabolic energy in form of ATP. Limited oxygen supply (hypoxia) alters expression of specific genes that allow physiological adaptation to the environmental conditions at the cellular, local and systemic levels. Expression of the glycoprotein hormone erythropoietin (Epo), the

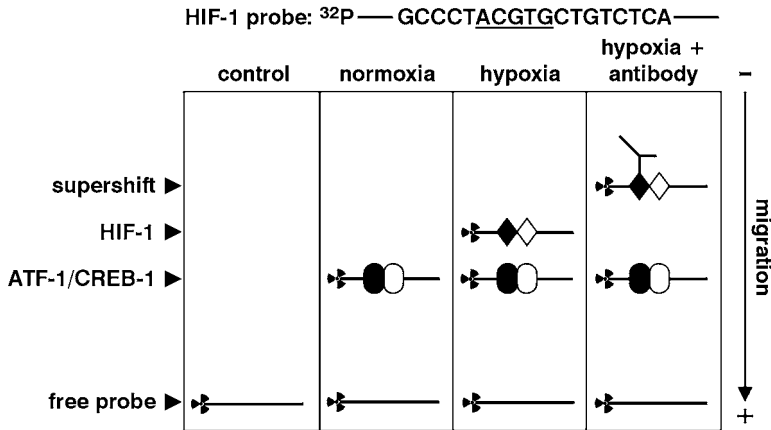


Fig. 1. Schematic drawing of electrophoretic mobility shift assays using a HIF-1-binding site containing probe.

primary regulator of mammalian erythropoiesis, increases in response to reduced oxygen tension.

Analysis of the 3' flanking region of the Epo gene revealed the presence of a hypoxia-response element (HRE) and the existence of a transcription factor specifically binding to this element named hypoxia-inducible factor-1 (HIF-1) (2). HIF-1 is a heterodimer composed of HIF-1 α and HIF-1 β . Whereas HIF-1 α was a newly identified protein, HIF-1 β turned out to be identical to the aryl hydrocarbon receptor nuclear translocator (ARNT), the dimerization partner of the aryl hydrocarbon receptor (AhR), better known as the dioxin receptor.

Performing EMSAs, we and others showed that no HIF-1 DNA-binding activity can be detected in nuclear extracts of normoxically cultured cells. On the other hand, when these cells were exposed to hypoxia (1% O₂), a strong DNA-binding activity was observed (*see Fig. 2*).

Recently, HIF-2 α , that is expressed mainly in endothelial cells in vivo (4), and HIF-3 α (5) have been found. These novel α -subunits also heterodimerize with ARNT and confer hypoxic response upon stimulation. The HIF-1 α subunit is rapidly ubiquitinated and degraded in proteasomes under normoxic conditions (6-8). Under reduced oxygen concentrations, however, the hypoxia-inducible factors (HIFs) are stabilized, translocate to the nucleus, and form a functional DNA-binding complex leading to differential gene expression. We investigated the role of ARNT in hypoxic induction and nuclear translocation properties of HIF-1 α using the ARNT-mutant mouse hepatoma cell line Hepa1c4. We showed by EMSA that ARNT-mutant Hepa1c4 cells are unable to form a functional HIF-1 DNA-binding complex (*see Fig. 3*). This result shows

that, despite the lack of wildtype ARNT protein, HIF-1 α is still hypoxically induced and translocates to the nucleus. Indeed, we showed by immunofluorescence experiments that hypoxic induction and nuclear accumulation of HIF-1 α are independent of ARNT (9). On the other hand, ARNT expression is not regulated by oxygen tension and the ARNT level stays almost constant.

HIF-1 binds its recognition sequence as a heterodimer. The sequence specificity of DNA binding of HIF-1 is not fully understood. Analyzing 26 HIF-1 DNA binding sites, we found in 24 cases the asymmetric core hypoxia-response element (HRE) ACGTG (reviewed in ref. 10). We also demonstrated that even non-Epo producing cells can keep this site methylation free, raising the question whether the constitutive factors, consisting of the activating transcription factor (ATF) and cAMP response element binding protein (CREB) (12–14) occupy this site in normoxia when HIF-1 is absent and thereby protecting the HIF-1-binding site from methylation.

2. Materials

2.1. Equipment

2.1.1. Preparation of Nuclear Extracts

1. Normoxic/hypoxic tissue incubators.
2. Centrifuge.
3. Dounce homogenizer.
4. Dialysis tubes.
5. Liquid nitrogen.
6. UV-VIS spectrophotometer.

2.1.2. Oligonucleotide Purification and Labeling

1. PAGE unit.
2. Power supply.
3. Heating block.
4. Thin layer chromatography plate.
5. UV-handlamp (259 nm).
6. Centrifuge.
7. Shaker.
8. Vortex.
9. UV spectrophotometer.
10. Scintillation counter.

2.1.3. Electrophoretic Mobility Shift Assay

1. PAGE unit.
2. Power supply.
3. Gel dryer.
4. X-ray film exposure cassettes and developing facilities.

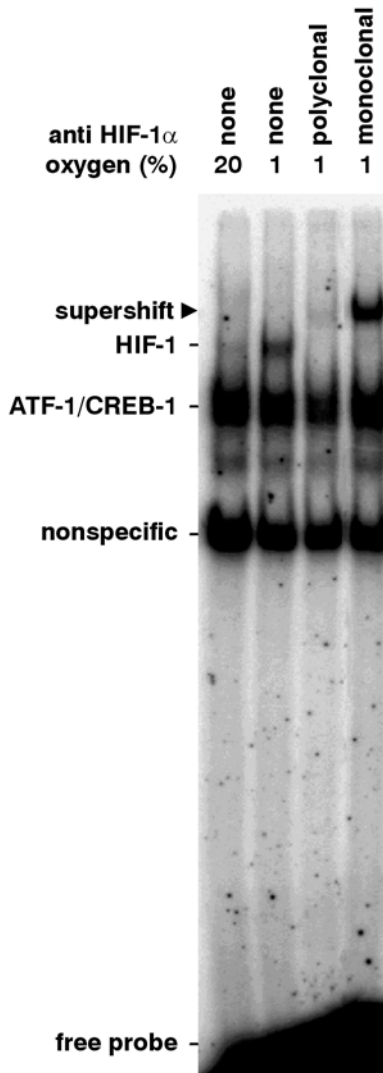


Fig. 2. The generation of both, monoclonal and polyclonal antibodies raised against HIF-1 α (3) verified the presence of this HIF-1 subunit in the DNA-binding complex found in hypoxic cells.

2.2. Reagents

2.2.1. Preparation of Nuclear Extracts

1. DMEM medium (high glucose) supplemented with 10% heat-inactivated fetal calf serum (FCS), 100 I.U./mL penicillin, 100 μ g/mL streptomycin, 1X MEM nonessential amino acids, 2 mM L-glutamine, and 1 mM sodium pyruvate.

2. Phosphate-buffered saline (PBS).
3. Buffer A (10 mM Tris-HCl, pH 7.8, 1.5 mM MgCl₂, 10 mM KCl).
4. Buffer C (20 mM Tris-HCl, pH 7.8, 1.5 mM MgCl₂, 420 mM KCl, 20% glycerol).
5. Buffer D (20 mM Tris-HCl, pH 7.8, 100 mM KCl, 0.2 mM EDTA, 20% glycerol).
6. Protease inhibitor cocktail (0.5 mM dithiothreitol [DTT]; 1 mM Na₃VO₄; 0.4 mM phenylmethylsulfonyl fluoride (PMSF); and 2 µg/mL each of leupeptin, pepstatin, and aprotinin).
7. Bradford protein assay (BioRad).
8. Bovine serum albumin (BSA).

2.2.2. Oligonucleotide Purification and Labeling

1. Urea.
2. Acrylamide-bisacrylamide solution (29:1 w/w).
3. TBE buffer: 89 mM Tris, 89 mM Boric acid, 5 mM EDTA.
4. Ammonium persulfate (10% w/v), freshly prepared.
5. N, N, N', N'-tetramethylethylenediamine (TEMED).
6. Formamide.
7. Size-marker (10 mL formamide, 10 mg xylene cyanole ff (BioRad), 10 mg bromophenol blue (BioRad), 200 µL 0.5 M EDTA).
8. TNES buffer: 10 mM Tris-HCl, pH 8.0, 1 mM EDTA, 0.3 M NaCl, 2% SDS.
9. Phenol-chloroform-isoamylalcohol (25:24:1, v/v).
10. Chloroform-isoamylalcohol (49:1, v/v).
11. Ethanol.
12. 0.3 M NaAc, pH 4.8.
13. TE buffer: 10 mM Tris-HCl, pH 7.6, 1 mM EDTA.
14. 10X bacteriophage T4 polynucleotide kinase (PNK) buffer: 500 mM Tris-HCl, pH 7.6, 100 mM MgCl₂, 50 mM DTT, 1 mM spermidine, 1 mM EDTA (Fermentas).
15. T4 polynucleotide kinase (PNK) (10 U/µL, Fermentas).
16. [γ -³²P] ATP (3000Ci/mmol, 10µCi/µL, Hartmann Analytic).
17. Biogel P-60 (BioRad).
18. 1 M MgCl₂.

2.2.3. Electrophoretic Mobility Shift Assay

1. Repel-Silane ES (dimethyldichlorosilane solution, 2% [w/v], in octamethylcyclotetrasiloxane, Pharmacia Biotech).
2. 30% acrylamide-bisacrylamide solution (80:1 w/w).
3. TBE buffer: 89 mM Tris, 89 mM Boric acid, 5 mM EDTA.
4. Glycerol.
5. Ammonium persulfate (10% w/v), freshly prepared.
6. N, N, N', N'-tetramethylethylenediamine (TEMED).

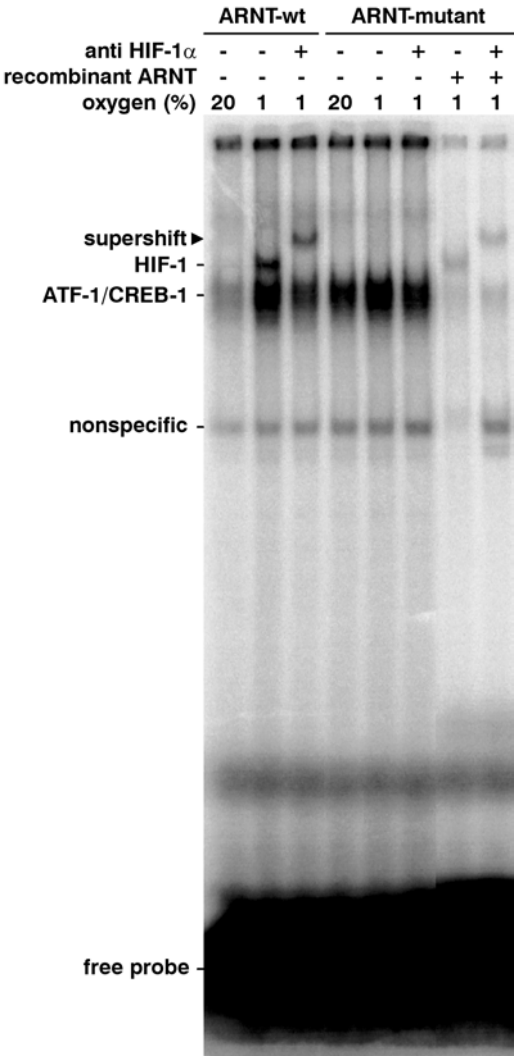


Fig. 3. Supplementation of HepalC4 nuclear extracts with in vitro synthesized ARNT protein reconstituted the HIF-1 DNA-binding activity.

- 7. Size-marker (10 mL formamide, 10 mg xylene cyanole ff (BioRad), 10 mg bromophenol blue [BioRad], 200 μ L 0.5 M EDTA).
- 8. Binding buffer: 10 mM Tris-HCl, pH 7.5, 50 mM KCl, 50 mM NaCl, 1 mM MgCl₂, 1 mM EDTA, 5 mM DTT, 5% glycerol.
- 9. Carrier DNA (denatured sonicated calf thymus DNA, Sigma).

3. Methods

3.1. Cell Culture and Hypoxic Induction

1. Medium: DMEM (high glucose) supplemented with 10% heat-inactivated (FCS), 100 I.U./mL penicillin, 100 µg/mL streptomycin, 1X MEM nonessential amino acids, 2 mM L-glutamine, and 1 mM sodium pyruvate.
2. Cell culture: culture cells in a humidified atmosphere containing 5% CO₂ at 37°C.
3. Induction: oxygen tensions in the incubator are either 140 mm Hg (20% O₂ [v/v] normoxia) or 7 mm Hg (1% O₂ [v/v] hypoxia). Perform hypoxic induction by exposing the cells for 4 h to hypoxia.

3.2. Nuclear Extract Preparation

1. Wash 1×10^8 cells twice with ice-cold PBS.
2. Add 5 mL ice-cold PBS to the cells and scrape them from the dish. Pellet the cells by centrifugation at 400g for 5 min at 4°C.
3. Estimate the packed cell volume (pcv), resuspend the pellet in 4X pcv buffer A with freshly added protease inhibitor cocktail and incubate for 10 min on ice.
4. Lyse the cells by 10 strokes of a Dounce homogenizer and centrifuge at 4,500g for 5 min at 4°C. Cytoplasmic fractions are obtained by re-centrifugation of the supernatant for 10 min at 20,000g.
5. Extract the pelleted nuclei in 2X pcv of buffer C previously complemented with freshly prepared protease inhibitor cocktail at 4°C for 30 min with gentle agitation. Centrifuge the extracted nuclei at 10,000g for 30 min at 4°C and transfer the nuclear extracts into dialysis tubes (Spectra/Por®, MWCO 5,000).
6. Dialyse twice for 2 h at 4°C in 2 L of buffer D.
7. Centrifuge the extracts at 10,000g for 10 min at 4°C, aliquot the supernatant and immediately freeze in liquid nitrogen. For permanent storage keep the aliquots at -80°C.
8. Determine the protein concentrations of 2 µL nuclear extract using the Bradford protein assay (BioRad) with BSA as standard. Depending on the cell type, the expected yield of nuclear proteins is around 2–8 µg/µL.

3.3. Oligonucleotide Probes: Purification and Labeling

Synthetic oligonucleotides are purified by separating them in urea-containing polyacrylamide gels. The 18 bp oligonucleotide probe is derived from the Epo 3' enhancer (5'-GCCCTACGTGCTGTCTCA-3') and synthesized by Microsynth (Balgach, Switzerland) (13).

1. Preparation of a 10% polyacrylamide gel (100 mL): dissolve 48 g urea in 50 mL of doubled-distilled H₂O heated to 37°C. Add 33.3 mL 30% acrylamide-bisacrylamide solution (29:1 w/w) and 10 mL 10X TBE buffer. Adjust the

volume to 100 mL with doubled-distilled H_2O . Start the polymerization process by adding 700 μL ammoniumpersulfate and 35 μL TEMED. After polymerization, prerun the gel for 20 min at 400 V.

2. Preparation of the oligonucleotides: take 20 μg oligonucleotide, the volume should not exceed 30 μL . Add the same volume of pure formamide and heat the sample for 5 min to 55°C.
3. Directly following the prerun, load the heated probes onto the gel. Separate the probes by an empty slot and load a size marker of a mixture of bromophenol blue and xylene cyanole in the outer slots. Run the gel at 400 V at room temperature until the size marker is about 5 cm ahead the bottom of the gel.
4. After finishing the run, cover the gel with Saran wrap and place it on a thinlayerchromatography plate. Visualize the oligonucleotide by UV light shadowing at 259 nm and excise the main band. Transfer the gel piece into a microcentrifuge tube that contains a small hole in the bottom. Place the gel containing tube into another tube that contains 600 μL TNES buffer and centrifuge for 5 min at 15,000g until the whole gel piece is homogenized by squeezing through the small hole. Incubate the gel in TNES buffer over night at 30°C in a shaker to elute the oligonucleotide.
5. For efficient recovery, heat the gel pieces for 1 h at 50°C and vortex every 5–10 min. After cooling down on ice for 30 min, spin the tube at 15,000g for 10 min at 4°C and transfer the supernatant into a fresh tube. Save the gel pieces and store them in the fridge.
6. Extract the oligonucleotide containing supernatant once with phenol-chloroform-isoamylalcohol and once with chloroform-isoamylalcohol, then precipitate by adding 2.5 volumes of 100% ethanol and 1/10 volume 0.3 M NaAc, pH 4.8, for 1 h at –80°C. Centrifuge at 15,000g for 30 min at 4°C and wash the pellet with 70% ethanol, vacuum-dry, and resuspend in 20 μL TE. Determine the oligonucleotide concentration and repeat the elution with the stored gel pieces in case of low yield.
7. End-label the oligonucleotide by using the polynucleotide kinase (PNK) from the bacteriophage T4. This enzyme catalyzes the transfer of the terminal (γ) phosphate of ATP to the 5'-hydroxyl termini of the oligonucleotide. Perform the kinase reaction before annealing to label only the sense strand. Incubate 2 pmol sense strand oligonucleotide with T4 PNK buffer (Fermentas), [γ - ^{32}P] ATP (3000 Ci/mmol, use 40 μCi) and T4 PNK (5 U) (Fermentas) at 37°C for 1 h. Remove unincorporated nucleotides by gel filtration over Bio-Gel P60 (fine) columns (BioRad). Fill a pasteur pipet to the nick with Bio-Gel P60 and equilibrate with 400 μL TE. Apply the label reaction to the column and add 400 μL TE. Elute the column with 600 μL TE and count 1 μL for Cerenkov counts in a scintillation counter to determine the specific activity (cpm/ μL). A typical binding reaction will result in about 5,000 to 20,000 cpm. Add the antisense strand oligonucleotide in a twofold molar excess (4 pmol), heat for 3 min at 95°C and anneal by switching off the heating block and letting cool-down to room temperature over night. The probes can be stored for to 4–6 wk at 4°C.

3.4. EMSA: Binding Reaction and Electrophoresis

1. Preparation of a 4% nondenaturing gel: assemble washed glass plates and 1.5 mm spacers for casting the gel. Siliconize the smaller glass plate with repel-silane (Pharmacia Biotech). Pay attention that all traces of detergent are carefully removed because detergent will disrupt protein-DNA interactions. Prepare the gel solution (80 mL) by mixing 66.2 mL double-distilled H₂O, 9.9 mL 30% acrylamide-bisacrylamide (80:1 w/w), 2.4 mL 10X TBE, 0.8 mL 87% glycerol, 200 μ L 10% ammoniumpersulfate, and 50 μ L TEMED. Pour the gel, insert the comb, and allow polymerization for at least 30 min. Add 0.3X TBE running buffer and prerun the gel at 200 V for 20 min at 4°C.
2. Carry out the DNA-protein binding reaction for 30 min at 4°C in a total volume of 20 μ L. The binding reactions contain 4–5 μ g nuclear extract, 0.2 μ g sonicated denatured calf thymus DNA, and 5,000–20,000 cpm radiolabeled oligonucleotide probe in 10 mM Tris-HCl, pH 7.5, 50 mM KCl, 50 mM NaCl, 1 mM MgCl₂, 1 mM EDTA, 5 mM DTT, and 5% glycerol.
3. Load each binding reaction into the appropriate well of the prerun gel and perform electrophoresis at 200 V in TBE buffer at 4°C. Load a size marker into the outer wells and stop the run before the bromophenol blue front line approaches the bottom of the gel.
4. Slowly pry up the upper (siliconized) glass plate, lay a sheet of Whatmann 3MM filter paper onto the gel and remove it from the glass plate. Cover the gel with Saran wrap and dry under vacuum with heat (2 h at 70°C). Autoradiograph the dried gel.

3.5. Results

1. Nuclear extracts from HeLa cells cultured under normoxic (20% O₂) or hypoxic (1% O₂) conditions were analyzed by EMSA (see **Fig. 2**). In nuclear extracts from normoxic HeLa cells no HIF-1 DNA-binding activity could be observed but a constitutive band consisting of the ATF-1/CREB-1 heterodimer. Upon hypoxic exposure, HIF-1 is stabilized and accumulates in the nucleus where a functional DNA-binding complex is formed. Addition of affinity-purified polyclonal chicken IgY anti-human HIF-1 α antibodies (**3**) reduced HIF-1 DNA-binding activity and resulted in a partial supershift. This indicates that the polyclonal antibodies interact with epitopes critical for DNA binding and therefore partially abolish DNA-binding activity. Addition of the monoclonal anti-human HIF-1 α antibody mgc3 resulted in a complete supershift, identifying the HIF-1 α subunit as part of the DNA-binding complex.
2. ARNT-wildtype mouse Hepa1 and ARNT-mutant Hepa1c4 cells were cultivated under normoxic or hypoxic conditions and nuclear extracts were prepared. Hepa1 cells strongly induced HIF-1 DNA-binding activity when cultured under hypoxic conditions and supershift analysis using the monoclonal anti-human HIF-1 α antibody identified HIF-1 α in the DNA-binding complex (see **Fig. 3**). In contrast, HIF-1 DNA-binding activity is completely abolished in ARNT-mutant

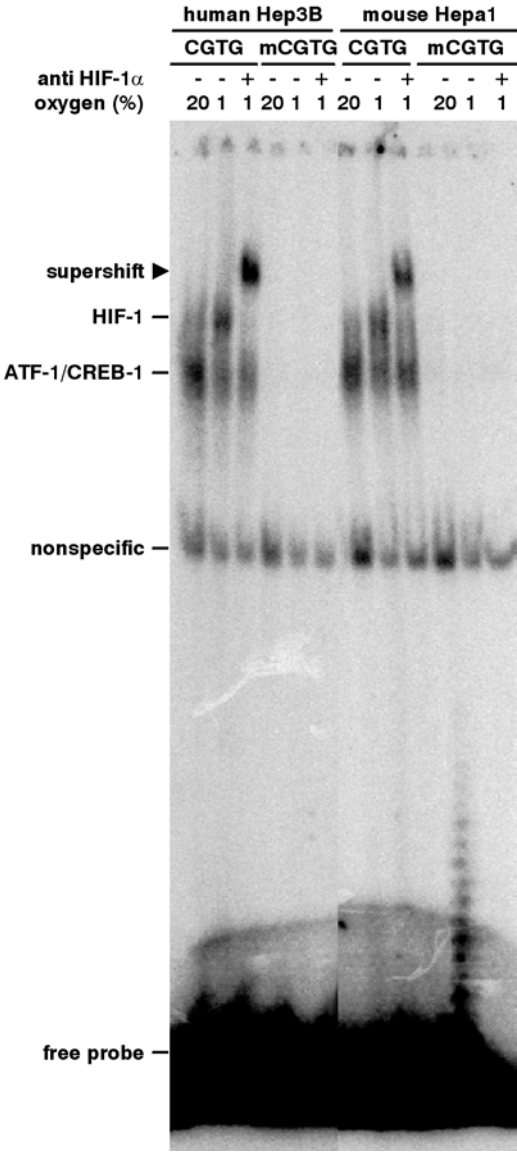


Fig. 4. Since the HIF-1 consensus binding site contains a CpG dinucleotide that is usually methylated in humans if not located within a so-called CpG island, we examined the impact of methylation on HIF-1 DNA binding. We observed that CpG methylation impairs HIF-1 DNA binding and transactivation, and that Epo gene expression, where the 3' HIF-1 binding site is located outside of a CpG island, is dependent on a methylation-free HIF-1 binding site (11).

Hepal4 cells, independent of the oxygen concentrations. Addition of in vitro synthesized ARNT protein to nuclear extracts of Hepal4 cells reconstituted HIF-1 DNA-binding activity and proved that the HIF-1 α subunit is induced under hypoxic conditions and accumulates in the nucleus even in the absence of functional ARNT protein.

3. Mouse Hepal and human Hep3B cell lines were exposed to either normoxia or hypoxia for 4 h and nuclear extracts were prepared (*see Fig. 4*). An 18 bp oligonucleotide (5'-GCCCTACGTGCTGTCTCA-3') derived from the human Epo 3' enhancer was used as probe. Where indicated, the cytosine residue at position 7 was replaced by 5-methylcytosine in both strands (mCGTG). This methylation abolished DNA-binding of HIF-1 in hypoxic extracts. Supershift experiments using the monoclonal anti-human HIF-1 α antibody mgc3 confirmed the identity of the HIF-1 α subunit in these extracts. Binding of the constitutive factor, composed of ATF-1 and CREB-1, was also abolished whereas DNA-binding activity of the nonspecific factor was not affected.

4. Notes

1. The amount of carrier DNA is a critical factor and has to be optimized for every oligonucleotide probe and nuclear extract. Sufficient carrier DNA is needed to prevent nonspecific proteins from binding to the probe. Most sequence-specific DNA-binding proteins have low nonspecific DNA affinities. Therefore, titration of the optimal amount of carrier DNA is a crucial step in establishing an EMSA. Weak band intensities of the free probe and/or smears over the entire gel often indicate that more carrier DNA is required.
2. The type of carrier DNA is also of great importance. Optimally, the sequence of the carrier DNA should be different from the sequence of the specific DNA-binding site. Using synthetic carriers such as poly(dA-dT) or poly(dI-dC), we did not obtain satisfying results. Heterologous sequence DNA will reduce the amount of specific protein-DNA complex because binding sites of varying affinities will occur at some frequency. Best results in our hands were obtained when using sonicated denatured calf thymus DNA as carrier.
3. When using an alternative method of nuclear extract preparation using detergents to lyse the nuclei, attention should be paid to completely remove these detergents. Traces of detergents will disrupt the formation of a protein-DNA complex.
4. We also performed EMSAs with recombinant proteins. In vitro transcription and translation of recombinant proteins were performed using the TNT[®] coupled transcription-translation rabbit reticulocyte lysate system (Promega) under conditions recommended by the manufacturers. Prior to addition of the binding reaction mix, the in vitro synthesized proteins were allowed to interact for 30 min at room temperature. After this time the binding reaction mix containing the probe, carrier DNA and binding buffer were added and the sample proceeded as described earlier.

5. A common expansion of the EMSA technology is the use of antibodies to identify specific proteins present in a DNA-binding activity. Several effects can be observed. If the protein specifically recognized by the antibody is not involved in the DNA-binding complex, addition of the antibody has no effect. If the protein that forms the DNA-binding complex is recognized by the added antibody, the later will either block complex formation (observed with the polyclonal IgY anti-human HIF-1 α antibodies) or will form an antibody-protein-DNA complex (observed with the monoclonal anti-human HIF-1 α antibody mgc3) resulting in a further reduction in the mobility (supershift). For supershift analysis, 1 μ L of hybridoma culture supernatant was added to the completed binding reactions followed by incubation for 2 h at 4°C prior to loading.
6. The cell density is an important factor to be considered. Culturing cells at confluency leads to the induction of HIFs even under normoxic conditions. It is important to grow the cells subconfluently and maintain them in an exponential growth phase (15).

Acknowledgments

We are grateful to P. Spielmann, I. Kvietikova, and F. Parpan for excellent technical assistance. This work was supported by the Swiss National Science Foundation (31-56743.99) and the “Stiftung für wissenschaftliche Forschung an der Universität Zürich.” R.H.W. is a recipient of the “Sondermassnahmen des Bundes zur Förderung des akademischen Nachwuchses.”

References

1. Bunn, H. F. and Poyton, R. O. (1996) Oxygen sensing and molecular adaptation to hypoxia. *Physiol. Rev.* **76**, 839–885.
2. Wang, G. L., Jiang, B. H., Rue, E. A., and Semenza, G. L. (1995) Hypoxia-inducible factor 1 is a basic-helix-loop-helix-PAS heterodimer regulated by cellular O₂ tension. *Proc. Natl. Acad. Sci. USA* **92**, 5510–5514.
3. Camenisch, G., Tini, M., Chilov, D., Kvietikova, I., Srinivas, V., Caro, J., et al. (1999) General applicability of chicken egg yolk antibodies: the performance of IgY immunoglobulins raised against the hypoxia-inducible factor-1 α . *FASEB J.* **13**, 81–88.
4. Tian, H., McKnight, S. L., and Russell, D. W. (1997) Endothelial PAS domain protein 1 (EPAS1), a transcription factor selectively expressed in endothelial cells. *Genes Dev.* **11**, 72–82.
5. Gu, Y. Z., Moran, S. M., Hogenesch, J. B., Wartman, L., and Bradfield, C. A. (1998) Molecular characterization and chromosomal localization of a third α -class hypoxia inducible factor subunit, HIF-3 α . *Gene Expr.* **7**, 205–213.
6. Salceda, S. and Caro, J. (1997) Hypoxia-inducible factor-1 α (HIF-1 α) protein is rapidly degraded by the ubiquitin-proteasome system under normoxic conditions. Its stabilization by hypoxia depends on redox-induced changes. *J. Biol. Chem.* **272**, 22642–22647.

7. Huang, L. E., Gu, J., Schau, M., and Bunn, H. F. (1998) Regulation of hypoxia-inducible factor-1 α is mediated by an O₂-dependent degradation domain via the ubiquitin-proteasome pathway. *Proc. Natl. Acad. Sci. USA* **95**, 7987–7992.
8. Kallio, P. J., Wilson, W. J., O'Brien, S., Makino, Y., and Poellinger, L. (1999) Regulation of the hypoxia-inducible transcription factor-1 α by the ubiquitin-proteasome pathway. *J. Biol. Chem.* **274**, 6519–6525.
9. Chilov, D., Camenisch, G., Kvietikova, I., Ziegler, U., Gassmann, M., and Wenger, R. H. (1999) Induction and nuclear translocation of hypoxia-inducible factor-1 (HIF-1): heterodimerization with ARNT is not necessary for nuclear accumulation of HIF-1 α . *J. Cell Sci.* **112**, 1203–1212.
10. Wenger, R. H. and Gassmann, M. (1997) Oxygen(es) and the hypoxia-inducible factor-1. *Biol. Chem.* **378**, 609–616.
11. Wenger, R. H., Kvietikova, I., Rolfs, A., Camenisch, G., and Gassmann, M. (1998) Oxygen-regulated erythropoietin gene expression is dependent on a CpG methylation-free hypoxia-inducible factor-1 DNA-binding site. *Eur. J. Biochem.* **253**, 771–777.
12. Ebert, B. L. and Bunn, H. F. (1998) Regulation of transcription by hypoxia requires a multiprotein complex that includes hypoxia-inducible factor 1, an adjacent transcription factor, and p300/CREB binding protein. *Mol. Cell. Biol.* **18**, 4089–4096.
13. Kvietikova, I., Wenger, R. H., Marti, H. H., and Gassmann, M. (1995) The transcription factors ATF-1 and CREB-1 bind constitutively to the hypoxia-inducible factor-1 (HIF-1) DNA recognition site. *Nucleic Acids Res.* **23**, 4542–4550.
14. Kvietikova, I., Wenger, R. H., Marti, H. H., and Gassmann, M. (1997) The hypoxia-inducible factor-1 DNA recognition site is cAMP-responsive. *Kidney Int.* **51**, 564–566.
15. Wenger, R. H., Marti, H. H., Bauer, C., and Gassmann, M. (1998) Optimal erythropoietin expression in human hepatoma cell lines requires activation of multiple signalling pathways. *Int. J. Mol. Med.* **2**, 317–324.

Analysis of Heat-Shock Transcription Factor and Element-Binding Activity

Yong J. Lee

1. Introduction

Stress response is nearly universal. Living organisms respond to the changes in their chemical, physical, and biological environments by synthesizing a group of proteins called stress or heat-shock proteins (*1*). The preferential synthesis of these proteins appears to be involved in induced transient thermal resistance (*2*). It is well known that transcription of heat-shock genes is regulated by heat-shock transcription factors (HSFs), which bind to heat-shock elements (HSEs) located in the promoter region of genes encoding heat-shock proteins (*3*). Heat-shock protein gene promoter contains three heat-shock elements (HSE, 5'-GAAnnTTCnnGAA-3') (*4*). The HSE is known as a conserved motif present in the promoters of many heat-inducible heat-shock protein genes. Many studies have demonstrated that stress-induced denatured, unfolded, or malformed proteins trigger the activation of heat shock transcription factors (HSFs) (*5-7*). In mammalian cells, the activated HSF binds to the HSE and then stimulates transcription.

The gel mobility shift assay is an assay used to quantitatively determine the binding of heat shock transcription factor to double stranded DNA. This is an in vitro assay that can be applied to any number of DNA binding proteins, as long as a DNA oligomer containing the appropriate binding base sequence is available.

Although this is a very useful assay, there is one limitation that is frequently overlooked. The assay involves treating intact cells to induce changes that will result in protein binding to the oligomer sequence. However, the binding to the oligomer occurs in a cell-free lysate made from the treated cells. The

assumption made is that the HSF in the lysate retains the same affinity for DNA binding as they do in the intact cells.

2. Materials

2.1. Equipment

1. Centrifuge.
2. Microfuge (Fisher Scientific, Pittsburgh, PA).
3. Spectrophotometer (Beckman Coulter, Fullerton, CA).
4. Electrophoresis gel units (Hoefer, Model SE 600, San Francisco, CA).
5. Gel dryer (Bio-Rad, Model 583, Hercules, CA).
6. Vortex.
7. Power supply (Hoefer PS500X).
8. Radioactivity shields.
9. Scintillation counter (Beckman Coulter).
10. Stainless steel cassettes with intensifying screen.

2.2. Reagents

The following chemical reagents are molecular grade obtained from Bio-Rad, Sigma Chemical (St. Louis, MO), Pharmacia Biotech (Piscataway, NJ), and Boehringer Mannheim (Indianapolis, IN): Tris-HCl, EDTA disodium, Ethanol, Phosphoric acid, Acrylamid, ammonium persulphate, TEMED, Tris base, Boric acid, Yeast tRNA, *E. coli* DNA, Poly(dI-dC), BSA, NaCl, DTT, glycerol.

3. Methods

3.1. Harvesting Cells

Following the experimental treatment the cells must be harvested. Each cell sample should contain 2×10^6 to 4×10^6 cells in order to provide sufficient DNA-binding protein in the lysate. Cells from a 70–80% confluent T-25 or a P-60 provide sufficient cells for the assay. Cells in suspension are merely collected in an aliquot from the culture that provides sufficient cells. Cells growing attached to a substrate are trypsinized or scrapped from the substrate. Although both trypsinizing and scraping appear to work equally well, trypsinization is preferred. There appear to be less adverse effects on the cells. This latter point may be particularly important when using the assay to investigate the heat-shock factors for the different heat-shock proteins.

1. Trypsinize cells from the p-60 or T-25. Harvest cells into 15 mL centrifuge tube and spin them down at 1200 rpm for 6 min.
2. Resuspend pellet in 10 mL phosphate buffered solution (PBS; pH 7.4) and spin down at 1200 rpm for 6 min.
3. Aspirate PBS from cell pellet and quick-freeze cell pellet by dropping tube directly into liquid nitrogen, store cells at -70°C (see **Note 1**).

3.2. Preparation of Cell Extract

1. Place tubes with frozen cell pellets on ice. Estimate the volume of each pellet: This is usually between 20–50 μL . Add a volume of extraction buffer to the frozen cell pellet that is approx 5X that of the cell pellet.

Extraction Buffer (EB)

10 mM HEPES	0.486 g
422 mM NaCl	4.68 g
0.1 mM EGTA	7.6 mg
5.3% Glycerol	10 mL
*A-dH ₂ O	120 mL

*autoclaved, distilled water

Also needed: Stock solutions of 0.1 M dithiothreitol (DTT) and 200 mM PMSF (in ethanol); both are stored at -20°C .

Add HEPES, NaCl and EGTA to A-dH₂O and then adjust pH to 7.9. Add glycerol and sufficient water to bring final volume to 190 mL. Filter EB and aliquot into 10 mL tubes and store at -20°C .

Before using, add 5.0 μL of 0.1 M DTT and 2.5 μL of 200 mM PMSF per mL of EB. This completed EB can be re-aliquoted and frozen for later use. It is good for approx 3 wk.

2. After pellet has thawed, resuspend pellet with a pipeter using 4–6 up and down strokes. Be firm but not overly vigorous; do not perform this step such that air bubbles form and the lysate foams. Transfer samples into microfuge tubes.
3. Freeze/thaw samples three times in liquid nitrogen or dry ice/ethanol bath and room temperature water, vortex cells quickly after each thaw.
4. Spin tubes in fixed angle microfuge or at top speed on variable-speed microfuge for 5 min at 4°C . The advantage of the variable-speed microfuge is that it produces flat pellets that may make the next step somewhat easier.
5. Transfer supernatant to a new, appropriately labeled microfuge tube. At this point, sample can be either refrozen at -70°C or kept on ice while performing the remaining steps.

3.3. Determination of Lysate Protein Concentration:

Bradford Assay

1. Turn on visible light source (VIS) on spectrophotometer.
2. Prepare protein standard solutions for the assay.

<u>Protein content (μg)</u>	<u>μL BSA (1.0 mg/mL)</u>	<u>μL TE buffer</u>
5	5	55
10	10	50
20	20	40
30	30	30
40	40	20
50	50	10

Make bovine serum albumin (BSA) stock up in TE buffer (1X TE: 10 mM Tris and 1 mM EDTA, pH 8.0).

- 3. For cell lysates, add 5 μL of lysate to 55 μL of TE buffer.
- 4. Add 2.0 mL of Bradford Reagent to each sample tube, mix by inversion (parafilm over tube) and incubate for 5 min at room temperature.
- 5. Transfer samples to plastic, disposable cuvetts and read samples at 595 nm.

Bradford Reagent Preparation

100 mg Coomassie Blue G-50 (*see Note 2*)
50 mL of 100% ethanol
100 mL of 85% phosphoric acid
850 mL of distilled water

3.4. Preparation of 4.5% Acrylamide Gel

	<u>1 Gel</u>	<u>2 Gels</u>
22.5% Acrylamide solution	10 mL	20 mL
(22.5/0.27, Acrylamide/Bisacrylamide)		
10X TBE	2.5 mL	5.0 mL
Water	37.5 mL	75 mL
10% ammonium persulphate	0.4 mL	0.8 mL
TEMED	50 μL	100 μL

Mix together the first three ingredients in a filter flask and degas for 5 min. Add the ammonium persulphate and TEMED, swirl to mix (*see Note 3*).

10X TBE, pH 8.0

Tris base 108 g
Boric acid 55 g
EDTA disodium 9.3 g
add A-dH₂O to 1 L.

3.5. Binding Reaction

- 1. Calculate the number of samples (reactions) to be run in order to determine the total volume of the premix that needs to be prepared. Add one to the total number and an additional one for every 10 samples to be run. This will help protect against running short of the premix (see example below).
- 2. Calculate the total volume of the premix needed; each sample requires 12 μL of premix.

EXAMPLE: Setup for 30 reactions (2 gels)

- a. 30 reactions + 1 extra + 3 extra (for the three groups of 10 in 30) = 34 total reactions.
- b. Total volume of premix to make is: $34 \times 12 \mu\text{L} = 408 \mu\text{L}$.
- c. Premix

5X binding buffer	170 μL	(5 μL /reaction)
10 mg/mL Yeast tRNA	34 μL	(1 μL /reaction)
1 mg/mL <i>E. coli</i> DNA	34 μL	(1 μL /reaction)
2 mg/mL Poly(dI-dC)	34 μL	(1 μL /reaction)
50 mg/mL BSA	34 μL	(1 μL /reaction)
A-dH ₂ O	34 μL	(1 μL /reaction)

5X BINDING BUFFER (Procedure to make 100 mL)

50 mM Tris-HCl, pH 7.5	5.0 mL from 1 M stock
250 mM NaCl	25.0 mL from 1 M stock
5.0 mM EDTA	1.0 mL from a 0.5 M stock
25% Glycerol	25 mL of glycerol
A-dH ₂ O	43.5 mL

Make this solution and freeze at -20°C as 1.0 mL aliquots.

Make a 1 M stock of dithiothreitol (DTT) in A-dH₂O and freeze at -20°C in 50 μL aliquots. Add 5.0 μL of this DTT stock per mL of the 5X binding buffer to complete it. The DTT is kept separate as the DTT lasts longer this way.

- d. Mix all the premix components in one microfuge tube and keep this on ice. If more than one probe is to be used (e.g., HSP-70 and HSP-28 HSE), divide the premix up proportionally to accommodate the number of samples to be used with each different probe.
- e. Calculate the total volume of probe to be used (2 μL probe/reaction). SEE SECTION ON PROBE PREPARATION. For 30 samples, you will need 68 μL of the probe; 60 μL for the 30 samples plus 8 μL of probe for the extra samples used to account for liquid loss during aliquoting.
3. Take the cell lysate samples out of the -70°C freezer and place them on ice to thaw.
4. Label microfuge tubes that will be used to hold the reaction samples; these are the reaction tubes.
5. Calculate the volume of each cell lysate sample (μL lysate = 20 μg protein) and the volume of diluted extraction buffer (4 parts extraction buffer + 1 part H₂O) to be used per reaction.
Sample volume + diluted extraction buffer volume = 13 μL
6. Pipet the proper, calculated volume of diluted extraction buffer into the appropriately numbered reaction tubes.
7. Add cell lysate sample (20 μg protein) to the reaction tubes; keep these on ice. Then, refreeze the original cell lysate samples at -70°C .
8. Add probe to premix and mix well by finger vortexing.
9. Add the probe-premix to the reaction tubes. Incubate at room temperature for 15 min. If needed, prepare cold competitor reaction at this time.

CONTROL WITH COLD COMPETITOR

Cold, unlabeled HSE (200 ng/ μL)	1 μL
Cell extract (20 μg protein)*	X μL
A-dH ₂ O	12-X μL
Premix with probe	12 μL

Incubate the cold competitor reaction mixture for 15 min at room temperature along with the other reaction mixtures.

10. Add 5 μL of bromophenol blue dye mixture (DNA bromophenol blue) per reaction tube.
11. Prepare 0.5X TBE to be used as the running buffer (make 500 mL per gel).

12. Load samples onto gel and run at 140 volts for approx 2.5 h, or until dye band is 1.5 cm from the bottom of the gel.
13. Following the run, separate one glass plate from the gel and use the other glass plate as a support for the gel. Obviously, the plate selected as the support plate should be that to which the gel preferentially adheres to.
14. If the gel is to be dried immediately it does not need to be fixed; simply transfer the gel to the drying paper and dry at 80°C for approximately 1.5 h/gel.
15. Expose dried gel to X-ray film in metal cassettes with intensifying screens. Make exposure at -70°C; usually 18 h to 72 h, depending upon age of ^{32}P label.

3.6. Probe Preparation

1. Set up the fill-in reaction in a microfuge tube as follows:

200 ng of oligonucleotide	20 μL
5X LB	20 μL
^{32}P dATP (SA>6000 Ci/mmol)	5 μL
^{32}P dCTP	5 μL
Klenow (15 U)	1 μL
A-dH ₂ O	49 μL

Incubate at room temperature overnight. A double stranded HSE oligonucleotide of the hsp70 gene promoter (45-mer upper strand and 36-mer lower strand) can be used.

5X LB reagent mix

- a. Solution O: 1 M Tris-HCl, pH 8.0, 0.125 M MgCl_2 (Dissolve 0.254 g in 10 mL of 1 M Tris). Store at 4°C.
- b. Solution A: 200 μL solution O, 3.6 μL β -mercaptoethanol, 5 μL 20 mM dGTP (Prepared in water and stored at -20°C), 5 μL 20 mM dTTP.
- c. Solution B: 2 M MOPS, pH 6.6 (use NaOH to pH) Stored at 4°C.
- d. Solution C: TE buffer (10 mM Tris-HCl, pH 7.5, and 1 mM EDTA), 5X LB is 10 μL solution A, 25 μL solution B, and 15 μL solution C. The labeled oligonucleotide is purified by using a NucTrap Probe purification column (Stratagene, La Jolla, CA).

3.7. Results

A representative autoradiogram is shown in **Fig. 1**. The activation of HSF during heat shock was detected by gel mobility shift assays. The HSE-protein complex found in extracts from unheated cells had an electrophoretic mobility distinct from that found in extracts made from heated cells. The latter is known as HSF-HSE complex (lane 2 in **Fig. 1**): activated HSF binds to HSE (4). The HSF binding activity was highly specific to HSE. The signal was abolished by adding a 200-fold molar excess of unlabeled HSE (lane 4 in **Fig. 1**); adding a 200-fold molar excess of unlabeled SP1 did not show the same effect (lane 7

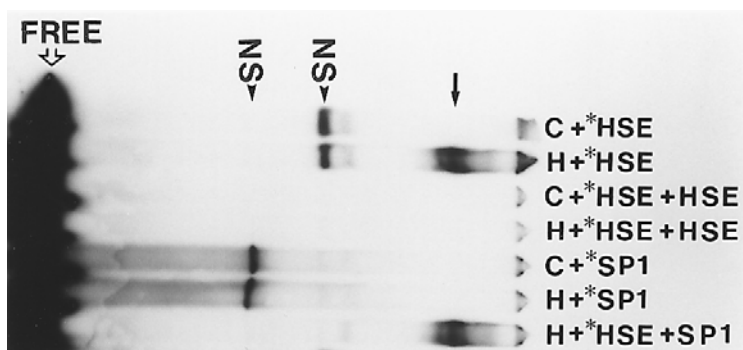


Fig. 1. Detection of a heat-shock element (HSE)-binding factor in whole-cell extracts prepared from control (C) and heated (H) cells. The gel mobility shift assay was performed with a ^{32}P -labeled HSE (*HSE) or SP1 (*SP1) oligonucleotide and whole cell extracts (20 $\mu\text{g}/\text{mL}$) prepared from cells incubated at 37°C or heated at 43°C for 1 h. Competition assays were performed by adding a 200-fold molar excess of a nonlabeled HSE oligonucleotide (lanes 3 and 4) or a nonlabeled SP1 oligonucleotide (lane 7). Closed arrow indicates a heat-specific HSE-binding activity. Closed arrowheads indicate a nonheat-specific interaction (NS). Open arrow indicates a free ^{32}P -labeled oligonucleotide fragment (FREE).

in **Fig. 1**). The activated HSF did not bind to SP1 consensus binding sequence (lane 6 in **Fig. 1**).

4. Notes

1. Harvested cells can be stored a long time at -70°C . Previously the aspirated pellets were frozen in liquid nitrogen. However, this is not necessary. Our experience indicates that the -70°C freezing provides results equal to those attained by the liquid nitrogen freezing.
2. To prepare Bradford reagent, dissolve the Coomassie Blue dye in the ethanol and then add the phosphoric acid and the water sequentially; filter using cotton balls in a funnel (try Whatman #1 using a Buchner funnel).
3. More often than not gels will either be rerun or samples will be used for several different gels. Therefore, to save time it is wise to make a sample dilution that is good for 5 gels. Thus, take an aliquot of each extract that contains 100 μg of protein and dilute this to 65 μL with the diluted extraction buffer; mix well by finger vortexing. Now use 13 μL of this dilution for each reaction ($5 \times 13 \mu\text{L} = 65 \mu\text{L}$) and refreeze the remainder at -70°C for later use.

References

1. Lindquist, S. and Craig, E. A. (1988) The heat-shock proteins. *Ann. Rev. Genet.* **22**, 631–677.

2. Li, G. C. and Werb, Z. (1982) Correlation between synthesis of heat shock protein synthesis in Chinese hamster fibroblasts. *Proc. Natl. Acad. Sci. USA* **79**, 3218–3222.
3. Pelham, H. R. B. (1982) A regulatory upstream promoter element in the *Drosophila* hsp70 heat-shock gene. *Cell* **30**, 517–528.
4. Schiller, P., Amin, J., Ananthan, J., Brown, M. E., Scott, W. A., and Voellmy, R. (1988) Cis-acting elements involved in the regulated expression of a human HSP70 gene. *J. Mol. Biol.* **203**, 97–105.
5. Ananthan, J., Goldberg, A. L., and Voellmy, R. (1992) Abnormal proteins serve as eukaryotic stress signals and trigger the activation of heat shock genes. *Science* **232**, 522–524.
6. Mosser, D. D., Kotabauer, P. T., Sarge, K. D., and Morimoto, R. I. (1990) *In vitro* activation of heat shock transcription factor DNA-binding by calcium and biochemical conditions that affect protein conformation. *Proc. Natl. Acad. Sci. USA* **87**, 3748–3752.
7. Baler, R., Welch, W. J., and Voellmy, R. (1992) Heat shock gene regulation by nascent polypeptides and denatured proteins: hsp70 as a potential autoregulatory factor. *J. Cell Biol.* **117**, 1151–1158.
8. Wu, C. (1985) An exonuclease protection assay reveals heat-shock element and TATA-box binding proteins in crude nuclear extracts. *Nature* **317**, 84–87.

Slot-Blot Hybridization in Studying Gene Expression During Oxygen Deprivation

Enbo Ma and Gabriel G. Haddad

1. Introduction

Gene expression plays an important role in many biological processes. During development, for example, early developmental genes are turned on first to guide embryonic pattern formation (*1–3*). A stress, either a physiological/pathophysiological or an environmental one, can also regulate the expression of certain genes. To meet the stressful challenges, an organism has to produce more chaperones or protective proteins (*4–6*). A growing body of evidence shows that O₂ deprivation differentially regulates gene expression (*7–9*).

There are many approaches which can be used to examine or investigate gene expression in certain situations. Each of these has advantages and disadvantages. Immunochemistry, for example, can be used to study gene expression at a protein level, but these methods are unavailable without having an appropriate antibody. Nucleic acid approaches overcome the limitations met in immunochemistry and directly examine the activities of a certain gene, even before its full characterization. Among these nucleic acid techniques, slot-blot hybridization is relatively easy and quick approach to be used in practice. We describe here in detail the use of slot hybridization in the study of gene expression during O₂ deprivation in the central nervous system of *Drosophila melanogaster*.

2. Materials

2.1. Equipment

1. MINI-SIEVE INSERT-ASTD (Bel-Art Products, Pequannock, NJ; openings of 707 and 500 μm).

From: *Methods in Molecular Biology*, vol. 196: *Oxidants and Antioxidants: Ultrastructure and Molecular Biology Protocols*
Edited by: D. Armstrong © Humana Press Inc., Totowa, NJ

2. Beckman oxygen analyzer.
3. Slot blot apparatus-Bio-Dot SF (Bio-Rad).
4. Computer imaging system (ImageQuaNT, Molecular Dynamics).
5. UV-VIS spectrophotometer.
6. Centrifuge.
7. Polytron homogenizer.
8. Hypoxia-chamber.

2.2. Reagents

1. Trizol Reagent kit (Gibco-BRL) for total RNA isolation.
2. FastTrack mRNA isolation kit (Invitrogen) for mRNA isolation.
3. Nitrogen to freeze dry tissues.
4. TE buffer: 10 mM Tris-HCl, pH 7.5, 1 mM EDTA, pH 8.0.
5. SSC buffer: dissolve 175.3 g of sodium chloride and 88.2 g of sodium citrate into 800 mL of water. Adjust pH to 7.0 with sodium hydroxide and the volume with water. Sterilize by autoclave.

3. Methods

3.1. *Drosophila* Stocks

Drosophila melanogaster stock Canton-S is maintained at room temperature (~22°C) on standard food medium consisting of 82.5% water, 6.5% cornmeal, 0.74% agar, 1.6% yeast, and 8.7% molasses. Either 0.56% propionic acid or 0.87% Tegosept is added to prevent the growth of mold. The flies from each stock are collected into 50 mL Corning tubes and divided into two groups, one used as control (normoxia) and another used for anoxia. The flies used as control are immediately frozen in liquid N₂ after being collected. The tubes containing the flies used for anoxia experiment are covered with nylon mesh and placed in a one-liter plastic box connected to a N₂ tank. Following the introduction of N₂ at a certain rate, the level of oxygen within the box (measured with a Beckman oxygen analyzer) declines to 0.02% within 1 min.

3.2. Head Collection

In order to obtain mass-isolated head RNA, Canton-S flies from both groups are frozen in liquid N₂, shaken vigorously, and pass through a number of sieves of successively smaller pore sizes. Specifically, shaken material is passed through two sieves (MINI-SIEVE INSERT-ASTD from Bel-Art Products, Pequannock, NJ; openings of 707, and 500 µm). Most heads pass through 707-µm sieve and accumulate on the 500-µm sieve; most bodies and some intact flies are collected on the 710-µm sieve; antennae, very small embryos, halteres and the fragments of legs pass through 500-µm sieve. In order to obtain clean heads, the collected heads are sieved one more time.

3.3. RNA Isolation

3.3.1. Total RNA Isolation

Total RNA is extracted from fly heads using Trizol Reagent. The procedure to isolate total RNA is summarized below.

1. Weigh about 300 mg of tissue (*see Note 1*).
2. Add 5 ml of Trizol Reagent (1.5 mL per 100 mg). Quickly homogenize the tissue with a homogenizer and incubate the homogenized samples 5 min at room temperature.
3. Add 1.0 mL of chloroform into each sample. Shake the tubes vigorously, and incubate the samples for 3 min at room temperature.
4. Centrifuge the samples at 11,500g for 10 min at 4°C and transfer the up-supernatant to new tubes.
5. Add 2.5 mL of 2-propanol into the tubes containing the up-supernatant. Incubate the samples for 10 min at room temperature before a centrifugation at 11,500g for 10.0 min at 4°C.
6. Discard the liquid. Wash the pellet with 8 mL of 75% of ethanol and centrifuge at 7,400g for 5 min at 4°C.
7. Discard the ethanol and let the pellet dry for 5 min at room temperature.
8. Dissolve the pellets with 100 μ L of TE buffer. Take 1 μ L of the dissolved total RNA into 499 μ L of H₂O to measure OD₂₆₀ and calculate the concentration of total RNA. RNA concentration (μ g/ μ L) can be calculated by the formula of $20 \times \text{OD}_{260}$.

3.3.2. mRNA Isolation

Poly(A)⁺ RNA can be isolated either from total RNA or directly from tissue using FastTrack mRNA isolation kit (Invitrogen). Our experience, however, indicates that more mRNA can be obtained from total RNA rather than directly from fly tissues. The procedure to isolate mRNA is described in detail in the Instruction Manual from Invitrogen.

3.4. Procedure for Slot-Blot Hybridization

3.4.1. Preparation of Slot Blots

To quantify the expression of certain genes from two groups of flies, slot blotting is performed with Bio-Dot Apparatus (Bio-Rad). Serial dilutions of mRNAs are blotted onto Nytran membrane (Schnell and Schuell). The procedure is detailed below:

1. Wet a 9 cm \times 13 cm Nytran membrane in DEPC-treated H₂O.
2. Transfer the wet Nytran membrane into 6X SSC (*see Note 2*).
3. Assemble the apparatus and tighten the apparatus while applying vacuum.

4. After assembly, apply 100 μL of 6X SSC into each well.
5. Gently remove the buffer from the wells. As soon as the buffer solution drains from all the wells, adjust the flow valve to atmospheric pressure.
6. Adjust mRNA sample to 50 μL with TE buffer, pH 7.5.
7. Add 30 μL of 20X SSC plus 20 μL of a 37% formaldehyde solution.
8. Incubate at 65°C for 15 min.
9. After adding 400 μL of 6X SSC to each sample, apply the samples into the wells immediately.
10. Pull the samples through by applying a gentle vacuum.
11. Rinse all wells with 500 μL of 6X SSC.
12. Apply vacuum until all wells dry.
13. Disassemble the apparatus, mark the membrane and rinse it in 2X SSC plus 0.1% SDS briefly.
14. Fix the mRNA membrane by UV cross-linking.

3.4.2. Preparation of Isotope Probes

As for Northern or Southern blot analyses, there are different probes which can be used in slot blot hybridization. To study expression profiles of different isoforms with a high homology in the gene, labeled antisense oligonucleotide (Oligo) as a probe is an appropriate choice. The 5'-end of an Oligo can be efficiently labeled in the following reaction:

2.0 μL	Oligo (5 pmol/ μL)
2.0 μL	10X T4 Kinase buffer
12. μL	$\gamma\text{-P}^{32}\text{ATP}$ (3 $\mu\text{Ci}/\text{pmol}$)
2.8 μL	H_2O
<u>1.2 μL</u>	<u>T₄ Kinase (10 U/μL)</u>
20.0 μL	

After an incubation for 75 min at 37°C, the labeled cDNA can be separated from un-incorporated $\gamma\text{-P}^{32}\text{ATP}$ using G25 column from Boeringer Mannheim. The following Oligos are examples used in this manuscript:

Ubiquitins (UB):

UB3: 5'-GTA GTG ACG ATC TTC GTG GGC AGC CAT GAA-3'

UB4: 5'-GGT CTT TCC GGT CAA AGA CTT CAC AAA GAT CTG-3'

Heat shock proteins (HSP):

HSP70: 5'-GTC GAT GGT CAG GAT GGT GAC ATC GAA GGT-3'

HSP26: 5'-CTC CTG GAG TTC ATC CAC AAG CGA AAG CAG-3'

3.4.3. Slot-Blot Hybridization

After 3 h of prehybridization in a buffer containing 40% formamide, 4X SSC, 5X Denhardt's and 200 $\mu\text{g}/\text{mL}$ of spermidine DNA, blots are hybridized (42°C overnight) with the $\gamma\text{-P}^{32}\text{ATP}$ -labeled antisense Oligo probes. After hybridiza-

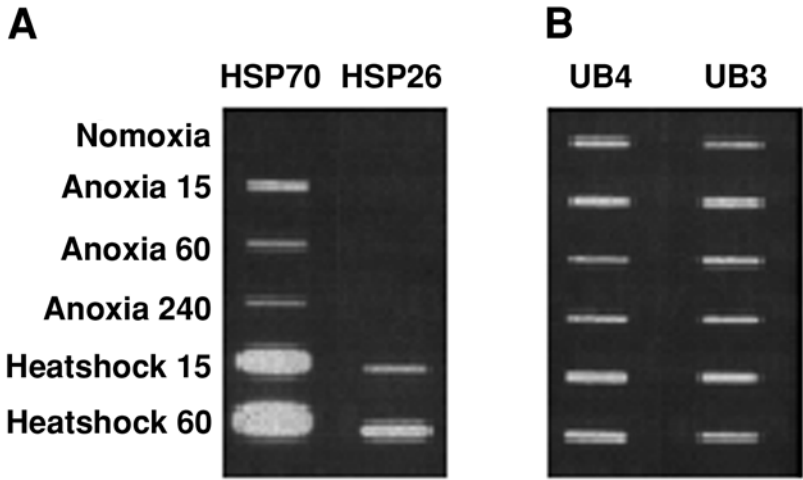


Fig. 1. Slot-blot hybridization. Six unique oligonucleotide probes were used to hybridize the blotted mRNAs from flies subjected to normoxia, anoxia (15, 60 and 240 min.) and heat shock (15 and 60 min.). HSP = heat shock proteins; UB = ubiquitins. *Note:* 1), HSP mRNA bands in normoxia are very weak because these genes are barely active at 20°C; 2), HSP26 expression in anoxic groups (15 min, 60 min. and 240 min.) is also very low.

tion, the blots are washed 30 min in 4X SSC with 0.5% SDS, 2X SSC with 0.25% SDS, 1X SSC with 0.1% SDS, and 0.5X SSC with 0.1% SDS, respectively. A final wash is performed at 55°C for 30 min in 0.2X SSC with 0.1% SDS. The membranes are then ready to be exposed to X-ray film 1–3 d at –70°C.

3.4.4. Measurement of Hybridization Signals

After the slots are exposed to X-ray film for a certain time, the films are scanned with a density scanning machine (ImageQuaNT, Molecular Dynamics). To quantify mRNA levels detected in anoxia and normoxia samples, the comparison is carried out in a linear portion between the blotted mRNA amount and the integrated optical density (area under the peak, IOD).

3.5. Results

1. Heat-shock proteins (HSP). To study the effects of anoxia on the expression of HSP genes and to determine their patterns of expression under different forms of stress, we treated the flies with either anoxia or heat shock. Interestingly, anoxia and heat shock regulate the expression of HSP genes in different ways. Data in **Fig. 1A** and **Table 1** show that HSP, especially HSP70, are significantly

Table 1
Relative Changes in mRNA Levels During Anoxia^a

		15 min	60 min	240 min
HSP70	Exp.1	808.99	494.82	365.55
	Exp.2	1743.01	1165.82	980.41
HSP26	Exp.1	2.84	0.01	3.74
	Exp.2	56.59	26.58	54.48
UB4	Exp.1	1.01	0.74	0.89
	Exp.2	0.91	0.71	0.91
UB3	Exp.1	1.55	1.51	1.37
	Exp.2	1.47	1.32	1.14

^amRNA levels during anoxia normalized to levels during normoxia. HSP = heat shock proteins; UB = ubiquitins. Exp.1 is abbreviation for experiment 1; and Exp. 2, for experiments 2. Note: the large difference between experiments 1 and 2 shown in this table for HSPs is mostly due to the extremely low expression during normoxia.

Table 2
Relative Changes in mRNA Levels During Heat Shock^a

		15 min	60 min
HSP70	Exp.1	6710.61	9304.84
	Exp.2	9186.91	12277.91
HSP26	Exp.1	136.97	601.79
	Exp.2	1390.21	4508.78
UB4	Exp.1	1.23	1.91
	Exp.2	1.31	1.44
UB3	Exp.1	1.45	1.24
	Exp.2	1.37	0.95

^amRNA levels during heat shock normalized to levels during normoxia. HSP = heat shock proteins; UB = ubiquitins. Exp.1 is abbreviation for experiment 1; and Exp. 2, for experiments 2. Note: again, the large difference between the two experiments is mostly due to the very low level during normoxia.

up-regulated during severe anoxia up to a thousand fold. HSP70 mRNA reach a maximum level within the first 15 min of anoxia and then decrease after one hour to a steady level that is still highly above baseline (**Table 1**). In contrast, both HSP70 and HSP26 mRNAs are remarkably increased up to few thousand fold by heat shock treatment (**Fig. 1A** and **Table 2**).

2. Ubiquitins (UB). Ubiquitins show a mixed response to anoxia. UB4 was down-regulated during anoxia by 10–30% while UB3 is upregulated by 1.4 times (**Fig. 1B** and **Table 1**). Heat shock up-regulates the expression of ubiquitins by 1.2–1.9 times (**Table 2**).

3. In summary, anoxia differentially regulates gene expression, and this regulation can be easily examined using slot blot analyses.

4. Notes

1. Always handle tissues on dry ice, never let the tissues thaw before homogenization.
2. Never let blots dry during hybridization and post-hybridization washes.

References

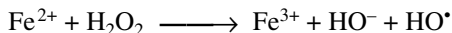
1. Ingham, P. W. (1988) The molecular genetics of embryonic pattern formation in *Drosophila* [Review] [85 refs]. *Nature* **335**(6185), 25–34.
2. Nusslein-Volhard, C. and Wieschaus, E. (1980) Mutations affecting segment number and polarity in *Drosophila*. *Nature* **287**(5785), 795–801.
3. Carroll, S. B. and Scott, M. P. (1986) Zygotically active genes that affect the spatial expression of the fushi tarazu segmentation gene during early *Drosophila* embryogenesis. *Cell* **45**(1), 113–126.
4. Benjamin, I. J., Kroger, B., and Williams, R. S. (1990) Activation of the heat shock transcription factor by hypoxia in mammalian cells. *Proc. Natl. Acad. Sci. USA* **87**, 6263–6267.
5. Buchner, J. (1996) Supervising the fold: functional principles of molecular chaperones. *FASEB J.* **10**, 10–20.
6. Das, D. K., Engelman, R. M., and Kimura, Y. (1993) Molecular adaptation of cellular defenses following pre-conditioning of the heart by repeated ischemia. *Cardiovasc Res.* **27** 578–584.
7. Norris, M. L. and Millhorn, D. E. (1995) Hypoxia-induced protein binding to O₂-responsive sequences on the tyrosine hydroxylase gene. *J. Biol. Chem.* **270** 23774–23779.
8. Semenza, G. L., Koury, S. T., Nejfelt, M. K., Gearhart, J. D., and Antonarakis, S. E. (1991) Cell-type-specific and hypoxia-inducible expression of the human erythropoietin gene in transgenic mice. *Proc. Natl. Acad. Sci. USA* **88**, 8725–8729.
9. Ma, E. and Haddad, G. G. (1997) Anoxia regulates gene expression in the central nervous system of *Drosophila melanogaster*. *Mol. Brain Res.* **46**, 325–328.

An Expression System for a Transporter of Iron and Other Metals

Michael D. Garrick and Kevin G. Dolan

1. Introduction

One major source of reactive oxygen species (ROS) is the Fenton reaction:



Mass action implies that ROS generated by the Fenton reaction depend on the intracellular concentration of ferrous ions ($[\text{Fe}^{2+}]$) although other metabolic fluxes make it difficult to capture this concentration dependence. Other metals such as Cu^+ may participate in a Fenton reaction and others may even have antioxidant activity; but, until recently, it was also difficult to affect intracellular $[\text{Fe}^{2+}]$ or the intracellular concentration of other divalent metals by experimental manipulation. This chapter reviews the discovery of a transporter that is involved in Fe^{2+} flux and potentially in the flux of other divalent metals and describes some ways to manipulate expression of this transporter.

Three papers led to the discovery of this transporter: Hediger's group (1) used expression in *Xenopus* oocytes to clone a cDNA from rat duodenum with properties that indicated that it could be the gastrointestinal (GI) Fe^{2+} transporter. Andrew's group (2) mapped the genetic locus for the *microcytic* (*mk*) mutation that causes a hypochromic, microcytic anemia in mice and inferred that a gly \rightarrow arg mutation at residue 185 (G185R) in a protein Nramp2 was the mutation and that the protein should be a GI transporter of iron. Our group collaborated with the latter group (3) to map the *Belgrade* (*b*) mutation that causes a somewhat similar anemia in rats and found an identical G185R mutation in the rat homolog. This paper eliminated the possibility that the G185R mutation was a linked genetic variation, indicating that it was respon-

sible for the anemia. Given that we had established that *b/b* rats had an intracellular defect in the transferrin cycle (4–6), the paper also showed that the transporter was responsible for endosomal exit of iron. The protein had been called Nramp2 (natural resistance associated macrophage protein 2) because it was first identified due to its sequence similarity to Nramp1 (7); however, many now prefer the name DMT1 (divalent metal transporter 1) or DCT1 (divalent cation transporter 1), reflecting the transporter's apparent ability to take up other metals in the oocyte system (1). We will use DMT1 henceforth.

The evidence above indicates that DMT1 is responsible for mammalian GI transport of Fe^{2+} and for intracellular flux of Fe^{2+} . In retrospect, DMT1 is also involved in uptake of iron that is not dependent on transferrin (8–10). Thus *mk/mk* mice and *b/b* rats provide researchers with animal models in which intracellular $[\text{Fe}^{2+}]$ is decreased and ROS are likely also to be decreased. Although we are currently testing the hypothesis that ROS are decreased in *b/b* rats, it is difficult to manipulate ROS or intracellular $[\text{Fe}^{2+}]$ in rats beyond the effects of the mutation. Transient overexpression of DMT1 in cell culture, however, can be coupled with controlled exposure of the cells to extracellular iron sources or to ROS generation so this chapter describes an expression system for DMT1. Because DMT1 may also transport other divalent metals (1) that may have pro-oxidant or anti-oxidant effects, it may turn out that this expression system will be useful not only to study metal uptake, but also to study controlled alteration of ROS by manipulating intracellular metal concentrations.

2. Materials

2.1. HEK293T Cells

1. HEK293T cells (American Type Culture Collection, Manassas, VA, <http://www.atcc.org>, CRL-1573).

2.2. Media

1. DMEM (Grand Island Biologicals (GIBCO), Grand Island, NY, <http://www.lifetech.com>, GIBCO 12100-046).
2. Fetal bovine serum (FBS, Atlanta Biologicals, Norcross, GA, S11150).
3. Opti-MEM® I Reduced Serum Medium (GIBCO 31985).

2.3. pMT2 Plasmid Constructs

1. Wild-type DMT1 (described in **ref. 3**).
2. G185R DMT1 (described in **ref. 3**).
3. Controls (appropriate additional controls could include vector alone and antisense but *see Notes*).

2.4. Transfection Reagent

1. DMRIE-C reagent (LIFE Technologies, Rockville, MD, <http://www.lifetech.com>, 10459).

2.5. Radioisotopes

1. $^{59}\text{FeCl}_3$ (NEN Life Science Products, Boston, MA, <http://www.nenlifesci.com>, NEZ037).
2. $^{54}\text{MnCl}_2$ (NEN Life Science Products, NEZ040).
3. $^{59}\text{FeSO}_4$ (NEN Life Science Products, NEZ049).

2.6. Cell Culture Materials

1. T-25 flasks, T-75 flasks and 35 mm culture plates (Becton-Dickinson, Franklin Lakes, NJ, Falcon 3108, 3111 and 3001, respectively).
2. Six well 35 mm culture plates (Marsh Biomedical Products, Rochester, NY, Greiner Labortechnik Cellstar 657 160).
3. Cell scrapers (Costar Corporation, Cambridge, MA).

2.7. Other Reagents

1. Other compounds were reagent grade.

3. Methods

3.1. Growth of Cells

HEK293T cells are grown in DMEM with 10% FBS at 37°C in 95% O₂/5% CO₂ in a CO₂ incubator. Cells grow well and must be split and passaged twice a week. We usually use T-25 flasks. As for most cultures, it is wise to freeze down an early passage in 90% FBS/10% dimethylsulfoxide using a cell-freezing container and store it in liquid N₂ as a precaution to replace contaminated cultures. We also have found that cultures occasionally decline at high passage number and need to be replaced.

3.2. Transfection and Subsequent Growth

Transfections are performed according to the flyer that accompanies the DMRIE-C reagent (*see Note 1*). Briefly, cells are seeded at 2×10^5 cells per 35 cm plate and are grown in high glucose DMEM supplemented with 10% FBS (*see Note 2*). Cells are transfected with one μg of the pMT2-DMT1 expression plasmid 18–24 h after seeding. Protein concentration is determined by BCA assay (*II*). Metal uptake assays should be done 48–72 h after transfection (*see Note 3*).

3.3. Metal Uptake Assays (Radioactive)

Uptake of ^{59}Fe or ^{54}Mn is assayed 48–72 h after transfection. Transfected cells are washed twice with prewarmed (37°C) incubation buffer (10 mM HEPES, 150 mM NaCl, 1% glucose, 1 mM CaCl_2 , 1 mM MgCl_2 , pH 6.0, or a selected pH). One μM $^{54}\text{Mn}^{2+}$ or $^{59}\text{Fe}^{2+}$ (or a selected concentration) is then added in incubation buffer and cells incubated at 37°C in a CO_2 incubator for 20 min (or a selected time). A saturation curve and time course for Mn were done to determine appropriate conditions. Ice cold PBS is added to stop the reaction then a cell scraper detaches the cells. The cells are transferred to a centrifuge tube on ice. Cells are spun at $7,800g$ for 5 min at 4°C . Cells are washed in ice cold PBS two more times. Cells are solubilized in 2.5% SDS and counted in a γ counter.

3.4. Metal Competition Assays

Incubations were as described above except that ~ 10 nM $^{54}\text{Mn}^{2+}$ or $^{59}\text{Fe}^{2+}$ was incubated with selected concentrations of nonradioactive MnCl_2 or FeSO_4 , respectively (*see Note 4*).

3.5. Possible Nonradioactive Metal Assays

The radioisotope assays above are valuable for assessing whether transfection and expression are functioning properly. One can use nonradioactive approaches, however, when the interest is ROS. If one wishes to check on uptake, atomic absorption spectrophotometry can be used. We recommend that conditions be similar to those in **Subheading 3.3.** above except that longer incubations should be investigated because they may lead to more ROS.

3.6. Results

1. **Figures 1** and **2** illustrate typical time and concentration dependence for uptake by transfected cells. Incorporation is linear for at least 1 h. The K_m is approx $1 \mu\text{M}$ for both metals.
2. **Figure 3** depicts the ability of Mn^{2+} to inhibit Fe^{2+} uptake and *vice versa*. Each metal competitively inhibits uptake of the other with the K_i approx $1 \mu\text{M}$ for both metals. Thus it appears that the two metals are transported via the same mechanism and utilize the same binding site.
3. **Figure 4** represents the effect of external pH (with a HEPES-MES buffer replacing the HEPES buffer to assure buffering over the range studied). Cells detached from plates at pH 5.5 so one can conclude that the optimum is pH 6.0 or lower for transport. **Figure 5** shows that the *b* mutation abrogates the stimulation of metal uptake, demonstrating that wild type DMT1 is responsible for the stimulation (*see Note 4*).
4. Using the conditions described, we find that $\sim 25\%$ of the cells are transfected transiently with pMT2-DMT1 (not shown). If one is in a position to compare

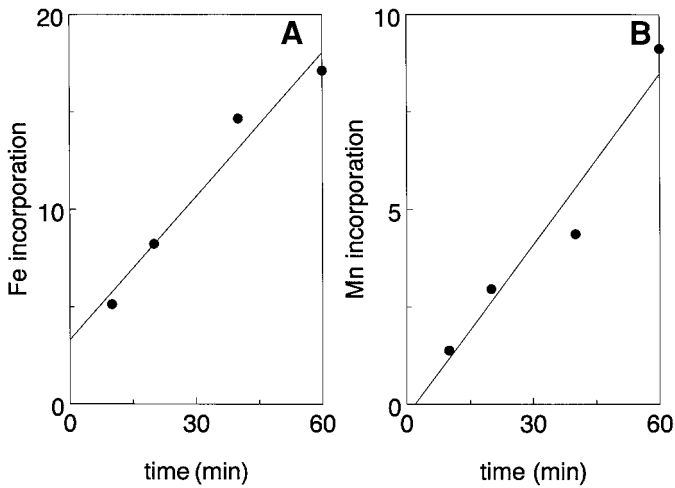


Fig. 1. Time course for uptake of Fe^{2+} or Mn^{2+} by HEK293T cells after transfection with pMT2-DMT1. Incorporation is expressed relative to uptake by untransfected cells in a 10 min incubation.

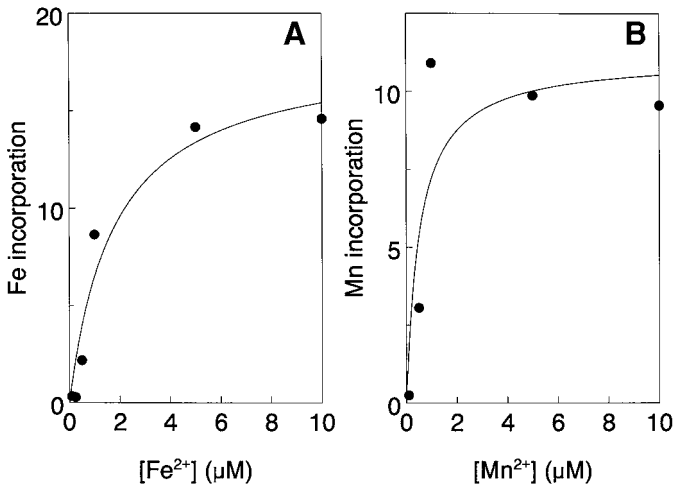


Fig. 2. Effect of metal concentration on uptake of Fe^{2+} or Mn^{2+} by HEK293T cells after transfection with pMT2-DMT1. Incorporation is expressed relative to uptake by untransfected cells at 100 nM of metal ion.

effects on cells within the same culture, then the untransfected cells can serve as a control for those expressing DMT1. If not, one should keep in mind that only a portion of the cells is expressing DMT1. We have not yet established how long beyond 1 h transiently transfected cells may be exposed to metals and still exhibit linear uptake. Attempts to obtain permanently transfected cells have been

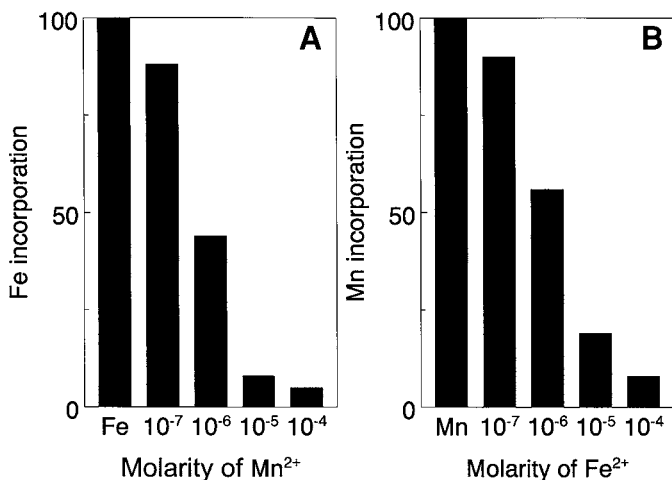


Fig. 3. Inhibition of uptake of Fe^{2+} or Mn^{2+} by HEK293T cells by Mn^{2+} or Fe^{2+} , respectively, after transfection with pMT2-DMT1. Incorporation is expressed as a percent of the Fe^{2+} only incubation for (A) and as a percent of the Mn^{2+} only incubation for (B).

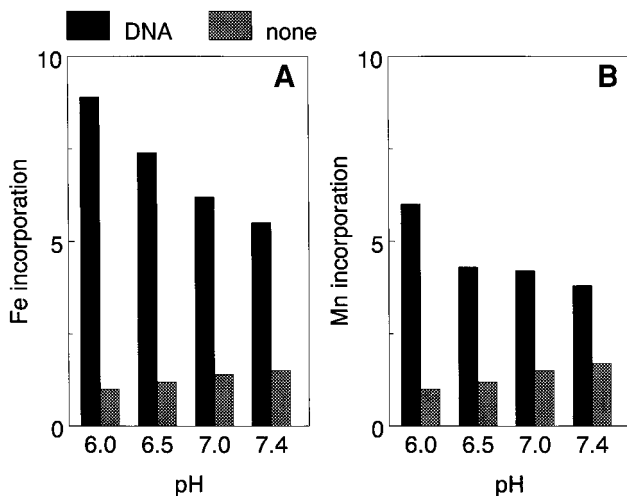


Fig. 4. Effect of external pH on uptake of Fe^{2+} or Mn^{2+} by HEK293T cells after transfection with pMT2-DMT1. Incorporation is expressed relative to uptake by untransfected cells (1.0) at pH 6.0.

unsuccessful so far, suggesting that continuous overexpression of DMT1 is toxic. Future plans include efforts to transfect HEK293T cells with constructs in which one can turn DMT1 expression on or off as desired. Such cell lines will yield deeper insight into this suggested toxicity.

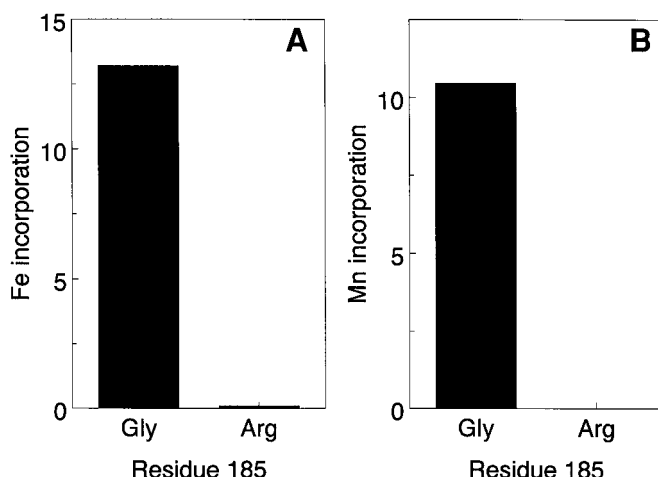


Fig. 5. Effect of the *b* mutation on uptake of Fe^{2+} or Mn^{2+} by HEK293T cells after transfection with pMT2-DMT1. Incorporation is expressed relative to uptake by untransfected cells as 1.0 after subtracting the same level of uptake. Thus G185R eliminates stimulation of Mn^{2+} uptake and nearly eliminates Fe^{2+} uptake.

4. Notes

1. Using 2 μL of DMRIE-C reagent per 35 mm well is sufficient. We have also used CaPO_4 precipitation in place of DMRIE-C reagent (3). CaPO_4 precipitation frequently yielded a higher efficiency of transfection but the efficiency of DMRIE-C reagent was much less variable (~25%). Presumably many of the other methods now available for transfection would also work. All of the Fe^{2+} uptake studies shown were done with CaPO_4 precipitation to transfect cells with DNA.
2. Frequently 1% penicillin and streptomycin are employed to minimize the risk of contamination. Although we use these antibiotics for routine growth of HEK293T cells, they are omitted for cultures after transfection preceding uptake assays. This omission prevents interference with the assays by the metals binding to the antibiotics. We are indebted to Dr. Marcel Conrad of the University of South Alabama (Mobile, AL) for drawing our attention to the ease of omitting the antibiotics.
3. Generally we have seen little or no difference between untransfected control cells and those transfected with the G185R mutant (Fig. 5) or with the antisense construct. This result implies that it is usually safe to omit the vector-only control or any of the other controls except untransfected cells.
4. It is much less expensive to order ^{59}Fe as NEZ037 (FeCl_3) than NEZ049 (FeSO_4), but DMT1 transports Fe^{2+} not Fe^{3+} . Moreover, the dilute FeSO_4 stock begins to convert to the ferric form as soon as it is exposed to oxygen. We therefore routinely mix $^{59}\text{FeCl}_3$ with a 10X excess of nonradioactive FeSO_4 to dissimulate

the iron to the ferrous form and add a 10X excess of ascorbic acid (relative to FeSO_4) to stabilize it for the length of the experiment. One can also order the more expensive form and add 1 mL of 10^{-5} M ascorbic acid to the $^{59}\text{FeSO}_4$ before dispensing it from the manufacturer's anaerobic container. The radio-labeled ferrous ascorbate can then be dispensed into tissue culture cell media containing 2-mercaptoethanol (10^{-4} M) to maintain the iron in a reduced state. We are indebted to Dr. Marcel Conrad of the University of South Alabama (Mobile, AL) for teaching us this alternative.

References

1. Gunshin, H., Mackenzie, B., Berger, U. V., Gunshin, Y., Romero, M. F., Boron, W. F., et al. (1997) Cloning and characterization of a mammalian proton-coupled metal-ion transporter. *Nature (London)* **388**, 482–488.
2. Fleming, M. D., Trenor, C. I., Su, M. A., Foernzler, D., Beier, D. R., Dietrich, W. F., and Andrews, N. C. (1997) Microcytic anaemia mice have a mutation in *Nramp2*, a candidate iron transporter gene. *Nature Genet.* **16**, 383–386.
3. Fleming, M. D., Romano, M. A., Su, M. A., Garrick, L. M., Garrick, M. D., and Andrews, N. C. (1998) *Nramp2* is mutated in the anemic Belgrade (*b*) rat: Evidence of a role for *Nramp2* in endosomal iron transport. *Proc. Natl. Acad. Sci. USA* **95**, 1148–1153.
4. Garrick, L. M., Gniecko, K., Hoke, J. E., Al-Nakeeb, A., Ponka, P., and Garrick, M. D. (1991) Ferric-salicylaldehyde isonicotinoyl hydrazone, a synthetic iron chelate, alleviates defective iron utilization by reticulocytes of the Belgrade rat. *J. Cell. Physiol.* **146**, 460–465.
5. Garrick, L. M., Gniecko, K., Liu, Y., Cohan, D. S., Grasso, J. A., and Garrick, M. D. (1993) Iron distribution in Belgrade rat reticulocytes after inhibition of heme synthesis with succinylacetone. *Blood* **81**, 3414–3421.
6. Garrick, M. D., Gniecko, K., Liu, Y., Cohan, D. S., and Garrick, L. M. (1993) Transferrin and the transferrin cycle in Belgrade rat reticulocytes. *J. Biol. Chem.* **268**, 14867–14874.
7. Gruenheid, S., Cellier, M., Vidal, S., and Gros, P. (1995) Identification and characterization of a second mouse *Nramp* gene. *Genomics* **25**, 514–525.
8. Garrick, L. M., Dolan, K. G., Romano, M. A., and Garrick, M. D. (1999) Non-transferrin-bound iron uptake in Belgrade and normal rat erythroid cells. *J. Cell. Physiol.* **178**, 349–358.
9. Eged, A. (1991) Na^+ modulates carrier-mediated Fe^{2+} transport through the erythroid cell membrane. *Biochem. J.* **275**, 635–638.
10. Hodgson, L. L., Quail, E. A., and Morgan, E. H. (1995) Iron transport mechanisms in reticulocytes and mature erythrocytes. *J. Cell. Physiol.* **162**, 181–190.
11. Smith, P. K., Krohn, R. I., Hermanson, R. I., Mallia, A. K., Gartner, F. H., Provenzano, M. D., et al. (1985) Measurement of protein using bicinchoninic acid. *Anal. Biochem.* **150**, 76–85.

Analysis of Gene Expression Following Oxidative Stress

Dana R. Crawford, Toshihide Suzuki, Jan Sesay,
and Kelvin J. A. Davies

1. Introduction

The modulation of gene expression by cellular stress is a universal phenomena that has been described in organisms ranging from bacteria to animals to plants, and in response to a wide range of stress agents including heat shock, glucose deprivation, oxidants, radiation, and heavy metals (*1*). For oxidative stress alone, many genes have been identified whose steady-state mRNA product levels are modulated by a multitude of oxidant stress agents (*1*). These genes were identified using various techniques that are still popular, such as two-dimensional gel electrophoresis, subtractive hybridization, differential display (DD), restriction fragment differential display (RFDD), serial analysis of gene expression (SAGE), and gene arrays; as well as other techniques that have lost their popularity, including one-dimensional protein gel electrophoresis and differential hybridization (*1*). Differential display (DD) is a polymerase chain reaction (PCR)-based technique that requires only small amounts of sample, is relatively sensitive, and able to identify both induced and reduced species (*2,3*). Its main drawbacks are a high number of false-positives and products that are strongly biased for the 3' untranslated region of the mRNA. These drawbacks have been addressed by a more recent technique called restriction fragment differential display (RFDD), which uses restriction enzyme-generated cDNA fragments as PCR templates (*1*). This modification allows for the use of much higher temperature and more specific annealing conditions as well as the ability to generate products that include the coding region and 5' untranslated region. Both techniques remain popular, in part due to

From: *Methods in Molecular Biology*, vol. 196: *Oxidants and Antioxidants: Ultrastructure and Molecular Biology Protocols*
Edited by: D. Armstrong © Humana Press Inc., Totowa, NJ

continuing improvements such as the combination of subtractive hybridization with DD (4) and the application of gene chip technology to RFDD.

Here, we describe our use of the basic DD and RFDD technologies to identify mRNAs that are modulated in response to acute hydrogen peroxide exposure (DD) as well as chronic resistance to hydrogen peroxide (RFDD).

2. Materials

2.1. Differential Display

2.1.1. Equipment

1. Spectrophotometer.
2. Electrophoresis unit (e.g., Gibco Model H4).
3. PCR thermocycler (e.g., MJ Research Model PTC-200 DNA engine).

2.1.2. Reagents

1. Commercial Differential display kit (e.g., GenHunter, Nashville, TN).
2. Oligolabeling kit (Amersham Pharmacia Biotech, Piscataway, NJ).
3. [γ - ^{33}P]-dATP (New England Nuclear, Boston, Mass; 2000 Ci/mmol).

2.2. Restriction Fragment Differential Display PCR (RFDD)

2.2.1. Equipment

As above for DD as well as an Eppendorf Tabletop Microfuge.

2.2.2. Reagents

1. displayPROFILE kit (Display Systems Biotech, Vista, CA).
2. Oligolabeling kit (Pharmacia, Piscataway, NJ).
3. [γ - ^{33}P]-ATP (ICN, Costa Mesa, CA; 3000 Ci/mmol).

3. Methods

3.1. Differential Display

3.1.1. Sample Collection and Preparation

1. Expose cultured cells to an oxidant of choice (for this study, hydrogen peroxide). At appropriate time points, extract total RNA using commercially available kits (e.g., RNA Isolator, Genosys, The Woodlands, Texas).
2. Treat RNA with RNase-free DNase according to the manufacturer (Boehringer Mannheim, Indianapolis, IN), check for integrity by ethidium bromide-staining of formaldehyde gels, and quantify spectrophotometrically using standard techniques (5).

3.1.2. Differential Display Procedure

1. cDNA subgroups are synthesized using arbitrary 13-mer primers containing a HindIII restriction site, with anchor primers containing a HindIII-site, oligo-dT

stretch, and terminal nucleotide, either A, C, or G. First strand cDNA template is synthesized by mixing 9.4 μL diethyl pyrocarbonate (DEPC)-treated water, 4 μL 5X reverse transcriptase buffer, 1.6 μL of a 250 μM mix of each dNTP, 2 μL of the 0.1 $\mu\text{g}/\mu\text{L}$ DNase RNA, and 2 μL of the oligo-dT primer of choice (10 μM). Heat for 5 min at 65°C and incubate at 37°C for 10 min. Start reaction by adding 1 μL of MMLV reverse transcriptase (Gibco BRL, Gaithersburg, MD) to each tube, and incubate the tubes at 37°C for 50 min more. Heat the tubes for 5 min at 95°C, centrifuge briefly, and store at -20°C for the subsequent PCR reaction.

2. For PCR amplification of a given subgroup, mix 10 μL water, 2 μL 10X PCR buffer, 1.6 μL of a 25 μM solution-containing a mix of each dNTP, 2 μL of an arbitrary primer (2 μM) of choice, 2 μL of an anchor primer (10 μM) of choice, 2 μL from the above reverse transcription reaction, 0.25 μL [α -³³P]-dATP, and 0.2 μL Taq polymerase (Perkin Elmer, Wilton, CT). A core mix of all of these reagents, except the primer(s) and reverse transcription reaction mix is made first and dispensed into each tube for more uniform results. After mixing, overlay reaction contents with 25 μL mineral oil (if necessary for chosen PCR thermocycler) and PCR amplify 40 cycles in a thermocycler using the following cycle parameters: 94°C, 30 s (denaturation), then 40°C, 2 min (annealing), then 72°C, 30 s (elongation) with a 5 min 72°C elongation extension at the last cycle (*see Note 1*).
3. Electrophorese samples through a standard 6% denaturing polyacrylamide gel, dry the gel, and expose to X-ray film. Compare band intensities on adjacent lanes (e.g., control vs treated) and excise modulated bands with a razor blade. Place in 400 μL water in a siliconized eppendorf tube for 10 min, heat to 95°C for 15 min in a heating block, and reamplify the DNA for 40 cycles as before except with no radiolabeled ATP and a final 20 μM dNTPs concentration in a final volume of 40 μL . Run out these reamplified DNAs on a low-melt agarose gel stained with ethidium bromide, excise the PCR bands, and place in separate pre-weighed eppendorf tubes. Add three times the mg weight of the gel slice as μL of water and store at 4°C or -20°C.
4. Radiolabel this DNA using the random priming Oligolabeling kit as described by the manufacturer and probe a Northern blot for final confirmation (*see Note 2*), and mRNA sizing using standard procedure (5).

3.2. RFDD

3.2.1. Sample Collection and Preparation

RNA is extracted and DNase-treated as above for DD, this time using hydrogen-peroxide resistant (HP50 and HP100) and nonresistant control HL-60 promyelocytes as a cell source (8).

3.2.2. RFDD Procedure

1. For this procedure, double-stranded cDNA is required. First-strand cDNA is prepared from DNase-treated RNA samples by mixing 10.0 μL of 0.1 $\mu\text{g}/\mu\text{L}$ DNase RNA, 1.5 μL of the anchored primer of choice (12.5 μM), 2.5 μL cDNA buffer

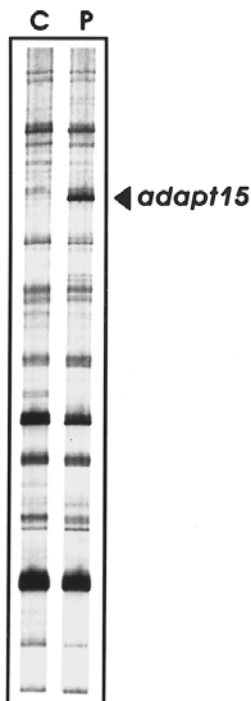
1. 5.0 μL of a 5 mM mix of each dNTP, 1 μL of reverse transcriptase (100 U/ μL displayREVERSE), and 5.0 μL DEPC-treated water. Incubate at 42°C for 2 h. For second strand synthesis, add 50 μL of the following mix to the 25 μL first strand reaction: 7.5 μL cDNA buffer 2, 2.5 μL of dNTP (5 mM each), 1.2 μL of DNA polymerase I (10 U/ μL), 0.8 μL of RNase H (2 U/ μL), and 38.0 μL water. Incubate for 2 h at 16°C. Extract with phenol/chloroform, centrifuge 5 min at high speed in a Microfuge, collect the aqueous phase, and precipitate by adding 0.1 volume of 3 M sodium acetate, pH 5.2, and 2 volumes of cold 100% ethanol as described (5). Store overnight at -20°C, centrifuge, wash the pellet with 75% ethanol, partially dry the pellet, and resuspend in 20 μL water (*see Note 3*).
2. For template preparation, add 2 μL of 10X displayBUFFER to 10 μL of double-stranded cDNA sample, followed by 0.5 μL TaqI restriction enzyme (10 U/ μL) and 7.5 μL of water. Incubate at 65°C for 2 h. The anchors are then ligated by adding the following to the above reaction (using a ligation core mix based on the number of TaqI reactions): 0.75 μL 10X displayBUFFER, 0.75 μL adaptor mix (15 μM), 1.25 μL ATP (10 mM), 0.30 μL T₄ DNA ligase (1 U/ μL), and 4.45 μL water. Incubate 3 h at 37°C (*see Note 4*).
3. End-label the 0 extension primer by combining the following per label: 0.10 μL 10X display Buffer, 0.40 μL of 0 extension primer (10 μM), 0.20 μL [γ -³³P]-ATP, 0.02 μL T₄ polynucleotide kinase, and 0.28 μL water. Incubate at 37°C for 30 min.
4. PCR amplify by scaling up the following reaction mix: 2.0 μL displayTAQ FL 10X reaction buffer, 0.8 μL dNTP mix (5 mM each), 1.0 μL labeled primer (4 μM), 0.3 μL displayTAQ FL (5 U/ μL), 4.0 μL displayPROBE (1 μM), 0.2 μL template, and 11.7 μL water. Heat to 94°C for 1 min, then follow with 10 cycles at 94°C for 30 s; 60°C down to 55°C with 0.5°C decrements in each cycle for 30 s; and 72°C for 1 min, followed by 25 cycles at 94°C, 30 s; 55°C, 30 s, and 72°C, 1 min.
5. After cycling, separate on a standard sequencing gel and analyze as above for DD. For candidate bands, reamplify by combining 4.0 μL displayTAQ FL 10X reaction buffer, 1.6 μL dNTP mix, 0.8 μL of 0 extension primer, 8.0 μL displayPROBE (1 μM), 5.0 μL gene fragment solution, 0.6 μL displayTAQ FL (5 U/ μL), and 20 μL water and PCR cycling 94°C for 30 s, 55°C for 30 s, and 72°C for 1 min for 30 cycles. Radiolabel and confirm, also as for DD.

3.3. Results

3.3.1. Differential Display

Figure 1A shows a representative Differential display gel. Comparison of the control- with treated-sample lanes identifies “candidate” modulated mRNAs. Excision of the candidate DNA band (designated by an arrow and in this case labeled “*adapt15*”), reamplification, and radiolabeling of the DNA to probe a Northern blot allows confirmation of the modulation (**Fig. 1B**). Subsequent cloning of confirmed Differential display bands is valuable for identification of

A Differential Display analysis



B Northern Blot analysis

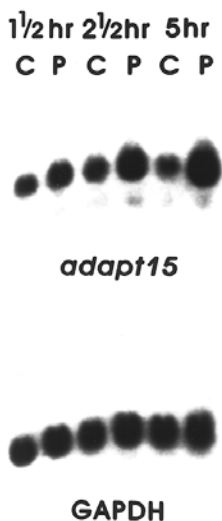


Fig. 1. Differential display analysis. (A) Representative differential display gel comparing the expression in HA-1 hamster control vs peroxide-treated cells. C, control sample lane; P, peroxide-treated cell sample lane. Arrow denotes candidate band (“*adapt15*”) (B) The candidate DNA band in **Fig. 1A** was excised, reamplified, radiolabeled, and used to probe a Northern blot containing RNA extracted from HA-1 hamster cells at multiple time points after peroxide exposure to confirm the modulation. The Northern blot was also probed with glyceraldehyde-3-phosphate dehydrogenase (GAPDH) cDNA as a loading control.

the “parent” mRNA species it represents for expression analyses, and for use as a probe to obtain full length clones (*see Note 5*). In the case of *adapt15*, these subsequent analyses indicated that no functional information had previously been published on *adapt15* (i.e., it was novel), that it was a member of the *gadd* stress response gene family, and that it was associated with active translation in the cell (3,6). Unfortunately, DD is also plagued by false-positives (*see Notes 6 and 7*). Often, candidate bands similar in differential band intensity to that observed for *adapt15* do not confirm at the Northern blot level.

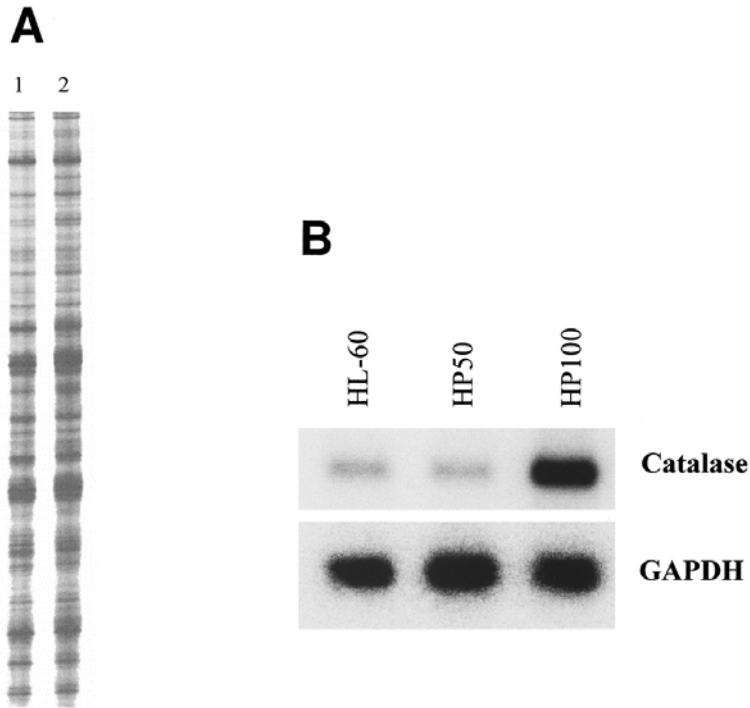


Fig. 2. Restriction fragment differential display analysis. (A) Representative RFDD gel using hydrogen-peroxide resistant (HP50 and HP100) and nonresistant control HL-60 promyelocytes as a cell source. Compared samples are referred to as 1 and 2. (B) Northern blot confirmation analysis of a RFDD candidate DNA band. Excision, reamplification, and radiolabeling were performed as above for DD. Subsequent cloning, sequencing, and GenBank database analysis identified the confirmed band as catalase.

3.3.2. RFDD

Figure 2A shows a representative RFDD. As with DD, comparison of the samples (sample 1 vs sample 2) lanes identifies “candidate” modulated mRNAs. Candidate bands are then excised and reamplified, followed by Northern blot hybridization; also the same approach used for DD (*see Note 8*). An example of a confirmation analysis is shown in **Fig. 2B**. The strongly induced, confirmed band in the HP100 hydrogen peroxide-resistant cells in **Fig. 2B** was identified as catalase. This result is consistent with previous studies where catalase mRNA levels were found to be elevated 16-fold in the most peroxide-resistant (HP100) versus control (HL-60 cells due to gene amplification (7). We have also identified reduced species in the resistant cells using this RFDD technique.

4. Notes

1. Although the standard number of PCR cycles is 40, less can be used. We have found that 33–35 cycles is sufficient for most analyses and can also lead to a modest increase in the observed differential signal between samples, presumably because the weaker band sample species does not have time to “catch up” once the stronger band sample species enters plateau phase.
2. False-positives are a major drawback to conventional Differential display. Many variations on the conventional technique have been developed in attempts to address this problem, with varying levels of success. We use reverse Northern blot analysis as described (7) to better screen for positives, which dramatically lowers the number of false-positives. For these analyses, we use the Convertible slot blotting apparatus (Gibco, Gaithersburg, MD).
3. It is useful to first check 10 μ L of the resuspended second-strand cDNA on an 0.8% agarose gel for a cDNA smear between 100 and 2000 base pairs. If the maximum observed size is 400 base pairs or less, stop here, discard samples, and repeat the RNA extraction.
4. Although the standard temperature for ligation is 37°C, we have found that changing the ligation temperature to 16°C overnight reduces variability.
5. Confirmed modulated bands can be cloned into a suitable vector (e.g., PCR-TRAP, GenHunter) for subsequent sequencing and identification using the GenBank database.
6. Because of the false-positive drawback of this technique, it is important to run the samples in at least duplicate and preferably in triplicate before deciding upon a candidate.
7. Multiple bands can sometimes occur at the same location, resulting in 2–4 bands that show the same modulation. These usually represent the same species with one-base exceptions, so that only one of these bands need to be excised.
8. An advantage to this procedure over DD is the use of a much higher annealing temperature to minimize the number of false-positives. This is due to the increased length of the PCR primers used for RFDD.

References

1. Crawford, D. R., Suzuki, T., and Davies, K. J. A. (2000) Oxidant-modulated gene expression, in *Antioxidant and Redox Regulation of Genes* (Sen, C. K., Sies, H., and Baeuerle, P. A., eds.), Academic Press, San Diego, CA, pp. 21–45.
2. Liang, P. and Pardee, A. B. (1992) Differential display of eukaryotic messenger RNA by means of the polymerase chain reaction. *Science* **257**, 967–971.
3. Crawford, D. R., Schools, G. P., Salmon, S. L., and Davies, K. J. A. (1996) Hydrogen peroxide induces the expression of *adapt15*, a novel RNA associated with polysomes in hamster HA-1 cells. *Arch. Biochem. Biophys.* **325**, 256–264.
4. Pardinas, J. R., Combates, N. J., Prouty, S. M., Stenn, K. S., and Parimoo, S. (1998) Differential subtraction display: a unified approach for isolation of cDNAs from differentially expressed genes. *Anal. Biochem.* **257**, 161–168.

5. Crawford, D. R., Edbauer-Nechamen, C. A., Lowry, C. V., Salmon, S. L., Kim, Y. K., Davies, J. M. S., and Davies, K. J. A. (1994) Assessing gene-expression during oxidative stress. *Methods Enzymol.* **234**, 175–217.
6. Crawford, D. R., Schools, G. P., and Davies, K. J. A. (1996) Oxidant-inducible *adapt15* is associated with growth arrest and DNA damage-inducible *gadd153* and *gadd45*. *Arch. Biochem. Biophys.* **329**, 137–144.
7. Francia, G., Mitchell, S. D., Moss, S. E., Hanby, A. M., Marshall, J. F., and Hart, I. R. (1996) Identification by differential display of annexin-VI, a gene differentially expressed during melanoma progression. *Cancer Res.* **56**, 3855–3858.
8. Yamada, M., Hashinaka, K., Inazawa, J., and Abe, T. (1991) Expression of catalase and myeloperoxidase genes in hydrogen peroxide-resistant HL-60 cells. *DNA Cell Biol.* **10**, 735–742.

Measurement of Immunoglobulin G Oxidation by Western-Blot Analysis

Andrew Chow, Shahid Ahmed, Larissa Chaplia,
and Joseph Mattana

1. Introduction

Oxygen radicals are chemical species that have an unpaired electron in their outer orbits. The unpaired electron gives the radical instability and it reacts easily with inorganic or organic chemicals. The three most important species are superoxide, hydrogen peroxide, and hydroxyl ions. The body keeps the system in balance by antioxidants, like vitamin E, ceruloplasmin, and transferrin, which act as scavengers for the oxygen radicals. Enzymes, like superoxide dismutase, catalase, and glutathione peroxidase, reduce oxygen radicals to oxygen and water.

Increased oxidative stress is useful in situations like microbial killing. However, oxidation of organic chemicals in the body may have harmful effects (*1–4*). For example, oxygen radicals generate atherogenic lipid products that may contribute to a higher incidence of cardiovascular disease (*5–9*). Oxidative modification of DNA can result in mutagenesis and an increased risk of malignant transformation (*10*).

While the susceptibilities of lipids and DNA to oxidation and the consequences of this are well known, less is known regarding how oxidation of other biological substrates can alter their structure and function. An increase in protein oxidation has been demonstrated in normal human aging (*11*) as well as inflammatory diseases (*12*). The pathophysiological consequences of protein oxidation are not yet fully understood although oxidation of a number of proteins appears to alter their function and different proteins appear to have different degrees of susceptibility to oxidation (*13–18*).

From: *Methods in Molecular Biology*, vol. 196: *Oxidants and Antioxidants: Ultrastructure and Molecular Biology Protocols*
Edited by: D. Armstrong © Humana Press Inc., Totowa, NJ

Oxidation of protein results in the formation of carbonyl groups, which can be labeled with 2,4-dinitrophenylhydrazine (DNPH) to form stable protein hydrazones, which can be measured spectrophotometrically (**16**). The development of antibodies specific for DNPH-labeled proteins has made possible Western-blot analysis by which a variety of proteins can be studied (**16**). Shacter et al. for example, have described a method for Western-blot analysis of plasma subjected to oxidation with a metal-catalyzed oxidation system (**17**). This protocol will provide the information needed for purifying and measuring oxidized immunoglobulin G using Western-blot analysis.

2. Materials

2.1. Equipment

1. Sterifil D-HA (0.45 μ m filter unit).
2. Trans-Blot Filter Paper.
3. Trans-Blot Nitrocellulose Membrane (0.45 μ m).
4. DEAE-Affi-Gel Blue IgG Purification Column (Bio-Rad).
5. 10 DG Desalting Column (Bio-Rad).
6. Mini-Protean II Electrophoresis Cell (Bio-Rad).
7. 4–15% acrylamide gradient gel (Bio-Rad).
8. Kodak X-OMAT AR film.

2.2. Reagents

1. Bovine serum albumin (BSA; Sigma, fraction V).
2. Sodium dodecyl sulfate (SDS).
3. Phosphate-buffered saline (PBS).
4. Transfer Buffer (12 mM Tris, 96 mM Glycine, 20% Methanol).
5. PBS-T (PBS, pH 7.2–7.5 containing 0.05% Tween 20).
6. OxyBlot™ Protein Oxidation Detection Kit (Intergen).
7. ECL chemiluminescent reagent (Amersham).
8. Micro BCA* protein assay kit (Pierce).

3. Methods

3.1. Collection of Human Plasma

1. Collect 3 mL whole human blood in Vacutainer-type tube containing 5.4 mg EDTA.
2. Place blood samples on ice until centrifugation.
3. Centrifuge blood samples at 2000 rpm at 4°C for 10 min.
4. Isolate plasma and determine protein concentration by Micro BCA* protein assay kit.
5. Analyze plasma immediately or store in aliquots at –70°C in a light shielded container.

3.2. Purification of Human Immunoglobulin G

3.2.1. Buffer Preparation

1. Loading buffer preparation.
 - a. Prepare 0.02 M K_2HPO_4 with distilled, deionized water (*see Note 1*).
 - b. Filter the buffer through Steril D-HA (0.45 μm filter unit).
 - c. Adjust pH to 8.0 ± 0.2 with 10 N KOH or 6 N HCl.
 - d. Store buffer at 4°C.
2. Regeneration buffer preparation.
 - a. Prepare 1.5 M sodium thiocyanate with the loading buffer (*see Note 2*).
 - b. Filter the buffer through Steril D-HA (0.45 μm filter unit).
 - c. Store buffer at 4°C; no pH adjustment is necessary.

3.2.2. Plasma Sample Preparation

1. Prepare a Desalting column (Bio-Rad) according to the manufacturer's instructions and equilibrate with a bed volume of loading buffer (*see Notes 3–5*).
2. Add 3 mL of plasma to the column and discard the elution (*see Note 6*).
3. Add 4 mL of loading buffer and collect the elution fraction.
4. If desired, store the desalted plasma elution fraction at -70°C ; or continue with the IgG purification process.
5. Wash the column with a bed volume of distilled, deionized water containing 0.02% sodium azide and store the column at 4°C (*see Note 7*).

3.2.3. Immunoglobulin G Purification

1. Prepare a column of DEAE-Affi-Gel Blue (Bio-Rad) according to manufacturer's instructions and equilibrate with 1.5X bed volume of loading buffer (*see Notes 3, 5, and 8*).
2. Add 2.5 mL (*see Note 9*) of the desalted plasma (*see Note 10*) to the column and discard the elution.
3. Add 20 mL (or a bed volume) of loading buffer to the column.
4. Collect the elution fractions in volumes approx equal to that of the sample applied.
5. Store the purified IgG elution fraction at -70°C (*see Note 11*).
6. Regenerate the column with a bed volume of regeneration buffer (*see Note 12*).
7. Wash the column with 1.5X bed volume of loading buffer containing 0.02% sodium azide and store the column at 4°C (*see Note 13*).
8. Run on SDS PAGE to determine IgG-rich fractions.
9. Determine each purified IgG elution fraction concentration by Micro BCA* protein assay kit.

3.3. In Vitro Oxidation of Immunoglobulin G

Incubate IgG with equal volume of metal-catalyzed oxidation system (phosphate buffered saline containing final concentration of 2 mM FeCl_3 , 25 mM

ascorbate and 2.4 mM EDTA, pH 7.4) or EDTA alone (control) for 60 min at 37°C. Samples are then extensively dialyzed against sodium phosphate buffer for 24 h at 4°C.

3.4. Western-Blot Analysis

1. Add SDS to IgG sample to make a final concentration of 6% SDS.
2. Mix the sample with an equal volume of 10 mM 2,4-dinitrophenylhydrazine (DNPH) and incubate at room temperature for 15 min.
3. Add 7.5 μ L of OxyBlot™ Neutralization Solution (*see Note 14*).
4. Mix the sample with an equal volume of 2X concentrated sample buffer.
5. Load IgG sample mixtures and a molecular mass marker (OxyBlot™) onto an acrylamide gel (4–15%).
6. Separate the samples electrophoretically at 90V initially, then at 140V.
7. Transfer the samples electrophoretically onto nitrocellulose membrane (NCM) at 20 V for 16 h at 4°C.
8. Incubate NCM with blocking buffer (PBS-T with 1% BSA) for 1–2 h at room temperature.
9. Incubate NCM with primary antibody (1 : 150 rabbit anti-DNPH [OxyBlot™] in blocking buffer) for one hour at room temperature.
10. Rinse NCM twice with PBS-T, then wash NCM with PBS-T once for 15 min and twice for 5 min each.
11. Incubate NCM with secondary antibody (1 : 300 HRP conjugated goat anti-rabbit antibody [OxyBlot™] in blocking buffer) for 1 h at room temperature.
12. Repeat the rinse and wash steps as in **Subheading 3.4., step 10**.
13. Incubate NCM with ECL chemiluminescent reagent.
14. Produce autoradiographs.

3.5. Results

3.5.1. Western-Blot Analysis of Oxidized Immunoglobulin G

Figure 1 demonstrates oxidation of IgG using the FeCl₃/ascorbate/EDTA system via Western blot analysis using a highly specific antibody to DNPH-labeled oxidized protein from a representative experiment. IgG was preincubated with the oxidizing system for 1 h and dialyzed as described previously. This shows increased protein oxidation by incubation with the oxidizing system at molecular masses corresponding to the heavy and light chains of IgG (**15**).

3.5.2. Western-Blot Analysis of Immunoglobulin G Purified from Plasma of Control and Hemodialysis Patients

Patients with end-stage kidney failure who are on hemodialysis appear to suffer enhanced oxidative stress (**5–7**). **Figure 2** illustrates the results of

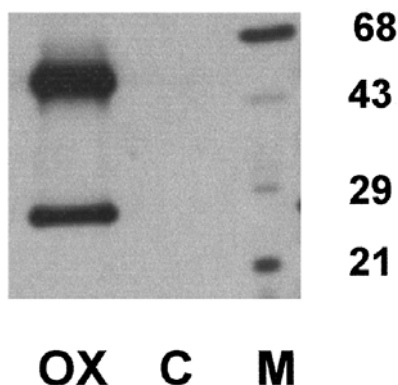


Fig. 1. Western-blot analysis of purified human IgG oxidized with a metal-catalyzed oxidation system and control. Control IgG (treated with EDTA alone) and IgG oxidized for 60 min using a FeCl_3 /ascorbate/EDTA oxidizing system were extensively dialyzed. The protein samples were incubated with 2,4-dinitrophenylhydrazine (DNPH), loaded at 3 μg per lane, and separated via SDS-PAGE. Western-blot analysis using an antibody specific for DNPH-labeled oxidized protein was then carried out.

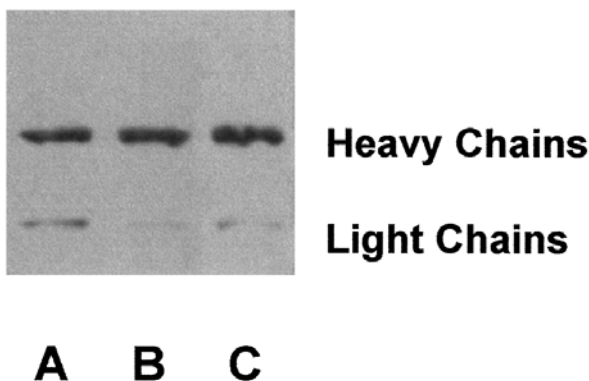


Fig. 2. Western-blot analysis of IgG purified from plasma of three hemodialysis patients. Whole human blood (3 mL) was obtained from each patient. The plasma was desalted, and IgG was purified using DEAE-Affi-Gel Blue columns (Bio-Rad). Purified IgG was incubated with 2,4-dinitrophenylhydrazine (DNPH), loaded at 3 μg per lane, and separated via SDS-PAGE. Western-blot analysis using an antibody specific for DNPH-labeled oxidized protein was then carried out. (A), (B), and (C) represent purified IgG from three patients.

Western-blot analysis of IgG purified from three hemodialysis patients. Two bands, one between 68 and 43 kD and the second between 29 and 21 kD corresponding to the heavy and light chains of IgG can be seen with greater antibody binding to the heavy chains.

4. Notes

1. For purification of IgG from rabbit plasma, it is recommended that 0.02 *M* Tris-HCl, pH 8.0 \pm 0.2, containing 0.028 *M* NaCl be used.
2. Another suitable regeneration buffer includes 2 *M* guanidine HCl in the loading buffer.
3. It is recommended that these steps should be carried out at 4°C.
4. Total bed volume to plasma volume ratio is 7:1.
5. Flow will stop when the buffer level reaches the top frit; the column will not run dry.
6. If the plasma sample is less than 3 mL, add loading buffer to make a total volume of 3 mL.
7. If the column is to be used again immediately, wash the column with a bed volume of loading buffer.
8. Total bed volume to sample volume ratio is 8:1.
9. If manufacturer's column is used, check label on column package for exact column sample capacity.
10. Desalted plasma samples obtained from **Subheading 3.2.2., step 3** or other alternate desalting procedure.
11. Transferrin (76,000 kD) usually coelutes with the IgG fraction.
12. An optional step before regenerating the DEAE-Affi-Gel Blue column: wash the column with loading buffer containing 1.4 *M* NaCl to elute the bound albumin.
13. If the column is to be used again immediately, wash the column with 1.5X bed volume of loading buffer.
14. If reduction of the protein sample is desired, add 2-mercaptoethanol to the sample mixture for a final concentration of 0.74 *M* 2-mercaptoethanol.

References

1. Halliwell, B. (1987) Oxidants and human diseases: some new concepts. *FASEB J.* **1**, 358–364.
2. Freeman, B. A. and Crapo, J. D. (1982) Biology of disease: free radicals and tissue injury. *Lab. Invest.* **47**, 412–426.
3. Slater, T. F. (1984) Free radical mechanisms in tissue injury. *Biochem. J.* **222**, 1–15.
4. Henson, P. M. and Johnston, R. B., Jr. (1987) Tissue injury in inflammation: oxidants, proteases and cationic proteins. *J. Clin. Invest.* **79**, 669–674.
5. Richard, M. J., Arnaud, J., Jurkovitz, C., Hachache, T., Meftahi, H., Laporte, F., et al. (1991) Trace elements and lipid peroxidation abnormalities in patients with chronic renal failure. *Nephron* **57**, 10–15.
6. Dasgupta, A., Hussain, S., and Ahmad, S. (1992) Increased lipid peroxidation in patients on maintenance hemodialysis. *Nephron* **60**, 56–59.
7. Maggi, E., Bellazzi, R., Falaschi, F., Frattoni, A., Perani, G., Finardi, G., et al. (1994) Enhanced LDL oxidation in uremic patients: an additional mechanism for accelerated atherosclerosis? *Kidney Int.* **45**, 876–883.
8. Witzum, J. L. (1994) The oxidation hypothesis of atherosclerosis. *Lancet* **344**, 793–795.

9. Steinberg, D., Parthasarathy, S., Carew, T. E., Khoo, J. C., and Witztum, J. L. (1989) Beyond cholesterol: modifications of low-density lipoprotein that increase its atherogenicity. *N. Engl. J. Med.* **320**, 915–924.
10. Imlay, J. A. and Linn, S. (1988) DNA damage and oxygen radical toxicity. *Science* **240**, 1302–1309.
11. Oliver, C. N., Ahn, B., Moerman, E. J., Goldstein, S., and Stadtman, E. R. (1987) Age-related changes in oxidized proteins. *J. Biol. Chem.* **262**, 5488–5491.
12. Stadtman, E. R. and Berlett, B. S. (1991) Fenton chemistry: amino acid oxidation. *J. Biol. Chem.* **266**, 17201–17211.
13. Oliver, C. N., Starke-Reed, P. E., Stadtman, E. R., Liu, G. J., Carney, J. M., and Floyd, R. A. (1990) Oxidative damage to brain proteins, loss of glutamine synthetase activity and production of free radicals during ischemia/reperfusion injury to gerbil brain. *Proc. Natl. Acad. Sci. USA* **87**, 5144–5147.
14. Oliver, C. N. (1987) Inactivation of enzymes and oxidative modification of proteins by stimulated neutrophils. *Arch. Biochem. Biophys.* **253**, 62–72.
15. Margiloff, L., Chaplia, L., Chow, A., Singhal, P. C., and Mattana, J. (1998) Metal-catalyzed oxidation of immunoglobulin G impairs Fc receptor-mediated binding to macrophages. *Free Rad. Biol. Med.* **25**, 780–785.
16. Levine, R. L., Williams, J. A., Stadtman, E. R., and Shacter, E. (1994) Carbonyl assays for determination of oxidatively modified proteins. *Methods Enzymol.* **233**, 346–357.
17. Shacter, E., Williams, J. A., Lim, M., and Levine, R. L. (1994) Differential susceptibility of plasma proteins to oxidative modification: examination by Western blot immunoassay. *Free Rad. Biol. Med.* **17**, 429–437.
18. Mattana, J., Margiloff, L., Chaplia, L., Chow, A., and Singhal, P. C. (1998) Metal-catalyzed oxidation of extracellular matrix increases macrophage nitric oxide generation. *Kidney Int.* **54**, 1581–1592.

Thioredoxin and Redox Regulation of the Nuclear Receptor

Yuichi Makino, Kensaku Okamoto, and Hirotoshi Tanaka

1. Introduction

Oxidative stress evokes various cellular responses including alteration of gene expression to preserve cellular homeostasis (1,2). Thioredoxin (TRX) is a small ubiquitous protein with protein thiol-reducing activity and has been shown to function as a cellular antioxidant buffering system in response to oxidative stress and play essential roles in maintenance of cellular function (3,4). Recently, a growing number of evidence has shown that TRX plays crucial roles in redox regulation of gene expression via either direct or indirect interaction with various transcription factors including NF- κ B (5), AP-1 (6), and PEBP2 (7). Alteration in expression and/or subcellular localization of TRX has been indicated to be involved in such redox-dependent control of the transcription factors (8,9), however, precise mechanisms remain unknown.

The glucocorticoid receptor (GR) is a ligand-inducible transcription factor that belongs to the superfamily of the nuclear receptors (10). Like other members of the superfamily, the GR is composed of a central DNA binding domain (DBD), nuclear localization signals, a ligand binding domain, and several transactivation functions (11,12). Each domain contains structurally and functionally crucial cysteine residues and thus the GR is shown to be susceptible to redox-mediated modification both in vitro and in vivo (13–16). We have shown that GR function is coordinately modulated by cellular redox status and TRX levels under oxidative conditions (17). Moreover, the estrogen receptor, a member of nuclear receptors as well, has been shown to be likewise regulated by cellular redox state and TRX (18), indicating that TRX might

widely participate in regulation of nuclear receptor-mediated signal transduction. Monitoring and illustration of the interplay between TRX and the nuclear receptors, thus, might be prerequisite for elucidation of a pathophysiological importance of TRX in conditional regulation of the nuclear receptor-mediated transcriptional regulation of gene expression.

In this line, we here describe variety of methodologies to monitor: 1) expression and subcellular localization of TRX, 2) effect of TRX on transcriptional control by the nuclear receptors, and 3) physical interaction between TRX and the nuclear receptors.

2. Materials

2.1. Equipment

1. Centrifuge.
2. UV-VIS spectrophotometry.
3. Electrophoresis apparatus.
4. Lumino-meter.
5. Confocal laser scanning microscope (or fluorescent microscope).

2.2. Reagents

Diamide, hydrogenperoxide (H_2O_2), dexamethasone (DEX) were purchased from Sigma (St. Louis, MO).

2.3. Plasmids (see Note 1)

1. The expression plasmids for: the wild-type GR, pRShGR α ; the wild-type TRX, pcDSR α ADF; the antisense TRX, pASADF.
2. Reporter plasmid: glucocorticoid-responsive luciferase reporter plasmid driven by the tandem repeat of glucocorticoid response element (GRE), pGRE-Luc.

2.4. Recombinant Proteins (see Note 2)

1. TRX.
2. Glutathione S-transferase (GST)-fused GR DBD (GST-GR DBD).

2.5. Cell Culture

COS7 and HeLa cells were purchased from RIKEN (Tsukuba Science City, Japan) and maintained in Dulbecco's modified Eagle's medium (DMEM, Invitrogen, Carlsbad, CA), pH 7.0, supplemented with 10% heat-inactivated fetal calf serum (FCS) and antibiotics.

2.6. Antibodies

1. Anti-TRX mouse monoclonal antibody was purchased from Oriental Yeast (Nagahama, Japan).
2. Anti-GST antibody was from Amersham Bioscience (Uppsala, Sweden).

3. Methods

3.1. Analysis of TRX Expression under Oxidative Stress

It has been reported that expression of TRX is induced by a variety of intra- and extracellular stresses including oxidative stress (19), UV irradiation (20), viral infection (21), and inflammatory cytokines (9). This stress-induced expression of TRX was observed in a number of cell lines such as keratinocytes, lymphoid cells (20), and a certain class of cancer cells (22); thus it seems to be a ubiquitous phenomenon.

3.1.1. Analysis of TRX mRNA Expression by Northern Blot

1. Treat cells with H₂O₂. Concentration of H₂O₂ and duration of treatment should be optimized.
2. Isolate total RNA by acid guanidine thiocyanate phenol chloroform extraction.
3. Separate total RNA (20 µg) on a 1% formaldehyde-agarose gel, then transfer and immobilize on a charge-modified polyvinylidene fluoride (PVDF) membrane by means of UV irradiation.
4. Label TRX cDNA probe with [α -³²P]dCTP using, for example, the Klenow fragment of DNA polymerase.
5. Hybridize RNA with the probe in a QuikHyb[™] hybridization solution (Stratagene, La Jolla, CA).
6. Results are visualized by autoradiography or phosphorimaging analysis.

3.1.2. Analysis of TRX Protein Levels by Western Immunoblot

1. Treat cells with H₂O₂. Concentration of H₂O₂ and duration of treatment should be optimized.
2. Prepare whole-cell extract by homogenization with a solution containing 10 mM Tris-HCl, 10% glycerol, and 0.4 M NaCl.
3. Separate protein samples on a 15% SDS-polyacrylamide gel and transfer to a PVDF membrane.
4. Probe with mouse monoclonal anti-TRX antibody (10 µg/mL in PBS containing 3% milk) followed by incubation with peroxidase-conjugated anti-mouse Ig antibody.
5. Detect antigen-antibody complex by an enhanced chemiluminescence (ECL) Western-blot detection kit according to the manufacturer's protocol (Amersham Bioscience).

3.2. Analysis of Subcellular Localization of TRX in Response to Oxidative Stress

Recent studies have shown that TRX translocates from the cytoplasm to the nucleus in response to oxidative stress (8), UV-irradiation (9), phorbol 12-myristate 13-acetate (PMA) (23), and inflammatory cytokines (9). Induc-

ible nuclear translocation of TRX by various cellular stresses suggests that conditional compartmentalization of TRX may play an important role in cellular homeostatic control including regulation of gene expression.

3.2.1. Indirect Immunofluorescent Study

1. Culture cells (e.g., HeLa cells) on 8-chambered sterile glass slides (Nippon Becton & Dickinson, Tokyo, Japan).
2. Treat cells with H₂O₂. Concentration of H₂O₂ and duration of treatment should be optimized.
3. Fix cells by a freshly prepared solution of 4% paraformaldehyde (w/v) in PBS overnight at 4°C.
4. Incubate with anti-human TRX monoclonal mouse antibody at 1 µg/mL in PBS containing 0.1% Triton X-100 for 12 h at 4°C.
5. Remove the antibody by washing five times with PBS.
6. Incubate with biotinylated anti-mouse IgG antibody from rabbit at a dilution of 1:200 in PBS containing 0.1% Triton X-100 for 1 h at room temperature.
7. Remove the antibody by washing five times with PBS.
8. Incubate with FITC-conjugated streptavidin at a dilution of 1:100 in PBS containing 0.1% Triton X-100 for 1 h at room temperature.
9. Wash five times with PBS, and mount the coverslip onto a glass slide.
10. Examine localization of the fluorescence by a laser scanning microscope (Zeiss LSM 510, Karl Zeiss Jena GmbH, Jena, Germany).

3.3. Monitoring the Effect of the Redox States and Cellular TRX Levels on the GR-Inducible Gene Expression

Numerous studies have shown that cellular levels of TRX is one of the critical determinants of various biological processes; overexpression and/or exogenous addition of TRX confers anti-apoptotic function (24), stimulation of cytokine expression (25), and cytoprotection from cytotoxic and DNA damaging agents (22,26), as well as augmentation of transcription factor function (5–8). Another prominent evidence is the fact that targeted disruption of TRX gene causes early embryonic lethality in mice (27). To further verify the intrinsic role of TRX in cellular processes including transcriptional control of certain gene expression, conditional alteration of cellular TRX levels may be necessary. We, for this purpose, negatively or positively manipulated cellular TRX levels by introduction of antisense or sense TRX expression plasmid, respectively, and examined the effect of TRX on glucocorticoid-inducible gene expression (17,26).

3.3.1. Modulation of Cellular TRX Levels by Transient Transfection

1. Transfect TRX and/or antisense TRX expression plasmid (pcDSRα.ADF and/or pASADF, respectively) into COS7 cells by the lipofection procedure. Note that

condition of transfection (e.g., amounts of plasmids) should be optimized for each cell line.

2. Incubate cells for 24 h.
3. Prepare whole cell extracts and analyze TRX protein levels by Western blot using anti-TRX antibody (*see Subheading 3.1.2.*).

3.3.2. Monitoring of Glucocorticoid-Inducible Gene Expression-Luciferase Assay

1. Cotransfect glucocorticoid-responsive luciferase plasmid (pGRE-luc), GR expression plasmid (RShGR α), and increasing amount of pcDSR α ADF and/or pASADF into COS7 cells by lipofection procedure.
2. Treat cells with DEX in the presence or absence of H₂O₂.
3. Harvest cells and prepare whole-cell extracts.
4. Determine the cellular luciferase activity using a luminometer.

3.4. Detection of Physical Interaction Between TRX and the GR

TRX has been shown to form an intermediate with various target molecules through disulfide linkage in exerting its reducing action (3). Recent NMR study on the interplay between DNA-binding loop of NF- κ B p50 subunit and TRX has shown direct association of these two molecules and further indicated the structure-based specificity and/or preference in substrate targeting by TRX (28). Verification of physical association between TRX and target protein, thus, is extremely important to elucidate the role of TRX in redox regulation of the protein function. Coprecipitation assay using, for example, GST-fusion protein and recombinant TRX in combination with diamide cross-linking is a useful method to demonstrate their direct interaction.

1. Incubate GST-GR DBD fusion protein (*see Note 2*) (10 μ g) or GST (5 μ g) with 45 μ g of glutathione Sepharose 4B beads (Amersham Bioscience) in 250 μ L of PBS at room temperature for 30 min.
2. Wash the beads five times in PBS.
3. Incubate the protein-conjugated beads with 10 μ g of recombinant TRX (*see Note 2*) in PBS containing 3% bovine serum albumin (BSA), 0.1% Triton X-100, and 5 mM diamide at room temperature for 30 min.
4. Wash the beads five times.
5. Elute bound proteins by boiling in 30 μ L of 2X loading buffer (20% v/v glycerol, 4.6% w/v SDS, 0.125 M Tris-HCl, pH 6.8, 4% 2-mercaptoethanol), and separate by a native polyacrylamide gel electrophoresis.
6. Detect proteins by immunoblotting using anti-TRX or -GST antibody.

3.5. Results

1. Oxidative Stress Induces TRX Expression. Representative results of northern blot and Western blot were shown in **Figure 1**. Treatment of HeLa cells with

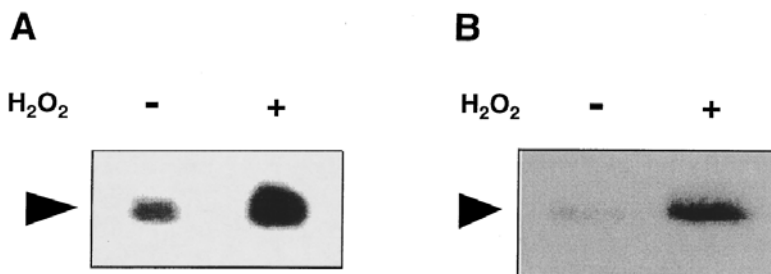


Fig. 1. Induction of TRX expression under oxidative condition. HeLa cells were treated with or without 1 mM H_2O_2 for 12 h and mRNA expression and protein levels of TRX were determined. **(A)** Northern blot assay. Twenty micrograms of total RNA were separated on a 1% formaldehyde-agarose gel and transferred to a PVDF membrane. The filter was hybridized with radiolabeled cDNA probe for TRX as described in **Methods**. Result was visualized by autoradiography. **(B)** Western blot assay. Twenty micrograms of whole cell extract were separated on a 15% SDS polyacrylamide gel electrophoresis and transferred to a PVDF membrane. Immunoblotting was performed with antibody against TRX as described in **Methods**. Numbers depict relative molecular masses (kD) determined by molecular marker run in parallel.

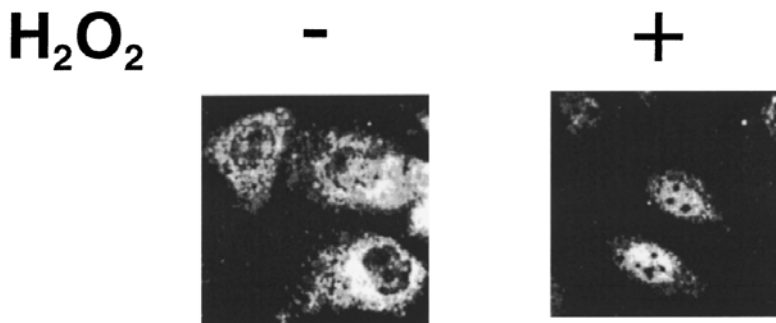


Fig. 2. Effect of oxidative treatment on subcellular localization of TRX in HeLa cells. HeLa cells were cultured in the absence or presence of 1 mM H_2O_2 for 2 h as indicated and subcellular localization of TRX was examined by immunocytochemical analysis using anti-human TRX monoclonal antibody as described in **Methods**.

H_2O_2 induced TRX mRNA expression (**Fig. 1A**) and increased TRX protein levels (**Fig. 1B**). Similar results were reported from other laboratories after UV irradiation (20) or stimulation with cytokines (9). Note that sensitivity of cells to oxidative treatment is extremely variable and optimization of experimental conditions is essential to obtain reproducible results.

2. Oxidative stress induces nuclear accumulation of TRX. Treatment of HeLa cells with H_2O_2 induced rapid translocation of TRX from the cytoplasm to the nucleus (**Fig. 2**). UVB irradiation and cellular treatment with TNF (9) or PMA (23),

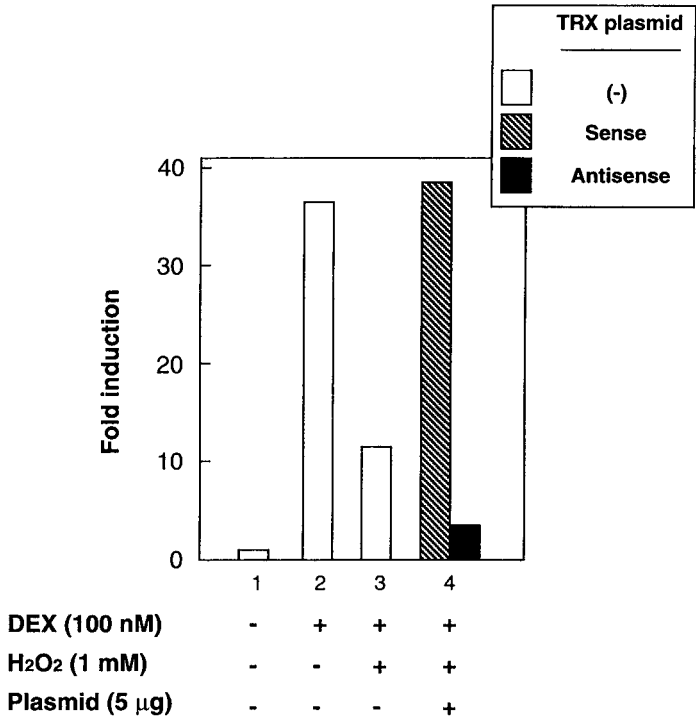


Fig. 3. Effect of oxidative treatment and overexpression of TRX or antisense TRX on transactivation function of the GR. COS7 cells were transfected with 10 ng GR expression plasmid pRShGR α , 5 μ g pGRE-Luc reporter plasmid, and 5 μ g TRX or antisense TRX expression plasmid (pcDSR α ADF, pASADF, respectively). Twenty-four hours after treatment with 1 mM H₂O₂ and/or 100 nM DEX, the cells were harvested and cellular luciferase activity was determined as described in **Methods**.

which have been shown to generate intracellular reactive oxygen intermediates, caused nuclear translocation of TRX as well.

- 3. Glucocorticoid-inducible gene expression is coordinately modulated by cellular redox state and TRX level. Glucocorticoid-inducible gene expression was repressed by treatment with 1 mM H₂O₂ (**Fig. 3**). When TRX was overexpressed, the repression effect of H₂O₂ was canceled (lanes 4, hatched columns). In contrast, reduction of cellular TRX levels, which was accomplished by expression of anti-sense TRX, resulted in increased sensitivity to H₂O₂ and hormone induction response was further decreased (lanes 4, filled columns). These results indicate that cellular TRX level is an important determinant of glucocorticoid-mediated gene expression.
- 4. TRX directly binds to the GR DBD. Results of GST pull-down assay in combination with diamide cross-linking were shown in **Fig. 4**. Neither Sepharose (lane 2)

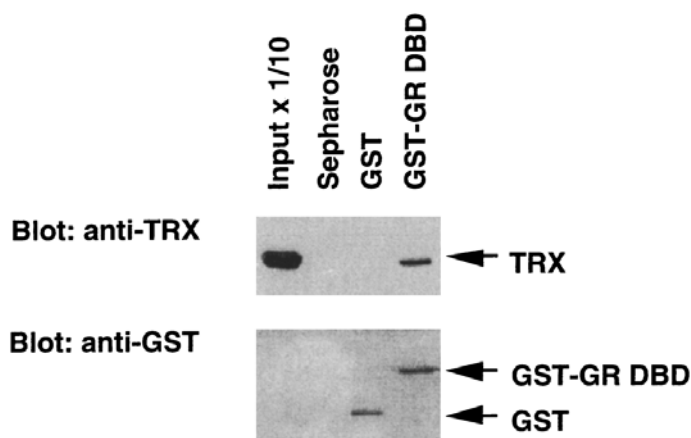


Fig. 4. Direct protein-protein interaction between GR DBD and TRX. Ten micrograms of recombinant TRX were incubated with glutathione-Sepharose beads (lane 2) or beads bound with GST (lane 3) or GST-GR DBD (lane 4) in the presence of 5 mM diamide for 1 h at room temperature as indicated. The beads were collected by centrifugation and washed in PBS. Bound materials were separated on a 15% SDS-polyacrylamide gel followed by immunoblot using anti-human TRX monoclonal antibody (upper panel) or anti-GST antibody (lower panel) as described in Methods. Lane 1 represents 10% of TRX input. Numbers at left represent molecular masses (kD) markers run in parallel.

nor GST-bound Sepharose (lane 3) was capable of precipitating TRX. On the other hand, TRX was precipitated when mixed with GST-GR DBD-bound Sepharose in the presence of diamide (lane 4), suggesting the presence of direct protein-protein interaction between TRX and the GR DBD in oxidative conditions. In support of this, domain analysis for functional interaction between the GR and TRX in transient transfection assay employing the deletion mutants of the GR also indicated that the DBD of the GR is one of the region to communicate with TRX (17).

4. Notes

1. The wild-type GR expression vectors, pRShGR α (20) was kindly supplied by Dr. R.M. Evans (Salk Institute, La Jolla, CA). The expression plasmid for TRX, pcDSR α ADF (29), was a gift from Dr. J. Yodoi (Kyoto University, Kyoto, Japan). To construct the antisense TRX expression plasmid pASADF, *Bam*HI-*Hind*III fragment from pcDSR α ADF was isolated and subcloned into the *Hind*III-*Bam*HI site of the pcDNA3 plasmid (Invitrogen, Carlsbad, CA). The noncoding strand sequence of glucocorticoid-response element in reporter construct pGRE-Luc was; 5'-CGGATCCTGTACAGGATGTTCTAGCTACGGATCCTGTACAGGATGTTCTAGCTACG-3'.

2. GST-GR DBD fusion protein containing Serine403–Leucine532 of the human GR was expressed in *Epicurian coli* BL21(DE3) by pGEX protein expression and purification system according to the manufacturer's protocol (Amersham Bioscience). Recombinant TRX was produced and kindly provided by Basic Research Laboratory, Ajinomoto Co. Inc., (Kawasaki, Japan) (30).

References

1. Yu, B. P. (1994) Cellular defenses against damage from reactive oxygen species. *Physiol. Rev.* **74**, 139–162.
2. Demple, B. and Amabile-Cuevas, C. F. (1991) Redox redux: the control of oxidative stress responses. *Cell* **67**, 837–839.
3. Holmgren, A. (1995) Thioredoxin structure and mechanism: conformational changes on oxidation of the active-site sulfhydryls to a disulfide. *Structure* **3**, 239–243.
4. Holmgren, A. (1985) Thioredoxin. *Annu. Rev. Biochem.* **54**, 237–271.
5. Schenk, H., Klein, M., Erdbrugger, W., Droge, W., and Schulze-Osthoff, K. (1994) Distinct effects of thioredoxin and antioxidants on the activation of transcription factors NF- κ B and AP-1. *Proc. Natl. Acad. Sci. USA* **91**, 1672–1676.
6. Meyer, M., Schreck, R., and Baeuerle, P. A. (1993) H₂O₂ and antioxidants have opposite effects on activation of NF- κ B and AP-1 in intact cells: AP-1 as secondary antioxidant-responsive factor. *EMBO J.* **12**, 2005–2015.
7. Akamatsu, Y., Ohno, T., Hirota, K., Kagoshima, H., Yodoi, J., and Shigesada, K. (1997) Redox regulation of the DNA binding activity in transcription factor PEBP2. The roles of two conserved cysteine residues. *J. Biol. Chem.* **272**, 14497–14500.
8. Makino, Y., Yoshikawa, N., Okamoto, K., Hiorota, K., Yodoi, J., Makino, I., and Tanaka, H. (1999) Direct association with thioredoxin allows redox regulation of glucocorticoid receptor function. *J. Biol. Chem.* **274**, 3182–3188.
9. Hirota, K., Murata, M., Sachi, Y., Nakmura, H., Takeuchi, J., Mori, K., and Yodoi, J. (1999) Distinct roles of thioredoxin in the cytoplasm and in the nucleus. *J. Biol. Chem.* **274**, 27891–27897.
10. Evans, R. M. (1988) The steroid and thyroid hormone receptor superfamily. *Science* **240**, 889–895.
11. Beato, M., Herrlich, P., and Schutz, G. (1995) Steroid receptors: many actors in search of a plot. *Cell* **83**, 851–857.
12. Picard, D. and Ymamato, K. R. (1987) Two signals mediate hormone-dependent nuclear localization of the glucocorticoid receptor. *EMBO J.* **6**, 3333–3340.
13. Simons, S. S. Jr. and Pratt, W. B. (1995) Glucocorticoid receptor thiols and steroid-binding activity. *Methods Enzymol.* **251**, 406–422.
14. Bodwell, J. E., Holbrook, N. J., and Munck, A. (1984) Sulfhydryl-modifying reagents reversibly inhibit binding of glucocorticoid-receptor complexes to DNA-cellulose. *Biochemistry* **23**, 1392–1398.
15. Okamoto, K., Tanaka, H., Ogawa, H., Makino, Y., Eguchi, H., Hayashi, S., et al. (1999) Redox-dependent regulation of nuclear import of the glucocorticoid receptor. *J. Biol. Chem.* **274**, 10363–10371.

16. Makino Y., Tanaka, H., Dahlman-Wright, K., and Makino, I. (1996) Modulation of glucocorticoid-inducible gene expression by metal ions. *Mol. Pharmacol.* **49**, 612–620.
17. Makino, Y., Okamoto, K., Yoshikawa, N., Aoshima, M., Hirota, K., Yodoi, J., et al. (1996) Thioredoxin: a redox-regulating cellular cofactor for glucocorticoid hormone action. Cross talk between endocrine control of stress response and cellular antioxidant defence system. *J. Clin. Invest.* **98**, 2469–2477.
18. Hayashi, S., Hajiro-Nakanishi, K., Makino, Y., Eguchi, H., and Tanaka, H. (1997) Functional modulation of estrogen receptor by redox state with reference to thioredoxin as a mediator. *Nucleic Acids Res.* **25**, 4035–4040.
19. Taniguchi, Y., Taniguchi-Ueda, Y., Mori, K., and Yodoi, J. (1996) A novel promoter sequence is involved in stress-induced expression of the adult T-cell leukemia-derived factor (ADF)/human thioredoxin (TRX) gene. *Nucleic Acids Res.* **24**, 2746–2752.
20. Sachi, Y., Hirota, K., Masutani, H., Toda, K., Okamoto, T., Takigawa, M., and Yodoi, J. (1995) Induction of ADF/TRX by oxidative stress in keratinocytes and lymphoid cells. *Immunol. Lett.* **44**, 189–193.
21. Wakasugi, N., Tagaya, Y., Wakasugi, H., Mitsui, A., Maeda, M., Yodoi, J., and Tursz, T. (1990) Adult T-cell leukemia-derived factor/thioredoxin, produced by both human T-lymphotrophic virus type I- and Epstein-Barr virus-transformed lymphocytes, acts as an autocrine growth factor and synergizes with interleukin 1 and interleukin 2. *Proc. Natl. Acad. Sci. USA* **87**, 8282–8286.
22. Sasada, T., Iwata, S., Sato, N., Kitaoka, Y., Hirota, K., Nakamura, K., et al. (1996) Redox control of resistance to cis-diamminedichloroplatinum (II) (CDDP). Protective effect of human thioredoxin against CDDP-induced cytotoxicity. *J. Clin. Invest.* **97**, 2268–2276.
23. Hirota, K., Matsui, M., Iwata, S., Nishiyama, A., Mori, K., and Yodoi, J. (1997) AP-1 transcriptional activity is regulated by a direct association between thioredoxin and Ref-1. *Proc. Natl. Acad. Sci. USA* **94**, 3633–3638.
24. Nakamura, H., Nakamura, H., and Yodi, J. (1997) Redox regulation of cellular activation. *Annu. Rev. Immunol.* **15**, 351–369.
25. Schenk, H., Vogt, M., Droge, W., and Schulze-Osthoff, K. (1996) Thioredoxin as a potent costimulus of cytokine expression. *J. Immunol.* **156**, 765–771.
26. Yokomizo, A., Ono, M., Nanri, H., Makino, Y., Ohga, T., Wada, M., et al. (1995) Cellular levels of thioredoxin associated with drug sensitivity to cisplatin, mitomycin C, doxorubicin, and etoposide. *Cancer Res.* **55**, 4293–4296.
27. Matsui, M., Oshima, M., Oshima, H., Takaku, K., Maruyama, T., Yodoi, J., and Taketo, M. (1996) Early embryonic lethality by targeted disruption of the mouse thioredoxin gene. *Dev. Biol.* **178**, 179–185.
28. Qin, J., Clore, G. M., Kennedy, W. M. P., Huth, J. R., and Gronenborn, A. M. (1995) Solution structure of human thioredoxin in a mixed disulfide intermediate complex with its target peptide from the transcription factor NFκB. *Structure* **3**, 289–297.

29. Matthews, J. R., Wakasugi, N., Virelizer, J.-L., Yodoi, J., and Hay, R. T. (1992) Thioredoxin regulates the DNA binding activity of NF- κ B by reduction of a disulphide bond involving cysteine 62. *Nucleic Acids Res.* **20**, 3821–3830.
30. Tagaya, Y., Wakasugi, H., Masutani, H., Nakamura, H., Iwata, S., Mitsui, A., et al. (1990) Role of ATL-derived factor (ADF) in the normal and abnormal cellular activation: involvement of dithiol related reduction. *Mol. Immunol.* **27**, 1279–1289.

Analysis of Phospholipid Hydroperoxide Glutathione Peroxidase mRNA

Xin Gen Lei and Wen-Hsing Cheng

1. Introduction

Phospholipid hydroperoxide glutathione peroxidase (PHGPX or GPX4, E.C. 1.11.1.12) is one of the four identified selenium-dependent glutathione peroxidases (GPX) in mammals (*1*). Both of the pig (2.8 kb) and the mouse (4.0 kb) GPX4 genes contain seven exons and six introns, with putative regulatory elements or binding sites for transcriptional factors (*2,3*). There is 95% homology among amino acid sequences deduced from the GPX4 cDNA of rat (*4*), mouse (*5*) and human (*6*). In contrast, the homology between GPX1 and GPX4 is less than 40%. There are two forms of GPX4: the long form (23 kDa) with a leader sequence for transportation to mitochondria, and the short form (20 kDa) or the non-mitochondrial form (*7*). Although GPX4 was initially considered mainly an antioxidant enzyme by reducing phospholipid hydroperoxides (*8*), it may be involved in sperm maturation (*9*) as there are abundant GPX4 activity and mRNA in testis (*10,11*) and rat epididymal spermatozoa (*12*). It exists as a soluble peroxidase in spermatids, but loses its activity in mature spermatozoa and persists as an oxidatively cross-linked insoluble protein (*13*). Besides, GPX4 is expressed in all major tissues studied so far. Comparatively, GPX4 mRNA and activity are less affected by changes in tissue selenium status than those of GPX1 or GPX3 (*14*). Because there is a selenium-independent enzyme that reduces phospholipid hydroperoxides (*15*), GPX4 mRNA analysis becomes a specific tool to distinguish these two enzymes for various biochemical and physiological studies. Herein, we describe the standard Northern-blot analysis and the increasingly popular

reverse transcriptase-polymerase chain reaction (RT-PCR) method for the determination of steady-state levels of GPX mRNA in tissues or cells.

2. Materials

2.1. Equipment (see Note 1)

1. Polytron homogenizer.
2. Microcentrifuge.
3. Spectrophotometer.
4. Microwave.
5. Horizontal gel electrophoresis apparatus and power supply.
6. Fume hood.
7. Hybridization oven (Hybaid, Middlesex, UK).
8. IS-1000 digital imaging system (Alpha Innotech Corp., San Leandro, CA).
9. FuJIX BAS 1000 Bio-imaging analyzer and imaging plate (Fuji Bas-III, Kanagawa, Japan) (see Note 2).

2.2. Reagents (see Note 1)

2.2.1. Northern Analysis of GPX4 mRNA Levels

1. RNAqueous™ phenol-free total RNA isolation kit (Ambion, TX).
2. 10X MOPS: dissolve 20.94 g 3-(N-morpholino) propanesulfonic acid (MOPS) and 3.28 g sodium acetate in DEPC water to a total volume of 400 mL. Add 10 mL of 0.5 M EDTA, pH 8.0. Adjust pH to 7.0 and the final volume to 500 mL. Autoclave and store it at 4°C.
3. DEPC (diethyl pyrocarbonate) water: add 1 mL DEPC to 1 L water (for all materials and reagents) in orange-capped autoclave bottle and stir overnight (cap loose) at room temperature (RT). Autoclave and stir at RT for 2 h or longer. Tighten the cap and store at RT.
4. RNA loading buffer: mix 0.8 mL 10X MOPS, 0.4 mL 80% glycerol, 0.4 mL bromophenol blue, 1.4 mL formaldehyde (37%), 4.0 mL formamide, and 80 µg ethidium bromide (EtBr). Store at -20°C.
5. 20X SSC: dissolve 175.3 g of NaCl and 88.2 g of sodium citrate in 800 mL of water. Adjust the pH to 7.0 and the volume to 1 L with water. Autoclave.
6. 50X Denhardt's reagent: add 1 g of Ficoll, 1 g of polyvinylpyrrolidone, 1 g of bovine serum albumin (BSA), and water to 100 mL. Filter (0.22 µm cellulose acetate filter, Corning, NY), dispense into 15 mL aliquots and store at -20°C.
7. 20X SSPE: dissolve 43.83 g of NaCl, 6.9 g of NaH₂PO₄•H₂O and 1.85 g of EDTA in 200 mL of water. Adjust the pH to 7.4 and the volume to 250 mL. Autoclave.
8. Ethyl alcohol, dehydrated 200 proof (EtOH): required for the RNA isolation kit.
9. 10% SDS: dissolve 10 g of sodium dodecyl sulfate (SDS) in 90 mL of water. Heat to 68°C. Adjust the pH to 7.2 and the volume to 100 mL.
10. Formamide.

11. Sperm DNA.
12. Agarose.
13. 3MM paper (Whatman, Maidstone, UK).
14. Nitrocellulose membrane (GibcoBRL, Rockville, MD).
15. ^{32}P (dCTP, Du Pont, Boston, MA).
16. DNA probes: a 637-bp *EcoRI/XhoI* fragment of rat GPX4 and a 1.4-kb *BamHI* fragment of human 18S rRNA (11, see **Note 3**).

2.2.2. RETROscript™ First-Strand Synthesis Kit (Ambion)

1. 10X RT-PCR buffer: 100 mM Tris-HCl, pH 8.3; 500 mM KCl; 15 mM MgCl_2 .
2. 10X first-strand buffer: 500 mM Tris-HCl, pH 8.3; 750 mM KCl; 30 mM MgCl_2 ; 50 mM DTT.
3. dNTP mix (2.5 mM each dNTP).
4. Random decamers, 50 μM .
5. Moloney-murine leukemia virus reverse transcriptase, 100 units/ μL .
6. Placental RNase inhibitor, 10 units/ μL .
7. Nuclease-free water.

2.2.3. QuantumRNA™ Alternative 18S Internal Standards (Ambion)

1. 18S Primers.
2. Competimers™.

2.2.4. Others

1. Taq polymerase (Fisher).
2. GPX4 primers (forward primer 5'ACCATGTGTGCATCCCCGGA3', reverse primer 5'TAGCTAGAGATAGCACGGCA3', synthesized by BioResource Center, Cornell University, Ithaca, NY).

3. Methods

3.1. Isolation of Total RNA

1. Homogenize 50 mg tissue samples in 600 μL lysis/binding solution on ice using polytron homogenizer. For mammalian cells, add 300 μL lysis/binding solution per 1×10^6 to 1×10^7 cells and homogenize by vigorous vortexing or pipetting.
2. Remove debris by centrifugation for 3 min at 12,000g at 4°C. Collect the supernatant.
3. Add an equal volume of 64% EtOH and mix well by repeating pipetting.
4. Apply the mixture to the filter cartridge that is held in a collection tube.
5. Microcentrifuge for 15 s or until all the solution is through. Discard the flow-through.
6. Add 700 μL wash solution #1 to the filter cartridge and microcentrifuge as **step 5**.

7. Add 500 μL wash solution #2/3 and microcentrifuge as **step 5**.
8. Repeat **step 7**.
9. Transfer the filter cartridge to a new collection tube. Add 60 μL elution buffer to the filter.
10. Incubate the tube with filter at 68°C for 10 min.
11. Recover the eluate by spinning the tube for 1 min at 12,000g.
12. Quantitate RNA concentration of the eluate by its absorbance (1:200 dilution) at λ 260 nm.

3.2. Formaldehyde Agarose Gel Electrophoresis

1. For an 11 \times 14 \times 0.5 cm gel, add 1.8 g agarose (for 1.5% gel) and 85 mL water in a baked Erlenmeyer flask.
2. Dissolve agarose in microwave for approx 2 min and add 12 mL 10X MOPS.
3. Cool the agarose solution to 50°C. Add 21.5 mL of 37% formaldehyde (final concentration 2.2 M) in a fume hood. Mix by swirling.
4. Pour the gel (in the hood). Remove any bubbles on the gel surface.
5. Add sufficient 1X MOPS as running buffer to cover the gel after the gel solidifies.
6. Prepare 15 μg RNA for each sample and adjust the total volume to 7.5 μL using DEPC water.
7. Add 1 volume of RNA loading buffer, and heat the mixture at 68°C for 15 min.
8. Load 15 μL samples to each well, run the gel for 5 h at 50 V (4 to 6 V/cm of gel). Circulate the running buffer using a peristaltic pump (CP-600, BRL) to improve gel electrophoresis.
9. Photograph gel using the gel documentation apparatus or any UV transilluminator to record positions of 28S and 18S rRNA.

3.3. Blotting Gel

1. Pre-wet nitrocellulose membrane cut to the size of gel with 2X SSC.
2. Soak the gel for 20 min in 10X SSC to remove formaldehyde.
3. In a flat plastic or glass dish, construct transfer stack (see general molecular biology manuals for more details). Place a small plastic pan upside-down in the middle of the dish and a plate (slightly larger than the gel) on top of the pan as a platform. Cut 2 wicks of Whatman 3 MM paper. Spread the first wick over the platform and the second wick over the first wick after the papers are saturated with 10X SSC. Use a baked graduated 1 mL pipet to remove bubbles between the wicks and(or) platform.
4. Add 10X SSC to the dish as transfer buffer.
5. On top of the wicks, flip the washed gel over and remove bubbles. Surround gel with X-ray film strips to keep the buffer flowing only through the gel.
6. Lay the nitrocellulose membrane on top of the gel with forceps. Add two layers of Whatman 3 MM paper over the membrane and remove bubbles at each layer. Place a stack of paper towel (dry) cut to fit the size of the gel on top of the Whatman 3 MM paper.

7. Place a glass plate on top of the towel and a light weight (250–300 g) on top of the plate. Pour sufficient 10X SSC into the transfer pan and cover with Saran wrap.
8. Allow transfer to proceed for 4 h or overnight.
9. At the end of transfer, carefully remove the membrane from the transfer stack into 2 pieces of Whatman 3 MM papers. Let the membrane air dry for 15 min to 1 h.
10. Use a hand UV lamp to mark positions of 18S and 28S rRNA and each loading well with a pencil. Bake the membrane in two pieces of Whatman 3 MM paper at 80°C oven for 2 h.
11. Store blot between clean Watman 3 MM papers in a sealed plastic bag at RT.

3.4. Using a Hybridization Oven for Pre-Hybridization, Hybridization, and Washing

1. Place the selected hybridization bottles (in pairs for rotation balance) in the oven at 42°C for warm-up (1 h).
2. Prepare 10 mL pre-hybridization buffer for each small bottle carrying 1 membrane, and increase the buffer to 15–20 mL for bottles with 2 or more (maximal 5) membranes: 5 mL formamide; 1 mL 50X Denhardt's reagent; 2.5 mL 20X SSPE; 1 mL 10% SDS; 0.3 mL water; 0.2 mL denatured (95°C, 10 min) sperm DNA (5 mg/mL).
3. Pre-warm the pre-hybridization buffer to 42°C.
4. Select a piece of support mesh appropriate for the size of membrane. Pre-wet the mesh and the membrane with 2X SSC in a tray.
5. Lay the membrane exactly over the mesh and wind both up into a tight roll. If more than one membrane is to be hybridized, make sure that membranes are separated from each other by a piece of mesh.
6. Insert the roll into the hybridization bottle in the orientation that both mesh and membrane will unroll with the rotation of the bottle. Add 10–15 mL of 2X SSC. On a flat surface, rock the bottle backwards and forwards to attach the first part of the membrane to the bottle. Then roll the bottle to unwind the mesh and membrane fully. If bubbles exist between the membrane and bottle wall, remove the membrane and mesh and re-roll.
7. Discard the 2X SSC, add 10 mL of pre-warmed pre-hybridization buffer, and insert the bottle into the rotisserie of the oven.
8. Rotate (speed 8) the membrane at 42°C for 2 h or overnight.
9. While the membrane is being pre-hybridized, label the GPX4 DNA probe (purified with the GeneClean kit or equivalent) with ^{32}P using a Ready-To-Go kit (-dCTP, Pharmacia Biotech, Piscataway, NJ). Follow the detailed instructions by the manufacturer. Briefly, add 5 μL ($> 0.05 \text{ mCi}$) ^{32}P and 20 ng ($< 45 \mu\text{L}$) denatured (95°C, 10 min) GPX4 probe. Add water to a total volume of 50 μL (good for two membranes) and incubate at 37°C for 30 min.
10. Remove the unincorporated ^{32}P from the reaction mixture using the ProbeQuantTM G-50 Micro Columns (Pharmacia Biotech.).
11. Collect the flow-through. Save 1 μL to check the incorporate rate if necessary.

12. Denature the probe by incubating it at 95°C for 10 min.
13. Add 25 μ L of the denatured probe to the pre-hybridization buffer. Make sure the probe is not applied to any spot in the membrane directly.
14. Rotate the membrane in a hybridization oven at 50°C overnight.
15. Pre-warm the washing buffer to 60°C.
16. Remove the bottle from the oven, discard the hybridization buffer into a liquid waste container of radioactive ^{32}P , and turn the oven temperature to 60°C.
17. Add 25 ml of 60°C 2X SSC to each bottle and rotate for 10 min. Decant the washing buffer and repeat (*see Note 4*).
18. Decant the washing buffer and increase the oven temperature to 65°C.
19. Add 50 mL of 65°C 2X SSC and rotate for 20 min.
20. Decant the washing buffer and check the radioactivity to see if additional washing is necessary. The last washing can be carried out in a plastic pan after the membrane is removed from the bottle.

3.5. Developing and Visualization of Phosphoimage

1. After washing, wrap membrane with Saran wrap. Do not let the membrane dry out completely.
2. Erase the Image Plate (IP) for at least 15 min using the BAS-1000 system.
3. Place the membrane (face-up) in the cassette and put IP on top (face-down). Close the cassette and keep it at RT.
4. Depending on the intensity of signal, expose the plate for hours or days.
5. At the end of exposure, warm-up the FUJIX BAS 1000 Phosphoimager system.
6. Develop IP in the Phosphoimager.
7. Using a FUJIX BAS software, quantify the intensity of the bands and print out the results.

3.6. Re-Stripping Membrane and Internal Control

1. If necessary, the hybridized probe in membrane can be stripped and the membrane can be re-hybridized with probes of other genes or internal controls. Place the membrane in 500 mL boiling 0.1X SSPE/0.1% SDS for 30 min with agitation. Check the residual radioactivity to see if another stripping is necessary.
2. Bake the membrane for 2 h at 80°C.
3. Repeat steps in **Subheadings 3.4.–3.5.** We routinely use 20 ng human 18S rRNA as an internal control. Due to its abundant expression, it takes only 15–30 min to develop highly visible bands.
4. Express the GPX4 mRNA levels relative to its pertinent 18S rRNA levels on the same blots (*see Note 5*).

3.7. Results

3.7.1. Image Intensity of Mouse Tissues GPX4 mRNA and 18S rRNA at 0 to 25 μ g Total RNA Per Lane

1. In **Fig. 1**, the image intensity of the 18S rRNA or GPX4 mRNA increases with the amount of total RNA loaded.

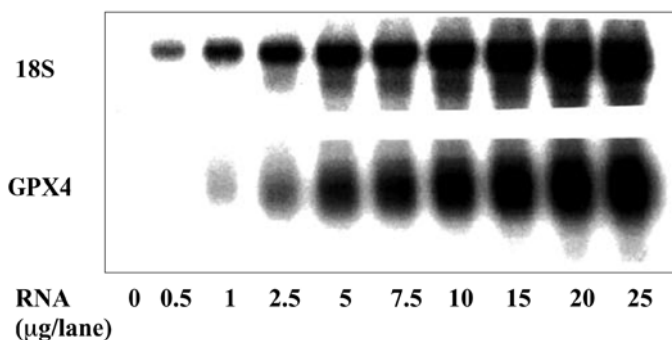


Fig. 1. Comparisons of GPX4 mRNA and 18S rRNA levels in mouse testis loaded with 0–25 μg of total RNA per lane.

2. Levels of body 18S rRNA are much higher than those of GPX4 mRNA, and can be detected with as low as 0.5 μg RNA per lane is loaded.
3. We found 15 μg RNA per lane is appropriate and were used for the following study.

3.7.2. Effects of Dietary Selenium on Expression Levels of GPX4 mRNA in Tissues of Mice

In **Fig. 2** dietary selenium deficiency (<0.02 mg Se/kg of diet to weanling mice as Na_2SeO_3 for 10 wk) does not significantly affect GPX4 mRNA levels in liver, kidney, or testis. Expression levels of GPX4 mRNA are lower in liver compared with those in kidney and testis. In contrast, GPX1 mRNA levels in tissues are significantly affected by dietary selenium deficiency (*14*).

3.8. Relative RT-PCR to Compare GPX4 mRNA Expression Among Tissues

The polymerase chain reaction has been used to determine steady-state RNA levels (*see Note 6*). The basic strategy is to transcribe RNA into cDNA using reverse transcriptase. Then, a pair of gene-specific primers is used to amplify the cDNA originated from the RNA. A pair of primers specific to an internal control is also necessary. Finally, the RNA levels are expressed by the ratios of the band intensity of GPX4 over that of the internal control. To conduct RT-PCR, we use a RETROscript[™] first-strand synthesis kit (Ambion) and a patented alternate 18S rRNA relative RT-PCR internal standards with two sets of primers (Ambion).

Figure 3 depicts that the relative expression levels of GPX4 mRNA are lower in liver compared with that in kidney and testis in selenium-adequate mice.

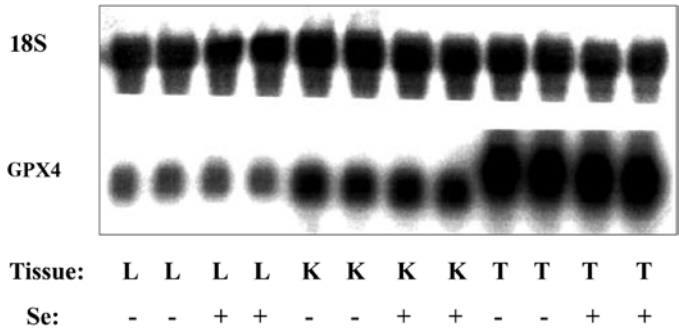


Fig. 2. Levels of GPX4 mRNA in mouse tissues determined by Northern analysis. Fifteen μ g of total RNA per lane was loaded. The abbreviations are as follows: L, liver; K, kidney; T, testis; -, samples from selenium-deficient mice; +, samples from selenium-adequate mice.

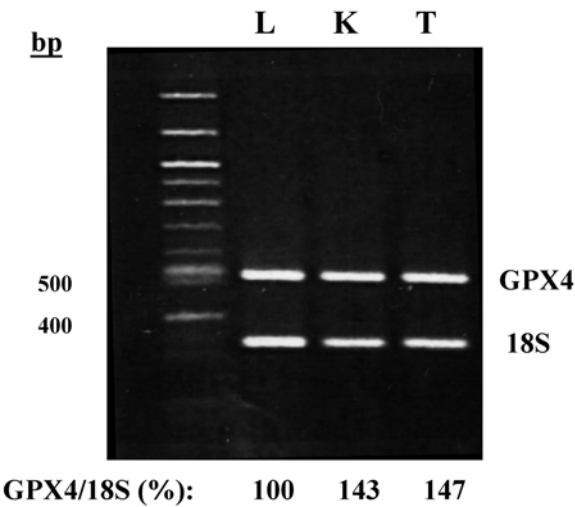


Fig. 3. Levels of relative GPX4 mRNA in mouse tissues determined by the relative RT-PCR assay. The length of the expected DNA products is 518 bp and 324 bp for GPX4 and 18S rRNA, respectively. The abbreviations are as follows: L, liver, K, kidney, T, testis. The band intensity of GPX4 over 18S rRNA in liver is designated as 100%.

3.8.1. Reverse Transcription Reaction

1. Add together (for one reaction): 1.5 μ g template RNA; 4 μ L dNTP mix; 2 μ L 10X first-strand buffer; add nuclease-free water to 16 μ L.
2. Mix, spin briefly, and heat 3 min at 80°C.

3. Add together to the tube of step 1 (for one reaction): 2 μL random decamers; 1 μL placental RNase inhibitor; 1 μL reverse transcriptase.
4. Mix, spin briefly, and incubate at 50°C for 1 h.
5. Incubate at 92°C for 10 min.
6. Store the reaction mixture at -20°C if not doing amplification immediately.

3.8.2. PCR Amplification

1. Add together (for one reaction): 1 μL reverse transcription reaction; 5 μL 10X PCR buffer; 2.5 μL dNTP mix; 1 unit of Taq polymerase; 20 pmol GPX4 primer pairs; 1.6 μL 18S primers; 2.4 μL competitor primers (*see Note 7*). Add nuclease-free water to a total of 50 μL .
2. PCR reaction condition: Heat 3 min, 94°C; 30 cycles: 94°C, 20 s; 53°C, 30 s; 72°C, 40 s. Hold 10 min, 72°C.
3. Run a 1.5% native agarose gel in the presence of EtBr (0.1 $\mu\text{g/mL}$ buffer).
4. Visualize the product under UV light.
5. Quantitate the band intensities of GPX4 and 18S rRNA using the IS-1000 digital imaging system. Express the results as ratios of GPX4 over those of 18S rRNA. Designate the control as 100% (*see Note 8*).

4. Notes

1. It is absolutely essential to keep all equipment apparatus and solutions RNase-free. If possible, all of these items should be for RNA analysis only. All glassware and metal apparatus should be baked and stored in a designated area. All solutions should be prepared with DEPC water. Also, wear gloves at all times to prepare reagents and handle the actual RNA analysis.
2. If this system is not available, autoradiography could be conducted using X-ray film (*see general molecular biology manuals for details*).
3. We have used the rat GPX4 cDNA to probe mouse and pig GPX4 mRNA satisfactorily (**13,16**).
4. Stringency refers to the salt concentration of buffer and the temperature at which washings are conducted. Increased temperature and/or decreased salt enhances stringency and is less conducive to hybridization. If the probe used for hybridization is very specific, increased stringency of washes will decrease background. On the contrary, decreased stringency may help enhance signal at the risk of a high background.
5. Quantitative mRNA levels are expressed as relative levels to assure the equal loading of RNA amount. Thus, an internal control with constant expression over treatments is needed. Good choices are GA3PD, 18S rRNA, actin, and so forth.
6. Generally, RT-PCR is more sensitive and less time-consuming than Northern analysis. Theoretically, copy number of mRNA as low as one is good enough to be detected using RT-PCR. This allows the detection of low levels of mRNA expression. However, the high sensitivity may also amplify sampling and pipeting errors. Also, make sure the number of PCR cycles is in the linear increase phase of the PCR amplification.

7. The ideal condition for GPX4 and 18S rRNA primers to amplify their respective targets is that both primers use the PCR machinery at a similar efficiency. A preliminary PCR reaction designed with different 18S rRNA to the competitor ratios along with a fixed concentration of GPX4 primers must be done. Choose the ratio that has similar expression levels between 18S rRNA and GPX4 bands.
8. The ideal RNA species for an internal control should be expressed at a constant level across all of the types of samples being analyzed. Normally, 18S rRNA expresses constantly and make up about 20% of total RNA. The huge difference between 18S rRNA and GPX4 mRNA abundance makes competition of using the PCR ingredient favors the former. Such drawback could be overcome by using a specially designed 18S rRNA competitor (Patented) along with the 18S rRNA primer pairs. Using the imaging system, the intensity of each band can be quantitated. The ratio of the band intensities of GPX4 over 18S rRNA controls is designated as 100%.

Acknowledgment

The rat GPX4 and human 18S rRNA probes were provided by R. A. Sunde, University of Missouri. Research in the authors' laboratory is funded by a NIH grant DK 53018.

References

1. Ursini, F., Maiorino, M., and Gregolin, C. (1985) The selenoenzyme phospholipid hydroperoxide glutathione peroxidase. *Biochim. Biophys. Acta* **839**, 62–70.
2. Brigelius-Flohé, R., Aumann, K. D., Blöcker, H., Gross, G., Kiess, M., Klöppel, K. D., et al. (1994) Phospholipid-hydroperoxide glutathione peroxidase: genomic DNA, cDNA and deduced amino acid sequence. *J. Biol. Chem.* **269**, 7342–7348.
3. Borchert, A., Schnurr, K., Thiele, B. J., and Kühn, H. (1999) Cloning of the mouse phospholipid hydroperoxide glutathione peroxidase gene. *FEBS Lett.* **446**, 223–227.
4. Pushpa-Rekha, T. R., Burdsall, A. L., Oleksa, L. M., Chisolm, G. M., and Driscoll, D. M. (1995) Rat phospholipid-hydroperoxide glutathione peroxidase: cDNA cloning and identification of multiple transcription and translation start sites. *J. Biol. Chem.* **270**, 26993–26999.
5. Knopp, E. A., Arndt, T. L., Eng, K. L., Caldwell, M., LeBoeuf, R. C., Deeb, S. S., and O'Brien, K. D. (1999) Murine phospholipid hydroperoxide glutathione peroxidase: cDNA sequence, tissue expression, and mapping. *Mamm. Genome* **10**, 601–605.
6. Esworthy, R. S., Doan, K., Doroshov, J. H., and Chu, F.-F. (1994) Cloning and sequencing of the cDNA encoding a human testis phospholipid hydroperoxide glutathione peroxidase. *Gene* **144**, 317–318.
7. Arai, M., Imai, H., Koumura, T., Yoshida, M., Emoto, K., Umeda, M., Chiba, N., and Nakagawa, Y. (1999) Mitochondrial phospholipid hydroperoxide glutathione peroxidase plays a major role in preventing oxidative injury to cells. *J. Biol. Chem.* **274**, 4924–4933.

8. Maiorino, M., Gregolin, C., and Ursini, F. (1990) Phospholipid hydroperoxide glutathione peroxidase. *Methods Enzymol.* **186**, 448–457.
9. Maiorino, M., Wissing, J. B., Brigelius-Flohé, R., Calabrese, F., Roveri, A., Steinert, P., et al. (1998) Testosterone mediates expression of the selenoprotein PHGPx by induction of spermatogenesis and not by direct transcriptional gene activation. *FASEB J.* **12**, 1359–1370.
10. Roveri, A., Casasco, A., Maiorino, M., Dalan, P., Calligaro, A., and Ursini, F. (1992) Phospholipid hydroperoxide glutathione peroxidase of rat testis. *J. Biol. Chem.* **267**, 6142–6146.
11. Lei, X. G., Evenson, J. K., Thompson, K. T., and Sunde, R. A. (1995) Glutathione peroxidase and phospholipid hydroperoxide glutathione peroxidase are differentially regulated by dietary selenium. *J. Nutr.* **125**, 1438–1446.
12. Godeas, C., Tramer, F., Micali, F., Soranzo, M., Sandri, G., and Panfili, E. (1997) Distribution and possible novel role of phospholipid hydroperoxide glutathione peroxidase in rat epididymal spermatozoa. *Biol. Reprod.* **57**, 1502–1508.
13. Ursini, F., Heim, S., Kiess, M., Maiorino, M., Roveri, A., Wissing, J., and Flohé, L. (1999) Dual function of the selenoprotein PHGPx during sperm maturation. *Science* **285**, 1393–1396.
14. Cheng, W.-H., Ho, Y.-S., Ross, D. A., Valentine, B. A., Combs, G. F., Jr., and Lei, X. G. (1997) Cellular glutathione peroxidase knockout mice express normal levels of selenium-dependent plasma and phospholipid hydroperoxide glutathione peroxidases in various tissues. *J. Nutr.* **127**, 1445–1450.
15. Fisher, A. B., Dodia, C., Manevich, Y., Chen, J.-W., and Feinstein, S. I. (1999) Phospholipid hydroperoxides are substrates for non-selenium glutathione peroxidase. *J. Biol. Chem.* **274**, 21326–21334.
16. Lei, X. G., Dann, H. M., Ross, D. A., Cheng, W.-H., Combs, G. F., Jr., and Roneker, K. R. (1998) Dietary selenium supplementation is required to support full expression of three selenium-dependent glutathione peroxidase in various tissues of weanling pigs. *J. Nutr.* **128**, 130–135.

Expression of Human Phospholipid Hydroperoxide Glutathione Peroxidase

Kunio Yagi, Sadaaki Komura, and Nobuko Ohishi

1. Introduction

Among lipid peroxides and related free radicals in the process of lipid peroxidation, the first stable products, lipid hydroperoxides, are unique from the viewpoint of pathogenicity. Because of their stability, these hydroperoxides can migrate throughout the body via the bloodstream. This disseminates the deleterious effects of these species, resulting in the provocation of secondary disorders of a disease. Accordingly, the elimination of lipid hydroperoxides would contribute to the prevention of lipid peroxide-mediated diseases. For this purpose, enzymatic decomposition of the hydroperoxides would be the most preferable approach. As enzymes capable of decomposing lipid hydroperoxides, at least four types of glutathione peroxidase (GPx) have been reported (**1**); that is, classical GPx; gastrointestinal GPx; plasma GPx; and phospholipid hydroperoxide GPx or monomeric GPx (PHGPx).

PHGPx is known to attack various kinds of lipid hydroperoxides including phospholipid hydroperoxides and to be present in both cytosol and mitochondrial fractions (**2**). Therefore, we had special attention on PHGPx and intended to express PHGPx gene in appropriate cells by transfection to see whether the expression of this enzyme could prevent host cells from the injury caused by lipid hydroperoxides (**3,4**). In this chapter, procedures to transfect cells with human PHGPx gene having a mitochondrial signal sequence (**Fig. 1**) and its expression in guinea pig 104C1 cells are described.

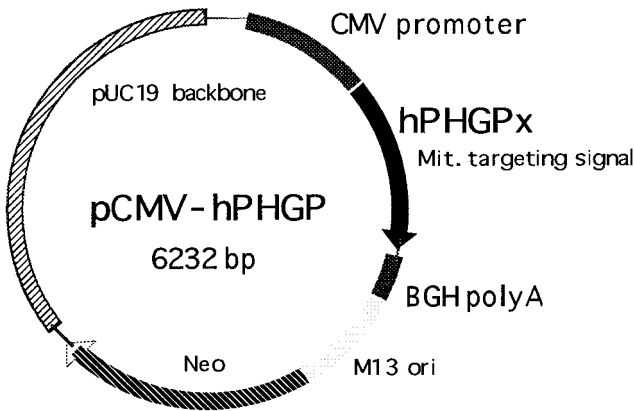


Fig. 1. Expression vector for human PHGPx. The relative locations of functional elements in the expression vector pCMV-hPHGPx are indicated. BGH poly A, bovine growth hormone-derived poly A signal sequence (3). Copyright (1996) Academic Press.

2. Materials

1. Cationic lipid solution: N-(α -trimethylammonioacetyl)-didodecyl-D-glutamate chloride (TMAG, Sogo Pharmaceutical Co., Tokyo), dilauroyl phosphatidylcholine (DLPC, Nichiyu Liposome Co., Tokyo), and dioleoyl phosphatidylethanolamine (DOPE, Nichiyu Liposome Co., Tokyo) in a molar ratio of 1:2:2 (total lipids, 1 μ mol/mL chloroform).
2. pCMV-hPHGPx: 20 μ g DNA/mL phosphate-buffered saline (PBS).
3. PHGPx antibody (*see Note 1*).
4. Cells: guinea pig cell line 104C1.
5. Medium: RPMI1640 medium supplemented with 10% fetal bovine serum (FBS), 100 units/mL penicillin, and 100 μ g/mL streptomycin.
6. G418 (Gibco BRL, Grand Island, NY).

3. Methods

3.1. Preparation of Cationic Multilamellar Liposomes Entrapped the Plasmid pCMV-hPHGPx

Entrapment of the plasmid in the cationic multilamellar liposomes was carried out as described by Yagi et al. (5).

1. Cationic lipid solution (total lipids, 1 μ mol) is taken in a 10-mL glass tube with a conical bottom.
2. The solvent is evaporated in vacuo.
3. The lipid film formed is wetted with 1 mL of PBS containing 20 μ g of plasmid and then vortexed for 2 min.

3.2. Transfection of Cells with pCMV-hPHGPx and Isolation of Stable Transfectants

1. 104C1 cells (1×10^6 cells) are seeded on a 25-cm² plate and incubated in RPMI 1640 medium containing 10% fetal bovine serum, 100 units/mL penicillin, and 100 µg/mL streptomycin at 37° overnight.
2. The next day, cells are incubated with cationic multilamellar liposomes entrapped pCMV-hPHGPx (2 µg DNA/0.1 µmol of lipids).
3. After 16 h of incubation with plasmid/liposomes, the medium is replaced with fresh medium and transfected cells are selected with G418 at its concentration of 400 µg/mL by replacing the antibiotic-containing medium every 3 d over a 15-d period until untransfected cells had detached from the culture flask.
4. By limiting dilution method, clones are isolated and thereafter, the selected cells were further cultured in the medium in the presence of 200 µg/mL G418.

3.3. Results

1. When 104C1 cells were transfected with pCMV-hPHGPx, four clones of transfectants, i.e., 104C1/O1F, 104C1/O2D, 104C1/O4C, and 104C1/O4D are isolated. Cells are disrupted in 0.1 M Tris-HCl buffer, pH 7.5, containing 5 mM β-mercaptoethanol, 17 µg/mL phenylmethylsulfonyl fluoride (PMSF), 5 µg/mL leupeptin, and 5 µg/mL pepstatin A with a Branson sonicator for 1 min at a power setting of 3 with a 50% pulse. The homogenate is centrifuged at 1,500g for 10 min, and the supernatant further centrifuged at 58,000g for 45 min to obtain the cytosol fraction. GPx activity in this fraction was measured with either dilinoleoyl phosphatidylcholine hydroperoxide (PCOOH), linoleic acid hydroperoxide (LAOOH) or *t*-butylhydroperoxide (*t*-BuOOH) as a substrate, as described previously (6).

Western-blot analysis is carried out with our polyclonal antibody against rat liver PHGPx (7).

2. GPx activity of 104C1 cells and of the transfectants is shown in **Table 1**. Since it is known that guinea pig cells scarcely produce selenium-dependent GPx, the GPx activity observed in the 104C1 guinea pig cell line should be due to glutathione S-transferase. Among the four clones, the transfectant 104C1/O4C had the highest GPx activity toward PCOOH, followed by 104C1/O2D and 104C1/O1F. Such activity was not found in 104C1/O4D. As is well known, PHGPx cannot react with *t*-BuOOH and thus it is reasonable that these transfectants did not show any increase in GPx activity toward this substrate. The degree of elevation of GPx activity toward LAOOH in the transfectants was nearly in parallel with that of the activity toward PCOOH.
3. Western-blot analysis of PHGPx is shown in **Fig. 2**. The control 104C1 cells (lane 1) and 104C/O4D cells (data not shown) had no protein immunoreactive with anti-rat PHGPx antibody. The band of the immunoreactive protein was clearly observed with the extract from 104C1/O2D cells (lane 3) and 104C1/O4C cells

Table 1
GPx Activity of 104C1 Cells Transfected with pCMV-hPHGPx

Cells	GPx activity (mU/mg protein)		
	PCOOH	LAOOH	<i>t</i> -ButOOH
Transfectants			
104C1/O1F	6.0	66.8	19.4
104C1/O2D	21.5	176.5	18.2
104C1/O4C	32.1	265.9	13.2
104C1/O4D	3.4	58.8	15.5
Control			
104C1	3.0	61.0	13.8

Cells were cultured on 75-cm² plates in RPMI 1640 medium supplemented with 10% fetal bovine serum. Typical data from a series of experiments are given (3). Copyright (1996), Academic Press.

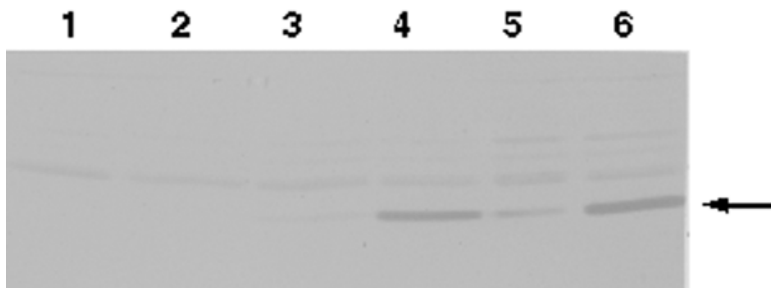


Fig. 2. Western-blot analysis of PHGPx. Cytosolic fraction containing 20 µg protein was subjected to sodium dodecylsulfate-polyacrylamide gel electrophoresis in a 15% gel. Lanes 1 and 2, the parent 104C1 cells; lanes 3 and 4, 104C1/O2D cells; and lanes 5 and 6, 104C1/O4C cells. Lanes 1, 3, and 5, cells were cultured in the RPMI medium without supplementation of selenium. Lanes 2, 4, and 6, cells were cultured in the same medium with the addition of selenium at the concentration of 250 nM. Arrow indicates the position of PHGPx.

(lane 5), and the level of PHGPx protein was higher in the latter than in the former, being consistent with their levels of GPx activity toward PCOOH. When these transfectants were cultured in the medium supplemented with 250 nM sodium selenite, the immunoreactive protein bands showed a marked increase (lanes 4 and 6). These results indicate that the expression of the protein is dependent on selenium. On the other hand, the immunoreactive protein was not seen in the parent 104C1 cells even when they were cultured in the selenium-supplemented medium.

4. Notes

1. Anti-rat PHGPx antibody is capable of reacting with human PHGPx. Anti-human PHGPx antibody is also available to cross-react with rat PHGPx.

References

1. Chu, F.-F. (1994) The human glutathione peroxidase genes GPX2, GPX3, and GPX4 map to chromosomes 14, 5, and 19, respectively. *Cytogenet. Cell Genet.* **66**, 96–98.
2. Godeas, C., Sandri, G., and Panfili, E. (1994) Distribution of phospholipid hydroperoxide glutathione peroxidase (PHGPx) in rat testis mitochondria. *Biochim. Biophys. Acta.* **1191**, 147–150.
3. Yagi, K., Komura, S., Kojima, H., Sun, Q., Nagata, N., Ohishi, N., and Nishikimi, M. (1996) Expression of human phospholipid hydroperoxide glutathione peroxidase gene for protection of host cells from lipid hydroperoxide-mediated injury. *Biochem. Biophys. Res. Commun.* **219**, 486–491.
4. Yagi, K., Shidoji, Y., Komura, S., Kojima, H., and Ohishi, N. (1998) Dissipation of mitochondrial membrane potential by exogenous phospholipid monohydroperoxide and protection against this effect by transfection of cells with phospholipid hydroperoxide glutathione peroxidase gene. *Biochem. Biophys. Res. Commun.* **245**, 528–533.
5. Yagi, K., Noda, H., Kurono, M., and Ohishi, N. (1993) Efficient gene transfer with less cytotoxicity by means of cationic multilamellar liposomes. *Biochem. Biophys. Res. Commun.* **196**, 1042–1048.
6. Duan, Y.-J., Komura, S., Fiszler-Szafarz, B., Szafarz, D., and Yagi, K. (1988) Purification and characterization of a novel monomeric glutathione peroxidase. *J. Biol. Chem.* **263**, 19003–19008.
7. Nakashima, M., Komura, S., Ohishi, N., and Yagi, K. (1993) Immunochemical differentiation between novel monomeric and classic tetrameric rat liver glutathione peroxidases. *Biochem. Mol. Biol. Int.* **29**, 1139–1144.

Superoxide Production in the Islet of Langerhans Detected by the MCLA Chemiluminescence Method

Takashi Sakurai and Susumu Terakawa

1. Introduction

It is well known that the superoxide anion radical (O_2^-) is produced in the body as a result of biochemical activities of many cells, such as neutrophils, macrophages, and Kupffer cells (1). Production of O_2^- is detectable by various methods, including cytochrome-c oxidation (1), nitroblue tetrazolium (NBT) staining, and chemiluminescence (CL) measurement (2). The site and amount of O_2^- production is variable with time and readily determined in vivo by applying the CL method. In earlier studies, the CL method was successfully applied for detection of O_2^- generation at a tissue level in the lung (3), liver (4), pancreas (5), heart (6), and brain (7). Combined with video imaging techniques, the CL method makes it possible to analyze O_2^- generation at a high spatial resolution, sometimes even at a single cell level. In this chapter, we describe the CL method applied to O_2^- detection from the islets of Langerhans in the perfused pancreas.

In an islet of Langerhans, more than 80% of cells are the same cells which function to secrete insulin for maintaining the level of blood glucose. By using 2-methyl-6-[p-methoxyphenyl]-3,7-dihydroimidazo [1,2-a] pyrazin-3-one (MCLA, a *Cypridina* luciferin analog) (2), the glucose-dependent O_2^- production in these cells was studied (8). CL was induced by the dioxetane cleavage reaction of MCLA in the presence of O_2^- or singlet oxygen (Fig. 1) (2). The quantitative analysis of CL was possible by counting the number of induced photons with a sensitive photomultiplier detector (9). The spatial analysis of CL was also possible by using a photon counting camera (9,10).

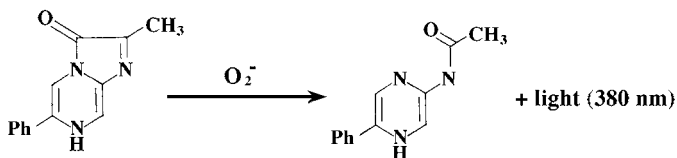


Fig. 1. Possible reaction in the MCLA-dependent chemiluminescence induced by O_2^- .

Combining the temporal and the spatial analyses together, we demonstrate a unique characteristic of the islet of Langerhans.

2. Materials

2.1. Equipment

1. Photon counter (BLR-301, Aloka, Japan).
2. Chamber for photon counting. An opaque acrylic well (2.5 mL in volume) was used as a recording chamber for the excised tissue (cell suspension was also available). The tissue was superfused with 1 mL of the control medium. To stabilize the preparation in the center of the recording chamber, the tissue was placed in a bag made of Teflon as shown in **Fig. 2**. The chamber was infused with a drug-containing medium by using a microsyringe (Hamilton, NV).
3. Photon counting camera system (ARGUS/VIM, Hamamatsu Photonics, Hamamatsu, Japan) composed of an image intensifier, a CCD camera, and a digital image processor. For printing the images, data stored in a computer were processed with a picture-handling program (Photoshop, Adobe, San Jose, CA).
4. Acryl-made animal box (size: approx $20 \times 20 \times 7.5$ cm³) warmed to 35°C with a rubber heater (**Fig. 3**), and placed in a dark room.
5. Light microscope (Labophot, Nikon, Tokyo, Japan) equipped with objectives of 4× (NA = 0.2) and 10× (Fluor, NA = 0.5) and placed in the dark room.

2.2. Reagents

1. Ringer-HEPES solution as a control medium containing 140 mM NaCl, 5 mM KCl, 2 mM $CaCl_2$, 1.2 mM $MgCl_2$, 1.5 mM glucose, 10 mM HEPES (pH 7.35, adjusted with NaOH). The control medium was well-oxygenated, and warmed to 35°C for superfusion or perfusion, and for the recording.
2. MCLA (Tokyo Kasei, Tokyo, Japan), 200 μ M (100× in dilution) in double-distilled water. MCLA solution was stored at −20°C until use.
3. D-glucose solution (750 mM) for stimulation (500× in dilution), stored in a refrigerator until use.
4. Superoxide dismutase (SOD, Sigma), 500 μ M (100× in dilution) in double-distilled water. SOD solution was stored at −20°C until use.
5. Urethane solution (1% in w/v) for anesthetization.

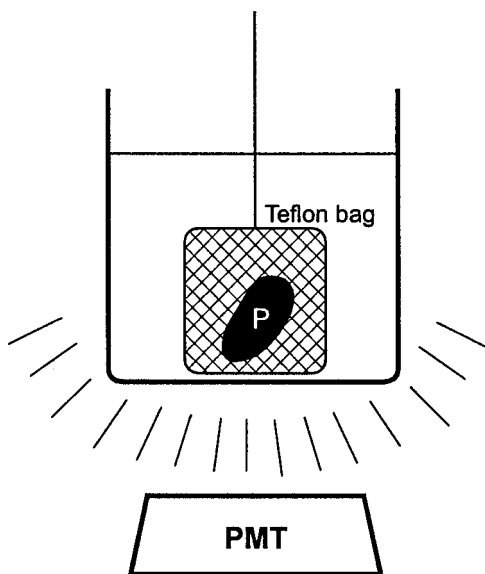


Fig. 2. Schematic diagram of the recording chamber used for the photon counting. The excised and superfused pancreas (P) was placed in a Teflon bag, and hung in the chamber. PMT, photomultiplier.

2.3. Animals

1. Male Wistar strain rats (4–8 wk in age, 250–350 g in body weight).

3. Methods

3.1. Pancreatic Tissue Preparation

1. From the urethane-anesthetized rat, the tail region of pancreas was excised. The tissue was immersed in the control medium.
2. It was then transferred to a Teflon bag, hung in the chamber of the photon counter, and superfused with the control medium. The preparation was incubated at 35°C for more than 10 min before MCLA infusion.

3.2. Perfusion of the Pancreas

1. Perfusion of the pancreas *in situ* was performed (**Fig. 3**) in the rat anesthetized with 1% urethane solution (1 mL i.p./100 g body weight). The body temperature of the animal was maintained at 35°C all the time.
2. The abdominal artery was cannulated with the polyethylene tube (24 gauge) for infusion of control medium containing heparin (0.1 U/mL) at a pressure of 130 cmHg. Within 10 s after the onset of medium infusion, the descending artery was clamped to introduce the control medium to the pancreas via the celiac artery.

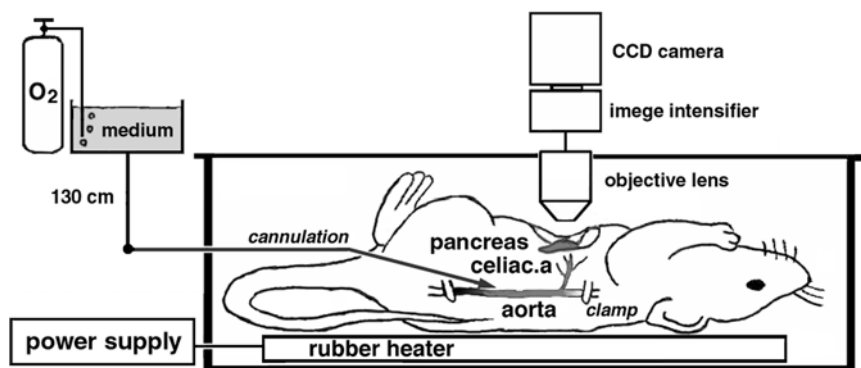


Fig. 3. Schematic diagram of the set up used for detection of chemiluminescence from a perfused pancreas.

3. Immediately after the clamp, the portal vein was cut to discharge the blood and the infusion medium. About 20 min after the perfusion, the islet of Langerhans was recognized as the so-called "island" under microscopic observation. The position of the islet of Langerhans was adjusted to the center of the field of camera view. MCLA ($2 \mu M$ as a final concentration) was added to the reservoir of control medium 10 min before the recording.

3.3. Measurement of MCLA-CL

1. Photon counting with a photomultiplier. According to the method described by Nakano et al. (2–6), the number of photons was counted in the recording chamber, and was printed on the paper or registered to a computer. Usually, the recording started after infusion of MCLA into the chamber. At a proper time, some reagents were added in the chamber to examine their effects.
2. Photon counting with a camera. Using a setup of photon counting camera similar to that described by Suzuki et al. (10), the CL from the superfused pancreas was two-dimensionally visualized. To amplify the efficiency of the conversion from a photon to electrons in the camera intensifier, the voltage applied to the intensifier had to be set at the highest level, as the photon productivity was quite low under the present condition. However, the high voltage generally increased the noise. Therefore, the exposure time was prolonged to more than 10 min for constructing an integrated image.

3.4. Results of MCLA-CL

3.4.1. O_2^- and Glucose-Dependent MCLA-CL from the Excised Pancreas

1. From the result shown in Fig. 4, we established that glucose stimulation specifically induced an increase in O_2^- -dependent MCLA-CL from the pancreatic tissue. At 1.5 mM of glucose in the control medium, the number of CL count was almost

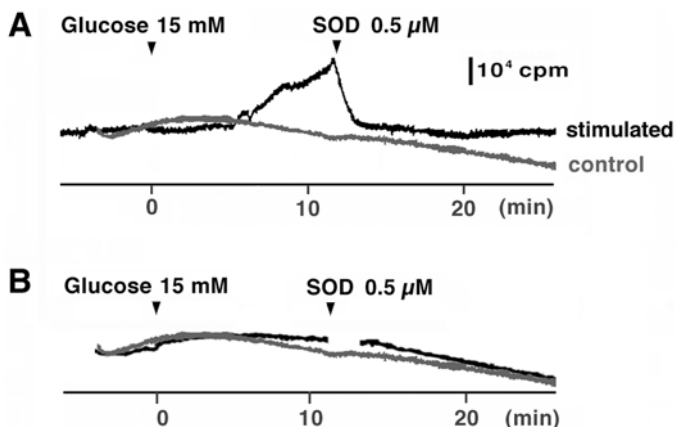


Fig. 4. Changes in chemiluminescence in the superfused pancreas. Experiments were performed at 35°C in (A) and at 25°C in (B). All reagents were added at the time indicated by arrowheads.

constant. The CL became strong when the tissue was stimulated by raising the glucose concentration to 15 mM.

2. To identify the substance that was directly responsible for elevation of the CL, medium containing 0.5 μ M SOD was used for infusion during the recording of an increased CL level. The glucose-evoked CL gradually decayed to the base line level by the SOD infusion.

3.4.2. Two-Dimensional Visualization of the O_2^- -Dependent MCLA-CL in the Perfused Pancreas

1. As shown in **Fig. 5**, CL activities were significantly higher in the pancreatic tissue than in the background, when the pancreas was stimulated with glucose for 30 min in the presence of MCLA.
2. There was a tendency that the CL accumulated from the islet was higher than that from the acinar region.

4. Notes

1. The CL probe should be selected by its properties, such as the detection sensitivity, pH-dependence, membrane permeability and the reaction time. Taking the advantage of the high sensitivity for probing O_2^- , we employed MCLA for the present study of the Langerhans islet. A low-membrane affinity and a slow reaction time (<1 s) of MCLA were not problematic for the detection under such a superfused or a perfused condition.
2. The level of MCLA-CL increased slightly even with the control medium and without tissue preparations. We regarded this small increase in CL as a baseline level, for it might be due to auto-oxidation of MCLA.

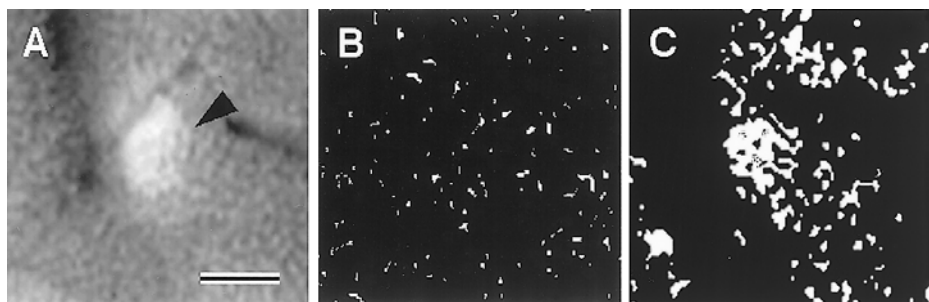


Fig. 5. Two-dimensional imaging with chemiluminescence from the perfused pancreas. (A) Micrograph of the perfused pancreas taken under ordinary illumination. Bar, 500 μm . (B) Image of photon counting with 30 min integration in control medium. (C) Image of photon counting with 30 min integration in 15 mM glucose-containing medium.

3. The glucose-induced O_2^- generation was recovered to control levels by lowering the concentration of glucose to 1.5 mM, and suppressed by reducing the temperature from 35°C to 25°C. However, we never detected any increase in CL from the tissue stimulated with other insulin secretagogues such as sulfonyl urea and calcium-ionophore.
4. The NBT staining (II) is comparable to photon counting imaging in terms of the 2D analysis for the O_2^- production. In fact, a formazan precipitation also appears in the Langerhans islet, when the pancreas is stimulated with 15 mM glucose for more than 30 min.
5. Interestingly, 15 mM glucose did not induce O_2^- production, when rat serum (only 1% v/v) was added to the control medium, or when Langerhans islets were isolated from the surrounding exocrine cells. These results may raise two possibilities, 1) O_2^- is not produced continuously under the normal state of blood flow, or 2) the islet of Langerhans alone is not sufficient for the O_2^- generation.

References

1. Halliwell, B. and Gutteridge, J. M. C. (eds.) (1989) *Free Radicals in Biology and Medicine*, 2nd ed. Clarendon Press, Oxford.
2. Nakano, M. (1998) Detection of active oxygen species in biological systems. *Cell Mol. Neurobiol.* **18**, 565–579.
3. Takahashi, A., Nakano, M., Mashiko, S., and Inaba, H. (1990) The first observation of O_2^- generation in situ lungs of rats treated with drugs to induce experimental acute respiratory distress syndrome. *FEBS Lett.* **261**, 369–372.
4. Nakano, M., Kikuyama, M., Hasegawa, T., Ito, T., Sakurai, K., and Hashimura, E. (1995) The first observation of O_2^- generation at real time in vivo from non-Kupffer sinusoidal cells in perfused rat liver during acute ethanol intoxication. *FEBS Lett.* **372**, 140–143.

5. Kishimoto, W., Nakao, A., Nakano, M., Takahashi, A., Inaba, H. and Takagi, H. (1995) Detection of superoxide free radicals in rats with acute pancreatitis. *Pancreas* **11**, 122–126.
6. Ushiroda, S., Maruyama, Y., and Nakano, M. (1997) Continuous detection of superoxide in situ during ischemia and reperfusion in the rabbit heart. *Jpn. Heart J.* **38**, 91–105.
7. Yamamoto, S., Terakawa, S., Sakurai, T., Matsumura, S., and Uemura, K. (1997) Production of reactive oxygen species and glutamate neurotoxicity in a rat organotypic hippocampal culture. *Adv. Neurotrauma Res.* **9**, 61–64.
8. Sakurai, T. and Terakawa, S. (1997) Radical production and degranulation in pancreatic islets induced by glucose. *Jpn. J. Physiol.* **47** (Suppl. 1), S15.
9. Mizuguchi, Y. (1998) Single photon counting, in *Methods in Molecular Biology*, vol. 108: *Free Radical and Antioxidant Protocols* (Armstrong, D., ed.), Humana Press, NJ, pp. 37–55.
10. Suzaki, E., Kobayashi, H., Kodama, Y., Masujima, T., and Terakawa, S. (1997) Video-rate dynamics of exocytotic events associated with phagocytosis in neutrophils. *Cell Motil. Cytoskeleton* **38**, 215–228.
11. DiGregorio, K. A., Cilento, E. V., and Lantz, R. C. (1987) A kinetic model of superoxide production from single pulmonary alveolar macrophages. *Am. J. Physiol.* **252**, C677–C683.

In Vivo Detection of Transition Metals and Nitrosyl-Heme Complexes Using Ex Vivo Electron Paramagnetic Resonance Spectroscopy

David M. Hall and Garry R. Buettner

1. Introduction

Cellular redox environment is a critical determinant of stress-induced cellular responses and the progression of disease (*1*). Under normal (nonstress) conditions, the cell maintains a strong reducing environment that favors reductive over highly compartmentalized oxidative biochemistry. Exposure of cellular macromolecules to reactive oxygen (ROS) and reactive nitrogen species (RNS) is tightly controlled. Environmental stress can shift the redox balance away from reductive biochemistry however, promoting transition metal activation, and nonprogrammed oxidative and/or nitrosative reactions. Metal-catalyzed oxidative and nitrosative stress have been implicated in the etiology of numerous clinical disorders including inflammation, ischemia-reperfusion injury, rheumatoid arthritis, and aging (*1*).

While the oxygen- and nitrogen-centered radicals themselves are labile and difficult to directly measure in biological systems without the aid of pharmacologic spin-trapping agents, endogenous biomolecules that have been modified by ROS/RNS can be relatively long-lived, allowing us to detect their presence using electron paramagnetic resonance spectroscopy (EPR). In this chapter, we present a technique for characterizing biomarkers of ROS/RNS production and metal activation in whole blood and intact tissues. With this method we have quantitated temporal changes in semiquinone radical (a biomarker of mitochondrial stress), ceruloplasmin (an acute phase ferroxidase antioxidant protein), transferrin, and nitrosyl-heme production in vivo, by sam-

pling arterial and venous blood across a tissue bed, and measuring radical concentrations *ex vivo* using low temperature EPR and a signal averaging approach (2). We have also utilized this technique to determine stress-related alterations in transition metal activation and semiquinone radical production in whole tissues. Simultaneous interpretation of vascular and tissue EPR spectra can provide a unique window into stress-induced alterations in local redox environment and oxidant production.

2. Materials

2.1. Equipment

2.1.1. Instrumentation and Equipment

1. Bruker ESP 300 EPR spectrometer (Bruker Instruments, Karlsruhe Germany), equipped with an ER035M gaussmeter, EIP-625A microwave frequency counter, and an ER4111VT variable temperature unit.
2. Quartz EPR tubes, 3 mm inner diameter (Wilmad, Beuna, NJ).
3. Teflon tubing, 3 mm inner diameter, 2.5 cm lengths.

2.1.2. Transcardial Perfusion Equipment

1. Masterflex perfusion pump (Cole-Parmer, Vernon Hills, IL) (flow rate of 25 mL/min).
2. 16-gauge I.V. catheter needle, connectors, silastic tubing.
3. Wire mesh surgical platform.
4. Large drip pan to catch fluids during transcardial perfusion.
5. Surgical scissors, hemostats, and forceps.
6. 1 and 3 mL Monoject[®] syringes.
7. Clinical benchtop microcentrifuge cooled to 4°C and sterile 1.5-mL spin tubes.

2.2. Reagents

1. Phosphate-buffered saline (PBS).
2. Five percent Heparin Sulfate.
3. Nitrogen gas.
4. Liquid nitrogen.
5. Standards.

3. Methods

3.1. Sample Processing

1. Place the animal on the wire mesh grid over a sink or drip pan and open the abdominal cavity to the height of the xyphoid process, via mid-line laparotomy. Isolate the artery perfusing the tissue bed of interest and its corresponding venous outflow site.

2. Collect 1.5–2.0 mL of whole blood from both the artery and vein, using Monoject® syringes (3), and immediately deliver 300 μ L of each sample into a quartz EPR tube. Cap and store at -80°C . (See **Note 1**).
3. Deliver the remaining venous and arterial blood into sterile microcentrifuge tubes and spin at 14,000 rpm for 5 min at 4°C to separate cell and plasma fractions.
4. Using 1 mL Monoject® syringes, separately aspirate 300 μ L each of the plasma and cell fractions and deliver them into quartz EPR tubes. Cap and store at -80°C .
5. For tissue processing, first remove blood by transcatheterially perfusing the animal with PBS plus 5% Heparin Sulfate.
 - a. Cut down the flank of the animal below the last rib to provide a channel for perfusate outflow.
 - b. Grasp the xyphoid process with hemostats and bend the handles toward the animal's head to expand the ribs and open the thoracic cavity.
 - c. Cut the diaphragm to expose the heart and insert the I.V. catheter into the left ventricle. Remove the needle and connect the catheter to the perfusion pump using a short length of silastic tubing and a connector.
 - d. Turn on the pump and cut the vena cava at the right heart. The perfusion is complete when the outflow from the vena cava clears (approx 500 mL).
6. Biopsy the tissue of interest. Clean the biopsy of blood and connective tissue in cold PBS, and insert it into a 2.5 cm length of Teflon tubing, 3 mm inner diameter, using forceps. Freeze at -80°C . Prior to EPR analyses, the tubing is warmed slightly and the tissue "icecycle" is displaced into a finger dewar of liquid nitrogen using a glass rod. The finger dewar is then placed into the spectrometer cavity.

3.2. EPR Procedure

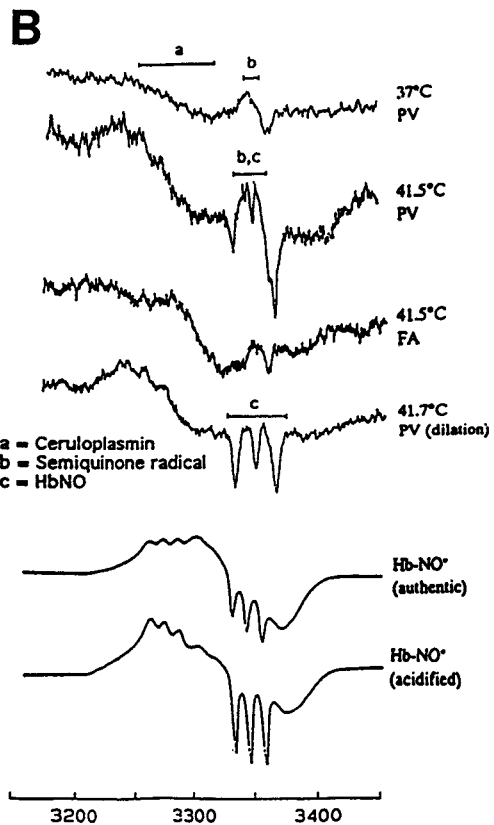
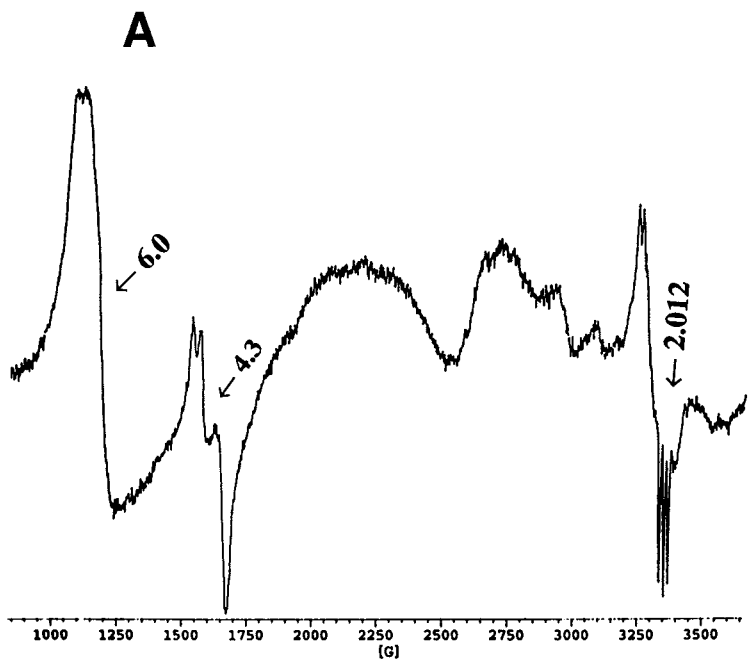
1. Analyses of cell and serum fractions from blood samples can be used to separate cell-based radicals ($\text{Hb}\cdot\text{NO}$) from large protein radicals in the serum such as ceruloplasmin and transferrin (see **Note 2**). Blood and tissue samples are analyzed for radical content using low temperature EPR where spectra can be collected at 77 K, by scanning samples immersed in liquid nitrogen, or at 100 K, using the variable temperature system, which maintains the sample at a pre-set temperature by passing cold nitrogen gas past the sample in the spectrometer cavity.
2. Both methods provide identifiable radical signals, but the signal-to-noise ratio is markedly improved with the variable temperature accessory. Specific radicals can be quantitated by determining area under the curve for their respective spectral features. Alterations in radical production between conditions are then presented in arbitrary units as a fold-increase relative to control samples.
3. To improve the spectral signal-to-noise ratio we also utilize a signal averaging approach with all spectra reported as the average of 20 scans. EPR conditions are

as follows: receiver gain, 5.00×10^5 ; modulation frequency, 100 kHz; modulation amplitude, 4.0 Gauss (G); microwave frequency, 9.43 GHz; microwave power, 10.0 mW; and scan rate 6.0 G/s.

3.3. Results

1. A variety of nitrosyl-heme complexes can be detected in the portal venous blood of heat-stressed rats (**Fig. 1A**). The hyperthermia-induced Hb- \cdot NO signal localized at $g = 2.012$ (between 3200 and 3400 G) in **Fig. 1B**; and **Fig. 2** (*see Note 3*), displays the classic nitrogen triplet hyperfine structure, $a^N = 17.5$ G and centered at $g = 2.012$ that is characteristic of a penta-coordinate heme complex of a ferrous-heme- \cdot NO moiety derived from rat hemoglobin (2). During heat stress, the intensity of this signal progressively increases with elevations in colonic temperature until the splanchnic vascular bed dilates independent of sympathetic nerve activity and circulating catecholamines (**Fig. 2**) (2,4). Similar radical signals are evident in blood and tissues collected from rats following endotoxin challenge, septic shock, and hemorrhagic shock (5,6). Simultaneous with the increase in heme- \cdot NO levels, the concentrations of iron(III)methemoglobin, $g = 6.0$, transferrin, $g = 4.3$ (**Fig. 1A**) and ceruloplasmin, $g = 2.06$ (**Fig. 2**) also increase, suggesting \cdot NO or ROS-mediated oxidation of hemoglobin and a compensatory production of antioxidant ferroxidase proteins. High levels of oxidized hemoglobin and reduced ceruloplasmin or transferrin production are synonymous with multorgan injury during acute heat illness.
2. In addition to nitrosyl-heme complexes and metal-binding proteins, a more narrow feature that is characteristic of a free radical, $\Delta H_{pp} \approx 10$ G at $g = 2.005$ is seen in blood and tissues (**Fig. 3**). In blood, this feature has been identified as a globin free radical (\cdot heme-iron(IV) = O) that evolves during hydrogen peroxide-mediated oxidation of hemoglobin (13). In tissues, this signal has been identified as semiquinone radical (2), a biomarker of mitochondrial reductive stress (*see Note 4*).

Fig. 1. (*see facing page*) Low-temperature (100 K) EPR spectra collected from rat whole blood. (A) presents a 3000 Gauss EPR scan of whole portal venous blood collected 2 h after heat stress. The deflections at $g = 6.0$ and 4.3 represent methemoglobin and ferritin, respectively, while the two triplets centered at $g = 2.012$ represent a penta-coordinate iron(II)nitrosyl-heme protein. In (B), rats were fitted with indwelling femoral artery and portal vein catheters and heated unanesthetized and unrestrained. Blood samples were drawn at the indicated colonic temperature. Spectra collected from hyperthermic rats contain multiple species. The broad feature at $g = 2.06$ (a) represents ceruloplasmin. The region around $g = 2.012$ contains 2 species: a semiquinone radical (b) and nitrosyl-heme (c). For comparison, authentic Hb- \cdot NO was made by briefly bubbling \cdot NO gas into a container of whole venous blood collected from a donor rat. PV, portal venous blood; FA, femoral artery blood.



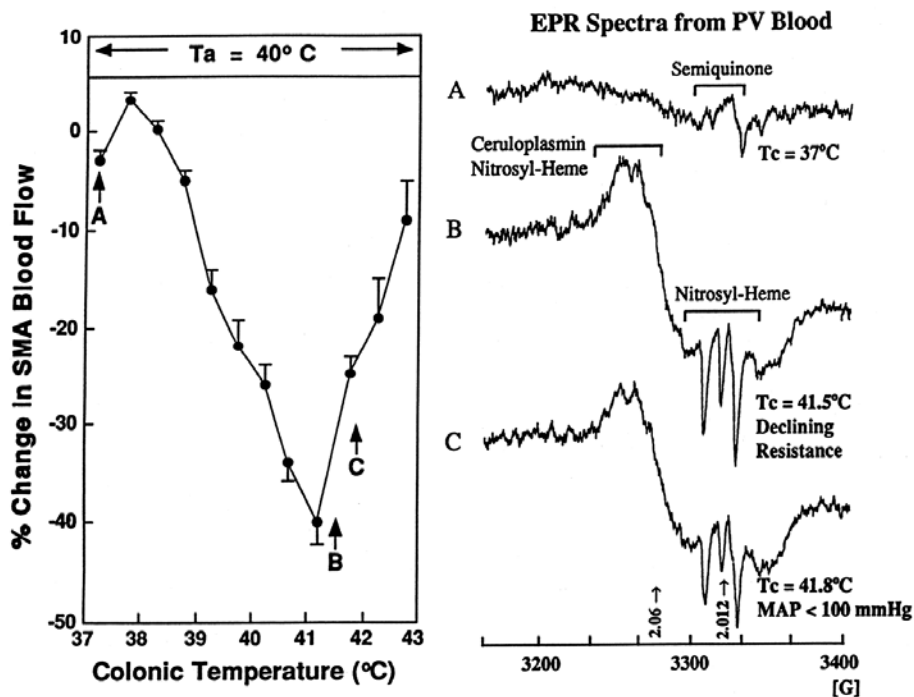


Fig. 2. Low-temperature (100 K) EPR spectra collected from rat whole blood presented with superior mesenteric artery blood flow. Letters denote the colonic temperature at which PV samples were collected. During heat stress, the intensity of the Hb- \bullet NO signal progressively increases with elevations in colonic temperature until the splanchnic vascular bed dilates at colonic temperature of 41.5°C . Note the upward displacement of the second line of the highfield Hb- \bullet NO triplet due to influence on these spectra from semiquinone radical. MAP, mean arterial pressure; T_a , ambient temperature; T_c , colonic temperature.

In liver and intestine (**Fig. 3**), a strong composite transition metal signal consisting of a $g = 2.25$ iron(III) moiety from cytochrome P450 (7) notably absent from intestine, a 480 gauss wide six line feature with g -values of 2.16, 2.12, 2.07, 2.007, 1.94, and 1.87 identified as manganese(II) (8), and $g = 1.935$ and 1.91 features assigned to mitochondrial iron-sulfur proteins (7). Heat stress increases the intensity of this signal in both liver and intestine, two critical target tissues for hyperthermia-induced injury, suggesting that heat stress may promote reduction of cellular iron-sulfur proteins leading to elevated tissue levels of low molecular-weight chelatable transition metals (*see Note 5*).

This EPR approach provides a window into the study of the respective roles of \bullet NO and ROS in the pathophysiology of whole body hyperthermia. Data collected with this technique have led us to hypothesize that \bullet NO and ROS produced

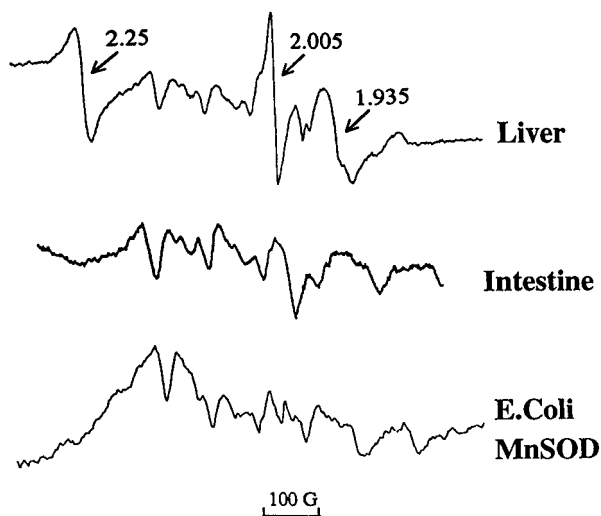


Fig. 3. EPR spectra collected from rat liver and intestine. Both liver and intestine show evidence of manganese (II), from MnSOD, as well as semiquinone radical at $g = 2.005$. Liver also shows evidence of a $g = 2.25$ iron (III) radical.

in splanchnic tissues contribute to the cardiovascular deficiency, consumptive coagulopathy, and multi-organ failure characteristic of heat stroke. We speculate that splanchnic oxidant generation and metal activation contribute to the pathophysiology of multiple shock syndromes.

4. Notes

1. Hb- \cdot NO and methemoglobin in whole blood cooled to -80°C have extremely long half-lives, on the order of days, even weeks. Also, samples are easily transported on dry ice, and can be briefly thawed and refrozen without losing appreciable concentrations of either radical.
2. Lancaster's kinetic models (9), detailing diffusion characteristics of \cdot NO in vivo, predict that alterations in vascular Hb- \cdot NO concentration are indicative of shifts in local tissue \cdot NO release. However, when using these techniques to quantitate \cdot NO release, the following reactions may complicate data interpretation (10):
 - a. \cdot NO can oxidize Hb- O_2 to paramagnetic Fe(III)-Hb;
 - b. \cdot NO binds slowly ($k_{\text{on}} \approx 10^3 - 10^4 \text{ M}^{-1} \cdot \text{s}^{-1}$) and reversibly to Fe(III)-Hb to form diamagnetic nitrosyl-methemoglobin (Fe(III)-Hb- \cdot NO), which auto-reduces by a first-order reaction ($k' \approx 10^{-3} \cdot \text{s}^{-1}$; $t_{1/2} \approx 12 \text{ min}$ at room temperature) to a paramagnetic, EPR-detectable Fe(II)-Hb- \cdot NO species. The ratio of rates of \cdot NO uptake and release for Fe(II)-Hb is 5 to 6 orders of magnitude greater than that of O_2 ($10^{-5} \cdot \text{s}^{-1}$ for \cdot NO and $20 \cdot \text{s}^{-1}$ for O_2), predicting that reduced methemoglobin is a more effective \cdot NO scavenger that can also rapidly release \cdot NO.

- c. Nitrite autocatalytically oxidizes Hb-O₂. Nitrite can also reversibly bind to methemoglobin to yield a mixture of EPR-detectable $S = 5/2$ and $S = 1/2$ complexes. These data suggest that local acid/base conditions and oxygen concentration are important considerations in EPR data interpretation.
3. A free radical ($g = 2.005$) often overlaps the high field line of the $\cdot\text{NO}$ triplet (centered at $g = 2.012$) in venous blood samples and the manganese(II) spectra in tissues. Lowering sample pH with glacial acetic acid removes these radicals and accentuates the $\cdot\text{NO}$ and metal features of respective spectra (2).
4. The precise spectral shape of Hb- $\cdot\text{NO}$ varies from hybrid to hybrid, therefore standards such as shown in **Fig. 1** must be established. Henry's reviews (11,12), include data on the EPR spectral characteristics of nitrosylated hemoproteins, iron-sulfur proteins, non-heme and non-iron-sulfur iron proteins, multicopper proteins, and hemerythrin.
5. The valency of iron ion is critical to its efficiency as a redox catalyst. Iron(II) is currently thought to be the primary valency state capable of participating in deleterious oxidant generation. However, the ratio of iron(II)/iron(III) has been shown to be important in determining rates of lipid peroxidation and iron(IV) radical generation in model systems. Determining alterations in their respective ratios can identify mechanisms of iron involvement in cellular responses to environmental stressors. Using appropriate metal chelators, iron(II) and iron(III) can be visualized in biological samples using EPR (7).

Acknowledgments

This work was supported by National Institutes of Health Grants AG12350, AG14687, and CA81090.

References

1. Schafer, F. Q. and Beuttner, G. R. (2001) Redox state of the cell as viewed through the glutathione disulfide/glutathione couple. *Free Radical Bio. Med.* **30**, 1191–1212.
2. Hall, D. M., Buettner, G. R., Matthis, R. D., and Gisolfi, C. V. (1994) Hyperthermia stimulates nitric oxide formation: electron paramagnetic resonance detection of $\cdot\text{NO}$ -heme in blood. *J. Appl. Physiol.* **77**(2), 548–553.
3. Buettner, G. R., Scott, B. D., Kerber, R. E., and Mugge, A. (1991) Free radicals from plastic syringes. *Free Radical Biol. Med.* **11**, 69–70.
4. Kregel, K. C., Wall, P. T., and Gisolfi, C. V. (1988) Peripheral vascular responses to hyperthermia in the rat. *J. Appl. Physiol.* **64**(6), 2582–2588.
5. Westenberger, U., Thanner, S., Ruf, H. H., Gersonde, K., Sutter, G., and Trentz, O. (1990) Formation of free radicals and nitric oxide derivative of hemoglobin in rats during endotoxin shock. *Free Radical Res. Commun.* **11**, 167–178.
6. Chamulitrat, W., Skrepnik, N. V., and Spitzer, J. J. (1996) Nitrosyl complex formation during endotoxin-induced injury in the rat small intestine. *Shock* **5**(1), 59–65.

7. Kozlov, A. V., Yegorov, D. U., Vladimirov, Y. A., and Azizova, O. A. (1992) Intracellular free iron in liver tissue and liver homogenate. *Free Rad. Biol. Med.* **13**, 9–16.
8. Hall, D. M., Oberley, T. D., Moseley, P. M., Buettner, G. R., Oberley, L. W., Weindruch, R. H., and Kregel, K. C. (2000) Caloric restriction improves thermotolerance and reduces hyperthermia-induced cellular damage in old rats. *FASEB J.* (In Press.)
9. Lancaster, J. R., Jr. and Hibbs, J. B., Jr. (1990) EPR demonstration of iron-nitrosyl complex formation by cytotoxic activated macrophages. *Proc. Natl. Acad. Sci. USA* **87**, 1223–1227.
10. Stamler, J. S., Singel, D. J., and Loscalzo, J. (1992) Biochemistry of NO and its redox activated forms. *Science* **258**, 1898.
11. Henry, Y., Lepoivre, M., Drapier, J., Ducrocq, C., Boucher, J., and Guissani, A. (1993) EPR characterization of molecular targets for NO in mammalian cells and organelles. *FASEB J.* **7**(12), 1124–1134.
12. Henry, Y., Ducrocq, C., Drapier, J.-C., Servant, D., Pellat, C., and Guissani, A. (1991) Nitric oxide, a biological effector. EPR detection of nitrosyl-iron-protein complexes in whole cells. *Eur. Biophys. J.* **20**(1), 1–15.

Spectral-Spatial Electron Paramagnetic Resonance Imaging (EPRI) in Skin Biopsies at 9.5 GHz

Jürgen Fuchs, Norbert Groth, and Thomas Herrling

1. Introduction

EPR spectroscopy can quantitatively detect free radicals with high specificity and sensitivity in biological samples. However, the natural free radical concentration in biological systems is usually too low for giving sufficient signal intensity which is necessary for EPR. In practice it is almost always necessary to use the indirect spin-trap method to detect radical spin adducts, which are in most cases nitroxide free radicals. The success of EPR-based studies relies heavily on the use of spin traps or the ability to follow the kinetics of nitroxides (*1*). Nitroxides are sensitive to motion, polarity, structural order and fluidity, oxygen tension, pH, and participate in one electron transfer reactions (*2*).

EPR imaging (EPRI) is a unique method used for visualizing spatial distribution of free radicals (*3,4*). In the recent years EPRI has been increasingly used for in vivo studies. Application of the EPRI technique to intact animals has been limited by several factors (*5*). The conventional EPR frequency of 9 GHz does not permit the use of large aqueous samples, due to the high dielectric loss, and the penetration depth of 9 GHz microwaves allows only studies at the body surface. For in vivo applications low (0.5–3.0 GHz) or very low (200–800 MHz) frequency has been used (*1,6–8*). Recent technical innovations of in vivo EPRI has been the design of instrumentation for pulsed EPR (*9*). An advanced technique is the integration and combination of different magnetic resonance techniques, as in proton electron double-resonance imaging (PEDRI) (*10,11*). In this chapter we describe the application of the EPR imaging at conventional 9 GHz frequency for measurement of nitroxide radicals in skin biopsies (*12,13*).

From: *Methods in Molecular Biology*, vol. 196: *Oxidants and Antioxidants: Ultrastructure and Molecular Biology Protocols*
Edited by: D. Armstrong © Humana Press Inc., Totowa, NJ

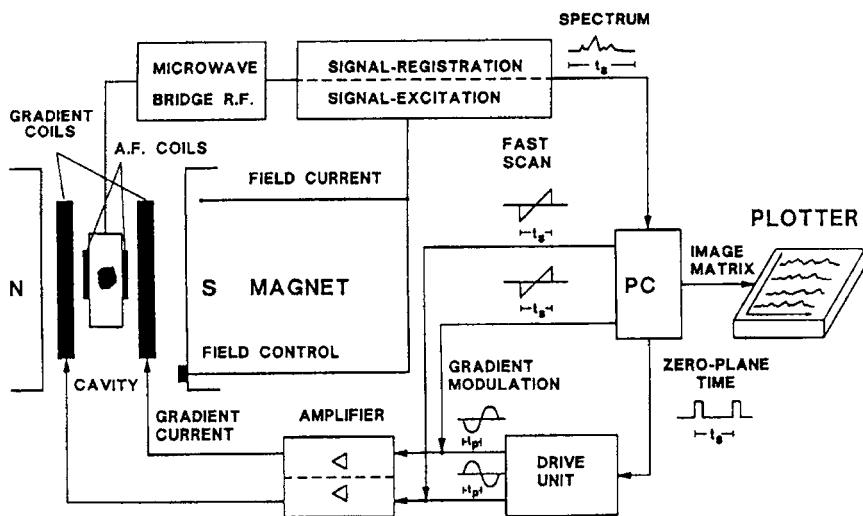


Fig. 1. Block diagram of the MOSS imaging system.

This approach does not require the use of highly sophisticated technology and can be performed with any commercially available EPR spectrometer after some technical modifications.

2. Materials and Methods

2.1. EPR Imaging in Mouse Skin Biopsies

The MOSS imaging system (Fig. 1) based on an EPR 221 spectrometer (developed and built at the Center of Scientific Instruments, Berlin) consists of an eight-inch iron magnet, a X-band (9.5 GHz) microwave bridge, and the EPR 221 console containing the power supply and the modules for signal excitation, recording, and control (14,15). The imaging unit consists of the gradient coils, which are arranged between the pole pieces and a rectangular standard resonance cavity with a H_{102} mode, the amplifier block, and the drive unit. The signal voltage is increased by the amplifier block, which is directly connected with the gradient coils. Both the gradient coils and its amplifier are water-cooled. The drive unit generating the gradient modulation and controlling the phase adjustment is connected with the amplifier block and a personal computer (PC). The driving part of the PC supplies the signal for shifting the spectral plane and the fast field scan. For data acquisition and for image processing, the PC is connected with the signal-recording block of the spectrometer. The data acquisition is triggered by the PC (14). The instrument settings were: Central magnetic field 339.0 mT, modulation frequency 50 kHz (second deriva-

tive), modulation amplitude 0.1–0.15 mT, field gradient 4 T/m, microwave frequency: 9.5 GHz, microwave power 50 mW, scan range 5 mT, scan time 4 min for 2D images, gradient frequency 70 Hz. Spectra were recorded in 128 spatial planes with 128 points, resulting in a 128×128 image matrix.

2.2. Chemicals

Perdeuterated ^{15}N 2,2,5,5-tetramethyl-3-pyrrolin-1-oxyl-3-carboxamide (pD- ^{15}N proxad) was purchased from IC Chemikalien GmbH, Ismaning, Germany.

2.3. Animals

Female hairless mice, 24 wk old, were purchased from Charles River Wiga, Sulzfeld, Germany. The animals were disease-free and had unrestricted access to a standard diet and water. Skin thickness was measured by histometry after GOLDBERGER staining. Total skin thickness (epidermis + dermis) was 400 μm . Epidermal thickness at the back of the animals was 35 ± 5 μm , at the belly 20 ± 3 μm , and follicular epidermis was 160 ± 10 μm .

2.4. Skin Preparation

The epidermal surface of a freshly excised 4 mm mouse skin biopsy from the belly was incubated with 5 μL of a 50 mM solution of pD- ^{15}N proxad in ethanol/water (50/50 = v/v). After incubation at 22°C for 5 min the nitroxide solution was washed off with isotonic saline. The biopsy was placed in the lower end of a quartz glass tube with 2.5 mm internal diameter (Spintec Inc., Remshalden, Germany) and centering the tissue sample in the middle of the EPR cavity. Repetitive measurements of different samples resulted in a tuning error of less than 5% of the total signal observed.

3. Results and Discussion

Using modulated field gradients with simultaneous field scan (MOSS) for surface imaging, we have measured the spatially resolved spectra (spectral spatial image) of the pyrrolidine type nitroxide pD- ^{15}N proxad in skin biopsies of euthymic hairless female mice at a microwave frequency of 9.5 GHz. Small skin samples, such as 4 mm biopsies, can be investigated in a rectangular standard resonance cavity with a H_{102} mode by EPRI. Perdeuterated ^{15}N substituted spin probes have narrow line widths due to the lack of a proton superhyperfine structure and thus the spectral resolution is increased. Time-dependent skin penetration of pD- N^{15} proxad can be visualized by EPR imaging. In **Fig. 2A** the 2nd derivative of the typical two-line resonance image of the pD- ^{15}N proxad is displayed, obtained 9 min after application of a small

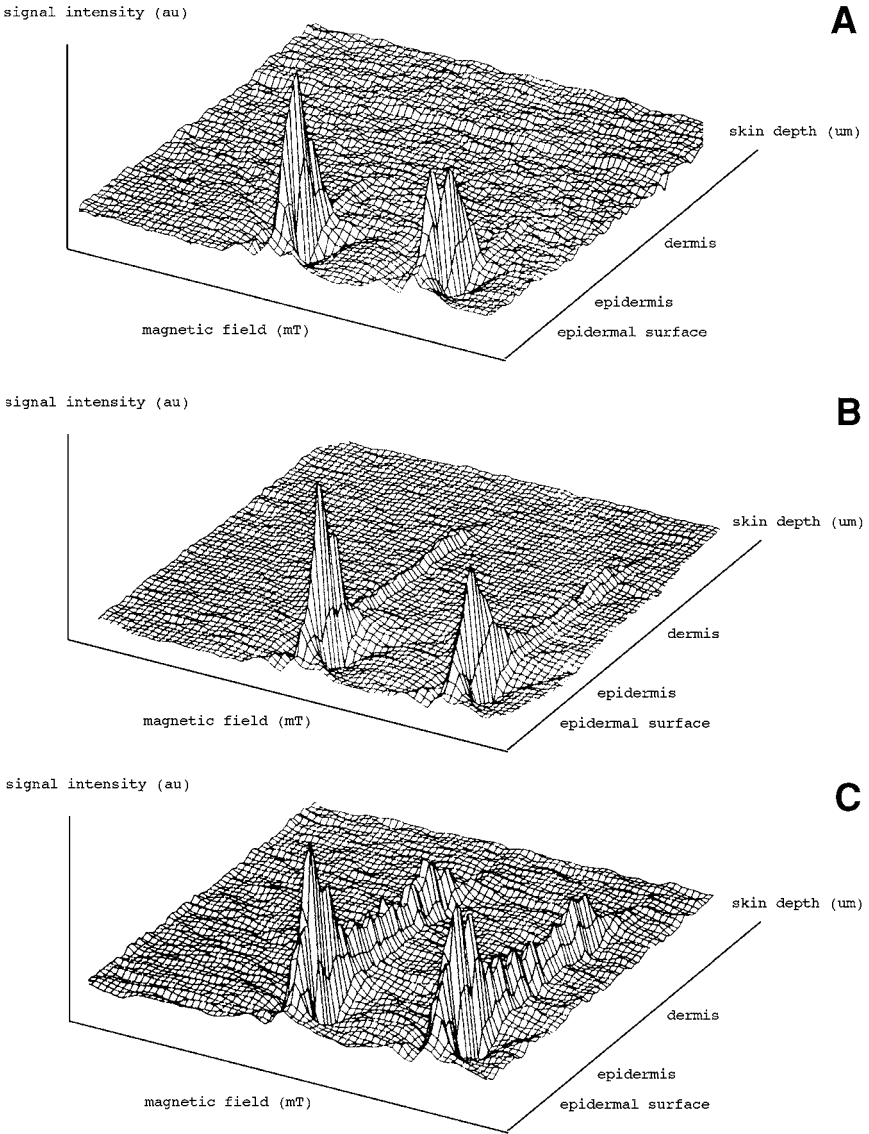


Fig. 2. Spectral spatial image of $\text{pD-}^{15}\text{N}$ proxad in epidermis/dermis of a freshly excised mouse skin biopsy (total skin thickness 0.4 mm). B, magnetic field, r , sample thickness. (A, 5 min; B, 20 min; C, 40 min).

spin probe reservoir at the epidermal surface. Subsequent scans after 20 min (**Fig. 2B**) and 40 min (**Fig. 2C**) show the penetration profile of pD-¹⁵N proxad into the skin sample. Significant penetration of pD-¹⁵N proxad into dermis is already observed after 40 min. Over this time period there is only minor EPR signal loss (8%). Proxad was used as a spin probe because pyrrolidine type nitroxides are relatively resistant to bioreduction in skin (**16**).

EPR imaging with modulated field gradients allows spatial resolution of paramagnetic centers in different tissues planes, and the possibility for obtaining an EPR spectrum in a selected volume part. A spatial resolution (actual point distinction) better than 10 μ m can be obtained (**12,13**), and X-band microwaves can be used for imaging full thickness skin biopsies of hairless mice in a rectangular H₁₀₂ resonant cavity. In contrast to ultrasound and nuclear magnetic resonance imaging, EPRI can provide information on skin biochemical and biophysical parameters, which cannot be obtained by other methods. Potential applications of EPRI include two- and three-dimensional studies on skin-membrane fluidity and polarity, one-electron redox processes, reaction of specifically targeted nitroxides with reactive chemical groups, transient free radical production, and detection of persistent free radicals. Furthermore, liberation, penetration and distribution of spin labeled drugs can be analyzed noninvasively in skin (**17**).

References

1. Sotgiu, A., Colacicchi, S., Placidi, G., and Alecci, M. (1997) Water soluble free radicals as biologically responsive agents in electron paramagnetic resonance imaging. *Cell. Mol. Biol.* **43**, 813–823.
2. Kocherginsky, N. and Swartz, H. M. (1995) Nitroxide spin labels: in *Reactions in Biology and Chemistry* (Kocherginsky, N. and Swartz, H. M., eds.), CRC Press, Boca Raton.
3. Berliner L. J. (1989) The development and future of ESR imaging and related techniques. *Phys. Med.* **5**, 63–75.
4. Swartz, H. M. and Walczak, T. (1993) In-vivo EPR: prospects for the 90's. *Phys. Med.* **9**, 41–50.
5. Colacicchi, S., Ferrari, M., and Sotgiu, A. (1992) In vivo electron paramagnetic resonance spectroscopy/imaging: first experiences, problems, and perspectives. *Int. J. Biochem.* **24**, 205–214.
6. Quaresima, V. and Ferrari, M. (1998) Current status of electron spin resonance (ESR) for in vivo detection of free radicals. *Phys. Med. Biol.* **43**, 1937–1947.
7. Fuchs, J., Groth, N., Herrling, T., and Packer, L. (1994) In vivo EPR skin imaging. *Methods Enzymol.* **203**, 140–149.
8. Gallez, B., Bacic, G., Goda, F., Jiang, J., O'Hara, J. A., Dunn, J. F., and Swartz, H. M. (1996) Use of nitroxides for assessing perfusion, oxygenation, and viability of tissues: in vivo EPR and MRI studies. *Magn. Reson. Med.* **35**, 97–106.

9. Murugesan, R., Cook, J. A., Devasahayam, N., Afeworki, M., Subramanian, S., Tschudin, R., et al. (1997) In vivo imaging of a stable paramagnetic probe by pulsed-radiofrequency electron paramagnetic resonance spectroscopy. *Magn. Reson. Med.* **38**, 409–414.
10. Alecci, M., Lurie, D. J., Nicholson, I., Placidi, G., and Sotgiu, A. (1996) A proton-electron double-resonance imaging apparatus with simultaneous multiple electron paramagnetic resonance irradiation at 10 mT. *MAGMA* **4**, 187–193.
11. Foster, M. A., Seimenis, I., and Lurie, D. J. (1998) The application of PEDRI to the study of free radicals in vivo. *Phys. Med. Biol.* **43**, 1893–1897.
12. Fuchs, J., Milbradt, R., Groth, N., Herrling, N., Zimmer, G., and Packer, L. (1991) One- and two dimensional EPR (Electron Paramagnetic Resonance) imaging in skin. *Free Rad. Res. Commun.* **15**, 245–253.
13. Fuchs, J., Milbradt, R., Groth, N., Herrling, T., Zimmer, G., and Packer, L. (1992) Electron Paramagnetic Resonance (EPR) imaging in skin: biophysical and biochemical microscopy. *J. Invest. Dermatol.* **98**, 713–719.
14. Herrling, T., Groth, N., Thiessenhusen, K. U., Fuchs, J., and Ewert, U. (1992) Spectral-spatial skin imaging with modulated gradient and simultaneous field scan (MOSS), in *Magnetic Resonance Microscopy* (Blümich, B. and Kuhn, W., eds.), VCH Verlagsgesellschaft mbH Weinheim, New York, pp. 563–572.
15. Herrling, T., Groth, N., and Fuchs, J. (1996) Biochemical EPR imaging of skin. *Appl. Magn. Res.* **11**, 471–486.
16. Fuchs, J., Groth, N., Herrling, T., and Zimmer, G. (1997) Electron paramagnetic resonance studies on nitroxide radical 2,2,5,5-tetramethyl-4-piperdine-1-oxyl (Tempo) redox reactions in human skin. *Free Radic. Biol. Med.* **22**, 967–976.
17. Freisleben, H. J., Groth, N., Fuchs, J., Rudolph, P., Zimmer, G., and Herrling, T. (1994) Penetration of spin-labeled dihydrolipoate into the skin of hairless mice: modification of epidermal and dermal polarity. *J. Pharm. Sci.* **23**, 234–245.

In Vivo/*In Situ* Detection of Nitric Oxide Using Low-Frequency EPR Spectroscopy

Pei Tsai, Supatra Porasuphatana, Howard J. Halpern, Eugene D. Barth, and Gerald M. Rosen

1. Introduction

Nitric oxide (NO•), generated by the catalytic action of nitric oxide synthase on L-arginine (1,2), regulates vascular tone, augments cell-cell communications, and governs many intracellular events (3–8). Further, NO• plays a critical role in host immunity, particularly effective against a number of intracellular pathogens (9–11). There are two distinct classes of nitric oxide synthases, constitutive and inducible (12), the latter of which is found in phagocytic cells (13) and can be induced in other cells by exposure to endotoxins and/or cytokines (14; *see Note 1*).

While there are numerous methods to detect free radicals, including NO•, in homogenous solutions of purified enzymes, cell suspensions, and isolated tissue preparations (15), spin trapping/EPR spectroscopy can characterize a variety of biologically generated free radicals in animal models in real time and at the site of their evolution (16). Of particular interest to this article are those recent studies that identify NO•. When considering spin traps for NO•, one is limited by the fact that nitrosoalkane and nitrones, most often used to detect oxygen-centered, carbon-centered, and sulfur-centered free radicals, do not react with NO• (17). Alternatives such as “activated” cis-conjugated dienes (18), nitronyl nitroxides (19), and ferrochelates (20–22) have proven to be valuable probes to identify NO• in a variety of experimental paradigms.

In this chapter, we will expand upon our earlier report in this Series (23) by focusing on the spin traps that will allow *in vivo in situ* detection of NO• in animal models in real time.

2. Materials

2.1. Equipment

1. EPR Spectra are attained with a low-frequency EPR spectrometer operating at 250 MHz (23,24). At 250 MHz, the skin depth (37% sensitivity) is approx 7 cm of tissue, more than deep enough to measure any part of the mouse.
2. The resonator assembly is a lumped circuit parallel inductance and capacitance.
3. The animal holder itself is the single turn inductive element of the resonant circuit.
4. The capacitive coupling of the resonator assembly to the RF source and the detection circuit is adjustable electronically, enabling suppression of spectral artifacts caused by animal motion and microphonic noise at frequencies out to several hundred hertz.

2.2. Reagents

1. Sodium N-methyl-D-glucaminedithiocarbamate (NaMGD).
2. Ammonium N-(dithiocarboxy)sarcosine ($[\text{NH}_4]_2\text{DTCS}$).
3. Potassium 2-(4-carboxyphenyl)-4,4,5,5-tetramethylimidazoline-1-oxyl 3-oxide (carboxy-PTIO).
4. (Z)-1-[N-[3-Aminopropyl]-N-[4-(3-aminopropylammonio)butyl]-amino} diazen-1-ium-1,2-diolate] (SPER/NO) (Alexis Biochemical, San Diego, CA).

3. Methods

3.1. Synthesis of Ammonium N-(dithiocarboxy)sarcosine (DTCS)

1. To a solution of sarcosine (Aldrich Chemical Co., 5 gm, 56.1 mmoles) dissolved in ammonium hydroxide (30%, 15 mL) at 10°C was added carbon disulfide (Aldrich Chemical Co., 5.6 mL, 93 mmoles) dissolved in absolute ethanol (15 mL). The rate of addition was such that the temperature of the reaction did not exceed 10–15°C.
2. Once completed, the mixture was stirred for 30 min, as the temperature of the reaction was allowed to reach ambient conditions, during which time a solid precipitated from the solution.
3. Upon filtering, this material was washed sequentially with ice-cold methanol (10 mL) and then dry ether (3×25 mL). Further purification was achieved by recrystallization from methanol. The resultant ammonium N-(dithiocarboxy)sarcosine was a white powder (6.7 gm, 60%), decomposing between 138–140°C. NMR (D_2O) δ : 3.46 (s, 3H), 4.57 (s, 2H) (26).

3.2. In Vivo In Situ Pharmacokinetics of NO-Fe(DTCS)₂ and NO-Fe(MGD)₂

Mice (C3H/sed, 10–25 wk old) were lightly anesthetized by i.p. injection of a mixture of ketamine (45 mg/kg) and diazepam (20 mg/kg) and restrained in the prone position in an acrylic hemicylindrical jig. Using the caudad tips of

the scapulae as an anatomical reference, animals were installed in the 3.2 cm long by 2.5 cm diameter resonator to include the entire abdomen—from the diaphragmatic domes to the bladder. Infrared radiant heating maintained the animal's core temperature at $37^{\circ}\text{C} \pm 1^{\circ}\text{C}$ as measured by thermocouple rectal probe before and after spectroscopy.

Normal saline solutions of $(\text{NH}_4)_2\text{DTCS}$ and NaMGD were each made by mixing the chelate at five times molar excess—two and one half times stoichiometric excess—with a stoichiometric amount of Fe^{2+} . A mixture of 5.4% nitric oxide and 94.6% argon (Matheson Gases, Joliet, IL) was passed through the iron chelate solutions as a fine stream of bubbles until maximal concentrations of $\text{NO-Fe}(\text{DTCS})_2$ [8] and $\text{NO-Fe}(\text{MGD})_2$ [9] were achieved. The bottles containing the solutions were regularly tapped to mix the solutions. The maximum concentrations were determined by the amplitude of the X-Band EPR signal, a $g \sim 2$ triplet signal. Nitric oxide bubbling was immediately followed by a 5 min purge with argon.

$\text{NO-Fe}(\text{DTCS})_2$ [8] solution developed a maximum signal after 3 min of bubbling at a rate of 24 mL of gas per min per mL of solution. One mL of $\text{NO-Fe}(\text{DTCS})_2$ [8] (10 mM, the Fe^{2+} concentration) was injected into the installed mouse by an i.p. infusion line and acquisition of spectra begun as soon as 50 s.

Formation of $\text{NO-Fe}(\text{MGD})_2$ [9] required more care. A stable, dark brown saline solution of $\text{Fe}(\text{MGD})_2$ [7] was bubbled with NO^{\bullet} (5.4% nitric oxide/94.6% argon) for 3 min at a rate of 24 mL of gas per min for mL of solution. The solution turned green and yielded a precipitate, with a concomitant decrease in the intensity of the EPR signal. The half-life of the X-Band signal was ~ 3 min. Reducing the bubbling time from 3 min to 90 s and the rate of bubbling from 24 to 12 mL per min per mL of solution increased the half-life of X-Band signal of $\text{NO-Fe}(\text{MGD})_2$ [9] from 3 to 20 min. Immediately after bubbling, 1 mL of $\text{NO-Fe}(\text{MGD})_2$ (20 mM, the Fe^{2+} concentration) was injected into the installed mouse by an i.p. infusion line and acquisition of EPR spectra begun as soon as 50 s.

3.3. Low-Frequency EPR Spectroscopy

At an incident radio-frequency power of 100 mW, and at a loaded Q (quality factor) of 65 typical for an installed mouse, the radio-frequency magnetic field (B_1) is ~ 0.15 G (25). The amplitude of the modulation field was 1 G at 5.12 KHz. Spectral acquisition was computer controlled. Each EPR spectrum was the sum of 10 individual scans of the magnetic window, with 64 data points per scan (*see* Fig. 1). The detection circuit time constant and the point acquisition time were both 0.1 s, yielding an acquisition time of just over 1 min.

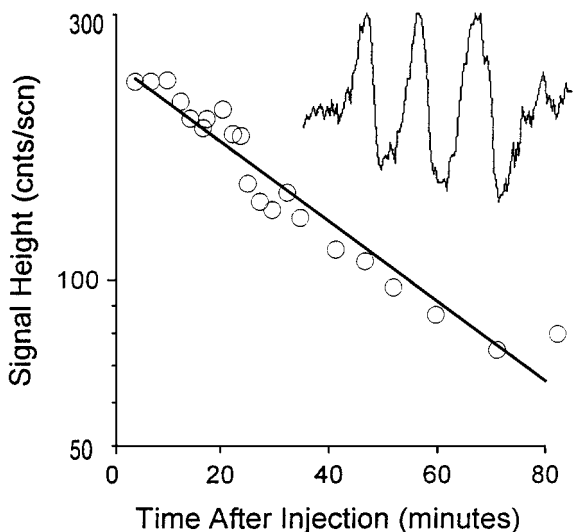


Fig. 1. A representative plot of the signal height versus time of the *in vivo* elimination of $\text{NO-Fe}(\text{DTCS})_2$. Each line of the $\text{NO-Fe}(\text{DTCS})_2$ triplet is plotted at the time the line was obtained. The inset shows the initial EPR spectrum for $\text{NO-Fe}(\text{DTCS})_2$. (Figure reprinted with permission from **ref. 26.**) Copyright (1999), Elsevier Science.

3.4. Results

3.4.1. Spin Traps for *In Vivo In Situ* Detection of $\text{NO}\bullet$

1. As discussed earlier, there are three distinct families of spin traps for $\text{NO}\bullet$. The first group of compounds, “activated” *cis*-conjugated dienes, such as 7,7,8,8-tetramethyl-*o*-quinodimethane [1], produced during the photolysis of 1,1,3,3-tetramethyl-2-indanone [2], react with $\text{NO}\bullet$; the resultant nitroxide, in this case 1,1,3,3-tetramethylisindolin-2-oxyl [3] exhibits a typical three-line EPR spectrum with $A_N \approx 15 \text{ G}$ (18) (Fig. 2). The necessity to photoactivate indanones to the corresponding *o*-quinodimethanes, as well as poor aqueous solubility, short half-life of isindolin-2-oxyls in biological milieu, a lack of specificity towards $\text{NO}\bullet$ and small second-order rate constant (18,27) makes the widespread use of *o*-quinodimethanes for the *in vivo in situ* spin trapping of this free radical problematic.
2. The second group, nitronyl nitroxides, including [4] react with $\text{NO}\bullet$. This leads to the loss of $\bullet\text{NO}_2$ and formation of imino nitroxides, such as [5] (19; Fig. 3). This reaction results in an accompanying change in the EPR spectrum from the five-lines of nitronyl nitroxide [4] to the seven-lines of the imino nitroxide [5]. Although there is sufficient discrimination between these nitroxides, at low fluxes of $\text{NO}\bullet$ it becomes exceedingly difficult to identify the EPR spectrum of the imino nitroxide with such a large background EPR spectrum of the nitronyl

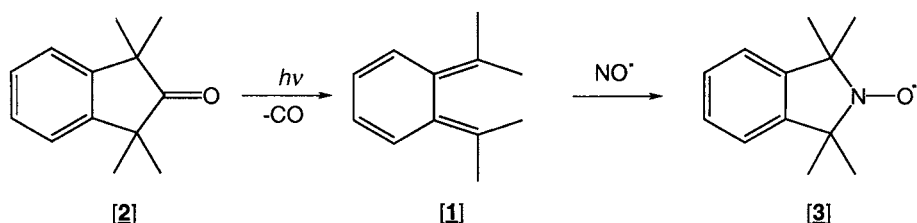


Fig. 2. Depiction of the reaction of NO^\bullet with 7,7,8,8-tetramethyl-*o*-quinodimethane [1]. The corresponding nitroxide, 1,1,3,3-tetramethylisoindolin-2-oxyl [3] exhibits a typical three-line EPR spectrum with $A_N \cong 15$ G.

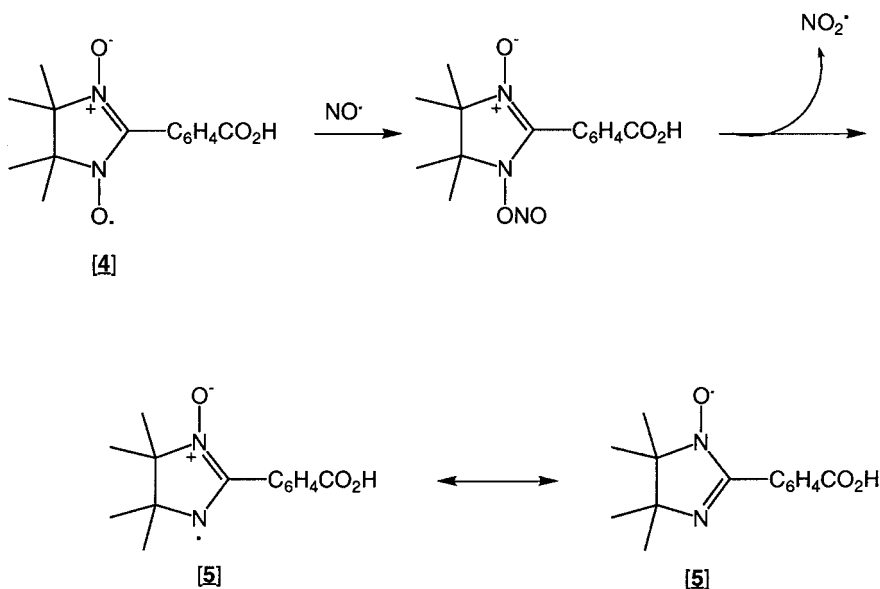


Fig. 3. Illustration of the reaction of NO^\bullet with the nitronyl nitroxide, 2-(4-carboxyphenyl)-4,4,5,5-tetramethylimidazoline-1-oxyl 3-oxide [4]. This results in the formation of the imino nitroxide [5] with a loss of NO_2^\bullet , concomitant with a shift in the EPR spectrum from 5 lines for nitronyl nitroxide [4] to an EPR spectrum of 7 lines for imino nitroxide [5].

nitroxide. When such conditions arise, experiments must be conducted for prolonged periods of time to assure accurate estimates of NO^\bullet production. This, unfortunately, leads to an additional limitation, nitronyl nitroxides are very susceptible to bioreduction, further restraining the utility of these reporters of NO^\bullet (28).

3. The third group of spin traps for NO^\bullet is chelates of iron. Nitrosylation of ferro-complexes result in the formation of paramagnetic species that can be detected

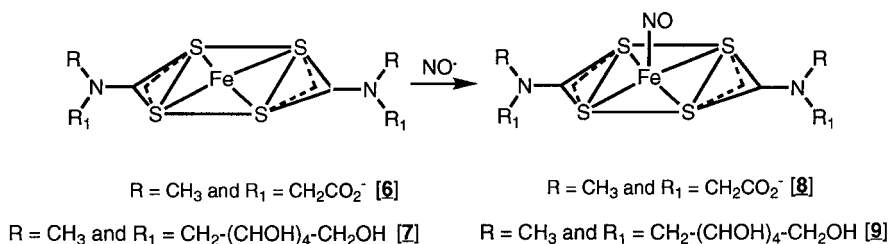


Fig. 4. The structure of ferro-chelates, $\text{Fe}^{2+}(\text{DTCS})_2$ [6] and $\text{Fe}^{2+}(\text{MGD})_2$ [7]. Reaction with $\text{NO}\bullet$ results in the formation of $\text{NO-Fe}(\text{DTCS})_2$ [8] and $\text{NO-Fe}(\text{MGD})_2$ [9].

by EPR spectroscopy (*see Note 3*). For identification of $\text{NO}\bullet$ in animal models in real time, $\text{Fe}^{2+}(\text{DTCS})_2$ [6] and $\text{Fe}^{2+}(\text{MGD})_2$ [7] have surfaced as the spin trap of choice (20–22; Fig. 4). Yet a careful examination of these findings reveal qualitative rather than quantitative assessments of *in vivo in situ* $\text{NO}\bullet$ production. In fact the lack of pharmacokinetic and pharmacodynamic data is troubling and makes it difficult to estimate the *in vivo* flux of $\text{NO}\bullet$ at relevant tissue sites. Recent pharmacokinetic studies in our laboratory (26) have begun to place these measurements on a sound footing by quantitating the utility of $\text{Fe}^{2+}(\text{DTCS})_2$ [6] and $\text{Fe}^{2+}(\text{MGD})_2$ [7] as spin traps to detect $\text{NO}\bullet$ in animal models in real time.

3.4.2. Rate Constants for the Spin Trapping of $\text{NO}\bullet$

1. Despite reports describing the spin trapping of $\text{NO}\bullet$ by Fe-chelates (20–22; *see Note 2*), there are, surprisingly, no data detailing either kinetics of NO-Fe-chelate formation or the resulting stability of these complexes in biological milieu. In fact, these studies are necessary prerequisites to real time estimates of $\text{NO}\bullet$ generation in animal models, as they define essential elements required to quantitate *in vivo* free radical production. For instance, do the Fe-chelates [6,7] spin trap a large percentage of $\text{NO}\bullet$ produced? These are important questions that must be addressed prior to undertaking *in vivo in situ* spin trapping experiments.
2. Rate constants for the reaction of $\text{NO}\bullet$ with either 7,7,8,8-tetramethyl-*o*-quinodimethane [1], nitronyl nitroxides [4] or the Fe-chelates [6,7] are presented in Table 1. In the case of “activated” *cis*-conjugated diene [1], the absolute rate constant was determined (27), whereas for nitronyl nitroxide [4] and Fe-chelates [6,7] apparent rate constants were determined in which oxyhemoglobin was used as the competitive inhibitor (26,29). Here, the oxidation of reduced oxyhemoglobin [$\text{Hb(Fe}^{+2}\text{)O}_2$] by $\text{NO}\bullet$, which has been found to be $3.7 \times 10^7 \text{ M}^{-1} \text{ s}^{-1}$ at 25°C (29), is an excellent model for such studies. From data presented in Table 1, the apparent rate constants for the spin trapping of $\text{NO}\bullet$ by the Fe-chelates [6,7] are a factor of ten greater than that calculated for nitronyl nitroxide [4]. Of interest was the finding that the apparent rate constant of

Table 1
Rate Constants for the Spin Trapping of Nitric Oxide

Compounds	Rate Constant $\times 10^3 \text{ M}^{-1} \text{ s}^{-1}$	Reference
[1]	0.06 ± 0.008^a	31
[4]	161 ± 48^a	This chapter
[6]	1710 ± 300^a	
	1490 ± 460^b	43
[7]	1210 ± 530^a	43
	1280 ± 150^b	43

^aRate constants were estimated using an anaerobic solution of nitric oxide gas in H₂O added to sodium phosphate buffer at pH 7.4.

^bRate constants were measured using the nitric oxide releasing compound, SPER-NO in sodium phosphate buffer at pH 7.4.

$1.6 \times 10^5 \text{ M}^{-1} \text{ sec}^{-1}$ for nitronyl nitroxide [4] is a factor of ten faster than a previous report (19), which in this case reported the absolute rate constant for this reaction.

3.4.3. Stability of Spin Trapped Adducts of NO•

1. While kinetic studies estimate the feasibility of spin trapping NO•, the ability to record EPR spectra from [5,8,9] is also dependent on the stability of these spin-trapped adducts. In particular, we need to know how steadfast are [5,8,9] in vivo, especially in the harsh environment created by stimulated phagocytes. To separate pharmacodynamic factors from bioreduction, we used an in vitro reductive model, which we (30) have previously shown, is a reliable model of the in vivo condition.
2. As shown in **Table 2**, in the absence of reductants, spin trapped adducts [5,8,9] are stable for prolong periods of time; however, in the presence of a low flux of O₂•⁻, generated from the action of xanthine oxidase on xanthine (30), all three spin-trapped adducts exhibited reduction with NO-Fe(MGD)₂ [9], demonstrating rapid elimination. In contrast, spin trapped adducts [5,8,9] showed considerably greater stability in the presence of GSH (1 mM) with NO-Fe(DTCS)₂ [8] displaying remarkable resistance toward reduction, doubling the rate of either imino nitroxide [5] or NO-Fe(MGD)₂ [9].

3.4.4. In Vivo Pharmacokinetics of NO-Fe(DTCS)₂ and NO-Fe(MGD)₂

1. Based on the discussion and kinetic and stability studies, it appears that ferro-chelates are the best of the spin traps for NO•. Yet, in vivo pharmacodynamics may limit the use of the complexes to specific environments. Studies were designed to estimate the in vivo half-life of ferro-chelates [8,9]. **Figure 1** depicts a representative plot of the elimination kinetics of NO-Fe(DTCS)₂ [8] after

Table 2
Stability of NO-Chelates and Imino Nitroxide

Compound	Half-life (min)	Experimental conditions
[5]	Unchanged ^a	Phosphate buffer, pH 7.4
	13.42 ± 2.36	2 μM/min superoxide, pH.7.4
	19.61 ± 2.83	1 mM GSH, pH 7.4
[8]	Unchanged ^a	Phosphate buffer, pH 7.4
	16.65 ± 3.11	2 μM/min superoxide, pH.7.4
	43.84 ± 0.23	1 mM GSH, pH 7.4
[9]	Unchanged ^a	Phosphate buffer, pH 7.4
	7.28 ± 1.29	2 μM/min superoxide, pH 7.4
	23.46 ± 3.08	1 mM GSH, pH 7.4

^aThe term unchanged refers to the fact that over 45 min there was no decrease in the concentration of [4,6,7].

intraperitoneal administration into mice (26). Of interest is the surprisingly long half-life of 41min. Similar, although a slightly shorter half-life of 35 min was found when [8] was introduced intravenously.

2. As the mouse, except for the tail, fitted within the cavity of the low-frequency EPR spectrometer, loss of the nitrosyl-ferrochelate [8] was undoubtedly the result of bioreduction, through a pathway that is currently unknown. In contrast to NO-Fe(DTCS)₂ [8], the half-life of NO-Fe(MGD)₂ [9] was determined to be only 2 min after intraperitoneal administration into mice (26).
3. When considering the variety of spin traps available to detect, quantify, and localize NO• in animal models in real time, it appears that Fe²⁺(DTCS)₂ [6] is the premiere spin trap (*see Note 3*). This is based on favorable kinetics for the reaction of the ferro-chelate [6] with NO•, reasonable stability of NO-Fe(DTCS)₂ [8] in the presence of O₂•⁻ and thiols and the exceptionally long *in vivo* lifetime of the nitrosyl-ferro-chelate [8].

4. Notes

1. While only one reference is cited, there is an extensive literature on cytokine induction of the inducible isozyme of nitric oxide synthase.
2. The reaction of NO• with ferro-chelates has been reported since the early part of this century; see, for instance, ref. (31). There is an extensive literature that has developed during this past decade on the spin trapping of NO• by ferrochelates in animal models in real time.
3. Even though our data demonstrate that Fe²⁺(DTCS)₂ [6] is the best of the current generation of spin traps for the *in vivo in situ* identification of NO•, this ferrochelate only reports NO• production in the vascular and/or interstitial space. There is no evidence that this chelate enter cells.

Acknowledgment

This research was supported in part by grants from the National Institutes of Health, AG-14829, CA-69538, and RR-12257.

References

1. Moncada, S. and Higgs, A. (1993) The L-arginine-nitric oxide pathway. *N. Engl. J. Med.* **329**, 2002–2012.
2. Marletta, M. A. (1993) Nitric oxide synthase structure and mechanism. *J. Biol. Chem.* **268**, 12231–12234.
3. Snyder, S. H. (1992) Nitric oxide: first in a new class of neurotransmitters? *Science* **257**, 494–496.
4. Huang, P. L., Dawson, T. M., Brecht, D. S., Snyder, S. H., and Fishman, M. C. (1993) Targeted disruption of the neuronal nitric oxide synthase gene. *Cell* **75**, 1273–1286.
5. Huang, Z., Huang, P. L., Panahian, N., Dalkara, T., Fishman, M. C., and Moskowitz, M. A. (1994) Effects of cerebral ischemia in mice deficient in neuron nitric oxide synthase. *Science* **265**, 1883–1885.
6. Huang, P. L., Huang, Z., Mashimo, H., Bloch, K. D., Moskowitz, M. A., Bevan, J. A., and Fishman, M. C. (1995) Hypertension in mice lacking the gene for endothelial nitric oxide synthase. *Nature* **377**, 239–242.
7. Förstermann, U., Gath, I., Schwarz, P., Closs, E. I., and Kleinert, H. (1995) Isoforms of nitric oxide synthase. Properties, cellular distribution and expressional control. *Biochem. Pharmacol.* **50**, 1321–1332.
8. Lander, H. M. (1997) An essential role for free radicals and derived species in signal transduction. *FASEB J.* **11**, 118–124.
9. MacMicking, J. D., Nathan, C., Hom, G., Chartrain, N., Fletcher, D. S., Trumbauer, M., et al. (1995) Altered responses to bacterial infection and endotoxic shock in mice lacking inducible nitric oxide synthase. *Cell* **81**, 641–650.
10. Wei, X.-Q., Charles, I. G., Smith, A., Ure, J., Feng, G.-J., Huang, F.-P., et al. (1995) Altered immune response in mice lacking inducible nitric oxide synthase. *Nature* **375**, 408–411.
11. Shiloh, M. U., MacMicking, J. D., Nicholson, S., Brause, J. E., Potter, S., Marino, M., et al. (1999) Phenotype of mice and macrophage deficient in both phagocytic oxidase and inducible nitric oxide synthase. *Immunity* **10**, 29–38.
12. Nathan, C. and Xie, Q.-W. (1994) Regulation of biosynthesis of nitric oxide. *J. Biol. Chem.* **269**, 13725–13728.
13. Deng, W., Thiel, B., Tannenbaum, C. S., Hamilton, T. A., and Stuehr, D. J. (1993) Synergistic cooperation between T cell lymphokines for induction of the nitric oxide synthase gene in murine peritoneal macrophages. *J. Immunol.* **151**, 322–329.
14. Bandaletova, T., Brouet, I., Bartsch, H., Sugimura, T., Esumi, H., and Ohshima, H. (1993) Immunohistochemical localization of an inducible form of nitric oxide synthase in various organs of rats treated with *Propionibacterium acnes* and lipopolysaccharide. *APMIS* **101**, 303–336.

15. Archer, A. (1993) Measurement of nitric oxide in biological models. *FASEB J.* **7**, 349–360.
16. Halpern, H. J., Yu, C., Barth, E., Peric, M., and Rosen, G. M. (1995) *In situ* detection, by spin trapping, of hydroxyl radical markers produced from ionizing radiation in the tumor of a living mouse. *Proc. Natl. Acad. Sci. USA* **92**, 796–800.
17. Pou, P., Keaton, L., Surichamorn, W., Frigillana, P., and Rosen, G. M. (1994) Can nitric oxide be spin trapped by nitron and nitroso compounds? *Biochim. Biophys. Acta* **1201**, 118–124.
18. Korth, H.-G., Ingold, K. U., Sustmann, R., De Groot, H., and Sies, H. (1992) Tetramethyl-ortho-quinodimethane. First member of a family of custom-tailored cheletropic spin traps for nitric oxide. *Angew. Chem., Int. Ed. Engl.* **31**, 891–893.
19. Akaike, T., Yoshida, M., Miyamoto, Y., Sato, K., Kohno, M., Sasamoto, K., et al. (1993) Antagonistic action of imidazolineoxyl N-oxides against endothelium-derived relaxing factor/ \bullet NO through a radical reaction. *Biochemistry* **32**, 827–832.
20. Komarov, A. Mattson, D., Jones, M. M., Singh, P. K., and Lai, C.-S. (1993) *In vivo* spin trapping of nitric oxide in mice. *Biochem. Biophys. Res. Commun.* **195**, 1191–1198.
21. Yoshimura, T., Yokoyama, H., Fujii, S., Takayama, F., Oikawa, K., and Kamada, H. (1996) *In vivo* EPR detection and imaging of endogenous nitric oxide in lipopolysaccharide-treated mice. *Nature Biotechnol.* **14**, 992–994.
22. Fujii, H., Wan, X., Zhong, J., Berliner, L. J., and Yoshikawa, K. (1999) *In vivo* imaging of spin-trapped nitric oxide in rats with septic shock: MRI spin trapping. *Magn. Reson. Med.* **42**, 235–239.
23. Rosen, G. M., Pou, S., and Halpern, H. J. (1998) *In vivo* detection of free radicals in real time by low-frequency electron paramagnetic resonance spectroscopy, in *Free Radical and Antioxidant Protocols*, vol. 108 (Armstrong, D., ed.), Humana Press, Totowa, NJ, pp. 27–35.
24. Halpern, H. J., Bowman, M. K., Spencer, P., Van Polen, J., Dowey, E. M., Massoth, R. J., et al. (1989) An imaging radiofrequency electron spin resonance spectrometer with high resolution and sensitivity for *in vivo* measurements. *Rev. Sci. Instr.* **60**, 1040–1050.
25. Halpern, H. J., Peric, M., Yu, C., Barth, E. D., Chandramouli, G. V. R., Makinen, M. W., and Rosen, G. M. (1996) *In vivo* spin-label murine pharmacodynamics using low-frequency electron paramagnetic resonance imaging. *Biophys. J.* **71**, 403–409.
26. Pou, S., Tsai, P., Porasuphatana, S., Halpern, H. J., Chandramouli, G. V. R., Barth, E. D., and Rosen, G. M. (1999) Spin trapping of nitric oxide by ferro-chelates: kinetic and *in vivo* pharmacokinetic studies. *Biochim. Biophys. Acta* **1427**, 216–226.
27. Bätz, M., Korth, H.-G., and Sustmann, R. (1997) A novel method for detecting nitric oxide (NO) by formation of fluorescent products based on cheletropic spin traps. *Angew. Chem., Int. Ed. Engl.* **36**, 1501–1503.

28. Haseloff, R. F., Zöllner, S., Kirilyuk, I. A., Grigor'ev, I. A., Reszka, R., Bernhardt, R., et al. (1997) Superoxide-mediated reduction of the nitroxide group can prevent detection of nitric oxide by nitronyl nitroxides. *Free Rad. Res.* **26**, 7–17.
29. Doyle, M. P. and Hoekstra, J. W. (1981) Oxidation of nitrogen oxides by bound dioxygen in hemoproteins. *J. Inorg. Biochem.* **14**, 351–358.
30. Finkelstein, E., Rosen, G. M., and Rauckman, E. J. (1984) Superoxide-dependent reduction of nitroxides by thiols. *Biochim. Biophys. Acta* **802**, 90–98.
31. Cambi, L. and Cagnasso, A. (1931) Iron dithiocarbamates and nitrosodithiocarbamates. *Atti Accad. Lincei* **13**, 809–813.

Introduction of NOS II Gene into Primary Cultures of Bovine and Human Endothelial Cells

Guan-Liang Cao, Bin Zhang, Joseph B. Domachowske,
and Gerald M. Rosen

1. Introduction

In recent years, endothelial cells, activated by cytokines (*1*) have been found to phagocytose Gram-positive and Gram-negative bacteria (*2–14*), and exhibit microbicidal activity toward *S. aureus* (*15*). One of the enzymes induced by cytokine treatment is nitric oxide synthase (NOS), which is responsible for the generation of nitric oxide (NO•) from the oxidative metabolism of L-arginine (*16,17*). Despite the voluminous literature pertaining to cytokine-activation of NOS II in macrophages and the role NO• plays in control of intracellular pathogens, there are few studies investigating the microbicidal activity of endothelial-derived NO•. Typical of such reports is that of Oswald et al. (*18*) in which immortalized brain endothelial cells were treated with combinations of different cytokines, monitoring NO• production and subsequent *Schistosomulum* killing. Although there were cytokine mixtures that resulted in a high killing rate concomitant with a high NO• flux, there were other cytokine combinations where such a correlation was not present (*18*). These findings point to the fact that cytokines induce a broad spectrum of enzymes, one of which happens to be NOS II. In the absence of more compelling data, it becomes difficult to assign microbicidal activity to specific reactions of NO•. We have recently developed techniques to stably introduce a retroviral vector encoding NOS II into primary cultures of endothelial cells (*19*). These methods will allow inquiries into the importance of cellular-derived NO• in host immune response. In this review, we will detail methods used to introduce the gene

for NOS II into primary cultures of bovine and human pulmonary artery endothelial cells.

2. Materials

1. Medium M199 (GIBCO, Grand Island, NY).
2. Iscove's Modified Dulbecco's Medium (IMDM) (GIBCO).
3. Fetal calf serum (FCS, GIBCO).
4. L-glutamine (GIBCO).
5. Gelfoam® (Upjohn/Pharmacia, Kalamazoo, MI).
6. Human pulmonary artery endothelial cells (Clonetics, San Diego, CA).
7. Endothelial cell growth media (ECGM, Clonetics).
8. Phosphate-buffered saline, pH 7.4 (PBS, Sigma Chemical Company, St. Louis, MO).
9. 4',6-diamindino-2-phenylindole (DAPI, Vector Lab, Burlingame, CA).
10. Goat anti-mouse iNOS antibody (Transduction Lab, Lexington, KY).
11. FITC-conjugated goat anti-mouse IgG (Jackson Immuno Research Lab, West Grove, PA).

3. Methods

3.1. Transduction of Endothelial Cells

1. One day before transduction, confluent bovine pulmonary artery endothelial cells, isolated as described previously (15,20), were split 1:3 and grown overnight to 40–50% confluence on T-75 polystyrene flasks. Likewise, the media covering each flask of the confluent ψ -crip packaging cells (21) were replaced with IMDM-containing 10% FBS and 2 mM glutamine (5 mL). On the following day, the media covering the endothelial cells were removed, and 5 mL supernatant containing retroviral particles encoding NOS II were transferred from the packaging cell culture flask to the endothelial cell culture flask. The transduction was conducted for 18 h in the presence of 8 μ g/mL protamine. At the end of the exposure, the retroviral media were replaced with fresh M199 containing 20% BCS. The endothelial cells were allowed to grow to confluence.
2. NOS II transduced bovine endothelial cells with different transduction efficiencies were obtained by exposing these cells to either diluted retroviral media or stock retroviral media. When transduced with retroviral media stock, bovine endothelial cells were treated for 1, 3, 5, and 7 days, whereas human endothelial cells were treated for 3 d (see Note 1). Fresh M199 medium was used to replace retroviral medium for 4 h between two consecutive transductions, giving bovine endothelial cells time to recover during this procedure, whereas for human endothelial cells, ECGM media was used. At the end of the transduction period, fresh M199 media, for bovine endothelial cells, and fresh ECGM media, for human endothelial cells, were added to replace retroviral media. Bovine and human endothelial cells were grown to confluence before seeding onto Gelfoam®. Stable NOS II gene expression in transduced endothelial cells was obtained by

culturing these cells on Gelfoam® (see **Note 2**). Culture media were changed every 48 h, and nitrite accumulation was measured as an estimation of NO• production (22). On day 10, the rate of NO• released from transduced bovine endothelial cells was normalized to cell number.

3.2. Nitrite Assay

Accumulation of nitrite was determined colorimetrically by mixing 0.5 mL each of culture medium and freshly prepared Griess reagent [0.1% N-(1-naphthyl) ethylenediamine in water and 1% sulfanilamide in 5% phosphoric acid, mixed 1:1] (22). Concentrations of nitrite were estimated by comparing absorbance at 550 nm against standard solutions of sodium nitrite prepared in the same medium.

3.3. Immunofluorescence Assay

Efficiency of retroviral vector mediated transduction of endothelial cells was estimated using an *in situ* immunofluorescence assay. Briefly, NOS II transduced endothelial cells with the purity (>99%) being confirmed by Factor VIII immunofluorescence staining (23), were seeded onto glass microscope coverslips. After 24 h culture, the cells were fixed with 4% paraformaldehyde in PBS, pH 7.4, and permeabilized in 0.05% Triton X-100. The sample was then blocked with 5% normal goat serum for 1 h and incubated with primary mouse anti-mouse NOS II antibody (1:25) for 1 h. After incubation, fluorescein isothiocyanate (FITC) conjugated with secondary goat anti-mouse antibody (1:50) was applied and further incubated for an additional h. Mounting media (Vectorshield) containing 4',6 diamidino-2-phenylindole (DAPI) was added to mount the sample which was observed using Nikon Eclipse E600 microscope (Tokyo, Japan). The transduction efficiency (TE) of retroviral particle mediated NOS II transfer was calculated as the ratio of number of fluoroscein stained cells divided by the number of DAPI stained cells $\times 100\%$.

3.4. Results

3.4.1. NOS II Gene Transfer into Bovine Artery Endothelial Cells

1. Monolayers of bovine pulmonary artery endothelial cells (passages 2 to 6) were passed (1:3) 1 d before transduction, rendering these cells into a proliferative phase. Endothelial cells were transduced with various concentrations of stock media of retroviral particles encoding NOS II (**Table 1**). During exposure to the retroviral vector encoding NOS II, the bovine endothelial cells changed morphology from a typical cobblestone morphology to one that took on the appearance of elongated rods (see **Note 3**). In contrast, endothelial cells grown in IMDM retained their cobblestone conformation. After the medium-containing retroviral particles was replaced with M199, the morphology of the infected

Table 1
Relationship Between Transduction Applications,
Transduction Efficiency (TE) and NO•

Groups	T0.2	T1	T3	T5	T7
NO• flux ($\mu\text{M}/\text{h}/10^6$ cells)	0.27	0.49	0.70	0.84	1.04
TE(%)	3	10	15	16	18

T0.2, 20% retroviral stock, 1-d treatment; T1, 100% retroviral stock, 1-d treatment; T7, 100% retroviral stock, 7-d treatment.

endothelial cells returned to that of a cobblestone formation. NOS II transduced endothelial cells were allowed to reach confluence prior to seeding onto Gelfoam®. This change in endothelial cell morphology was unique to the bovine source of cells, as human endothelial cells did not exhibit such morphological transformations during transduction.

2. Transduction efficiency (TE) of the retroviral supernant for NOS II gene transduction was estimated by immunocytochemical staining. As a control endothelial cells that had been transduced with either a control vector (PMFGSp47, a retrovirus-containing a control gene, p47^{phox}) or mock transduced with IMDM. Data showed that endothelial cells, receiving only retroviral particles encoding the cDNA for NOS II, demonstrated specific antigen binding. Further, expression of NOS II protein correlated with the number of transductions (**Table 1**). For example, bovine endothelial cells receiving 20% of the retroviral stock had a TE of 2.5%. As the frequency of transduction increased, higher TE was obtained. The highest TE, after 7 repeated retroviral particle exposures approached 18% (**Table 1**). In contrast, human endothelial cells, after 3 repeated retroviral particle exposures exhibited a TE in excess of 30% (**Fig. 1**).

3.4.2. Nitric Oxide Production

1. After seeding the transduced bovine endothelial cells onto Gelfoam®, these cells were cultured for 10 d. Media were changed every 2 d and nitrite accumulation was measured as an index of NO• released from these cells.
2. Nitrite accumulation increased during the 10-d culture, which correlated with proliferation of the endothelial cells over the matrix.
3. These data demonstrate that NOS II was stably expressed in these cells. By day 10, the NO• flux from each group was calculated and normalized to cell number. Our results demonstrated that NO• production increased with TE. The highest flux achieved was about 1 $\mu\text{M}/\text{h}/10^6$ cells (**Table 1**).

4. Notes

1. Data is presented for a 3-d treatment with retroviral-containing media, increased-frequencies of exposure can lead to even higher TEs.

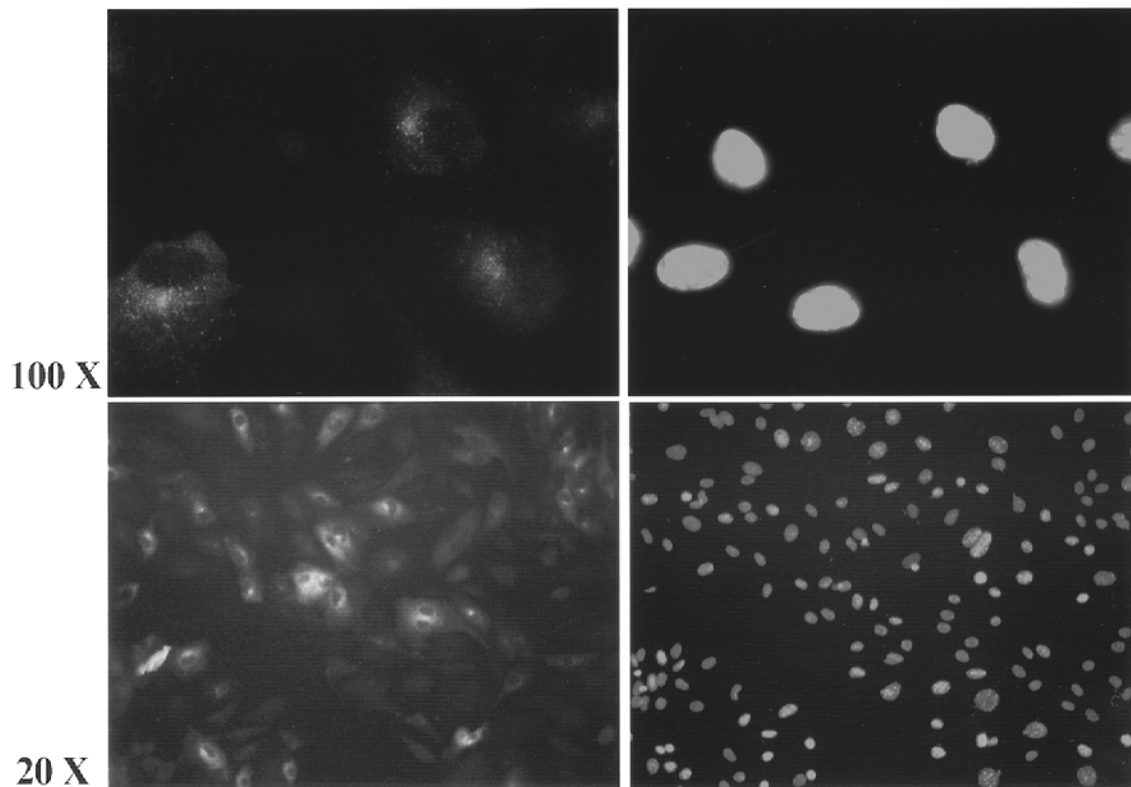


Fig. 1. Expression of NOS II protein in NOS II gene transduced primary human pulmonary artery endothelial cells. (Upper panel, left) is a representative image of NOS II-immunolabeled human endothelial cells. (Upper panel, right) is the image of total cells in the same field as in the left panel with DNA counterstained by DAPI. Images are an oil immersion at either 100 \times Objective (upper panel) or 20 \times Objective (lower panel) magnification. Nontransduced endothelial cells were used as the control (data not shown).

2. While we cultured NOS II transduced endothelial cells onto Gelfoam®, other experiments we conducted indicated that the gene was stable when cells were grown on plastic matrices.
3. This morphological change was only observed with bovine and not human endothelial cells.

Acknowledgment

This research was supported in part by grants from the National Institutes of Health, AG-14829, CA-69538, and RR-12257. Dr. Zhang would like to acknowledge support from the Geriatrics and Gerontology Education and Research and Isaac E. Emerson fellowships.

References

1. Mantovani, A., Bussolino, F., and Introna, M. (1997) Cytokine regulation of endothelial cell function: from molecular level to the bedside. *Immunol. Today* **18**, 231–240.
2. Ogawa, S. K., Yurberg, E. R., Hatcher, V. B., Levitt, M. A., and Lowry, F. D. (1985) Bacterial adherence to human endothelial cells *in vitro*. *Infect. Immun.* **50**, 218–224.
3. Hamill, R. J., Vann, J. M., and Proctor, R. A. (1986) Phagocytosis of *Staphylococcus aureus* by cultured bovine aortic endothelial cells: model for postadherence events in endovascular infections. *Infect. Immun.* **54**, 833–836.
4. Ryan, U. S. (1987) Endothelial cell activation responses, in *Pulmonary Endothelium in Health and Disease*, vol. 32 (Ryan, U. S., ed.), Marcel Dekker, NY, pp. 3–33.
5. Vann, J. M. and Proctor, R. A. (1987) Ingestion of *Staphylococcus aureus* by bovine endothelial cells results in time- and inoculum-dependent damage to endothelial cell monolayers. *Infect. Immun.* **55**, 2155–2163.
6. Ryan, U. S. (1988) Phagocytic properties of endothelial cells, in *Endothelial Cells*, vol. III (Ryan, U. S., ed.), CRC Press, Boca Raton, FL, pp. 33–49.
7. Vann, J. M. and Proctor, R. A. (1988) Cytotoxic effects of ingested *Staphylococcus aureus* on bovine endothelial cells: role of *S. aureus* α -hemolysin. *Micro. Pathogen.* **4**, 443–453.
8. Lowy, F. D., Fant, J., Higgins, L. L., Ogawa, S. K., and Hatcher, V. B. (1988) *Staphylococcus aureus*-human endothelial cell interactions. *J. Ultrastruct. Mol. Struct. Res.* **98**, 137–146.
9. Yao, L., Bengualid, V., Lowy, F., Gibbons, J. J., Hatcher, V. B., and Berman, J. W. (1995) Internalization of *Staphylococcus aureus* by endothelial cells induces cytokine gene expression. *Infect. Immun.* **63**, 1835–1839.
10. Huang, S. H., Wass, C., Fu, Q., Prasadara, N. V., Stins, M., and Kim, K. S. (1995) *Escherichia coli* invasion of brain microvascular endothelial cells *in vitro* and *in vivo*: Molecular cloning and characterization of invasion gene *ibe 10*. *Infect. Immun.* **63**, 4470–4475.

11. Meier, C., Oelschlaeger, T. A., Merkert, K., Korhonen, T. K., and Hacker, J. (1996) Ability of *Escherichia coli* isolates that cause meningitis in newborns to invade epithelial and endothelial cells. *Infect. Immun.* **64**, 2391–2399.
12. Prasadaraio, N. V., Wass, C. A., Weiser, J. N., Stins, M. F., Huang, S. H., and Kim, K. S. (1996) Outer membrane protein A of *Escherichia coli* contributes to invasion of brain microvascular endothelial cells. *Infect. Immun.* **64**, 146–153.
13. Yao, L., Lowy, F. D., and Berman, J. W. (1996) Interleukin-8 expression in *Staphylococcus aureus*-infected endothelial cells. *Infect. Immun.* **64**, 3407–3409.
14. Beekhuizen, H., van De Gevel, J. S., Olsson, B., van Benten, I. J., and van Furth, R. (1997) Infection of human vascular endothelial cells with *Staphylococcus aureus* induces hyperadhesiveness for human monocytes and granulocytes. *J. Immunol.* **158**, 774–782.
15. Zhang, B., Centra, M., Cao, G.-L., Taylor, R. M., Ratych, R. E., and Rosen, G. M. (1996) Penicillin G-induced microbicidal activity of endothelial cells cultured on Gelfoam blocks. *J. Infect. Dis.* **174**, 1001–1009.
16. Moncada, S. and Higgs, A. (1993) The L-arginine-nitric oxide pathway. *N. Engl. J. Med.* **329**, 2002–2012.
17. Marletta, M. A. (1993) Nitric oxide synthase structure and mechanism. *J. Biol. Chem.* **268**, 12231–12234.
18. Oswald, I. P., Eltoun, I., Wynn, T. A., Schwartz, B., Caspar, P., Paulin, D., Sher, A., and James, S. L. (1994) Endothelial cells are activated by cytokine treatment to kill an intravascular parasite, *Schistosoma mansoni*, through the production of nitric oxide. *Proc. Natl. Acad. Sci. USA* **91**, 999–1003.
19. Zhang, B., Centra, M., Cao, G.-L., Ratych, R. E., Domachowske, J. B., Malech, H. L., and Rosen, G. M. (1997) Are free radicals responsible for endothelial cell killing of *Staphylococcus aureus*? *Immunol. Lett.* **58**, 113–120.
20. Centra, C., Raytch, R. E., Cao, G.-L., Li, J., Williams, E., Taylor, R. M., and Rosen, G. M. (1992) Culture of bovine pulmonary artery endothelial cells on Gelfoam blocks. *FASEB J.* **6**, 3117–3121.
21. Domachowske, J. B., Rafferty, S. P., Singhanian, N., Mardiney, III, M., and Malech, H. L. (1996) Nitric oxide alters the expression of γ -globin, H-ferritin, and transferrin receptor in human K562 cells at the posttranscriptional level. *Blood* **88**, 2980–2988.
22. Green, L. C., Wagner, D. A., Glogowski, J., Skipper, P. L., Wishnok, J. S., and Tannenbaum, S. R. (1982) Analysis of nitrate, nitrite, and [^{15}N]nitrate in biological fluids. *Anal. Biochem.* **126**, 131–138.
23. Jaffe, E. A., Hoyer, L. W., and Nachman, R. L. (1973) Synthesis of antihemophilic factor antigen by cultured human endothelial cells. *J. Clin. Invest.* **52**, 2757–2764.

Detection of Peroxynitrite-Induced Protein and DNA Modifications

Scott Lorch, Richard Lightfoot, Hiroshi Ohshima, László Virág, Qiping Chen, Caryn Hertkorn, Marie Weiss, Jose Souza, Harry Ischiropoulos, Vladimir Yermilov, Brigitte Pignatelli, Mituharu Masuda, and Csaba Szabó

1. Introduction

Nitric oxide and superoxide rapidly combine to form a toxic reaction product, peroxynitrite anion (ONOO^-) (1,2). The oxidant reactivity of peroxynitrite is mediated by an intermediate with the biological activity of the hydroxyl radical. However, this product does not appear to be the hydroxyl radical *per se*, but peroxynitrous acid (ONOOH) or its activated isomer (ONOOH^*) (2). Peroxynitrite readily reacts with proteins, lipids, and DNA under conditions of inflammation.

Peroxynitrite is a highly reactive species, which causes rapid oxidation of sulfhydryl groups and thioethers, as well as nitration and hydroxylation of aromatic compounds, such as tyrosine and tryptophan. The most widely studied and best-characterized mechanism is tyrosine nitration (3): measurement of 3-nitrotyrosine is often used as a marker of peroxynitrite in vivo and in vitro. Peroxynitrite also injures DNA via a number of mechanisms. Prominent DNA modifications induced by exposure to peroxynitrite include formation of 8-nitroguanine and 8-oxoguanine as well as the induction of DNA single-strand breakage (4). DNA single-strand breakage induces a prominent secondary process, the activation of the nuclear enzyme poly(ADP ribose)synthetase (PARS) (also known as poly[ADP-ribose] polymerase [PARP]). PARS activation and subsequent cellular processes play an important role in the peroxynitrite-induced alterations in a variety of pathophysiological conditions (5).

From: *Methods in Molecular Biology*, vol. 196: *Oxidants and Antioxidants: Ultrastructure and Molecular Biology Protocols*
Edited by: D. Armstrong © Humana Press Inc., Totowa, NJ

In this chapter, we first describe the various methods of detecting peroxynitrite-induced tyrosine nitration, using immunohistochemical methods, enzyme-linked immunosorbent assay (ELISA), immunoprecipitation, and a new high-performance liquid chromatography (HPLC) electrochemical detector method. Subsequently, we describe the detection of 8-nitroguanine, which is probably one of the most prominent DNA modifications induced by peroxynitrite. Finally, we describe methods to detect PARS activation, a common peroxynitrite-triggered downstream process.

The protocols listed below in sections A-E utilize specific antibodies against protein 3-nitrotyrosine made in the laboratory of Joseph S. Beckman, University of Alabama at Birmingham, to detect and quantify 3-nitrotyrosine. Commercial sources of the anti-3-nitrotyrosine antibodies have not been tested by these protocols. The immunohistochemistry protocol includes both a chromogenic and a fluorescence detection method. Two solid-phase ELISA protocols, one using nitrocellulose for protein binding and chemifluorescence detection and the other binding of proteins onto 96-well plate and fluorescence detection. The immunoprecipitation protocol was developed for human plasma proteins but it can be applied to tissue extracts and other biological fluids as well. The Western-blot protocol can be used for both the polyclonal and monoclonal antibodies (PAb/MABs). Examples for immunohistochemistry, immunoprecipitation and western blotting are provided in **Figs. 1–3**, respectively.

A. Immunohistochemical Detection of 3-Nitrotyrosine

1. Introduction

The following protocol for immunohistochemical detection of 3-nitrotyrosine has been tested in a variety of tissues including brain, lung, heart, and blood vessels in human, rat, mice, and chicken. It is suitable for paraffin embedded tissue and tissue fixed with paraformaldehyde, and/or fresh frozen cryoprotected tissue.

2. Materials

2.1. Equipment

1. Vortex/mixer.
2. Organic solvent hood.
3. Water bath and slides staining jars.
4. Microscope.
5. Humidified chamber: A flat surface rectangular box 7" × 5" or larger lined with wet paper towels can be used for this purpose. All incubations are done in a humidified chamber.

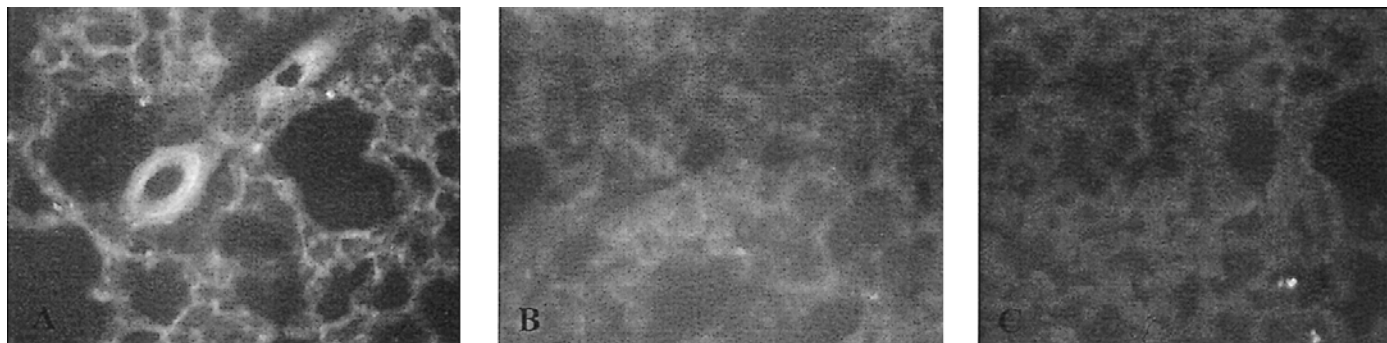


Fig. 1. Immunohistochemical localization of 3-nitrotyrosine in rat lung following 1 h of ischemia and 1-h of reperfusion. **(A)** Ischemia/Reperfusion stained with polyclonal anti-3-nitrotyrosine antibody. **(B)** Ischemia/Reperfusion stained with Antigen Competed anti-3-nitrotyrosine antibody. **(C)** Perfusion Control stained with polyclonal anti-3-nitrotyrosine antibody.

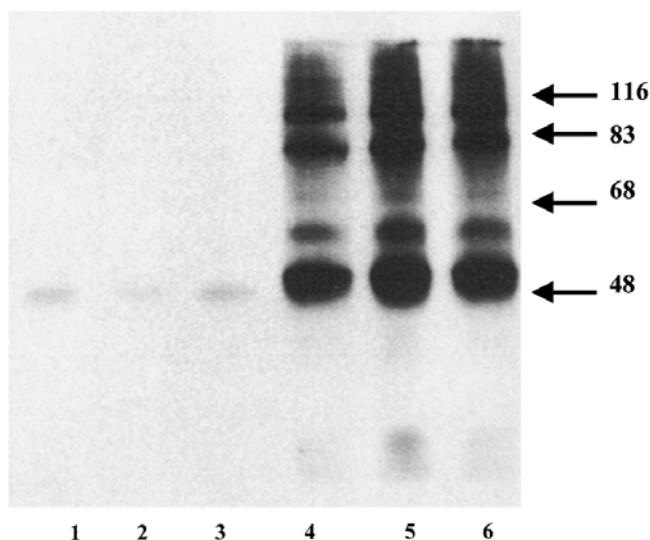


Fig. 2. Immunoprecipitation of nitrated human plasma proteins. (1–3) Unreacted plasma. (4–6) Plasma reacted with 1 mM SIN-1 for 1 h at 37°C. The proteins were immunoprecipitated with polyclonal anti-3-nitrotyrosine antibody and the Western blot was developed using monoclonal anti-3-nitrotyrosine antibody.

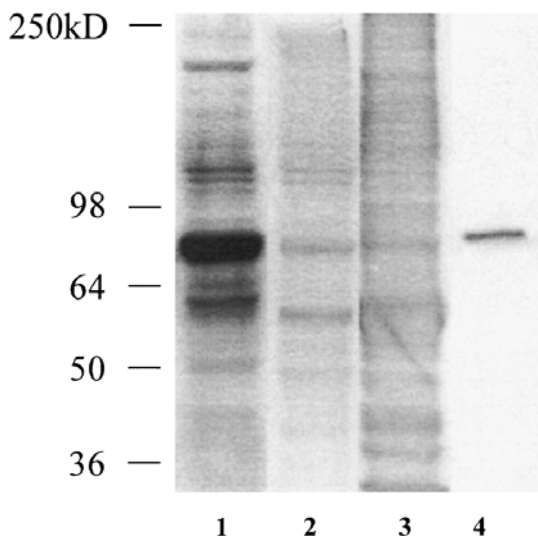


Fig. 3. Western blotting with anti-3-nitrotyrosine antibodies. Composite blot showing rat lung (1), spleen (2), and brain (3) homogenates nitrated by exposure to peroxynitrite. Nitrated BSA (4) included as positive control.

2.2. Reagents

1. PBS: For all staining procedures, 0.1 M PBS, pH 7.2 is used. To make 4 L PBS, dissolve 28.4 g of anhydrous sodium phosphate and 32 g sodium chloride in 3.5 L distilled water. After the solute dissolved, adjust the pH to 7.2 with HCl and bring the volume to 4 L.
2. BSA: When PBS-BSA is used, 0.1% Fraction V, fatty acid ultra free BSA is added to PBS. This solution should be made fresh daily before beginning the experiment.
3. ABC-kit (Vector).
4. Xylene.
5. Ethanol.
6. 3,3'-Diaminobenzidine tetrahydrochloride dihydrate (DAB) (Aldrich).
7. 30% H₂O₂ solution (Fisher).
8. Cytoseal (Vector).
9. ImmEdge pen (Vector).
10. Hematoxylin (Fisher).
11. Sodium hydrosulfite (Na₂S₂O₄) (Sigma).

3. Methods (see Note 1 in Section A)

3.1. Deparaffinization

For paraffinized slides, deparaffinization should be performed as follows:

1. Place slides at 60°C for 15 min.
2. Xylene #1 for 10 min.
3. Xylene #2 for 10 min.
4. 100% ethanol for 5 min, repeat **step 4**.
5. 95% ethanol for 5 min, repeat **step 5**.
6. 70% ethanol for 5 min.
7. Rinse slides in phosphate-buffered saline (PBS) briefly and then wash them in PBS for 10 min.

3.2. Blocking Endogenous Peroxidases

1. Make a circle on the slide around the tissue with ImmEdge pen. Do not write too close to the tissue in order to avoid the artifact of edge-effect.
2. Incubate slides with 5% H₂O₂ (30%) in methanol at room temperature for 20 min (see **Note 2** in Section A).
3. Wash slides twice with PBS.

3.3. Sample Treatment (only if positive or negative control is required)

1. Positive control: Apply peroxynitrite solution directly on the tissue, incubating at room temperature for 5 min.
2. Negative control: Make 0.5 M Na₂S₂O₄ by dissolving Na₂S₂O₄ powder in N₂ purged 0.01 N NaOH solution. Incubate the slides in the 0.5 M Na₂S₂O₄ solution for 5 min. Repeat the same three times in fresh 0.5 M Na₂S₂O₄ solution.

3. Negative control: Pre-absorb the antibody with 10-fold excess (w/w) 3-nitrotyrosine. The antibody dissolved in PBS, pH 7.2 is incubated overnight at 4°C with 3-nitrotyrosine (Aldrich). The antibody complex with 3-nitrotyrosine is diluted in antibody buffer prior to use.
4. Wash slides twice with PBS

3.4. Blocking

1. Incubate tissue at 37°C for 30 min with blocking solution, which contains 10 drops of goat serum in 10 mL of PBS-BSA buffer.
2. All the antibodies should be diluted in the blocking solution.

3.5. Incubation with Primary Antibody

1. Remove blocking solution by flinging the solution off or blotting off with absorbent paper. Do not rinse the sections.
2. Apply antibody solution at the desired dilution in blocking buffer (suggested starting dilution is 1:100 or 1:200).
3. Incubate at 37°C for 90 min or at 4°C overnight.
4. At the end of incubation, rinse slides with PBS-bovine serum albumin (BSA) buffer, and then wash slides in PBS-BSA buffer for 5 min. Wash another 5 min in a second dish.

3.6. Incubation with Secondary Antibody

1. Make up secondary antibody in blocking buffer at the dilution of 1:200. Apply the antibody solution to blotted tissue and incubate at 37°C for 40 min.
2. Rinse slides with PBS-BSA buffer, and then wash slides in PBS-BSA buffer for 5 min. Wash another 5 min in second dish.

3.7. Incubation with ABC Solution

1. Make ABC solution 20 min before use by mixing 1 drop of solution A and 1 drop of solution B in 2.5 mL of PBS-BSA buffer.
2. Blot excess PBS from slides and apply ABC reagent to sections. Incubate at 37°C for 30 min.
3. Wash slides twice in PBS-BSA buffer 5 min for each washing.

3.8. Color Development

1. Make up DAB solution by adding 5 mg DAB solid to 10 mL PBS-BSA. Draw into a syringe and expel through a filter. Add 10 μ L of 30% H_2O_2 solution right before use.
2. Apply DAB solution to the tissue section and incubate until desired color is attained.
3. Stop reaction by rinsing the slide with PBS and then rinse 2 min under running tap water.
4. Handling DAB with great caution. All the contaminated materials should be discarded into biohazard containers.

3.9. Counterstaining

1. Dip slides in Hematoxylin for 1 min, and then rinse them in water for 1 min.
2. Dip slides in acidic ethanol (1% HCl in 70% ethanol) for 2 s, and rinse.
3. 1 min in 0.25% $\text{NH}_4(\text{OH})$. And rinse in tap water.
4. 70% ethanol for 5 min.
5. 95% ethanol for 5 min.
6. 100% ethanol for 5 min, repeat **step 6**.
7. Xylene #1 for 10 min.
8. Xylene #2 for 10 min.

3.10. Use of Fluorescence-Labeled Secondary Antibody (see Note 3 in Section A)

1. Background blocking: Incubate slides four times for 3 min each in 1 mg/mL sodium borohydride (Sigma). Sodium borohydride will not reduce 3-nitrotyrosine to aminotyrosine but will significantly reduce tissue autofluorescence.
2. Blocking: Incubated slides for 30 min in blocking solution, made up of 0.3% Triton X-100, 5% fatty acid free-BSA, and 10% normal goat serum in 0.05 M PBS (pH 7.2).
3. Incubate with anti3-nitrotyrosine antibodies as above. At the end of incubation, rinse slides with PBS-0.3% Triton X-100 buffer, and then wash slides in PBS buffer for 5 min twice.
4. Secondary antibody: Incubate slides tissues for 1 h with anti-rabbit goat secondary antibody labeled with FITC (diluted at 1:200 concentration in blocking solution).
5. Wash with 0.05 M PBS three times for 5 min each time. Allow slides to air dry.

3.11. Cover Slips with Cytoseal

1. Place one drop of Cytoseal to the cover slip and gently place the cover slip onto the slide.
2. Remove bubbles by pressing the slides from center to the edges.
3. Dry the slides and examine under appropriate microscope.

4. Notes

1. Protocols for immunohistochemistry using anti-nitrotyrosine antibodies can be found in published work (6,7).
2. Wash slides extensively before applying H_2O_2 and limit the incubation with H_2O_2 to 20 min. Prolong incubations (>2 h) with H_2O_2 may result in low amount of 3-nitrotyrosine formation by the oxidation of nitrite present in the tissue.
3. Fluorescence images can be semi-quantitative by the use of computer-assisted image collection and processing software.

B. Solid-Phase ELISA for the Quantification of Protein 3-Nitrotyrosine

2. Materials

2.1. Equipment

1. Spectrophotometer.
2. Bio-dot microfiltration unit (96-well) (Bio-Rad, Hercules, CA).
3. Nitrocellulose paper (Schleicher & Schuell, Keene, NH).
4. Plastic disposable 96-well microplate.
5. Multichannel pipet.
6. STORM 840 (Molecular Dynamics, Sunnyvale, CA) or equivalent phosphoimager.

2.2. Reagents

1. Human plasma.
2. Peroxynitrite (Calbiochem, San Diego, CA or Alexis Corp., San Diego, CA).
3. 10 *M* NaOH.
4. 12 *N* HCl.
5. Tris-buffered saline (TBS) at pH 7.0: 500 *mM* NaCl, 20 *mM* Tris-HCl.
6. Tween tris-buffered saline (TTBS): 0.05% Tween-20 detergent in TBS.
7. Polyclonal anti-nitrotyrosine antibody (UBI, Calbiochem).
8. ECF Western Blotting Reagent Pack (Rabbit) includes: anti-rabbit alkaline phosphatase conjugate, dry milk powder, and ECF substrate (Amersham Life Science, Arlington Heights, IL).

3. Methods

1. Generate a 3-nitrotyrosine standard using human plasma. Add peroxynitrite to a final concentration of 1–2 *mM* to the human plasma.
2. To measure the concentration of 3-nitrotyrosine formed, make an aliquot of the reacted human plasma alkaline by the addition of 1/10 volume 10 *M* NaOH and a second aliquot of the reacted plasma acidic by the addition of 1/10 volume 12 *N* HCl. Scan both plasma solutions from 300–500 nm on a spectrophotometer. The alkaline solution should absorb maximally at 430 nm. To calculate the concentration of 3-nitrotyrosine in the reacted plasma, the absorbance at 430 nm of the plasma solution at acidic pH is subtracted from the same absorbance at alkaline pH and the resulting absorbance is divided by 4400 $\text{M}^{-1} \text{cm}^{-1}$ (extinction coefficient of 3-nitrotyrosine at 430 nm). A more accurate determination of 3-nitrotyrosine can be obtained by hydrolysis of the plasma and stable isotope dilution GC-MS detection or by HPLC coupled with electrochemical detection (e.g., 8; see also below in Section F).
3. The nitrated human plasma standard is loaded into a disposable 96-well microplate. The range of standards is usually between .30–0.003 ng of 3-nitrotyrosine in 50–0.005 μg protein per spot.

4. Prepare the samples of human plasma by diluting with *freshly prepared* TBS to the desired protein concentration (*see* **Notes 1** and **2** in Section B).
5. Load the samples into the disposable 96-well microplate accordingly. A final volume of 200 μL per well is achieved by adding TBS (*see* **Note 3** in Section B).
6. Soak a piece of nitrocellulose paper in TBS.
7. Assemble the Bio Dot microfiltration unit according to the manufacturer's instructions. Transfer the standards and samples from the disposable microplate to the nitrocellulose, under vacuum, using a multichannel pipet. To insure all standards and samples are loaded, wash the disposable microplate with 200 μL of TBS per well and transfer again to the nitrocellulose.
8. After all the standards and samples have been immobilized onto the nitrocellulose, block the nonspecific binding sites of the blot overnight with 10% dry milk in TTBS at 4°C with agitation.
9. After the blocking, wash the blot three times for 10 min with TTBS at room temperature with agitation.
10. Incubate the blot for 2 h at room temperature with agitation with the pre-conjugated antibody solution. The pre-conjugation is carried out as follows;
11. One $\mu\text{g/mL}$ of polyclonal anti-nitrotyrosine antibody and 1:10,000 dilution of anti-rabbit alkaline phosphatase linked antibody diluted in 0.5% dry milk in TTBS, incubated overnight at 4°C with agitation (*see* **Note 4** in Section B).
12. After the antibody incubation, wash the blot twice for 10 min with TTBS, then twice for 5 min with TBS at room temperature with agitation.
13. Develop the blot with the fluorescence scanning imager, STORM 840, using the chemifluorescence substrate provided in the Amersham ECF kit.
14. Plot the net counts of fluorescence measured in each sample (corrected for background from a sample blank) on a semilogarithmic plot.
15. Determine the concentration of the 3-nitrotyrosine in each sample from the linear portion of the sigmoidal curve from the semilog plot of net counts vs antigen concentration of the nitrated human plasma standard. Once the concentration of 3-nitrotyrosine per protein spot is determined, it can be plotted against the protein concentration per spot. The slope of the line from the linear regression analysis of this plot represents the concentration of 3-nitrotyrosine per μg of protein.

4. Notes

1. The TBS and TTBS solution should be prepared daily and filtered through a 0.2 μm filter.
2. Due to possible binding interference caused by some detergents and chemicals, the proteins in the plasma should only be diluted in TBS.
3. The binding capacity of proteins to nitrocellulose paper is 100.0 $\mu\text{g/cm}^2$. For this assay, a range of 1.0–50.0 μg protein/spot works ideally for the standard range used for quantification. However, the ratio of 3-nitrotyrosine to total protein present in a particular plasma sample varies, therefore the protein range for samples must be determined experimentally.

4. The pre-conjugation of antibodies overnight enhanced the specificity and reduced background.

C. Solid Phase ELISA—With Fluorescence Detection for the Measurement of 3-Nitrotyrosine

1. Introduction

The same principles of the above method apply for this protocol with the exception of using microplates for antigen binding and fluorescence-labeled secondary antibody for detection.

2. Materials

2.1. Equipment

1. Fluorometer (i.e. Spectra Max Gemini).
2. White Fluorometric Plates, 96-well capacity (i.e., FluoroNUNC C96 plates from NUNC brand products).

2.2. Reagents

Goat anti-rabbit IgG antibody, labeled with FITC (Zymed Laboratories, San Francisco, CA).

3. Methods

3.1. Preparation of Samples (see Note 1 in Section C)

1. For the unknown samples, dilute a portion of the serum in TBS solution to a concentration of 0.1 mg/mL. From this working solution, make dilutions to create a range of concentrations from 4 µg/mL to 18 µg/ml.
2. Prepare a set of standards (see Note 2 in Section C) from 0.2–10 ng/mL 3-nitrotyrosine in TBS.
3. Load 100 µL per well of each of the standards and samples into a white fluorometric plate such as those produced by NUNC brand products. The white plates are better suited for this method because of the higher binding affinity and low background fluorescence (see Note 5 in Section C).
4. For control purposes, at least one well on each plate needs to contain the following (see Note 3 in Section C):
 - a. TBS without primary or secondary antibodies;
 - b. Unknown sample (highest concentration made) with only secondary antibody added;
 - c. Unknown samples (highest concentration made) without primary or secondary antibody.
5. Let the protein bind to the PVC plate by incubating overnight in a humid chamber at 4°C (see Note 4 in Section C).

3.2. Blocking Procedure

Remove the samples from the wells. Wash each well four times with 200 μ L of TBS. Incubate wells with 200 μ L solution of 5% dry milk and 0.2% Tween-20 at room temperature for 2 h.

3.3. Addition of Antibodies

1. Remove the blocking solution from each well. Wash each well four times with 400 μ L of TBS in order to remove any residual blocking solution (*see Note 6* in Section C).
2. Prepare a dilution of the primary antibody (anti-3-nitrotyrosine) in TBS depending on the binding affinity of the antibody and concentration of the starting solution, ranging from 1 : 1000 to 1 : 5000 (approx 0.5–2 ng antibody per well) (*see Note 7* in Section C). Add 200 μ L of this dilution to each well of the plate that will receive primary antibody (remember that some of the control wells will not receive primary antibody and will instead get TBS) and incubate 2 h at room temperature.
3. Remove the primary antibody from each well and wash each well four times with 200 μ L of TBS to remove any unbound primary antibody.
4. Prepare a 1 : 5000 dilution of the secondary antibody (goat anti-rabbit IgG labeled with FITC) in TBS.
5. Add 200 μ L of this dilution to each well of the plate that will receive secondary antibody and incubate 1 h at room temperature.
6. Remove the secondary antibody from each well and wash each well four times with 200 μ L of TBS to remove any unbound secondary antibody.
7. Place the plate in a fluorometer and read the fluorescence output of each well.
8. Follow the same procedure as above to quantify the levels of 3-nitrotyrosine in the samples (*see Note 8* in Section C).

4. Notes

1. The ranges of both the standards and samples are dependent on the range that the relationship between the fluorescence output and the concentration of either the protein loaded or the total amount of 3-nitrotyrosine is linear. For most experiments these concentrations should be linear, but it is something that needs to be tested prior to any lengthy experiments are attempted.
2. Proteins such as transferrin and fibrinogen may be used for positive control. The proteins can be nitrated by the reaction with peroxynitrite in the presence of CO₂ containing buffer (**9**).
3. The controls will allow the measurement of autofluorescence (sample without antibodies), background fluorescence (sample with secondary antibody only), background binding of the primary antibody (TBS with antibodies).
4. Instead of incubating overnight at 4°C, the proteins may incubate for 2–4 h at room temperature. However, binding of the proteins to the PVC plate is maximized by an overnight incubation.

5. Similar results are obtained if a different volume of sample or standards is loaded into the plate. The maximum loading volume for the C96 white NUNC plates is 200 μ L.
6. It is imperative that the entire blocking buffer be removed from the plate prior to adding the primary antibody. This buffer will interfere with the binding of the primary antibody to the proteins bound in each well of the PVC plate.
7. Changing the concentration of primary antibody can affect the results of the study. Optimally, the concentration of anti-3-nitrotyrosine antibody needs to be several folds higher than the concentration of 3-nitrotyrosine in the plasma samples.
8. Other ELISA methodology for quantification of 3-nitrotyrosine is also available (*10–12*).
9. The major advantage of the ELISA methodology is that samples can be loaded without processing that may artificial alter the levels of 3-nitrotyrosine. However, these methodologies are not as sensitive as the GC-MS detection.

D. Immunoprecipitation of 3-Nitrotyrosine and Detection by Western Blot

1. Introduction

The following protocol is for use in immunoprecipitation of nitrated proteins, which can be precipitated from a variety of tissues and cell lines. The efficiency of precipitation can vary between proteins, although the indicated quantity of antibody has been sufficient to precipitate most of the proteins previously tested. MacMillan-Crow and Thompson have also developed a similar protocol for immunoprecipitation (*13*).

2. Materials

2.1. Equipment

1. Microcentrifuge.
2. Orbital shaker.
3. Bio-Rad Mini-PROTEAN II Cell using 0.75 mm spacers (Hercules, CA).
4. Bio-Rad Mini Trans-Blot Electrophoretic Transfer Cell.
5. Bio-Rad PowerPac 1000 Power Supply.
6. Schleicher & Schuell PROTRAN pure nitrocellulose membranes 0.2 μ m (Keene, NH).
7. Kodak BioMax Autoradiography Cassette (Rochester, NY).
8. Kodak X-Omat AR Film.

2.2. Reagents

1. Homogenization Buffer: 25 mM Tris HCl, 100 mM NaCl, 100 μ M DETPAC, 40 μ M phenylmethylsulfonyl fluoride (PMSF), 0.5 μ g/mL aprotinin (Sigma, St. Louis, MO), 20 μ M synthetic Lactacystin (Calbiochem, La Jolla, CA).

Add PMSF (40 μ L PMSF/100 mL buffer from freshly made 100 mM stock in ethanol), aprotinin, and lactacystin before each use after performing protein assay.

2. Lysis Buffer: 20 mM Tris base, 150 mM NaCl, 10% glycerol, 1% triton x-100, 4 mM EGTA, 1 mM PMSF (Sigma), 10 μ g/mL aprotinin (Sigma), 20 μ M synthetic Lactacystin (Calbiochem). Adjust pH to 7.4. Add PMSF (100 μ L PMSF/10 mL buffer from freshly made 100 mM stock in ethanol), aprotinin, and lactacystin before each use.
3. Amersham Pharmacia Biotech AB Protein G Sepharose beads.
4. Loading dye: 4 mL dH₂O, 1 mL 0.5 M Tris-HCl, pH 6.8, 0.8 mL Glycerol, 1.6 mL 10% SDS, 0.4 mL α -mercaptoethanol, 0.2 mL 0.05% bromophenol blue.
5. Bio-Rad goat anti-mouse IgG (H+L)-HRP conjugate.
6. 10X TBS: 1.5 M NaCl; 0.5 M Tris. Adjust pH to 7.4.
7. Amersham Pharmacia Biotech AB ECL Western blotting detection reagent.

3. Methods

3.1. Sample Preparation and Immunoprecipitation

1. Homogenize sample in homogenization buffer.
2. Bring 100 μ g of homogenate up to 500 μ L total volume with lysis buffer and add 8 μ L anti-nitrotyrosine polyclonal antibody. Incubate on orbital shaker at 4°C overnight.
3. Add 30 μ L Protein G Sepharose beads and incubate 1 h at 4°C. Centrifuge for 2 min at 10,000 rpm to precipitate beads. Discard supernatant, add 500 μ L lysis buffer, and vortex gently to mix. Precipitate beads by centrifugation and repeat three times.
4. Re-suspend washed beads in 40 μ L loading dye, boil 8–10 min, and centrifuge for 2 min at 10,000 rpm to precipitate beads. Transfer supernatant to a fresh tube and repeat centrifugation to fully remove beads. Sample can be run on gel or stored at –20°C.

3.2. Western Blot Procedure

3.2.2. Reagents

1. TBS-T: TBS with 0.05% Tween-20 (Sigma, Bio-Rad, etc.).
2. Nonfat dry milk.
3. ECL antibody detection system (Amersham) or equivalent.

3.2.3. Development

1. All steps below are performed at room temperature with gentle shaking.
2. Following blotting to nitrocellulose, block nonspecific antibody binding with 5% nonfat dry milk in TBS-T for 2 h (*see* **Notes 2, 3** in Section D).
3. Wash 3 times for 5 min each time in TBS-T.

4. Dilute anti-3-nitrotyrosine antibody in TBS-T with 1% dry milk. Dilutions of 1:5000 or 1:10000 of the primary antibody is a good starting point. Incubate blot with primary antibody for 2 h (*see* **Note 1** in Section D).
5. Rinse blot twice with TBS-T, followed by one 15 min wash and 4×5 min washes with TBS-T.
6. Dilute secondary antibody 1/5000 to 1/10000 in TBS-T and incubate with blot for 1 h.
7. Rinse and wash as in **step 5**, except perform last two 5-min washes with TBS (no Tween-20).
8. Detect antibody binding by standard methods recommended by manufacturer. We routinely use the Amersham ECL method.

4. Notes

1. The dilution of both the primary and secondary antibodies is determined partially by the sensitivity of the detection system employed, the properties of the antibodies themselves, as well as by the type and amount of immunoreactive material on the blot. It is advisable to determine the optimal dilution of the antibodies by serial dilution. Incubation times and temperature may vary as well. Pre-conjugation of the primary and secondary antibody as described earlier may also help reduce background and increase sensitivity. Typical western blot is shown in **Fig. 3**.
2. Include a positive control on the blot. We commonly load one lane of the gel with 25 ng of BSA nitrated by standard methods with peroxynitrite.
3. Do not allow the nitrocellulose membrane to dry at any time following protein transfer. Handle the membrane with gloved hands or clean forceps. Good general references for Western blotting are available from Bio-Rad, as well as from Current Protocols in Molecular Biology (Wiley).

E. Analysis of 3-Nitrotyrosine by HPLC Using a Postseparation, On-Line Reduction Column and Electrochemical Detection

1. Introduction

Nitrotyrosine is currently being used as a marker for tissue damage caused by reactive nitrogen species such as peroxynitrite and the myeloperoxidase- H_2O_2 -nitrite system (**14**). We describe a new high-performance liquid chromatography (HPLC)-electrochemical detector (ED) method to analyze nitrotyrosine in protein hydrolyzates or biological fluids (**15**). The sample is injected directly into the chromatograph and separated by a C18 reversed-phase column, and nitrotyrosine is subsequently reduced by a platinum column to aminotyrosine, which is then detected by ED.

2. Materials

2.1. Equipment

1. Vortex/mixer.
2. Centrifuge.
3. A Savan Speed-Vac Concentrator.
4. HPLC pump (ESA model 580 or equivalent).
5. Electrochemical detector (ESA Courochem II or equivalent).
6. Ultraviolet (UV) detector (Thermoseparation Spectra Series UV 100 or equivalent).
7. Beckman Ultrasphere ODS column (5 μ , 0.46 \times 25 cm).
8. Reduction column: a stainless-steel column (0.46 \times 10 cm) packed with platinum-black powder (Type RC-10-1, IRICA purchased from RIX, Souka-City, Saitama, Japan).
9. HPLC Software (KNAUER EuroChrom 2000 Integration Package).

2.2. Reagents

1. NTYR, L-tyrosine, L-DOPA, 3-chlorotyrosine, and L-tryptophan (Sigma).
2. 0.1 M sodium acetate buffer, pH 7.2.
3. Pronase E (E.C.3.4.24.31 from *Streptomyces griseus*; Sigma) is prepared by dialysis against excess 0.1 M sodium acetate buffer, pH 7.2.
4. Acetonitrile and methanol, HPLC-grade (Merck, Darmstadt, Germany).
5. Sodium phosphate (monobasic, NaH₂PO₄, SigmaUltra).
6. Sep-Pak C18 cartridge (Classic-type; Waters, Milford, MA), pre-washed with 2 mL 100% methanol, followed by 10 mL water.

3. Methods

(The method of Shigenaga et al. (16) with minor modifications.)

3.1. Purification of Free NTYR from Human Plasma

1. Add 3 vol of cold acetonitrile (4°C) to 1 mL human plasma and vortex.
2. Centrifuge (2000g) the mixture at 4°C for 10 min.
3. Resuspend the protein pellet in 0.5 mL of 0.1 M sodium acetate buffer, pH 7.2, and reprecipitate proteins with 3 vol of cold acetonitrile (repeat this procedure twice).
4. Combine the supernatants and dry in a Speed-Vac.
5. The protein precipitate will be used for the analysis of protein-bound nitrotyrosine (see Subheading 3.2.).
6. Dissolve the residue from Subheading 3.1., step 4 in 0.5 mL of 0.04 M ammonium sulfamate in 0.1 N HCl.
7. Apply the mixture to a pre-washed Sep-Pak C18 cartridge, pass 5 mL water through the Sep-Pak to eliminate water-soluble polar compounds.

8. Elute nitrotyrosine from the cartridge with 3 mL 100% methanol.
9. Evaporate methanol in a Speed-Vac and dissolve the residue in 100 μ L HPLC buffer (*see Subheading 3.3., step 2*).

3.2. Enzymatic Hydrolysis of Human Plasma Proteins

1. Resuspend the protein precipitate (from **Subheading 3.1., step 3**) in 1 mL of 0.1 M sodium acetate buffer, pH 7.2.
2. Incubate the samples overnight (16 h) at 50°C with 2 mg dialyzed pronase E.
3. Incubate also 1 mL of 0.1 M sodium acetate buffer, pH 7.2 (no sample), overnight (16 h) at 50°C with 2 mg dialyzed pronase E.
4. Add 3 vol of cold acetonitrile to the enzymatic hydrolysates, vortex, and centrifuge (2000g) at 4°C for 10 min.
5. Transfer the supernatant (1.4 mL) into a tube and evaporate the solvent in a Speed-Vac to dryness.
6. Dissolve the residue in 140 μ L HPLC buffer (*see Subheading 3.3., step 2*).

3.3. HPLC Procedure

1. HPLC system (the order of connection): pump (ESA model 580), guard cell (+1100 mV), injector, separation column (Beckman Ultrasphere ODS columns, 5 μ , 0.46 \times 25 cm), reduction post-column (IRICA RC-10-1), ED (ESA Coulchem II, Conditioning cell, -1000 mV, electrode 1, +900 mV; electrode 2, +1000 mV), UV-detector (Thermoseparation Spectra Series UV 100 at 280 nm) (*see Note 1* in Section E).
2. Mobile phase: 10 mM aqueous sodium phosphate (monobasic, NaH_2PO_4) containing 10% methanol at a flow rate of 1 mL/min.
3. Standards: Dissolve nitrotyrosine in water and tyrosine in 0.1 N HCl to give a concentration of 1 mM (stock solutions). Dilute stock solutions in water to prepare standard solutions in a range between 0.1 and 100 μ M.
4. Inject 20 μ L of each standard solution into the HPLC.
5. Using peak areas or peak heights detected by the electrode 1 and 2, draw calibration curves for NTYR.
6. Using peak areas or peak heights detected by a UV-detector, draw calibration curves for tyrosine.
7. Centrifuge (1000g) for 5 min the samples prepared in **Subheading 3.1., step 9** or **Subheading 3.2., step 6** and inject 20 μ L of the resultant supernatant into the HPLC.
8. A representative chromatogram is shown in **Fig. 4**.
9. In the case of free-nitrotyrosine analysis (**Subheading 3.1.**), calculate concentrations of nitrotyrosine using its standard curve and express the results as μ M concentrations (or μ mol/l plasma).
10. In the case of protein-bound nitrotyrosine (**Subheading 3.2.**), calculate concentrations of both nitrotyrosine and tyrosine using their standard curves.
11. Inject the blank (pronase E alone; **Subheading 3.2., step 3**) and calculate concentrations of tyrosine released during auto-hydrolysis of pronase E.

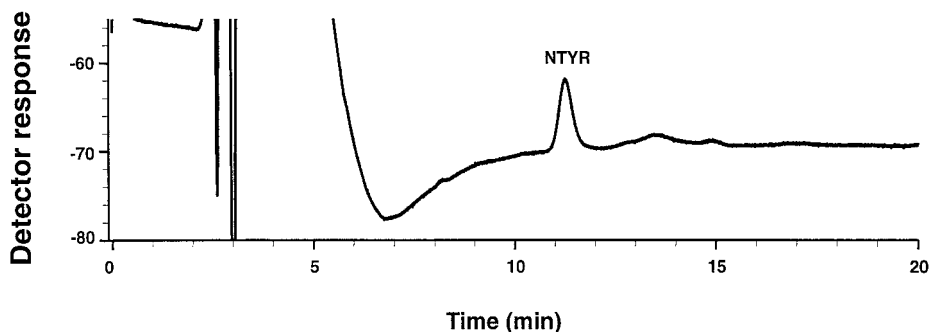


Fig. 4. A typical chromatogram obtained by HPLC-ED analysis of NTYR in the enzymatic hydrolyzates of peroxynitrite-treated BSA, which contained 0.03 mmol/mol TYR.

12. Calculate tyrosine concentrations in the sample hydrolysates by subtracting the background tyrosine derived from pronase E (**Subheading 3.3., step 11**).
13. Express results as the amount of nitrotyrosine (μmol or mmol) per mol tyrosine for protein-bound nitrotyrosine.

4. Note

1. We describe here a method using a coulometric detector. In order to optimize the potential applied, a hydrodynamic voltammogram for nitrotyrosine should be generated for each ED. Inject a constant amount of nitrotyrosine while varying potentials of the ED. Use the potential at which the maximum response from the detector is obtained. With our ED, setting a conditioning cell at the reduction mode (-700 to -1000 mV) and electrodes 1 and 2 at $>+800$ mV and $+1000$ mV, respectively, gave the highest response for nitrotyrosine (**15**).

F. Detection of 8-Nitroguanine in DNA and RNA by HPLC with an Electrochemical Detector

1. Introduction

8-Nitroguanine (nitro⁸Gua) is a unique base modification caused by reactive nitrogen species such as peroxynitrite (**17**) and the myeloperoxidase- H_2O_2 -nitrite system (**18**). Although nitro⁸Gua is not detectable by an electrochemical detector (ED), 8-aminoguanine (amino⁸Gua) has been reported to be electrochemically active (**19**). Nitro⁸Gua is easily reduced by sodium hydrosulfite to amino⁸Gua. On the basis of these observations, we have developed a method to analyze nitro⁸Gua in DNA (or RNA) sensitively and selectively that involves acid-hydrolysis of DNA (or RNA), and chemical conversion of nitro⁸Gua to

amino⁸Gua, which is then detected by HPLC-ED (**20**). RNA samples, but not DNA (*see* **Note 1** in Section F), can also be enzymatically hydrolyzed to nucleosides and analyzed similarly by HPLC-ED.

2. Materials

2.1. Equipment

1. Vortex/mixer.
2. Ultraviolet-visible (UV-VIS) absorbance spectrophotometer.
3. Centrifuge.
4. Block heater.
5. A Savan Speed-Vac Concentrator.
6. HPLC pump (Spectraphysics model SP8810, ESA model 580, or equivalent).
7. Electrochemical detector (ESA Courochem II, Waters model M460, or equivalent).
8. UV detector (Thermoseparation Spectra Series UV 100 or equivalent).
9. Beckman Ultrasphere ODS column (5 μ two columns of 0.46×15 cm or one column of 0.46×25 cm).
10. HPLC Software (KNAUER EuroChrom 2000 Integration Package).

2.2. Reagents

1. 8-Nitroguanine (nitro⁸Gua) can be synthesized by the reaction of guanine with peroxynitrite and purified by HPLC using a preparative reversed-phase column (**17**). Similarly, 8-nitroguanosine (nitro⁸Guo) can be synthesized from guanosine with peroxynitrite. Both compounds are also commercially available from BIOLOG Life Science Institute (Flughafendamm 9a, P.O.B. 107125, D-28071 Bremen, Germany). 8-Aminoguanosine (amino⁸Guo) is obtained from Sigma (St. Louis, MO), and 8-aminoguanine (amino⁸Gua) is prepared by acid hydrolysis of amino⁸Guo (**16**). 8-Oxoguanine (oxo⁸Gua) and 8-oxoguanosine (oxo⁸Guo) are obtained from Aldrich (Milwaukee, WI) and Cayman Chemical Co. (Ann Arbor, MI), respectively. Calf thymus DNA and calf liver RNA are obtained from Sigma.
2. Peroxynitrite is synthesized in a quenched-flow reactor and excess hydrogen peroxide is destroyed by granular manganese dioxide (**21**).
3. Sodium hydrosulfite (Sigma).
4. Nuclease P1 (*Penicillium citrinum*) and acid phosphatase type XA (Sweet potato) (Sigma).

3. Methods

3.1. Reaction of Calf Thymus DNA and Calf Liver RNA with Peroxynitrite and Other Reactive Nitrogen Species

1. Dilute peroxynitrite in a stock solution using cold 1 *N* NaOH and measure absorbance at 302 nm against 1 *N* NaOH. Calculate peroxynitrite concentration using $\epsilon_{302 \text{ nm}} = 1670/\text{M}/\text{cm}$ (**21**).

2. Add peroxynitrite prepared in 1 *N* NaOH at various concentrations (100 μ L) to a reaction mixture containing an appropriate buffer (e.g. 0.1 *M* phosphate buffer, pH 7.4), calf thymus DNA or calf liver RNA (0.2 mg/mL), 100 μ M diethylenetriaminepentaacetic acid (DTPA), a metal chelator, and an appropriate amount of HCl to neutralize the NaOH present in the peroxynitrite solution. Similar reactions can be performed with other reactive nitrogen species.
3. After the reaction, precipitate DNA with cold ethanol (2 volumes), wash twice with 75% ethanol and once with ethanol, and dry briefly in a Speed Vac.
4. Dialyze the peroxynitrite-RNA reaction mixture against water. The dialyzed sample can be used directly or after precipitation with 2.5 volumes of ice-cold ethanol in the presence of 0.3 *M* sodium acetate, pH 5.2.
5. DNA and RNA isolated from cells and tissues using conventional methods can also be used for the following analyses.

3.2. Acid or Enzymatic Hydrolysis of DNA and RNA (see Note 1)

1. Acid hydrolysis: The DNA (or RNA) samples can be hydrolyzed in 0.1 *N* HCl (~1 mL/mg DNA or RNA) at 100°C for 30 min in order to depurinate purines (guanine, adenine, and their derivatives). Remove HCl in a Speed Vac and dissolve the residue in 100 μ L of 0.1 *M* Tris-HCl buffer, pH 8.5.
2. Enzymatic hydrolysis: Dissolve the dialyzed or precipitated RNA sample (~100 μ g) in 100 μ L of 10 mM sodium acetate buffer, pH 4.5, containing 1 mM EDTA and incubate in the presence of 0.8 units nuclease P₁ and 1 unit acid phosphatase at 37°C for 30 min. Add 50 μ L chloroform to the mixture, vortex, and centrifuged.
3. To 50 μ L aliquots from acid (or enzymatic) hydrolysis, add a small amount of sodium hydrosulfite in order to reduce nitro⁸Gua (or nitro⁸Guo) to amino⁸Gua (amino⁸Guo).

3.3. HPLC Procedure

3.3.1. Analysis of Free Bases

1. HPLC system (the order of connection): pump (Spectraphysics model SP8810), injector, guard column (Beckman Ultrasphere ODS), separation column (two Beckman Ultrasphere ODS columns, 5 μ , 0.46 \times 15 cm), UV-detector (Thermoseparation Spectra Series UV 100 at 254 nm), and ED (Waters model M460 at a potential +600 mV) (see Note 2 in Section F).
2. Mobile phase: 12.5 mM citric acid-25 mM sodium acetate buffer containing 25 μ M EDTA, pH 5.2, at a flow rate of 1 mL/min.
3. Standards: Oxo⁸Gua and amino⁸Gua are dissolved in water to prepare solutions in a range between 0.01 and 1 μ M. Guanine standards (1–10 μ M in water).
4. Inject 20 μ L of each standard solution.
5. Using peak areas or peak heights, draw calibration curves for oxo⁸Gua and amino⁸Gua.

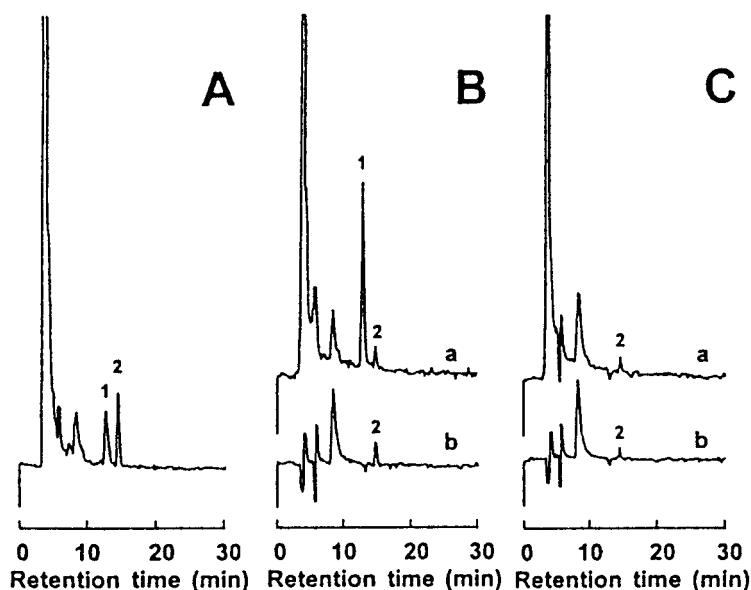


Fig. 5. Typical chromatograms obtained by HPLC-ED analyses of (A) standards, (B) acid-hydrolysates of DNA treated with peroxynitrite, and (C) those of DNA treated with decomposed peroxynitrite; (a,b) after and before reduction with sodium hydrosulfite, respectively. Peak 1 is nitro⁸Gua after reduction (i.e., amino⁸Gua) and peak 2 is oxo⁸Gua.

6. Using peak areas or peak heights detected by a UV-detector, draw calibration curves for guanine.
7. Centrifuge (1000g) for 5 min the samples prepared in **Subheading 3.2., step 1** before and after reduction with sodium hydrosulfite and inject 20 μ L of the resultant supernatant.
8. **Figure 5** shows representative chromatograms of acid-hydrolysates of calf-thymus DNA after incubation in vitro with 0.1 mM peroxynitrite (**Fig. 5Ba,b**) or decomposed peroxynitrite (**Fig. 5Ca,b**). Both samples show a peak corresponding to oxo⁸Gua before reduction with sodium hydrosulfite (**Fig. 5Bb,Cb**). After the reduction, bases from peroxynitrite-treated DNA show a new peak at a retention time corresponding to amino⁸Gua (**Fig. 5Ba**), but this peak is not observed in samples from DNA treated with decomposed peroxynitrite (**Fig. 5Ca**).
9. Concentrations of oxo⁸Gua are quantified by injecting the unreduced samples into HPLC-ED and using an oxo⁸Gua standard curve.
10. Concentrations of nitro⁸Gua are quantified by injecting the samples after reduction with sodium hydrosulfite using an amino⁸Gua standard curve.

11. Concentrations of unmodified guanine are measured by UV detection at 254 nm using a guanine standard curve.
12. The results are expressed as the amount of nitro⁸Gua or oxo⁸Gua (μmol or mmol) per mol guanine.

3.3.2. Analysis of Nucleosides from Enzymatic RNA Hydrolysis

1. HPLC system (the order of connection): pump (ESA model 580), guard cell (+350 mV), injector, separation column (Beckman Ultrasphere ODS columns, $5\ \mu\text{m}$, $0.46 \times 25\ \text{cm}$), electrochemical detector (ESA Coulochem II; conditioning cell, 0 mV; electrode 1, +150 mV; electrode 2, +300 mV), UV-detector (Thermoseparation Spectra Series UV 100 at 254 nm) (*see Note 2* in Section F).
2. Mobile phase: 20 mM citric acid-22 mM sodium acetate buffer containing 12% methanol (HPLC-grade from Merck), pH 3.75, at a flow rate of 1 mL/min.
3. Standards: Oxo⁸Guo and amino⁸Guo are dissolved in water to prepare solutions in a range between 0.01 and 1 μM . Guanosine standards (10–100 μM in water).
4. Inject 20 μL of each standard solution.
5. Using peak areas or peak heights detected by electrode 2, draw calibration curves for oxo⁸Guo and amino⁸Guo.
6. Using peak areas or peak heights detected by a UV-detector, draw calibration curves for guanosine.
7. Centrifuge (1000g) for 5 min the samples prepared in **Subheading 3.2., step 2** before and after reduction with sodium hydrosulfite and inject 20 μL of the resultant supernatant.
8. Representative chromatograms are shown in **Fig. 6**. After the reduction with sodium hydrosulfite, nucleosides from peroxynitrite-treated RNA show several peaks, one of which is at a retention time corresponding to amino⁸Guo (**Fig. 6A**). This peak is not observed in the same sample before reduction (**Fig. 6B**) or in the RNA treated with decomposed peroxynitrite even after reduction with sodium hydrosulfite (**Fig. 6C**).
9. Calculate concentrations of nitro⁸Guo, oxo⁸Guo and guanosine as described earlier (**Subheading 3.3.1., steps 7–9**) using standard curves for amino⁸Guo, oxo⁸Guo and guanosine, respectively, and express the results as the amount of nitro⁸Guo or oxo⁸Guo (μmol or mmol) per mol guanosine.

4. Notes

1. Nitro⁸Gua formed in DNA is unstable. It is rapidly depurinated from DNA to generate free nitro⁸Gua (the half-life of nitro⁸Gua in DNA incubated at 37°C in PBS has been estimated to be less than 4 h) (**20**). In contrast, nitro⁸Gua formed in RNA is stable. No apparent depurination is observed when RNA containing nitro⁸Gua is incubated under similar conditions. It is therefore possible to hydrolyze RNA enzymatically to nucleosides, which can then be analyzed by HPLC-ED in a similar way to that described for free bases.

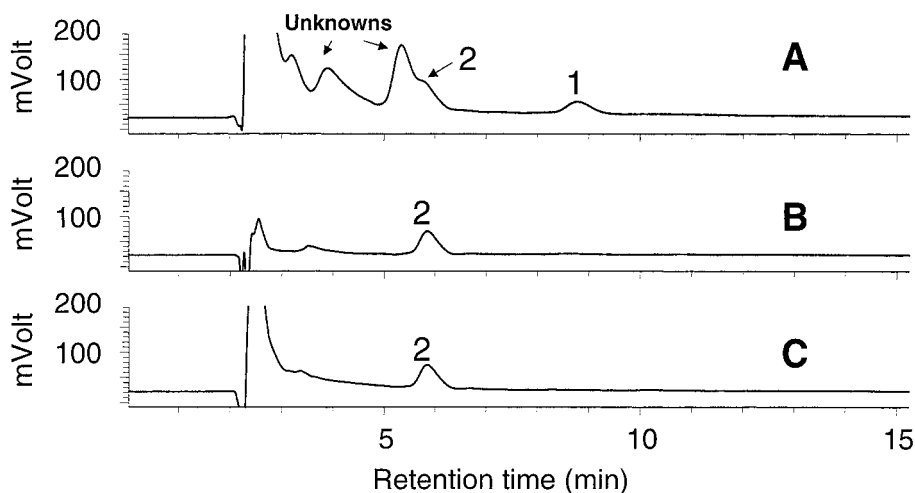


Fig. 6. Typical chromatograms obtained by HPLC-ED analysis of (A) nucleosides from enzymatic hydrolysis of peroxynitrite-treated RNA after reduction with sodium hydrosulfite; (B) those from the same RNA sample before reduction and (C) those from RNA treated with decomposed peroxynitrite, but after reduction. Peak 1 is nitro⁸Guo after reduction (i.e., amino⁸Guo) and peak 2 is oxo⁸Guo.

2. There is a multitude of instruments available that fulfill the requirements for the analyses. We describe here two different EDs, amperometric and coulometric detectors. Either type can be used. However, in order to optimize the potentials applied, hydrodynamic voltammograms of each analyte should be generated for each ED. Inject a constant amount of the analyte while varying the potentials of an ED. Use the potential at which the maximum response from the detector is obtained.

G. Detection of Peroxynitrite-Induced Poly(ADP-Ribose) Synthetase Activation

1. Introduction

Peroxynitrite is one of the most potent activator of the nuclear enzyme poly(ADP-ribose) synthetase (PARS) (also known as poly[ADP-ribose] polymerase [PARP], EC 2.4.2.30). PARS is a nick-sensor enzyme that becomes activated in response to DNA damage caused by various stimuli including ionizing radiation, alkylating agents, free radicals, reactive oxygen and nitrogen intermediates (ROI-s and RNI-s) (5,22). Upon activation, PARS cleaves NAD⁺ into nicotinamide and ADP-ribose and polymerises the latter on nuclear

acceptor proteins including histones and PARS itself. Poly ADP-ribosylation is involved in the maintenance of chromatine structure and genome integrity. However, excessive activation of PARS (by ROI-s and RNI-s) leads to necrotic cell death by depletion of cellular NAD⁺ and ATP.

The activity of the enzyme can be determined from peroxynitrite-treated cells (first protocol) and from tissue samples (e.g., vascular rings) (second protocol). Detection of poly(ADP-ribose) by immunofluorescence (third protocol), Western blotting (23), or by flow cytometry (24) also indicates PARS activation.

H. Peroxynitrite-Induced Poly(ADP-Ribose) Synthase Activation In Vitro (25,26)

2. Materials

2.1. Equipment

1. Liquid scintillation counter (e.g., Wallac 1409).
2. Incubator (set to 37°C).
3. Waterbath.
4. Microcentrifuge.

2.2. Reagents and Supplies

1. ³H-NAD (NEN, Cat. # NET-443).
2. NAD⁺ (Boehringer Mannheim).
3. Scintisafe scintillation fluid (Fisher).
4. Disposable cell scrapers (only if using adherent cells).

All other reagents including HEPES, sodium chloride, potassium chloride, magnesium chloride, digitonin and trichloroacetic acid (TCA) are from Sigma.

3. Methods

1. Prepare stock PARS buffer: 56 mM HEPES, pH 7.5, 28 mM KCl, 28 mM NaCl, 2 mM MgCl₂. Store at 4°C. Stable for months.
2. Treat cells with peroxynitrite in 12-well plates and incubate for 20–30 min in CO₂ incubator at 37°C.
3. While incubating the cells, make up 5% digitonin (in DMSO) and 125 μM NAD⁺ (in H₂O) and prepare assay buffer in a 50 mL conical tube by adding to 10 mL stock PARS buffer; 20 μL digitonin (final concentration 0.01%); 10 μL NAD⁺ (final concentration 0.125 μM); 50 μL ³H-NAD⁺. You will need 0.5 mL assay buffer/sample. Place tube in 37°C water bath.

4. Aspirate off medium from all wells and immediately add 0.5 mL assay buffer.
5. Put plates in 37°C incubator for 10 min.
6. Scrape the cells with a disposable cell scraper and transfer each well contents into labeled Eppendorf tubes.
7. To each tube add 0.2 mL ice-cold 50% (w/v) TCA, cap tubes, and refrigerate for 3 h.
8. Centrifuge samples in a microcentrifuge (10,000 rpm, 10 min).
9. Aspirate of supernatant and wash pellet twice with 1 mL ice-cold 5% TCA.
10. After aspirating off the second TCA wash, add 0.5 mL/tube 2% SDS (in 0.1 N NaOH), cap tubes, and solubilize pellet overnight in 37°C incubator.
11. Transfer the content of each tube to 7 mL scintillation vials previously filled with 6 mL scintillation fluid. Cap vials and vortex briefly.
12. Place samples into Beta scintillation counter and count 2 min in Tritium spectrum.
13. Calculate PARS activity using the following equation:

$$\text{PARS activity (nmol/min/}\mu\text{L)} = \frac{\text{total cpm} \times \text{reaction time (min)}^{-1} \times \text{sample volume (}\mu\text{L)}^{-1}}{\text{NAD specific activity (cpm/nmole)}^{-1}}$$

4. Notes

1. When nonadherent cells are used instead of adherent ones, the assay is easier to perform. With nonadherent cells, it is advisable to transfer the peroxynitrite-treated cells into Eppendorf tubes. Quick spin (15 s, max speed) cells and aspirate medium. Resuspend cells in assay buffer and proceed to **step 5**.
2. The kinetics of PARS activation in response to peroxynitrite or other oxidative and nonoxidative stimuli needs to be determined for each cell type. In most cases 20–30 min incubation is sufficient.
3. It is advisable to add PARS inhibitors (e.g., 3 mM 3-aminobenzamide) to some samples of cells before peroxynitrite treatment and use these samples as negative controls.

1. Poly(ADP-Ribose) Synthase Activation Ex Vivo (27)

2. Materials

2.1. Equipment (in addition to those listed in Section H)

1. Tissue homogenizer.
2. Sonicator.

2.2. Reagents and Supplies (in addition to those listed in Section H)

1. Phenylmethylsulfonyl fluoride (Sigma).
2. 0.2 μm nitro-cellulose analytical test filter funnels.

3. Methods

1. Place freshly obtained tissue samples into 1–2 mL ice-cold stock PARS buffer (see composition in previous protocol) containing 0.1 mM PMSF. (Stock PMSF = 100 mM in DMSO).
2. Homogenize tissues with a tissue tearer followed by sonication (3×15 s, maximal power) on ice.
3. Spin samples (3000g, 10 min, 4°C).
4. Use supernatants for protein and PARS activity assays.
5. Adjust the protein content of the samples to 0.5 mg/mL with stock PARS buffer.
6. Prepare PARS assay buffer by adding to 3 mL stock PARS buffer 5 μ L 125 μ M NAD⁺ and 25 μ L ³H-NAD.
7. Combine 40 μ L sample (tissue homogenate) with 60 μ L PARS assay buffer and allow the reaction to proceed for 1 min.
8. Stop the reaction by the addition of 900 μ L ice-cold TCA.
9. Leave tubes on ice for 30 min.
10. Collect TCA insoluble precipitate by filtration through 0.2 μ m nitro-cellulose analytical test filter funnels under vacuum and wash filters 5 times with 4 mL 5% ice-cold TCA.
11. Count the activity of membranes in 7 mL scintillation vials with ScintiSafe cocktail for 2 min beta spectrum in a scintillation counter.
12. Calculate PARS activity using the equation given in the previous protocol.

J. Immunohistochemical Detection of Poly(ADP-Ribose) (28–30)

2. Materials

2.1. Equipment

1. Fluorescent microscope.

2.2. Reagents and Supplies

1. Anti-poly(ADP-ribose) (monoclonal) (Alexis, Cat. # 804-220).
2. FITC-conjugated anti-mouse-IgG (goat) (Sigma).
3. Normal goat serum (Vector Laboratories).
4. Antifade (Vector Laboratories).
5. Trichloroacetic acid (Sigma).
6. Triton-X 100 (Sigma).
7. Coverslips (Fisher Scientific).
8. Coplin jars.

3. Methods

1. Grow cells on coverslips in 12-well plates or in multichamber slides.
2. Treat cells with peroxynitrite.

3. After 15 min, aspirate off medium and wash cells with ice-cold-PBS.
4. Fix cells in ice-cold 10% TCA for 10 min (*see* **Notes 1, 2** in Section J).
5. Dehydrate in 70%, 90% and absolute ethanol for 3 min each at -20°C .
6. Rehydrate cells in PBS for 10 min at room temperature.
7. Incubate slides in blocking serum (2% normal goat serum in PBS-0.1% Triton-X-100) for 20 min.
8. Incubate slides with anti-poly(ADP-ribose) antibody (1:200) for 1 h at room temperature (*see* **Note 3** in Section J).
9. Wash slides six times for 5 min in PBS.
10. Incubate slides with FITC-conjugated goat anti-mouse immunoglobulin for 1 h at room temperature.
11. Wash slides six times for 5 min in PBS.
12. Mount in Antifade and view under fluorescent microscope (*see* **Note 4** in Section J).

4. Notes

1. It is important to fix the cells in TCA as it inactivates poly(ADP-ribose) glycohydrolase (PARG). PARG, the enzyme that removes poly(ADP-ribose) from proteins is not inactivated during standard fixation procedures.
2. TCA fixation may interfere with the detection of antigens other than poly(ADP-ribose). This has to be considered when co-localization studies are performed (**30**).
3. The anti-poly(ADP-ribose) MAb (clone 10H) (**31**) can also be purchased from Serotec (Cat. # MCA148). A rabbit PAb (commercially available from Biomol) can also be used for the immunocytochemical detection of poly(ADP-ribose).
4. Immunofluorescent detection of poly(ADP-ribose) in cells has been widely demonstrated, detection of poly(ADP-ribose) in frozen or paraffin-embedded tissue sections has also been described (**32,33**).
5. Additional detection methods of PARP activation, using biotinylated NAD substrate have recently been described (**34,35**),

References

1. Beckman, J. S., Beckman, T. W., Chen, J., Marshall, P. A., and Freeman, B. A. (1990) Apparent hydroxyl radical production by peroxynitrite: implications for endothelial injury from nitric oxide and superoxide. *Proc. Natl. Acad. Sci. USA* **87**, 1620–1624.
2. Pryor, W. A. and Squadrito, G. L. (1995) The chemistry of peroxynitrite: a product from the reaction of nitric oxide with superoxide. *Am. J. Physiol.* **268**, L699–L722.
3. Ischiropoulos, H., Zhu, L., Chen, J., Tsai, M., Martin, J. C., Smith, C. D., and Beckman, J. S. (1992) Peroxynitrite-mediated tyrosine nitration catalyzed by superoxide dismutase. *Arch. Biochem. Biophys.* **298**, 431–437.
4. Szabo, C. and Ohshima, H. (1997) DNA damage induced by peroxynitrite: subsequent biological effects. *Nitric Oxide* **1**, 373–385.

5. Szabó, C. and Dawson, V. L. (1998) Role of poly(ADP-ribose) synthetase in inflammation and ischaemia-reperfusion. *Trends. Pharmacol. Sci.* **19**, 287–298.
6. Viera, L., Zu, Y., Eztevez, A. G., and Beckman J. S. (1999) Immunohistochemical methods to detect nitrotyrosine. *Methods Enzymol.* **301**, 373–381.
7. Haddad, I. Y., Pataki, G., Hu, P., Galliani, C., Beckman, J. S., and Matalon S. (1994) Quantitation of nitrotyrosine levels in lung sections of patients and animals with acute lung injury. *J. Clin. Invest.* **94**, 2407–2413.
8. Crowley, J. R., Yarasheski, K., Leeuwenburgh, C., Turk, J., and Heinecke, J. W. (1998) Isotope dilution mass spectrometric quantification of 3-nitrotyrosine in proteins and tissues is facilitated by reduction to 3-aminotyrosine. *Anal. Biochem.* **259**, 127–135.
9. Souza, J. M., Daikhin, E., Yudkoff, M., Raman, C. S., and Ischiropoulos, H. (1999) Factors determining the selectivity of protein tyrosine nitration. *Arch. Biochem. Biophys.* **371**, 169–178.
10. Banks, B. A., Ischiropoulos, H., McClelland, M., Ballard, P. L., and Ballard, R. A. (1998) Plasma 3-nitrotyrosine is elevated in premature infants who develop bronchopulmonary dysplasia. *Pediatrics* **101**, 870–874.
11. Khan, J., Brennan, D. M., Bradley, N., Gao, B., Bruckdorfer, R., and Jacobs, M. (1997) 3-Nitrotyrosine in the proteins of human plasma determined by an ELISA method. *Biochem. J.* **330**, 795–801.
12. Ter Steege, J. C. A., Koster-Kamphuis, L., van Straaten, E. A., Forget, P. P., and Buurman, W. A. (1998) Nitrotyrosine in plasma of celiac disease patients as detected by a new sandwich ELISA. *Free Rad. Biol. Med.* **25**, 953–963.
13. MacMillan, L. A. and Thompson, J. A. (1999) Immunoprecipitation of nitrotyrosine containing proteins. *Methods Enzymol.* **301**, 135–145.
14. Byun, J., Mueller, D. M., and Heinecke, J. W. (1999) 8-Nitro-2'-deoxyguanosine, a specific marker of oxidation by reactive nitrogen species, is generated by the myeloperoxidase-hydrogen peroxide-nitrite system of activated human phagocytes. *Biochemistry* **38**, 2590–2600.
15. Ohshima, H., Celan, I., Chazotte, L., Pignatelli, B., and Mower, H. F. (1999) Analysis of 3-nitrotyrosine in biological fluids and protein hydrolyzates by high-performance liquid chromatography using a postseparation, on-line reduction column and electrochemical detection: results with various nitrating agents [In Process Citation]. *Nitric Oxide* **3**, 132–141.
16. Shigenaga, M. K., Lee, H. H., Blount, B. C., Christen, S., Shigeno, E. T., Yip, H., and Ames, B. N. (1997) Inflammation and NO(X)-induced nitration: assay for 3-nitrotyrosine by HPLC with electrochemical detection. *Proc. Natl. Acad. Sci. USA* **94**, 3211–3216.
17. Yermilov, V., Rubio, J., Becchi, M., Friesen, M. D., Pignatelli, B., and Ohshima, H. (1995) Formation of 8-nitroguanine by the reaction of guanine with peroxynitrite *in vitro*. *Carcinogenesis* **16**, 2045–2050.
18. Byun, J., Mueller, D. M., and Heinecke, J. W. (1999) 8-Nitro-2'-deoxyguanosine, a specific marker of oxidation by reactive nitrogen species, is generated by the

- myeloperoxidase-hydrogen peroxide-nitrite system of activated human phagocytes. *Biochemistry* **38**, 2590–2600.
19. Sodum, R. S., Nie, G., and Fiala, E. S. (1993) 8-Aminoguanine: a base modification produced in rat liver nucleic acids by the hepatocarcinogen 2-nitropropane. *Chem. Res. Toxicol.* **6**, 269–276.
 20. Yermilov, V., Rubio, J., and Ohshima, H. (1995) Formation of 8-nitroguanine in DNA treated with peroxynitrite *in vitro* and its rapid removal from DNA by depurination. *FEBS Lett.* **376**, 207–210.
 21. Reed, J. W., Ho, H. H., and Jolly, W. L. (1974) Chemical syntheses with a quenched flow reactor. Hydroxytrihydroborate and peroxynitrite. *J. Am. Chem. Soc.* **96**, 1248–1249.
 22. de Murcia, G. and Menissier deMurcia, F. (1994) Poly(ADP-ribose) polymerase: a molecular nick-sensor. *Trends. Biochem. Sci.* **19**, 172–176.
 23. Rosenthal, D. S., Ding, R., Simbulan-Rosenthal, C. M., Vaillancourt, J. P., Nicholson, D. W., and Smulson, M. (1997) Intact cell evidence for the early synthesis, and subsequent late apopain-mediated suppression, of poly(ADP-ribose) during apoptosis. *Exp. Cell Res.* **232**, 313–321.
 24. Affar, E. B., Duriez, P. J., Shah, R. G., Winstall, E., Germain, M., Boucher, C., et al. (1999) Immunological determination and size characterization of poly(ADP-ribose) synthesized *in vitro* and *in vivo*. *Biochim. Biophys. Acta* **1428(2–3)**, 137–146.
 25. Virág, L., Scott, G. S., Cuzzocrea, S., Marmer, D., Salzman, A. L., and Szabó, C. (1998) Peroxynitrite-induced thymocyte apoptosis: the role of caspases and poly(ADP-ribose) synthetase (PARS) activation. *Immunology* **94**, 345–355.
 26. Virág, L., Scott, G. S., Antal-Szalmás, P., O'Connor, M., Ohshima, H., and Szabó, C. (1999) Requirement of intracellular calcium mobilization for peroxynitrite-induced poly(ADP-ribose) synthetase activation and cytotoxicity. *Mol. Pharmacol.* **56**, 824–833.
 27. Pulido, E. J., Shames, B. D., Selzman, C. H., Barton, H. A., Banerjee, A., Bensard, D. D., and McIntyre, R. C. (1999) Inhibition of PARS attenuates endotoxin-induced dysfunction of pulmonary vasorelaxation. *Am. J. Physiol.* **277**, L769–L776.
 28. Kupper, J. H., Van Gool, L., Muller, M., and Burkle, A. (1996) Detection of poly(ADP-ribose) polymerase and its reaction product poly(ADP-ribose) by immunocytochemistry. *Histochem. J.* **28**, 391–395.
 29. Kupper, J. H., Muller, M., Jacobson, M. K., et al. (1995) Trans-dominant inhibition of poly(ADP-ribosyl)ation sensitizes cells against gamma-irradiation and N-methyl-N'-nitro-N-nitrosoguanidine but does not limit DNA replication of a polyomavirus replicon. *Mol. Cell Biol.* **15**, 3154–3163.
 30. Lankenau, S., Burkle, A., and Lankenau, D. H. (1999) Detection of poly(ADP-ribose) synthesis in *Drosophila* testes upon γ -irradiation. *Chromosoma* **108**, 44–51.
 31. Kawamitsu, H., Hoshino, H., Okada, H., Miwa, M., Momoi, H., and Sugimura, T. (1984) Monoclonal antibodies to poly(adenosine diphosphate ribose) recognize different structures. *Biochemistry* **23(16)**, 3771–3777.
 32. Love, S., Barber, R., and Wilcock, G. K. (1999) Increased poly(ADP-ribosyl)ation of nuclear proteins in Alzheimer's disease. *Brain* **122**, 247–253.

33. Scott, G. S., Jakeman, L. B., Stokes, B. T., and Szabó, C. (1999) Peroxynitrite production and activation of poly(ADP-ribose) synthetase in spinal cord injury. *Ann. Neurol.* **45**, 120–124.
34. Garcia Soriano, F., Virag, L., Jagtap, P., et al. (2001) Diabetic endothelial dysfunction: the role of poly(ADP-ribose) polymerase activation. *Nat. Med.* **7**, 108–113.
35. Bakondi, E., Bai, P., Szabo, E., et al. (2002) Detection of poly(ADP-ribose) polymerase activation in oxidatively stressed cells and tissues using biotinylated NAD substrate. *J. Histochem/Cytochem* **50**, 91–98.

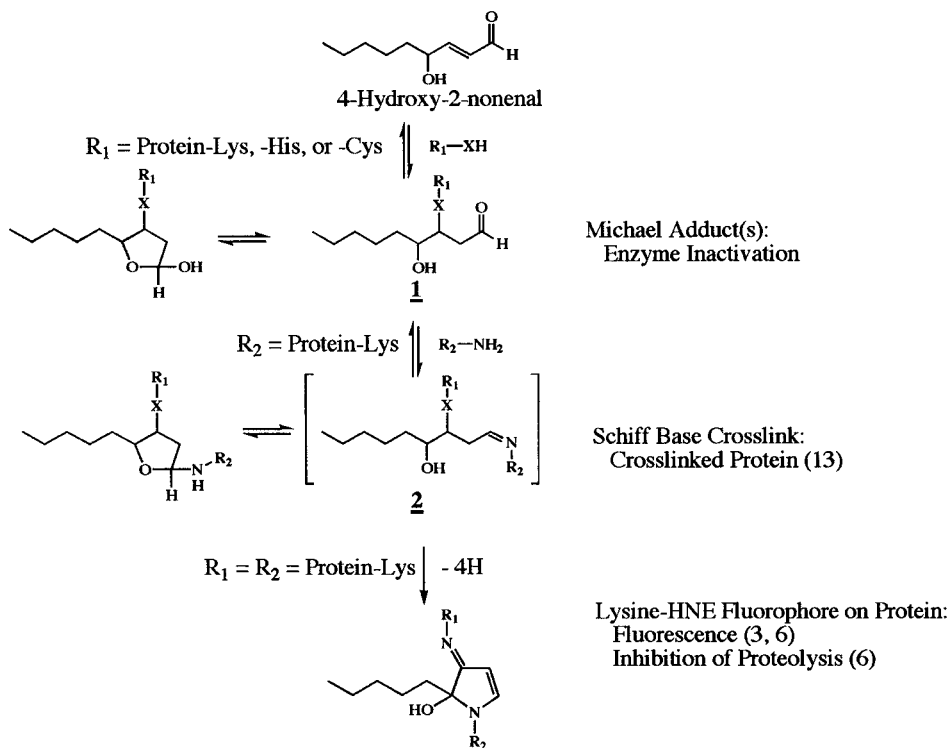
Immunochemical Detection of a Fluorophore Derived from the Lipid Peroxidation Product 4-Hydroxy-2-Nonenal and Lysine

Pamela A. Szweda, Lin Tsai, and Luke I. Szweda

1. Introduction

Aging and the progression of certain degenerative diseases are accompanied by increases in intra- and intercellular fluorescent material, termed lipofuscin and ceroid, respectively (for review, *see* **refs. 1,2**). These pigments are observed within granules composed, in part, of damaged protein and lipid. Modification of various biomolecules by aldehyde products of lipid peroxidation is believed to contribute to lipofuscin and ceroid formation. However direct evidence demonstrating the occurrence of lipid peroxidation product-derived fluorophores on protein components of lipofuscin or ceroid has yet to be obtained (for review, *see* **refs. 1,2**). We have recently identified a fluorescent product formed in the reaction of N_α-acetyllysine (NAL) and 4-hydroxy-2-nonenal (HNE) (**3**), a major product of lipid peroxidation and the most reactive of these compounds under physiological conditions (**4**). This fluorescent compound, characterized as a 2-hydroxy-3-imino-1,2-dihydropyrrol derivative (**3**, R₁ = R₂ = NAL), appears to form upon oxidative cyclization of the nonfluorescent 2:1 lysine-HNE Michael adduct-Schiff base cross-link (**Scheme 1**). Polyclonal antibody (PAb) to the NAL-HNE fluorophore was raised in rabbit and found to be highly specific to the chromophore structure of the compound (**3**). This antibody has been used to demonstrate the formation of the lysine-HNE derivative of this fluorophore upon exposure of protein to HNE in vitro. Thus, we have developed an immunochemical tool for assessing the occurrence of a distinct HNE-derived fluorophore on protein components within complex biological samples (**3**). The antibody has been successfully

From: *Methods in Molecular Biology*, vol. 196: *Oxidants and Antioxidants: Ultrastructure and Molecular Biology Protocols*
Edited by: D. Armstrong © Humana Press Inc., Totowa, NJ



Scheme 1. Reactions of HNE with nucleophilic amino acid residues on protein.

used in immunoblotting, immunoabsorption (enzyme-linked immunosorbent assay; ELISA), and immunohistochemical analysis (electron gold and light microscopy). We describe here general protocols for use of the antibody in Western-blot analysis, ELISA, and immunohistochemical evaluations. It is important to note that the following procedures should be modified based on tissue type and available apparatus and reagents (*see Note 1*).

2. Materials

2.1. Equipment

1. Tissue homogenizer, vortexer.
2. Refrigerated centrifuge.
3. UV-VIS spectrophotometer (Hewlett-Packard Model 8453) and spectrofluorimeter (Shimadzu).
4. High-performance liquid chromatography (HPLC) system (Hewlett-Packard Model 1050 with diode array detector) attached to a reverse phase (C18) HPLC column (Vydac).

5. Rig for gel electrophoresis and electroblotting, including power supply (Novex).
6. Film development system (Kodak).
7. If desired, scanner and software for densitometric analysis.
8. Microplate reader for ELISA (BioRad) and 96-well ELISA plates (Pierce).
9. Hitachi #-600 electron microscope.
10. Cryostat (Leico) with appropriate knife) and/or Sorvall MT2-B microtome equipped with Diatome knife.
11. Oven.

2.2. Reagents and Supplies

1. Protein assay reagents (bicinchronic acid assay, Pierce).
2. Sodium dodecyl sulfate polyacrylamide gel electrophoresis (SDS-PAGE) supplies:
 - a. 10X gel running buffer: 0.25 M Tris base, 1.9 M glycine, 1% SDS (do not adjust pH, which should be approx 8.5–8.8).
 - b. 20X transfer buffer: 0.25 M Tris base, 1.9 M glycine (do not adjust pH, which should be approx 8.5–8.8).
 - c. Gels of appropriate polyacrylamide content.
3. 10X phosphate-buffered saline (PBS): 0.017 M KH_2PO_4 , 0.05 M Na_2HPO_4 , and 1.5 M NaCl, pH 7.4.
4. Tris-buffered saline (TBS): 0.05 M Tris-HCl, 0.9% NaCl, pH 7.6.
5. PABs (raised in rabbit) specific to lysine-HNE fluorophore (CalBiochem).
6. Immunoblot (Western) and chemiluminescence reagents:
 - a. Blocking buffer. A recommended blocking reagent is 0.2% (w/v) I-Block™ (Novex) in 1X PBS containing 0.1–0.1% (v/v) tween-20 (Sigma).
 - b. 2X Gel loading buffer composed of 126 mM Tris HCl, 4% SDS, 20% glycerol, and 0.005% bromophenol blue, pH 6.8.
 - c. Anti-rabbit IgG conjugated to an appropriate enzyme (alkaline phosphatase or horseradish peroxidase) as secondary antibody (Dako).
 - d. Recommended chemiluminescence substrates: For alkaline Phosphatase, CSPD™ and Nitroblock™ (Novex). Buffer is composed of 20 mM Tris base, 1 mM MgCl_2 , pH 9.8. For horseradish peroxidase, SuperSignal® West Fento (or Pico) Luminol/Enhancer solution and Stable Peroxide Buffer (Pierce).
7. Protease inhibitors.
8. Appropriate competitor(s) for assessing the specificity of primary antibody binding.
9. Preimmune rabbit sera for control experiments, as desired.
10. HPLC solvents: Acetonitrile, trifluoroacetic acid (TFA).
11. Paraformaldehyde solution (16%, Electron Microscopy Sciences), OCT medium (Electron Microscopy Sciences)
12. Protein A conjugated to gold beads for immunogold electron microscopy (Electron Microscopy Sciences).
13. LR White resin (Electron Microscopy Sciences).

13. Detection system for immunolight microscopy. The Vectastain[®] ABC kit (Vector Laboratories and horseradish peroxidase substrate 3,3'-diaminobenzidine tablets (Sigma) are recommended.
14. Colorimetric alkaline phosphatase substrate for ELISA. p-Nitrophenylphosphate (Pierce) is recommended. Alternatively, horseradish peroxidase and appropriate substrates can be utilized.
15. Polyclonal antibodies to other forms of HNE-derived modifications to protein (anti-HNE Michael adducts are available from CalBiochem).
16. Immunofluorescence (and confocal) microscopy may also be performed, however the intrinsic fluorescence of 4-hydroxy-2-nonenal-derived fluorophores must be accurately taken into account.

3. Methods

3.1. Synthesis of N_{α} -Acetyllysine-HNE Fluorophore

1. Preparation of 4-Hydroxy-2-nonenal. 4-Hydroxy-2-nonenal (HNE) dimethylacetal was synthesized as previously described (5). The dimethylacetal was hydrolyzed to HNE with 0.05% TFA in a 50% acetonitrile solution in water. HNE was purified by RP-HPLC (Vydac C18 column, 1 mL/min, 0–50% acetonitrile vs water, 0.05% TFA, in 0–20 min). The concentration of HNE was determined by absorbance at 224 nm using $\epsilon_{224} = 13,750 \text{ M}^{-1} \cdot \text{cm}^{-1}$.
2. Preparation of the N_{α} -Acetyllysine-HNE Fluorophore (3). NAL is dissolved in 0.2 M Na_2HPO_4 , pH 7.4 to 1.0 M. To this mixture is added a solution of 20 mM HNE in water. The pH of the reaction mixture is adjusted to pH 7.4 and an aliquot of 100 mM aqueous CuSO_4 solution is added to a final concentration of 100 μM Cu^{2+} . The reaction is allowed to proceed at 37°C for 5 d with constant agitation. The reaction flask is periodically exposed to room air and the mixture vortexed to ensure the presence of oxygen. To monitor the progress of the reaction, aliquots of the reaction mixture are periodically withdrawn and analyzed by RP-HPLC (Vydac C18 column, 1 mL/min, 0–50% acetonitrile vs water, 0.05% TFA, in 0–20 min). Products are detected by UV absorbance at 210 and 360 nm. Relative levels of fluorophore in the reaction mixture are determined by measuring the area of absorbance at 360 nm under the peak with a retention time of 13.9 min (see Fig. 1).
3. The fluorophore is isolated by three successive HPLC runs over a reverse-phase column (Vydac C18). The first purification step is accomplished by an acetonitrile-water (0.05% TFA) gradient (0–50% acetonitrile in 20 min). The subsequent two HPLC runs employ a methanol-water (0.05% TFA) gradient (0–50% methanol in 20 min). The collected fractions are concentrated under a gentle stream of nitrogen and then lyophilized to yield a light yellow solid. The yield of a typical reaction is approx 4.1% based on HNE (3).
4. The spectroscopic properties of purified NAL-HNE fluorophore have been previously reported (3). FAB/MS: MH^+ 511. HR-MS: Observed 511.3128. Calculated for $\text{C}_{25}\text{H}_{43}\text{O}_7\text{N}_4$: 511.3132. UV: λ_{max} (H_2O , pH 7.0) 360 nm; $\epsilon_{360} =$

$11,250 \text{ M}^{-1} \cdot \text{cm}^{-1}$. Fluorescence: $\lambda_{\text{ex}} = 360 \text{ nm}$, $\lambda_{\text{em}} = 430 \text{ nm}$. For NMR data, see ref. 3.

3.2. Formation of the Lysine-HNE Fluorophore on Protein

We have previously found that prolonged exposure of the model protein glucose-6-phosphate dehydrogenase (Glu-6-PDH) from *Leuconostoc mesenteroides* with HNE leads to the formation of the lysine-HNE fluorophore on the protein (3,6). In contrast, minimal levels of lysine-HNE fluorophore form upon prolonged treatment of carbonic anhydrase (CA) with HNE, although for both proteins, amino acid-HNE Michael adducts (1:1) are rapidly produced (3). Thus, various proteins are differentially susceptible to HNE-derived fluorophore formation.

1. To prepare HNE-modified protein, Glu-6-PDH or carbonic anhydrase (CA) are suspended in $50 \text{ M K}_2\text{HPO}_4$, 200 mM KCl , pH 7.4, by passage through a PD-10 column (Pharmacia) previously equilibrated with the buffer. The reaction is initiated by addition of 10 mM HNE to an equal volume of protein (5.0 mg/mL) in $50 \text{ mM K}_2\text{HPO}_4$, 200 mM KCl , pH 7.4, and allowed to proceed at 37°C .
2. After 0, 0.5, 1.0, 2.0, and 4.0 h, an aliquot of the reaction mixture is treated with 5.0 mM NaBH_4 in 0.1 M NaOH for 5 min to stabilize the nonfluorescent 2:1 amino acid-HNE protein cross-links as previously described. We have determined that the 2:1 lysine-HNE fluorophore is not reduced under these conditions. After neutralization with 1 M HCl , the protein solution was passed over a PD-10 column with $100 \text{ mM Na}_2\text{HPO}_4$, pH 7.4, as eluant.
3. Protein concentration is determined by the bicinchoninim assay (BCA) with BSA as standard. An estimate can be obtained by measuring the absorbance of the protein solution at 280 nm (at pH ~ 7.2 $\epsilon^{1\%}$ Glu-6-PDH = 11.5 and $\epsilon^{1\%}$ CA = 19.0).

3.3. Preparation and Characterization of Anti-Lysine-HNE Fluorophore

PAb specific to the chromophore structure formed in the reaction of HNE and lysine was prepared as previously described (3). Briefly, fluorophore-linked KLH was prepared by reacting 2.0 mg KLH , $3.5 \text{ mg NAL-HNE fluorophore}$ ($6.9 \text{ } \mu\text{mol}$), and 0.5 mg EDC ($2.6 \text{ } \mu\text{mol}$) in $750 \text{ } \mu\text{L}$ 0.1 M 2-(N-morpholino)ethanesulfonic acid (MES), 0.9 M NaCl , pH 4.7. After 2 h at 25°C , unreacted NAL-HNE fluorophore and reaction byproducts were removed by gel filtration over a PD-10 column with $0.083 \text{ M Na}_2\text{HPO}_4$, 0.9 M NaCl , stabilizers, pH 7.2 as eluant. Polyclonal antibody was generated in New Zealand White female rabbits (see Note 2). To initiate the immunization protocol, a 0.5 mL aliquot of fluorophore-linked KLH (1.0 mg/mL) was diluted

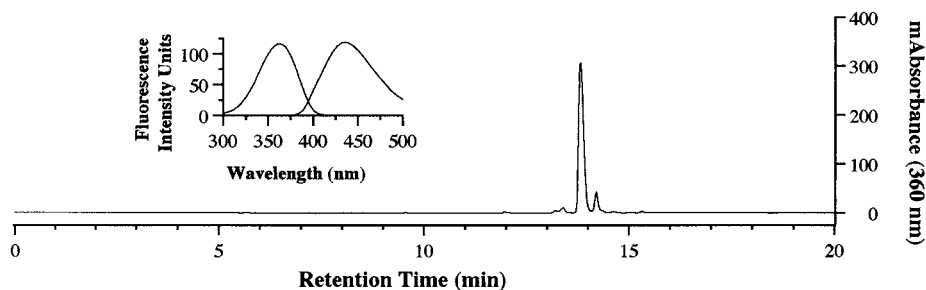


Fig. 1. HPLC resolution of products formed in the reaction of NAL and HNE.

with an equal volume of Freund's incomplete adjuvant (FIA) and injected into the rabbit (intradermal back). Thereafter, booster injections (125–250 μg immunogen diluted in FIA, subcutaneous dorsal) were made every 21 d. Test bleeds were obtained 10 d after each inoculation and antibody titer monitored by ELISA.

Anti-lysine-HNE fluorophore was characterized by ELISA. As previously reported (3), the affinity-purified antibody can readily detect as little as 15 fmol of lysine-HNE fluorophore (3, $R_1 = R_2 =$ lysine residues on protein) and recognizes analogous fluorophores produced by reaction of primary amines with HNE (3, $R_1 = R_2 =$ primary amines) (**Fig. 2**). In contrast, the antibody does not bind 1:1 N_α -acetylhistidine- and N_α -acetylcysteine-HNE Michael adducts or 1:1 and 2:1 N_α -acetyllysine-HNE adducts (**Fig. 3**). Thus, polyclonal antibody raised to the NAL-HNE fluorophore is specific to the chromophore portion of the lysine-HNE fluorophore and, under the conditions of our experiments, displays a sensitivity in the fmol range. It should be noted that similar properties are observed for protein A-purified preparations of the antibody (see **Note 3**).

3.4. ELISA

ELISA is useful for estimating the levels of lysine-HNE fluorophore present on purified protein treated with HNE. The fluorophore-modified protein can then be used in Western blots to provide a means for determining the lysine-HNE fluorophore content of given proteins in a complex biological sample by densitometry.

1. Standard coating antigen is prepared by covalently linking the NAL-HNE fluorophore to CA via EDC coupling. Typically, 0.4 mg of NAL-HNE fluorophore (0.8 μmol) in 100 μL water is mixed with 0.9 mg CA in 0.5 mL 20 mM Na_2HPO_4 , 0.1 M NaCl, pH 7.2. To this solution is added 0.15 mg (0.8 μmol) EDC $\cdot\text{HCl}$. The reaction is allowed to proceed for 2 h at 25°C. The NAL-HNE fluorophore-

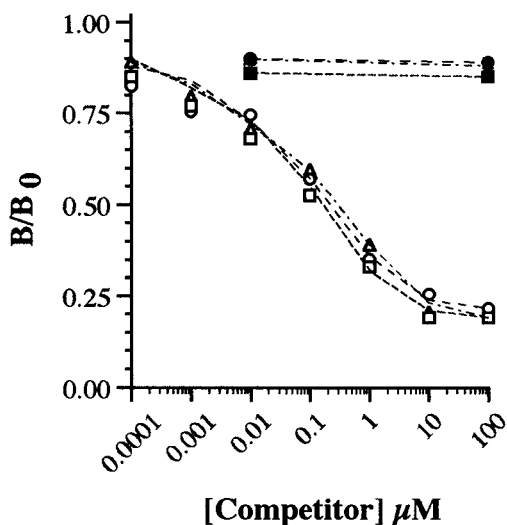


Fig. 2. Binding of anti-lysine-HNE fluorophore to HNE-treated Glu-6-PDH (3). Anti-body binding to fluorophore-modified Glu-6-PDH (60 fmol lysine-HNE fluorophore/well) was evaluated in the presence of NAL-HNE fluorophore (○), fluorophores produced in the reactions of HNE with γ -aminobutyric acid (□) and ethylamine (Δ), and nonderivitized NAL (●), γ -aminobutyric acid (■), and ethylamine (▲). Values of B/B_0 were determined as described in the legend to Fig. 2. Background (bkg) values were obtained using Glu-6-PDH treated with HNE for 0 min.

linked CA is passed over a PD-10 column with the same buffer as eluant. The degree of fluorophore incorporation is determined following HPLC purification of NAL-HNE fluorophore-linked CA (Vydac C18 column, 0–50% acetonitrile vs water, 0.05% TFA, in 20 min). Protein concentration is determined using the BCA assay with BSA as standard. Fluorophore content is estimated by comparing the intensity of signal at 360 nm to a standard curve constructed by using known quantites of NAL-HNE fluorophore. In general, under the conditions of our coupling reactions, approx 2.5 nmol of fluorophore is linked to 1.0 mg carbonic anhydrase (3).

2. In a typical ELISA, an aliquot of coating antigen solution is diluted into 0.2 M $\text{NaHCO}_3/\text{Na}_2\text{CO}_3$ buffer, pH 9.4, and applied to a microtiter plate (400 ng/well). After 1 h at 25°C, the wells are rinsed with $3 \times 100 \mu\text{L}$ PBS containing 0.05% Tween-20 and 0.1% BSA (wash buffer) and blocked (1% BSA in PBS) for 1 h (25°C). A 100 μL aliquot of anti-lysine-HNE fluorophore (1/100–1,200 n blocking buffer containing 0.5% Tween-20) is applied to the wells and incubated for 1 h (25°C). In competition studies, varying concentrations of competitors are added to the wells prior to addition of 1° Ab.

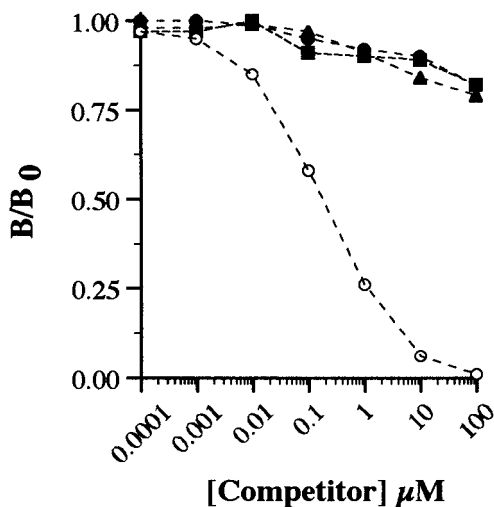


Fig. 3. Specificity of polyclonal antibody raised to NAL-HNE fluorophore (3). Competitive ELISA was performed as described (3) using immunopurified anti-NAL-HNE fluorophore as primary antibody and NAL-HNE fluorophore-linked CA (1.0 pmol NAL-HNE fluorophore/well) as coating antigen. Antibody binding was evaluated in the presence of NAL-HNE fluorophore (○) and Michael adducts produced in the reactions of HNE with N_α -acetylhistidine (▲), N_α -acetylcysteine (■), and N_α -acetyllysine (●), at concentrations indicated on the *abscissa*. $B/B_0 = [(OD/s) - (OD/s)_{\text{bkg}}] / [(OD/s)_{\text{no competitor}} - (OD/s)_{\text{bkg}}]$ where OD/s = change in absorbance at 405 nm per s in the linear range. Background (bkg) values were obtained using CA exposed to EDC in the absence of NAL-HNE fluorophore as coating antigen.

3. The wells are rinsed with $3 \times 100 \mu\text{L}$ of wash buffer and incubated in $100 \mu\text{L}$ goat anti-rabbit IgG conjugated to alkaline phosphatase (1:7500 in blocking buffer) for 1 h (25°C). After $3 \times 100 \mu\text{L}$ rinses with wash buffer and $2 \times 100 \mu\text{L}$ rinses with 20 mM Tris-Base, pH 9.8, containing 1 mM MgCl_2 (assay buffer), a $100 \mu\text{L}$ aliquot of 1 mg/mL p-nitrophenylphosphate (PNPP).
4. The microtiter plate is read in a BioRad model 500 microplate reader (405 nm) in the kinetic mode (30 min at 25°C). Typically, two readings/min are taken. Relative rates of PNPP hydrolysis, within the linear range, are then used to evaluate primary antibody binding.

3.5. SDS-PAGE and Western-Blot Analysis

1. Polyacrylamide gels are prepared to the desired percentage according to standard protocols. We use a stock polyacrylamide solution composed of 30% polyacrylamide (2.6% C). For most initial experiments, 100% polyacrylamide gels work well.
2. For analysis of purified protein(s), dissolve the protein(s) of interest in an appropriate buffer (typically 100 mM Na_2HPO_4 , pH 7.4). Protein concentration

should be such that, following a 1:2 dilution, approx 2 $\mu\text{g}/\text{lane}$ of protein can be loaded.

3. For analysis of tissue homogenate and subfractions, excise organ of interest, rinse in ice cold buffer (typically an isotonic solution buffered by Tris, MOPS, or other appropriate biological buffer), and blot excess liquid. Homogenize tissue ($\sim 20 \text{ mL/g}$ wet weight) and subfractionate by differential centrifugation as desired. It is recommended that protease inhibitors and EDTA be included in the homogenization buffer. If necessary, antioxidants should be present. Protein concentrations of at least 1.0 mg/mL are optimal.
4. Dilute protein samples with an equal volume of 2X sample buffer (126 mM Tris HCl, 4% SDS, 20% glycerol, 0.005% bromophenol blue) containing an appropriate amount of β -mercaptoethanol (BME). A reasonable content of BME in 2X sample buffer is in the range of 0.5–5.0% (v/v). Samples are heated at 60°C for 2 min prior to SDS-PAGE.
5. Samples are loaded onto gels ($2.0 \mu\text{g}/\text{lane}$ of pure protein, $12.5 \mu\text{g}/\text{lane}$ tissue homogenate or subfraction). For complete analyses, two identically loaded gels are run in parallel. One gel of a series is stained with Coomassie brilliant blue to visualize the protein profile. The other gel is used for Western-blot analysis.
6. SDS-PAGE is performed using running buffer (25 mM Tris base, 0.19 M glycine, 0.1% SDS). With the Novex system, 2 h at 135 v is sufficient.
7. Proteins are electroblotted onto nitrocellulose or PVDF membrane in 12.5 mM Tris base, 95 mM glycine, 10% methanol. With the Novex system, 1 h at 32–35 v is sufficient.
8. To determine the efficiency of transfer, the membrane is stained briefly with Ponceau's reagent (10X solution is composed of 2% Ponceau S [w/v], 30% trichloroacetic acid [w/v], and 30% sulfosalicylic acid [w/v]). Ponceau staining is visualized after brief rinses with deionized water. Stain is removed from the electroblotted protein blot by rinsing with 1X PBS.
9. The following protocol has been optimized for chemiluminescence visualization of immunoblotted protein. The detection system consists of alkaline phosphatase linked to the secondary antibody and chemiluminescence reagents CSPDTM and Nitro-Block[®] (Tropix). It should be noted that anti-lysine-HNE fluorophore has been successfully used for Western-blot analysis with goat anti-rabbit IgG conjugated to horseradish peroxidase as secondary antibody and appropriate substrates.
10. All antibodies are diluted into blocking buffer (1X PBS containing 0.2% I-BlockTM [w/v] from Tropix and 0.01% Tween-20). Note: The stringency of antigen-antibody interactions can be adjusted by varying the Tween-20 content (0.01–0.1% is recommended).
11. Anti-lysine-HNE fluorophore is diluted 1/200cp: blot, the typical volume of antibody solution is 20 mL.
12. The blot is washed $3 \times 10 \text{ min}$ with 1X PBS containing 0.01% tween-20.
13. The blot is incubated with goat anti-rabbit IgG conjugated to alkaline phosphatase (Tropix) and diluted 1/20000 in blocking buffer, for 1 h at room temperature.

14. The blot is washed 3×5 min with 1X PBS containing 0.01% Tween-20 and then 2×5 min with alkaline phosphatase buffer (20 mM Tris base, 1 mM MgCl_2 , pH 9.8).
15. The blot is incubated with CSPD™ and Nitro-Block® in alkaline phosphatase buffer for 5 min at room temperature according to Tropix protocol. After removal of excess solution, the blot is wrapped in plastic wrap and exposed to X-ray film for varying periods of time.
16. If desired, densitometric analyses can be performed.

3.6. Immunohistochemical Analyses

1. Tissue Fixation.
 - a. Immunolight microscopy. Depending on the organ(s) of interest, tissue is fixed by transcardial perfusion, perfusion of the isolative organ, or soaking small tissue pieces, approx $10 \times 10 \times 3$ mm, in fixative (4% neutral buffered formalin) for 1 h at room temperature (7–10).
 - b. Immunogold electron microscopy. Tissue can be fixed by transcardial perfusion or by perfusion of the isolated organ. It is also possible to soak small tissue portions, approx 1 mm^3 , in Carson-Millonig's fixative (4% paraformaldehyde in 0.16 M NaH_2PO_4 , pH 7.2) for 1 h at room temperature (7–10).
 - c. The conditions described previously have been successfully utilized for anti-lysine-HNE fluorophore (not shown) and antibodies to other HNE-derived protein modifications (7,8). However, numerous methodologies for fixing tissue samples have been previously described (7–10). Experiments to determine optimal conditions for analysis of samples of interest may be required.
2. Embedding and Sectioning.
 - a. Immunolight microscopy. Following fixation, tissue samples are saturated with sucrose. Briefly, fixed tissue is serially soaked in 10% sucrose (in PBS) overnight at 4°C and 15 mL 20% sucrose (in PBS) for 1–2 d at 4°C. Tissue is mounted in OCT embedding media and frozen sections ($10 \mu\text{m}$) are cut using a cryostat and picked up on gelatin-subbed slides.
 - b. Immunogold electron microscopy. After a 30-min rinse in 0.1 M NaH_2PO_4 , pH 7.2, samples are serially dehydrated (30 min per step) with 70, 80, and 90% ethanol followed by LR White resin/90% ethanol (2/1, v/v). Samples are then immersed in LR White resin overnight and rinsed with one further change (1 h) of fresh LR White resin. Polymerization of tissue embedded in LR White resin (sealed gelatin capsules) is thermally induced (55°C for 12 h). Ultrathin sections (70–80 nm) are cut using an ultramicrotome. And transferred to nickel grids For ultrastructural analysis, sections can be immediately stained with 4% uranyl acetate and lead citrate.
2. Staining and Detection
 - a. Immunolight microscopy. Tissue slides are rinsed with several changes of PBS and then incubated with blocking buffer (10% horse serum in PBS, 0.02% triton x-100) for 30 min at room temperature. Anti-lysine-HNE fluorophore

is diluted 1/100–1/500 in blocking buffer and sections are exposed to primary antibody for 30–60 min at room temperature. After several rinses with PBS, sections are exposed to secondary antibody, typically biotinylated anti-rabbit IgG and the ABC complex. Biotinylated universal antibody can also be used. The slides are then rinsed several times with PBS and incubated with diaminobenzidine (DAB) solution prepared by dissolving 10 mg DAB in 13.5 mL PBS containing 0.015% (v/v) H_2O_2 (filter through Whatman #1 or similar filter paper). After a suitable incubation time (approx 10 min), rinse with PBS or water, and dehydrate the tissue (0, 25, 50, 75, 95, and 100% ethanol for a minimum of 3–5 min each). Slides are then mounted with Permount (or other suitable mounting medium) and cover slip affixed.

- b. Immunogold electron microscopy. Sections are treated as previously described. Briefly, tissue grids are rinsed with several changes of tris-buffered saline (TBS) composed of 0.05 M tris, 0.9% NaCl, pH 7.6 and blocked with blocking buffer (2% BSA in TBS containing 0.2% Tween-20) for 3 min. Grids are then incubated with anti-lysine-HNE fluorophore diluted 1/80 in blocking buffer (overnight at 4°C). After extensive washing with blocking buffer diluted 1/10, the section are rinsed in alkaline TBS, pH 8.2, for 10 min and incubated with gold-conjugated goat anti-rabbit IgG (EM.GAR15) diluted 1/75 in blocking buffer (90 min at room temperature). Sections are then rinsed with TBS (2 × 10 min) and distilled water 2 × 5 min). After counterstaining with 4% uranyl acetate (aqueous) for 10 min, gold beads are visualized with a transmission electron microscope operated at 75 kV.

3.7. Results

3.7.1. Formation of Fluorophore from NAL and HNE

1. Reaction of N_α -acetyllysine (NAL, 0.5 M) with 4-hydroxy-2-nonenal (HNE, 10 mM) in Na_2HPO_4 (0.1 M, pH 7.4) at 37°C for 20 h results in the formation of a compound, which is resolved by RP-HPLC (**Fig. 1**) and exhibits a UV absorbance maximum of 360 nm (*see Note 4*). This compound is fluorescent, with excitation and emission maxima at 360 and 430 nm, respectively (**Fig. 1**, inset), and was characterized as a 2-hydroxy-3-imino-1,2-dihydropyrrol (3).

3.7.2. Formation of the Fluorophore on Protein

2. Treatment of glucose-6-phosphate dehydrogenase (Glu-6-PDH) from *Leuconostoc mesenteroides* with HNE for extended periods of time leads to the appearance of fluorescent, cross-linked protein (3,6). It was therefore important to determine whether the fluorophore formed on HNE-treated Glu-6-PDH was structurally analogous to the fluorescent product of the model reaction between NAL and HNE. The data presented in **Fig. 2** corresponds to approx 0.15 nmol of lysine-HNE fluorophore per mg of protein relative to an ELISA standard curve constructed using known amounts of NAL-HNE fluorophore/well (as NAL-HNE fluorophore-linked CA). Further evidence is provided by competitive ELISA. As

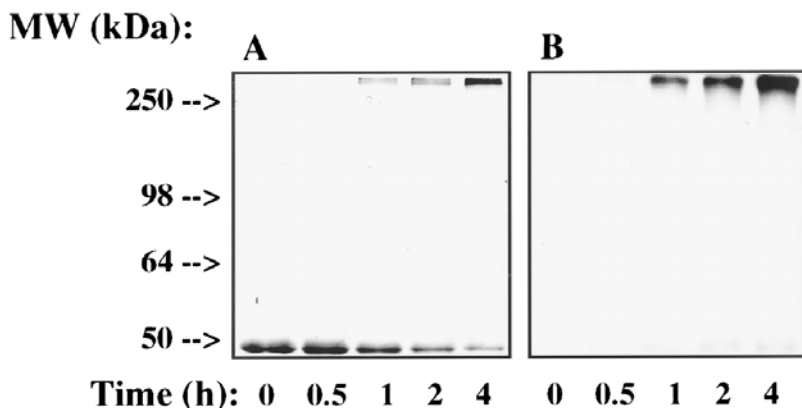


Fig. 4. SDS-PAGE and Western-blot analysis of Glu-6-PDH treated with HNE (3). Glu-6-PDH (2.5 mg/mL) was incubated with HNE (5.0 mM) for 0, 0.5, 1.0, 2.0, and 4.0 h at 37°C as detailed in Materials and Methods. Samples were loaded onto two 10% polyacrylamide gels (2.0 μ g/well). One gel of the series was stained with Coomassie blue for evaluation of the molecular weight distribution of HNE-treated Glu-6-PDH (A). The other gel was electroblotted onto nitrocellulose membrane (0.45 μ m) for Western-blot analysis with immunopurified antilycine-HNE fluorophore (1/2000) as primary antibody (B). Antibody binding was visualized after exposure of the blot to a chemiluminescent substrate.

shown in **Fig. 3**, antibody binding to HNE-treated Glu-6-PDH can be competed by authentic NAL-HNE fluorophore and by analogous fluorophores produced by reaction of γ -butyric acid and ethylamine with HNE (reaction conditions similar to that described for NAL and HNE). The kinetics of competition are identical, with the IC_{50} for antibody binding being approximately 0.1 μ M for each fluorophore tested. These observations demonstrate that the epitope recognized by the antibody is the 2-hydroxy-3-imino-1,2-dihydropyrrol structural feature of fluorophores produced by reaction of primary amines with HNE and that this structure forms when Glu-6-PDH is exposed to HNE.

3. To evaluate the distribution of fluorophore-modified Glu-6-PDH as a function of time of exposure to HNE, Glu-6-PDH treated with HNE for 0, 0.5, 1.0, 2.0, and 4.0 h was analyzed by SDS-PAGE and Western-blot analysis. As shown in **Fig. 4A**, this resulted in the formation of cross-linked, multimeric protein, the relative levels of which increased in a time-dependent fashion. Di- and tetrameric forms of Glu-6-PDH, visible in the gel but not readily seen in **Fig. 4A**, were rapidly converted to aggregated protein under the conditions of our experiments. Increases in the level of multimeric protein were paralleled by increases in the intensity of protein-associated fluorescence (not shown) and in the level of anti-lysine-HNE fluorophore binding (**Fig. 4B**). The distribution of antibody binding indicates that fluorescent, lysine-HNE cross-links are present primarily

on multimeric protein (**Fig. 4B**). This observation suggests that fluorescent cross-links represent relatively stable end products of HNE modification(s). However, some binding to monomeric protein is evident, indicating the presence of relatively low levels of intramolecular lysine-HNE fluorescent cross-links.

3.7.3. Immunohistochemical Analysis

Few immunohistochemical studies utilizing anti-lysine-HNE fluorophore are yet in print. However, we have successfully probed tissue excised from certain diseased organs with this antibody.

4. Notes

1. Detailed protocols on immuno(histo)chemical techniques are beyond the scope of this chapter. For a comprehensive review, *see* **ref. 11**. Clearly, tissue can be fixed and embedded using a variety of approaches and/or homogenized in different buffers using a wide array of available tissue disruptors. Further, optimal antibody blocking/staining procedures for different tissue types may require changes in triton x-100 content, Tween-20 or other treatments prior to immuno(histo)chemical staining. The procedures outlined above are meant to provide general guidelines for use of anti-lysine-HNE fluorophore.
2. To ensure the specificity of antibody binding, it may be necessary to perform competition studies (ELISA, Western, or immunohistochemistry). Such experiments require either preparation of authentic model compounds bearing the epitope recognized by the antibody or the desired HNE adduct covalently attached to protein.
3. Distinguishing between various forms of HNE-derived modifications to protein. HNE can react with protein to form 1:1 amino acid-HNE Michael adducts, 2:1 lysine-HNE nonfluorescent crosslinks, and the 2:1 lysine-HNE fluorophore (**Scheme 1**). In addition to anti-lysine-HNE fluorophore (**3**), polyclonal antibodies to Michael adducts and the chemically stabilized form of the nonfluorescent lysine-HNE crosslink have been described (**12,13**). Use of this series of antibodies in parallel is likely to provide additional insight on the selectivity, specificity, and subcellular distribution of different forms of HNE-derived protein modifications.
4. HPLC resolution of various materials is a function of the column and HPLC system. We have described here use of a Vydac C18 column and the Hewlett-Packard 1050 attached to a diode-array UV detector. It may be of interest, for some analyses, to utilize electrochemical and/or fluorescence detectors.

References

1. Porta, E. A. (1991) Advances in age pigment research. *Arch. Gerontol. Geriatr.* **12**, 303–320.
2. Harman, D. (1989) Lipofuscin and ceroid formation: the cellular recycling system. *Adv. Exp. Med. Biol.* **266**, 3–15.

3. Tsai, L., Szweda, P. A., Vinogradova, O., and Szweda, L. I. (1998) Structural characterization and immunochemical detection of a fluorophore derived from 4-hydroxy-2-nonenal and lysine. *Proc. Natl. Acad. Sci. USA* **95**, 7975–7980.
4. Esterbauer, H., Schaur, R. J., and Zollner, H. (1991) Chemistry and biochemistry of 4-hydroxynonenal, malonaldehyde and related aldehydes. *Free Radic. Biol. Med.* **11**, 81–128.
5. De Montarby, L., Tourbah, H., and Gree, R. (1989) *Bull. Soc. Chim. Fr.* **3**, 419–432.
6. Friguet, B., Stadtman, E. R., and Szweda, L. I. (1994) Modification of glucose-6-phosphate dehydrogenase by 4-hydroxy-2-nonenal. Formation of cross-linked protein that inhibits the multicatalytic protease. *J. Biol. Chem.* **269**, 21639–21643.
7. Oberley, T. D., Toyokuni, S., and Szweda, L. I. (1999) Localization of hydroxynonenal protein adducts in normal human kidney and selected human kidney cancer. *Free Radic. Biol. Med.* **27**, 695–703.
8. Zainal, T. A., Weindruch, R., Szweda, L. I., and Oberley, T. D. (1999) Localization of 4-hydroxy-2-nonenal-modified proteins in kidney following iron overload. *Free Radic. Biol. Med.* **26**, 1181–1193.
9. Coursin, D. B., Cihla, H. P., Oberley, T. D., and Oberley, L. W. (1992) Immunolocalization of antioxidant enzymes and isozymes of glutathione-S-transferase in normal rat lung. *Am. J. Physiol.* **263**, L666–L691.
10. Muse, K. E., Oberley, T. D., Sempf, J. M., and Oberley, L. W. (1994) Immunolocalization of antioxidant enzymes in adult hamster kidney. *Histochem. J.* **26**, 734–753.
11. Harlow E. and Lane, D. (1999) *Using Antibodies: A Laboratory Manual*. Cold Spring Harbor Laboratory Press, Cold Spring Harbor, NY.
12. Uchida, K., Szweda, L. I., Chae, H. Z., and Stadtman, E. R. (1993). Immunochemical detection of 4-hydroxynonenal protein adducts in oxidized hepatocytes. *Proc. Natl. Acad. Sci. USA* **90**, 8742–8746.
13. Cohn, J. A., Tsai, L., Friguet, B., and Szweda, L. I. (1996) Chemical characterization of a protein-4-hydroxy-2-nonenal cross-link: immunochemical detection in mitochondria exposed to oxidative stress. *Arch. Biochem. Biophys.* **328**, 158–164.

Liver Slice Technology as an In Vitro Model for Metabolic and Toxicity Studies

Sanjeev Thohan and Gerald M. Rosen

1. Introduction

Liver Slice Technology is a relatively new addition to the battery of in vitro assays of xenobiotic metabolism and toxicity evaluation. As with any developing technology, evaluation and refinement of the technique will be an essential component of its implementation to routine use. Three goals of this article will be to: (1) provide a brief survey of currently used methods for immediate and cultured liver slices, (2) review the use of liver slices in the assessment and quantification of pharmacological and toxicological responses, and (3) discuss the possible use of Liver Slice Technology for the investigation of drug interactions.

Liver Slice Technology has been developed as an in vitro model for the assessment of hepatic drug metabolism. Decided advantages over other techniques include: maintenance of the functional acinar architecture of the liver and patency of integrated drug metabolism. It is this latter application that has allowed mechanistic inquiries into the metabolic fate of drugs and xenobiotics with a model that takes into account the balance between Phase I and Phase II biotransformations. Further, an accurate understanding of the in vivo metabolic state dictates that the in vitro model account for cellular heterogeneity and metabolic competency. As such, Liver Slice Technology is ideally suited to probe the consequences of drug-drug interactions in the cellular environment of an intact isolated tissue. Finally, one of the important advantages of Liver Slice Technology is the ability to generate subcellular fractions from the same tissue for direct comparative metabolic profiling. This

study design has been used with hepatocytes, but it is technically difficult to achieve with reproducible data (1–3).

Cytochrome P-450 has emerged as one of the important Phase I enzymes responsible for a diversity of oxidative and reductive biotransformations. Of the many Phase II reactions, glucuronidation, sulfation, and glutathione conjugation have gained recognition as primary enzymes in the metabolism of a broad spectrum of endo- and xenobiotic compounds. Phase I and Phase II drug metabolism may be operationally considered to be integrated or sequential in nature, such that substrates undergoing Phase I metabolism can become substrates for Phase II enzymes; although enzymes catalyzing these reactions may be in distinct intracellular compartments. It is now realized that metabolism of drugs and other foreign compounds can result in the production of reactive intermediates, which often lead to toxic intermediates that initiate tissue necrosis, carcinogenesis, or teratogenesis. As will be documented herein, Liver Slice Technology can play an important role in the assessment of the metabolic fate of drugs, including toxicological sequelae. Although it is beyond the scope of this review, the interested reader should be aware that Tissue Slice Technology has been adapted for use with renal (4), lung (5), and cardiac tissues (6).

Cultured liver slices have been used as models for induction and metabolic profiling; however, their use has been limited in other arenas. This is due, primarily, to difficulties in achieving incubation times with liver slices that are traditionally associated with long-term tissue culture. Operationally, incubation duration of longer than 24 h is rare, as extended times frequently result in diminished enzymatic activity. For example, studies by Lake et al. (7) have shown the need to include inducing agents, such as phenobarbital, β -naphthoflavone, or aroclor 1254, in RPMI 1640 culture media to stem the loss of cytochrome P-450 activity when experimental conditions require incubation times greater than 24 h. Likewise, rat liver slices, cultured in either RPMI 1640 media or Williams Medium E, required the peroxisome proliferators, clofibrate, nafenopin, ciprofibrate, or Wy-14,643, to maintain peroxisomal integrity (8).

Supplemented Chee's medium, for instance, has been reported to sustain mouse and rat liver slices for up to 96 h without loss of normal lobular structure of the liver and were found to be responsive to induction upon exposure to β -naphthoflavone, dioxins such as TCDD and phenobarbital (9). Rifampicin was found to induce cytochrome P-450 3A4 in human liver slices cultured in RPMI 1640 culture media for up to 72 h (10). A more recent comprehensive evaluation of human liver slices has found that tissue viability was maintained in Waymouth's media for up to 24 h and declined during the next 72 h culture

period (11). Similar patterns of decreased activity were seen for isoform specific substrate metabolism in homogenates generated from these cultured liver slices (11).

As stated earlier, slice viability is of great concern in studying the metabolism of drugs and other foreign compounds and there have been a number of strategies to further improve the quality of the preparation (12). One approach has been to “washout” residual hydrolytic enzymes and allow acclimation of the tissue to the incubation medium. A background or baseline release of intracellular components is to be anticipated from the process of generation of liver slices. No threshold has been established for the release of intracellular enzymes that will indicate viable vs nonviable preparations however, background levels should be kept low such that increases in enzyme release may be reliably quantified. Ambient release of enzymes from intracellular compartments may arise from cells at the cut borders. If not damaged overtly, these border cells may have been compromised by the slicing procedure. Histological analyses by Thohan and Kane (13) confirmed observations of damage at the cut faces of the liver slice. Cut surfaces may appear compromised with regard to cellular integrity; however, deeper cellular architecture maintains viability as may be confirmed by histological evaluation.

In our studies, a total release of LDH was observed to be 17, 18, and 24% at 30, 60, and 120 min, respectively ($n = 6$ slices/incubation). This observation coupled with time-dependent increases in the metabolism of several substrates for cytochrome P-450 demonstrate the stability of the liver slice preparation and maintenance of the membrane integrity. Our findings are in agreement with LDH release patterns from liver slices as reported by Ekins et al. (14). In fact, the stability of the baseline release of intracellular marker enzymes, such as LDH or SDH, from liver slices indicate that the integrity of the tissue has not been compromised (13).

Cytotoxicity may be envisioned as a cascade of cellular events that begins with early intracellular changes in homeostatic mechanisms. In attempts to better understand these early events, many *in vitro* and *in vivo* models have been developed. Of these, hepatocytes have emerged as a standard of comparison between *in vitro* isolated enzyme preparations and *in vivo* models, since they retain both Phase I and Phase II biotransformation capabilities (15,16). With improvements in Liver Slice Technology noted earlier, primarily based on the work of Smith et al. (17), dramatic improvements in tissue slice preparation and use in metabolic studies have been observed. In fact, these studies provide the foundation for development of Liver Slice Technology as an alternative *in vitro* model for acute exposures and assessment of drug metabolism and xenobiotic-mediated toxicity.

2. Materials

2.1. Equipment

1. Microtome.
2. Tissue slicer (Krumdieck or Brendel types, Vitron, Tucson, AZ).

2.2. Reagents

1. 7-Ethoxycoumarin (Sigma Chemical Company, St. Louis, MO).
2. 7-Hydroxycoumarin (Sigma).
3. β -Glucuronidase (glucurase, Sigma).
4. Saccharic acid 1,4 lactone (Sigma).
5. Phenylmethylsulfonylfluoride (PMS; Sigma).
6. Butylated hydroxy toluene (BHT; Sigma).
7. Lactate dehydrogenase (LDH) determination (Sigma, Kit # 228-UV).
8. Waymouth's MB medium (Sigma).
9. Krebs Henseleit buffer (Sigma).
10. HEPES (N-[2-hydroxyethyl]piperazine-N'-[2-ethanesulfonic acid]) (Sigma).
11. 7-Methoxycoumarin (7-MC, Aldrich Chemical Company, Milwaukee, WI).
12. Coomassie Blue (BioRad, Richmond, CA).

2.3. Animals

Male Sprague Dawley Rats (180–220g, Charles River Laboratories) were housed in the Walter Reed Army Institute of Research (WRAIR) animal facility under standard operating procedures. Food and water were allowed *ad libitum*. Animals were restricted from food for 16 h prior to euthanasia. Animals were prepared for terminal surgical anesthesia with pentobarbital (60 mg/kg) by intraperitoneal injection.

3. Methods

3.1. Preparation of Liver Slices

1. Liver slices, from organs perfused with ice-cold 0.9% saline before excision, may be generated by a variety of manual and semi-automated means (*see Note 1*). Manual methods of slice production such as the McIlwain, Stadie Riggs, and microtome-based tissue slicers do not produce uniform slices under physiologically controlled situations. The Krumdieck tissue slicer (and similar slicing mechanisms) are able to produce a large number of uniform slices using physiologically based buffer systems under temperature-controlled situations. Since its introduction in the mid-1980s only Brendel/Vitron slicer has been included in the catalog of tissue slicers.
2. Livers were dissected into lobes and cores produced using a cylindrical stainless-steel corer (11.0 mm internal diameter). Cores were placed into the Krumdieck tissue slicer; slice thickness was controlled via a micrometer-based adjustment. Slices generated by movement of a weighted tissue core over an oscillating razor

blade were swept away to a collection chamber by a stream of saline. A slice may be generated every 3–4 s. Slices were transferred from the collection area to a shallow tray containing ice-cold 0.9% saline for selection and loading onto the incubation supports.

3. A detailed description of the slicing and incubation procedure with illustrations may be found in Kane and Thohan (**13**) and Thohan and Chung (**18**). Selection criteria were based on the physical appearance of the tissue slice. Slices that had portions of the hepatic capsule associated with them or those not uniform in thickness or cellular integrity were also not selected for use.

3.2. Dynamic Factors for Tissue Preparation

1. The advent of the “dynamic organ culture” methods of incubation by investigators at the University of Arizona demonstrated that exposure of the liver slice to a gas and liquid phase was advantageous to static methods of tissue preparation (**19**). A comprehensive evaluation of commonly used incubation techniques has been evaluated for short-term incubation of liver slices (**20**). It is well-established that the liver is an organ in which oxygen tensions are low and the presence of an oxygen-rich environment, such as those for many tissue-culture environments, may result in oxidative stress and a compromise of tissue viability. Despite this, there are examples where no significant change in metabolic profiling with the use of an oxygen-rich environment has been noted (**20**).
2. A variety of tissue-culture media and simple salt solutions have been explored as preservation solutions to retain the metabolic activity of tissue slices. Devising such a buffer has in no way been a trivial task. Commonly used media such as William’s Medium E or Waymouth’s MB, contain, for instance, a number of nucleophiles and antioxidants that may stabilize the liver slice and extend its viability beyond 24 h; however, some of the components of the medium may react with electrophiles and scavenge free radicals, thereby complicating data interpretation. For instance, millimolar concentrations of thiols can react with a variety of reactive metabolic intermediates, eliminating such electrophiles that would otherwise have reacted with tissue targets. Likewise, inclusion of fetal calf serum (FCS) or hormones may result in skewed observations, not pertinent to the homeostatic state of the tissue. Krebs Henseleit buffered with either HEPES or bicarbonate has been used as an alternative incubation medium to support metabolic processes without confounding the metabolic and/or the toxic cascade(s). In fact such simple buffers have been shown to sustain drug metabolism for up to 6 h and may be extended to 24 h with interval changes of the incubation medium (**13,19,21**).

3.3. Results

3.3.1. Measures of Toxicity

1. The use of liver slices in the arena of cytotoxicity evaluation is recent in comparison with the vast hepatocyte literature. The range of chemicals evaluated

Table 1
Acetaminophen Toxicity Profile for LDH and SDH Release^a

Concentration (mM)	Control		Phenobarbital	
	LDH	SDH	LDH	SDH
0.05	0.73 ± 0.08	0.53 ± 0.14	0.98 ± 0.19	0.60 ± 0.25
0.1	0.92 ± 0.12	0.63 ± 0.08	1.18 ± 0.08	0.63 ± 0.15
0.5	0.84 ± 0.14	0.79 ± 0.12	1.09 ± 0.10	1.81 ± 0.73*
1.0	0.93 ± 0.04	0.80 ± 0.13	1.07 ± 0.11	2.45 ± 0.75*

^aLDH and SDH values are presented as mean ± standard deviation of the Toxicity Index (generated from the percent of enzyme released in treatment groups normalized to vehicle controls). Values in the vicinity of 1 (one) on the toxicity index suggest little or no toxicity. *Indicates statistical difference from control values from $n = 3$ rats, 3 slice replicated/rat ($p < 0.1$).

for in vitro toxicity using liver slices consists of a small number of compounds (see **Note 2**), including allyl alcohol and bromobenzene (**22**), carbon tetrachloride and 1,2 dichloroethane (**23**), cocaine (**24**), and endotoxin and ethanol (**25**).

2. Tissue slices have been successfully used for biochemical and histochemical characterization of cellular damage (**9,13,17,22,23,26**). A major goal in the assessment of cytotoxicity requires techniques that are highly sensitive, reproducible, applicable to large-scale screening procedures for a variety of species, and advantageous in an economical sense.
3. Dose ranges of model compounds, such as acetaminophen and paraquat, were narrowed to better define the “effect” and “no-effect” levels of cytotoxicity. Additionally, the effects of in vivo induction on toxicity profiles in vitro was also examined. The toxicity index used in our investigations is a factor generated from the percent of enzyme released in treatment groups normalized to vehicle controls. Values that are in the vicinity of 1 (one) on the toxicity index suggest little or no toxicity. The long-term goal of this research is to provide a framework within which to create a database of information such that compounds may be ranked with regard to toxicity potential. This will allow more stringent limits to be placed on toxicity indexes and allow better definition of “effect” and “no-effect” levels of exposure.
4. Thohan and Chung (**18**) described no overt toxicity from the release patterns of lactate dehydrogenase (LDH) from liver slices in both the control and phenobarbital-pretreated rat liver slices when exposed to concentrations in the range from 0.05 mM to 1 mM acetaminophen (see **Table 1**). A significant increase in sorbitol dehydrogenase (SDH) was noted at concentrations greater than 0.5 mM. Taken together, the LDH and SDH results indicate a localization of the damage to the mitochondria of the liver slice.
5. Liver slices were exposed to concentrations of paraquat from 50 mM to 1 mM for 2 h. No overt toxicity was found for LDH or SDH release patterns in the control

Table 2
Paraquat Toxicity Profile for LDH and SDH Release^a

Concentration (mM)	Control		Phenobarbital	
	LDH	SDH	LDH	SDH
0.05	0.79 ± 0.07	0.85 ± 0.11	1.08 ± 0.17	2.60 ± 0.90*
0.1	0.89 ± 0.08	0.81 ± 0.10	0.91 ± 0.09	3.52 ± 0.73*
0.5	0.88 ± 0.08	0.81 ± 0.13	1.22 ± 0.09	3.03 ± 0.78*
1.0	1.02 ± 0.13	0.75 ± 0.14	1.18 ± 0.10	2.48 ± 0.24*

^aLDH and SDH values are presented as mean ± standard deviation of the Toxicity Index (generated from the percent of enzyme released in treatment groups normalized to vehicle controls). Values in the vicinity of 1 (one) on the toxicity index suggest little or no toxicity. *Indicates statistical difference from control values from $n = 3$ rats, 3 slice replicated/rat ($p < 0.1$).

rat liver slices or LDH release patterns from phenobarbital-induced rat liver slices. In contrast, paraquat-exposed liver slices from phenobarbital-pretreated rats demonstrated a significant release of SDH over 0.05 mM to 1 mM exposure range (**Table 2**). In fact, for paraquat, there was no noted difference in the amount of SDH released at any of the concentrations investigated. It seemed as though there were a quantal response to the release of SDH from the phenobarbital pretreated liver slices (**18**).

6. The production of superoxide by redox cycling of paraquat creates an environment for free radical generation limited by the flow of electrons to the substrate and the availability of oxygen. This places an enormous stress on cellular reduced glutathione stores and ultimately results in cell death. This potential for unabated production of reactive species from paraquat may have contributed to the quantal response observed for SDH release in the phenobarbital-pretreated rat liver slices. Considering these results, further investigation using quantification of cellular sulfhydryls and possible quantification of reactive species would allow greater understanding of the progression of cytotoxicity in liver slices.

3.3.2. Confirmation of Metabolic Profile: Liver Slice and Microsomal Metabolites

1. Microsomal fractions generated from liver slices or remnant tissues have also been used as comparators for metabolite identification or assessment of alterations to the liver slice enzyme profile. Brodfuehrer et al. (**26**) showed that the binding of reactive metabolites of benzene in liver slices from rat, mouse, and human was positively correlated with microsomal production of metabolites in each of these species. By design microsomal rates of xenobiotic metabolism are optimal, not dependent on pharmacodynamic properties of the parent compound and subsequent metabolites. It would, therefore, be likely that the liver slice

preparation, due to its architecture and similarity to the *in situ* condition, would yield rates that may be different.

2. A comparison of liver slice and microsomal metabolism was performed in our laboratory. A detailed description of analytical methods used for metabolite quantification may be found elsewhere (13). Although we limited our survey to a few xenobiotics, it appears that metabolic profiles from liver slices were found to be distinct from those generated from microsomal fractions isolated from the same tissue. In microsomal fractions, for example, no difference was noted in the O-dealkylation of 7-methoxycoumarin and 7-ethoxycoumarin (Fig. 1). In contrast, similar metabolic studies with liver slices revealed a significant difference between O-demethylation and O-deethylation of the alkoxy coumarins at early time points; thereafter, such differences waned with incubation time. These observations suggest that the initial difference in the metabolic rate of O-dealkylation can be assigned to disparate rates for 7-methoxycoumarin and 7-ethoxycoumarin diffusion to cytochrome P-450 and not associated with differential metabolism. **Figure 1** depicts the metabolic profile for 7-hydroxycoumarin in the absence of Phase I metabolism. These data confirm the well-established observation of capacity limited metabolism with the predominance of glucuronidation over sulfation.
3. Difference in substrate accessibility to metabolism has likewise been described for 2-(5'-chloro-2'-phosphorylphenoxyphenyl)-6-chloro-4-(3H)-quinazolinone (21). Here, it was proposed that the existence of a diffusional barrier in liver slices hindered substrate access to the metabolizing enzymes. More recently, Worboys et al. (27) examined the metabolism of a series of chemicals of distinct physicochemical characteristics. Liver slice content of xenobiotics was found to positively correlate with the lipophilicity, whereas subsequent metabolic rates were equated with enzyme function.
4. Patterns for Phase I metabolism were found to be qualitatively similar between liver slice and microsomal preparations in that there were no significant differences in metabolic profile. However, in consideration of the early time points for metabolism in liver slices, pharmacodynamic effects on the rates of drug metabolism must be reiterated. These effects include substrate uptake, biotransformation, and metabolite elimination. In the example cited previously, the increased rate of O-demethylation of 7-methoxycoumarin vs O-deethylation of 7-ethoxycoumarin at the 30-min interval illustrates the importance of physicochemical considerations and the utility of liver slices to investigate the pharmacodynamics of drugs and other foreign compounds. Differences in xenobiotic diffusion may have been previously overlooked since metabolic studies with microsomes focus primarily on K_m and V_{max} and functionally are not intended to differentiate metabolic rates based on pharmacodynamic characteristics of the drug or xenobiotic.
5. Continued interest into mechanisms involved in drug metabolism and toxicity will provide insight for the development and implementation of newer, more

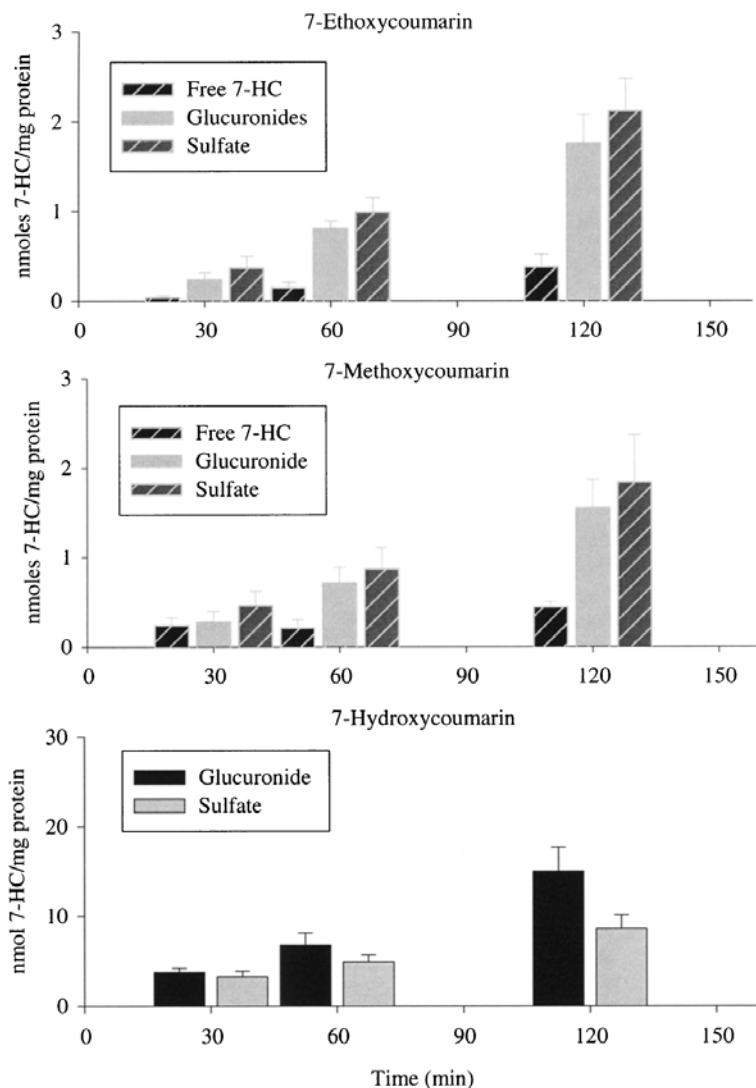


Fig. 1. Alkoxy coumarin metabolism in rat liver slices. Rat liver slices ($n = 7$, triplicate determination/rat) were exposed to either 7-ethoxycoumarin ($100 \mu M$), 7-methoxycoumarin ($100 \mu M$) or 7-hydroxycoumarin ($100 \mu M$). Substrates were added after a 60-min period to stabilize the tissue. Metabolites were assayed as described previously (13). Tight integration of metabolism was demonstrated by the low level of 7-hydroxycoumarin in the 7-ethoxycoumarin and 7-methoxycoumarin incubations. A high level of 7-hydroxycoumarin conjugation was quantified, indicating Phase II biotransformation was more active than Phase I metabolic processes.

sensitive technologies. These studies will provide a framework in which to conduct experiments to better understand biotransformation and assessment of bioactivation-based toxicity. To date, Liver Slice Technology has maintained a primary focus on cytochrome P-450 mediated metabolism; however, a complete assessment of Phase I drug metabolism should embody other oxidative enzymes such as FAD-containing monooxygenase and hydrolytic enzymes, including epoxide hydrolases (*see Note 3*).

6. Using Liver Slice Technology, pharmacokinetic characterization of Phase I and Phase II enzymes will enhance the understanding of metabolic processes and their relationship to pharmacological and toxicological sequelae. Moreover, these studies may offer insight into factors that impact xenobiotic metabolism such as enzyme induction or inhibition, gender, age, nutritional and environmental stressors (*see Note 4*).
7. Drug interactions have become a primary concern in the evaluation of existing and novel compounds being considered for lead optimization and candidate selection for drug development. Liver Slice Technology provides the complexity of an organ-perfusion system, but retains a metabolic simplicity of hepatocytes or microsomal fractions. The nature of the dynamic incubation provides flexibility in the exposure of multiple compounds, multiple sampling from the same tissue, and temporal exposure of compounds to better study pharmacokinetic and pharmacodynamic factors. These may result in drug induction, inhibition, or alteration of metabolic pathway(s).
8. Future investigations into this model would reinforce the concept that toxicity is indeed a balance in retaining homeostasis, where Phase I and Phase II sequential metabolism is an important contributor to the amelioration of potential cytotoxicity. Using this method, it will become possible to correlate metabolic bioactivation with markers of toxicity (*see Note 5*).

4. Notes

1. While only one reference is cited, there is an extensive literature on liver slices methods that readers should consult before undertaking these experiments. For a typical preparative scheme, *see ref. 6*.
2. For brevity, we have not incorporated all the compounds reported. Others include dichlorobenzenes, acetaminophen, chloroform, and bromotrichloromethane.
3. Substrates have been characterized for FAD-containing monooxygenase in microsomal preparations; however, sensitive analytical quantification methods, such as HPLC-mass spectrometry, have not been developed for these metabolic probes for Liver Slice Technology.
4. Recent studies have served to highlight caveats and pitfalls with the use of liver slices as a metabolic scaling model for understanding the behavior of compounds *in vivo*; however, their use in elucidation of toxicological processes involving integrated metabolism has yet to be explored.

5. Construction of a database from metabolic profiles of defined families of xenobiotics will enable this technology to be used as a rapid *in vitro* tool to support drug discovery and development.

References

1. Ekins, S., Williams, A., Murray, G. I., Burke, M. D., Marchant, N. C., Engeset, J., and Hawksworth, G. M. (1996) Xenobiotic metabolism in rat dog, and human precision-cut liver slices, freshly isolated hepatocytes and vitrified precision-cut liver slices. *Drug Metab. Dispos.* **24**, 990–995.
2. Sidelmann, U. G., Cornett, J., Tornelund, J., and Hansen, S. H. (1996) A comparative study of precision cut liver slices, hepatocytes and microsomes from wistar rat using metronidazole as a model substrate. *Xenobiotica* **26**, 709–722.
3. Carlile, D. J., Katayoun, Z., and Houston, B. J. (1997) Scaling factors to relate drug metabolic clearance in hepatic microsomes, isolated hepatocytes and the intact liver: Studies with induced livers using Diazepam. *Drug Metab. Dispos.* **25**, 903–911.
4. Ruegg, C. E., Gandolfi, A. J., Nagle, R. B., and Brendel, K. (1987) Differential patterns of injury to the proximal tubule of renal cortical slices following *in vitro* exposure to mercuric chloride, potassium dichromate, or hypoxic conditions. *Toxicol. Appl. Pharmacol.* **90**, 261–273.
5. Stefaniak, M. S., Krumdieck, C. L., Spall, R.D., Gandolfi, A. J., and Brendel, K. (1992) Biochemical and Histological characterization of agar-filled precision cut lung slices in dynamic organ culture as an *in vitro* tool. *In Vitro Toxicol.* **5**, 7–19.
6. Parrish, A. R., Shipp, N. G., Spall, R. D., Dorr, R. T., Krumdieck, C. L., Gandolfi, A. J., and Brendel, K. (1992) Organ culture of rat myocardial slices: An alternative *in vitro* tool in organ-specific toxicology. *Toxicol. Methods* **2**, 101–111.
7. Lake, B. G., Beamand, J. A., Japenga, A. C., Renwick, A., Davies, S., and Price, R. J. (1993) Induction of cytochrome P 450 dependent enzyme activities in cultured rat liver slices. *Food Chem. Toxicol.* **31**, 377–386.
8. Beamand, J. A., Price, R. J., Cunninghame, M. E., and Lake, B. G. (1993) Culture of precision-cut liver slices: effect of some peroxisome proliferators. *Food Chem. Toxicol.* **31**, 137–147.
9. Ghokale, M. S., Bunton, T. E., Zurlo, J., and Yeager, J. D. (1997) Cytochrome P 450 isozyme activities in cultured rat and mouse liver slices. *Xenobiotica* **27**, 341–355.
10. Lake, B. G., Ball, S. E., Renwick, A., Tredger, J. M., Kao, J., Beamand, J. A., and Price, R. J. (1997) Induction of CYP 3A isoforms in cultured precision cut human liver slices. *Xenobiotica* **27**, 1165–1173.
11. VandenBranden, M., Wrighton, S. A., Ekins, S., Gillespie, J. S., Binkley, S. N., Ring, B. J., et al. (1998) Alterations of the catalytic activities of drug-metabolizing enzymes in cultures of human liver slices. *Drug Metab. Dispos.* **26**, 1063–1068.

12. Dogetrom, P. and Rothuzien, J. (1993) A species comparison of tolbutamide metabolism in precision-cut liver slices from rats and dogs. *Drug Metab. Dispos.* **21**, 705–709.
13. Kane, A. S. and Thohan, S. (1996) Dynamic culture of fish hepatic tissue slices to assess phase I and phase II biotransformation, in *Techniques in Aquatic Toxicology* (Ostrander, G.K., ed.), CRC Press, Boca Raton, FL, pp. 371–391.
14. Ekins, S. (1996) Short term maintenance of phase I and phase II metabolism in precision-cut liver slices in dynamic organ culture. *Drug Metab. Dispos.* **24**, 364–366.
15. Chenery, R. J. (1988) The utility of hepatocytes in drug metabolism studies, in *Progress in Drug Metabolism and Disposition*, vol. 11 (Gibson, G. G., ed.), Taylor and Francis, London, pp. 217–265.
16. Paine, A. J. (1990) The maintenance of cytochrome P-450 in rat hepatocyte cultures to the study of drug metabolism, toxicity and induction of the P-450 system. *Chem. Biol. Interact.* **74**, 1–31.
17. Smith, P. F., Gandolfi, A. J., Krumdieck, C. L., Putnam, C. W., Zukoski, C. F., Davis, W. M., and Brendel, K. (1985) Dynamic organic culture of precision cut liver slices for *in vitro* toxicology. *Life Sci.* **36**, 1367–375.
18. Thohan, S. and Chung, H. (1999) Cytotoxicity profiles for a series of investigational compounds using Liver Slice Technology and human derived cell cultures, in *Toxicity Assessment Alternatives: Methods Issues and Alternatives* (Salem, H. and Katz, S. A., eds.), Humana Press, Totowa, NJ, pp. 35–52.
19. Barr, J., Brendel, K., Sipes, I. G., and Weir, A. J. (1991) Liver slices in dynamic organ culture. I. An alternative *in vitro* technique for the study of rat hepatic drug metabolism. *Xenobiotica* **21**, 331–339.
20. Fisher, R. L., Shaughnessy, R. P., Jenkins, P. M., Austin, M. L., Roth, G. L., Gandolfi, A. J., and Brendel K. (1995) Dynamic organ culture is superior to multiwell plate culture for maintaining precision-cut tissue slices: optimization of tissue culture. *Toxicol. Methods* **5**, 99–113.
21. Ekins, S., Murray, G. I., Burke, M. D., Williams, A., Marchant, N. C., and Hawksworth, G. M. (1995) Quantitative differences in phase I and II metabolism between rat precision-cut liver slices and isolated hepatocytes. *Drug Metab. Dispos.* **23**, 1274–1279.
22. Smith, P. F., Fisher, R., Shubat, P. J., Gandolfi, A. J., Krumdieck, C. L., and Brendel, K. (1987) *In vitro* cytotoxicity of allyl alcohol and bromobenzenes in a novel organ culture system. *Toxicol. Appl. Pharmacol.* **87**, 509–522.
23. Thomas, L., DeFeo, B., Mariani, M. F., and Van Rossum, G. D. V. (1989) Comparison of metabolic effects of carbon tetrachloride and 1,2-dichloroethane added *in vitro* to slices of rat liver. *In Vitro Toxicol.* **3**, 59–68.
24. Connors, S., Rankin, D. R., Gandolfi, A. J., and Brendel, K. (1990) Cocaine hepatotoxicity in cultured liver slices: A species comparison. *Toxicology* **61**, 171–190.

25. Sawyer, J. S., Daller, J. A., Brendel, K., Yohem, K., and Putnam, C. (1994) The hepatotoxicities of endotoxin and ethanol: comparisons *in vitro* using the precision-cut liver slice model. *Life Sci.* **55**, 1407–1417.
26. Brodfuehrer, J. I., Chapman, D. E., Wilke, T. J., and Powis, G. (1990) Comparative studies of the *in vitro* metabolism and covalent binding of ¹⁴C-benzene by liver slices and microsomal fraction of mouse, rat, and human. *Drug Metab. Dispos.* **18**, 20–27.
27. Worboys, P. D., Bradbury, A., and Houston, J. B. (1997) Kinetics of drug metabolism in rat liver slices: Relationship between metabolic clearance and slice uptake rate. *Drug Metab. Dispos.* **25**, 460–467.

Cytofluorescence Techniques for the Visualization of Distinct Pools of Protein Thiols at the Single Cell Level

Alfonso Pompella, Silvia Dominici, Caterina Cambiaggi,
Jürgen Frank, and Hans K. Biesalski

1. Introduction

Thiol groups of cysteine residues in protein have long been known as vulnerable sites, prone to alkylation by electrophiles as well as to oxidation by prooxidant agents, with formation in the latter case of intra- and intermolecular disulfide bridges. A number of studies have shown that such modifications of protein thiols are responsible of the cytotoxic effects of several toxins and drugs (*see, e.g., 1–3*). Recent experimental evidence has however documented that alterations in the redox status of cellular protein thiols can also mediate the nontoxic, physiological role exhibited by free radicals and other prooxidant species in modulating the function of growth factor receptors, protein kinases, and transcription factors (*4–6*). Also, the pathophysiological potential of reactions of S-thiolation and dethiolation in the modulation of several enzymatic activities has been established (*7,8*). A simplified outline of the main factors involved in modification of redox status of protein thiols is reported in **Fig. 1**.

Convenient labeling of protein thiols in isolated cells can be achieved by means of thiol-specific reagents, such as iodacetamides or maleimides. Quite a number of such compounds are commercially available, conjugated with a variety of fluorescent or nonfluorescent tags. Here we report procedures employing two distinct conjugated maleimides: 1) tetramethyl-rhodamine-5 (and-6)-maleimide (TRM), which proved in our hands an efficient tool for labelling of whole cellular protein thiols in fixed cells; and 2) 3-(*N*-maleimidylpropionyl) biocytin (MPB), which is a cell-impermeable, nonfluorescent compound useful

From: *Methods in Molecular Biology*, vol. 196: *Oxidants and Antioxidants: Ultrastructure and Molecular Biology Protocols*
Edited by: D. Armstrong © Humana Press Inc., Totowa, NJ

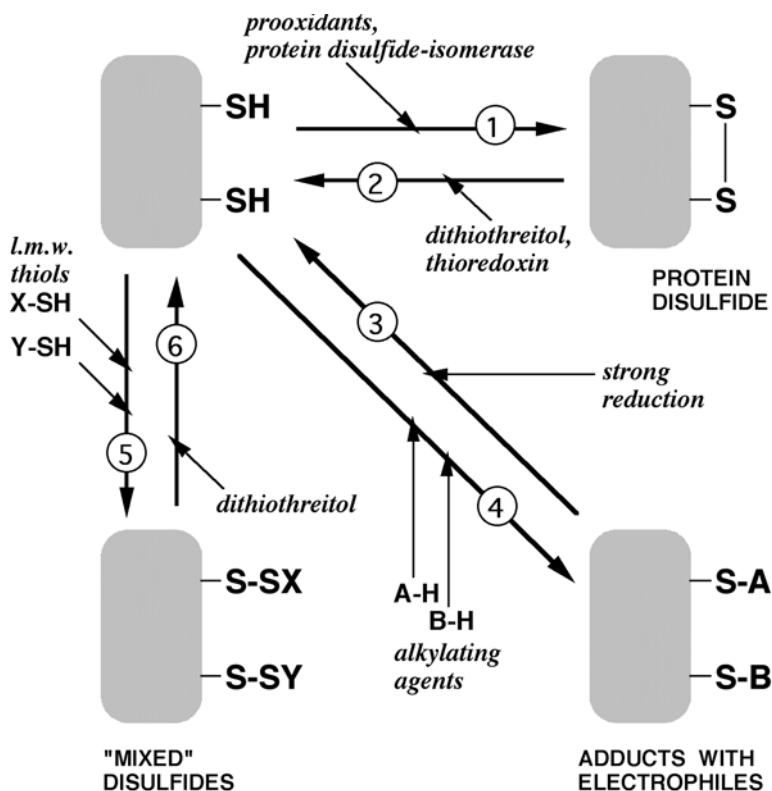


Fig. 1. Factors involved in reversible modification of protein sulfhydryl groups. [1] Protein thiols may be oxidized and form intra- and intermolecular disulfide bonds, due to the action of prooxidant agents (e.g., diamide, hydrogen peroxide, free radicals) as well as following the action of enzyme activities (protein disulfide isomerase). [2] Several reducing agents (e.g., dithiothreitol, 2-mercaptoethanol) can reduce disulfides back to free thiols; such action is enzymatically performed by thioredoxin as well. [3] Electrophilic alkylating agents (e.g., N-ethylmaleimide, iodacetamide, aldehydic compounds) can become covalently bound to protein thiols. [4] Such adducts can be sometimes removed by the action of strong reducing agents, such as Raney nickel. [5] Following the interaction with low molecular-weight thiol compounds (GSSG in the first place), with thiolate anions and with thiyl radicals, protein thiols can be involved in the formation of "mixed disulfides" (protein-S-S-nonprotein compound), a process often termed "protein S-thiolation" (see **ref. 7**). Even in this case, reducing agents such as dithiothreitol can usually recover protein thiols in their reduced form [6].

for labeling surface protein thiols in intact, unfixed cells; the adducts are then made fluorescent by reaction with fluoresceinated avidin. Procedures are presented with special reference to suspensions of isolated cells, but they are also suitable, with minor changes, for labeling of cultured cells growing in monolayers.

2. Materials

2.1. Equipment

1. Polylysine-coated glass slides (Polysine™ microslides, Menzel-Gläser Cat. # 041400); or alternatively, 8-well multitest slides (ICN Biomedicals, Cat. # 6040805). The latter should be coated before use with poly-L-lysine (Sigma, Cat. # P 8920; *see Note 1*).
2. Coplin jars.
3. Humid chambers for processing of slides (e.g., petri dishes with a piece of wet filter paper).
4. Thermostatic water bath.
5. Fluorescence microscope, or confocal fluorescence microscopy apparatus with fluorescein and rhodamine filter sets and adequate computer equipment for image analysis and mass storage of recorded images.

2.2. Reagents

2.2.1. For Labeling of Whole Cell Protein Thiols

1. Diethylether:ethanol, 1:1 (v/v).
2. Tetramethyl-rhodamine-5(and-6)-maleimide (TRM; Molecular Probes, Cat. # T-489).
3. Hank's medium (prepared from powdered salts: Sigma, Cat. # H 6136), Adjust pH to 8.5 with 1N NaOH.
4. Serial dilutions of ethanol: 100, 95, 70, 50, 30% in deionized water.
5. Methanol.
6. Methanol:water, 9:1 (v/v) containing 1 mM HCl.
7. Methanol:saline, 1:1 (v/v).
8. Fluorescein-isothiocyanate (FITC)-extravidin (Sigma, Cat. # 104H-4804).
9. Mounting solution: glycerol, 90% (v/v) in Tris-HCl buffer, pH 8.8.

2.2.2. For Selective Labeling of Cell Surface Protein Thiols

1. Paraformaldehyde (Sigma, Cat. # P 6148), 2% solution (w/v) in PBS. Alternatively, trichloroacetic acid, 10% solution (w/v) in deionized water.
2. 3-(*N*-maleimidylpropionyl)biocytin (MPB; Molecular Probes, Cat. # M-1602).
3. Na-acetate buffer, pH 3.9.
4. Phosphate-buffered saline (PBS), pH 7.4 and pH 8.5.
5. Fluorescein-isothiocyanate (FITC)-extravidin (Sigma, Cat. # 104H-4804).
6. Mounting solution: glycerol, 90% (v/v) in Tris-HCl buffer, pH 8.8.

3. Methods

3.1. Fluorescent Labeling of Whole Cell Protein Thiols

All steps are performed at room temperature for the indicated times.

1. Smears of cells from suspensions can be performed on Polysine™ microslides, and allowed to air-dry prior to fixation with one of the fixatives described below. Alternatively, drops (25–35 μ L) of cell suspensions can be applied to polylysine-precoated multitest slides and let to adhere for 30 min at room temperature in a humid chamber prior to fixation (*see Note 1*).
2. Fix cells in diethylether:ethanol, 1:1 (v/v), for 15 min (*see Note 2*).
3. Rehydrate samples by sequentially immersing slides through serial dilutions of ethanol (95, 70, 50, 30%) for 3 min each (*see Note 3*).
4. React fixed cell overnight with 250 μ M tetramethyl-rhodamine-5(and-6)-maleimide (TRM) in Hank's medium, pH 8.5, at 30°C in a thermostatic water bath.
5. Wash the samples in three changes of Hank's medium (3 min each).
6. Dehydrate samples by sequentially immersing slides through serial dilutions of ethanol (30, 50, 70, and 95%) for 3 min each.
7. Immerse samples in methanol for 20 min.
8. Immerse samples in methanol:water, 9:1 (v/v) containing 1 mM HCl (5 min).
9. Immerse samples in methanol:saline, 1:1 (v/v) for 5 min (*see Note 4*).
10. Rehydrate samples by sequentially immersing slides in 50% ethanol, 30% ethanol, and then deionized water.
11. Mount slides in 90% glycerol/Tris, pH 8.8, carefully removing excess mounting solution.
12. Analyze samples with a fluorescence microscope or a confocal apparatus, using a red fluorescence filter set (excitation 514 nm, barrier filter 550 nm). Slides can be stored at 4°C in the dark up to several days.

3.2. Selective Fluorescent Labeling of Protein Thiols of the Cell Surface

In this case, cells are best processed without prior fixation (*see Note 5*). All steps are performed at room temperature.

1. Apply aliquots of cell suspension to polylysine-precoated wells of multitest slides (25–35 μ L/well) and let cells to adhere for 30 min at room temperature in a humid chamber.
2. Carefully remove excess liquid with the aid with the aid of micropipets and filter paper (*see Note 6*).
3. Wash gently wells with PBS, pH 7.4 (3 times, 3 min each).
4. React samples for 30 min with MPB, 25 μ g/mL in PBS, pH 8.5, in a humid chamber.

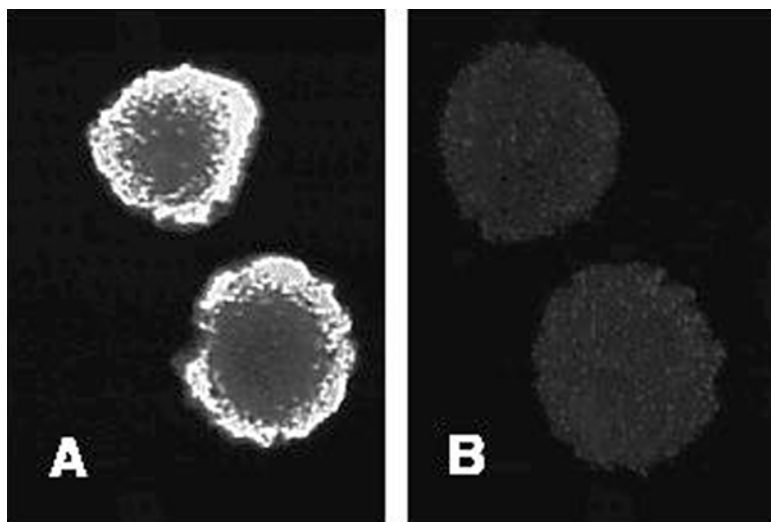


Fig. 2. Loss of protein thiols following exposure of HPBALL leukaemic cells to the reactive product of lipid peroxidation, 4-hydroxynonenal (4-HNE). Visualization of total cell protein thiols by means of TRM. Confocal images of fluorescence intensities were obtained with a BioRad MRC-500 apparatus equipped with an argon laser (*see ref. 10* for details of analytical conditions). (A) Control, untreated cells; the reaction is considerably higher in cytoplasm as compared to cell nucleus. (B) Cells treated with 10 μM 4-HNE for 20 min; extensive loss of TRM-reacting protein thiols has occurred.

5. Wash the samples once in PBS, pH 7.4, and then in three changes of Na-acetate buffer, pH 3.9 (5 min each).
6. Remove excess liquid. Add 25–35 μL /well of a 1 : 100 dilution of FITC-extravidin in PBS, pH 7.4 and incubate for 30 min in a humid chamber.
7. Wash the samples in Na-acetate buffer, pH 3.9 for 5 min at room temperature.
8. Mount slides in 90% glycerol/Tris, pH 8.8, carefully removing excess mounting solution.
9. Analyze samples with a fluorescence microscope or a confocal apparatus, using a green fluorescence filter set (excitation 488 nm, barrier filter 515 nm). Slides can be stored up to several days at 4°C in the dark in a humid chamber.

3.3. Results

Examples of detection of protein thiols in isolated cells by means of the described procedures are shown in **Figs. 2** and **3**. Analysis of specimens is improved when a confocal fluorescence microscopy apparatus can be used, as is the case of images reported. However, satisfactory results can be obtained

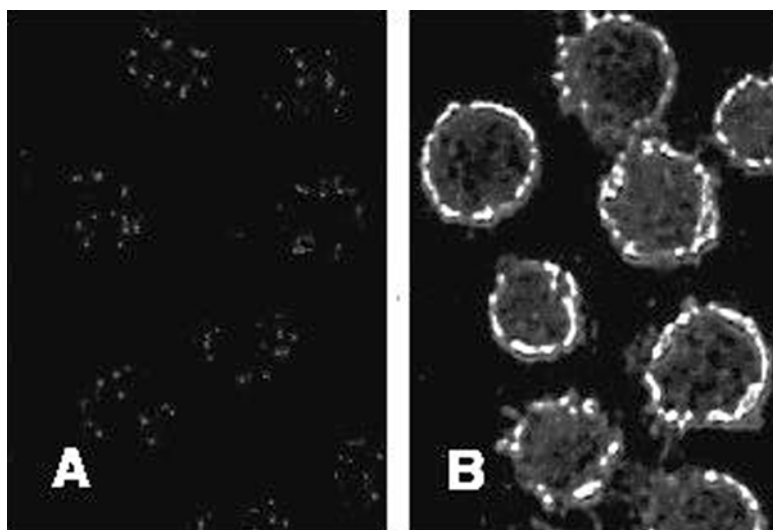


Fig. 3. Reduction of protein thiols at the cell surface following the treatment of U937 lymphoma cells with dithiothreitol (DTT). Selective labeling of cell surface protein thiols by means of MPB. Confocal images of fluorescence intensities were obtained with a BioRad MRC-500 apparatus equipped with an argon laser (*see ref. 10* for details of analytical conditions). (A) Control, untreated cells. (B) Cells exposed to 5 mM DTT for 15 min; a thin rim of fluorescence indicates the appearance of protein thiols at the cell surface, likely as a result of the reduction of preexisting disulfides.

with conventional fluorescence microscopy as well. MPB-labeling of cell surface protein thiols has been recently employed for the demonstration of prooxidant effects of membrane-bound gamma-glutamyl transpeptidase activity in histiocytic lymphoma cells (9).

4. Notes

1. Multitest slides are useful in order to process simultaneously up to 8 different samples (e.g., different cell treatments) on the same slide. Precoating with polylysine is easily accomplished by immersing multitest slides in 0.1% polylysine solution for 30 min at room temperature; slides are then gently rinsed with deionized water and let to air dry before use. After cell adherence, fixative (35–50 μ L/well) is added to multitest slides lying horizontally on their back. After fixation, multitest slides can be then immersed vertically in Coplin jars for washes and all other steps.
2. 10% TCA or 2% paraformaldehyde can also be used for fixation. Choice of fixative should be done by attempts, depending on the cell type and/or the experimental treatments to which cells are exposed before cytochemical processing.

3. This step is omitted with samples fixed in aqueous media (10% TCA or 2% paraformaldehyde), and substituted for with three washes in deionized water (3 min each).
4. Extensive washing of TRM-treated samples in methanol etc. is required in order to remove soluble thiols species and all reagent nonspecifically bound to cellular lipids.
5. MPB cannot cross the plasma membrane of intact cells, and its reaction is therefore restricted to thiols of proteins of the cell surface.
6. Depending on the cell types and/or the experimental treatments used, adherence of cells to multitest slides may be unsatisfactory. In this case, we have verified that fixation with 10% TCA (5 min) followed by three washes in deionized water (3 min each) can be conveniently used, without affecting the selectivity of MPB reaction with the cell surface.

Acknowledgments

The financial support of the Associazione Italiana Ricerca sul Cancro (A.I.R.C.), the Association for International Cancer Research (UK), and of the Italian Ministry for Education and Scientific Research (Cofinanziamento 98) is gratefully acknowledged. The authors wish to thank Prof. M. Comporti (University of Siena, Italy) for his ongoing guidance during their efforts to develop new techniques for the visualization of oxidative stress.

References

1. Moore, M., Thor, H., Moore, G., Nelson, S., Moldeus, P., and Orrenius, S. (1985) The toxicity of acetaminophen and N-acetyl-p-benzoquinone imine in isolated hepatocytes is associated with thiol depletion and increased cytosolic Ca^{2+} . *J. Biol. Chem.* **260**, 13035–13040.
2. Casini, A. F., Maellaro, E., Pompella, A., Ferrali, M., and Comporti, M. (1987) Lipid peroxidation, protein thiols and calcium homeostasis in bromobenzene-induced liver damage. *Biochem. Pharmacol.* **36**, 3689–3695.
3. Pascoe, G. A. and Reed, D. J. (1989) Cell calcium, vitamin E and the thiol redox system in cytotoxicity. *Free Rad. Biol. Med.* **6**, 209–224.
4. Monteiro, H. P. and Stern, A. (1996) Redox modulation of tyrosine phosphorylation-dependent signal transduction pathways. *Free Rad. Biol. Med.* **21**, 323–333.
5. Lander, H. M. (1997) An essential role for free radicals and derived species in signal transduction. *FASEB J.* **11**, 118–124.
6. Sen, CK. (1998) Redox signaling and the emerging therapeutic potential of thiol antioxidants. *Biochem. Pharmacol.* **55**, 1747–1758.
7. Thomas, J. A., Chai, Y.-C., and Jung, C.-H. (1994) Protein S-thiolation and dethiolation. *Methods Enzymol.* **233**, 385–394.
8. Cabiscol, E. and Levine, R. L. (1996) The phosphatase activity of carbonic anhydrase III is reversibly regulated by glutathiolation. *Proc. Nat. Acad. Sci. USA* **93**, 4170–4174.

9. Dominici, S., Valentini, M., Maellaro, E., Del Bello, B., Paolicchi, A., Lorenzini, E., and Tongiani, R. (1999) Redox modulation of cell surface protein thiols in U937 lymphoma cells: the role of γ -glutamyl transpeptidase-dependent H_2O_2 production and S-thiolation. *Free Rad. Biol. Med.* **27**, 623–635.
10. Pompella, A., Cambiaggi, C., Dominici, S., Paolicchi, A., Tongiani, R., and Comporti, M. (1996) Single-cell investigation by laser scanning confocal microscopy of cytochemical alterations resulting from extracellular oxidant challenge. *Histochem. Cell Biol.* **105**, 173–178.

Preparation of Microspheres and Incorporation of Lipid Hydroperoxide for Sustained Release Studies

Donald Armstrong, Hideya Kimura, Kazushi Tamai,
Tsutomu Yasukawa, Mohammed Afzal, and Richard W. Browne

1. Introduction

The development of controlled-release drug-delivery systems that can achieve an effective concentration for a specific period has been investigated using various drug carriers (1).

From the formulation point of view, different drug-delivery systems involving liposomes, mixed micelles, and nanoparticles have shown much promise, as have controlled-release implants based on the use of biodegradable polymers. The latter are one of the more promising drug carriers following incorporation into the microsphere where drugs diffuse through the polymers and diffusion is enhanced by degradation of the matrix. Both pore diffusion and degradation depend on the molecular weight of the polymer and the composition of the copolymers.

Drugs can be delivered by injection (2) or parenterally (3). A variety of compounds have been incorporated into microspheres including steroids (4), angiogenic factors to promote therapeutic neovascularization (5–7), or anti-angiogenic agents to inhibit pathological vascular disorders (7,8). The eye appears to be a promising target organ (9–10), as well as gene therapy in cancer (11). Other applications involve quantification of phagocytosis (12), transport across cells (13,14), induction of excitatory or edematous injury (15), and polymorphic genotyping (16).

On the other hand, caution is advised since some types of microspheres may provoke an inflammatory response (17), or be antimicrobial through their cationic nature (18).

From: *Methods in Molecular Biology*, vol. 196: *Oxidants and Antioxidants: Ultrastructure and Molecular Biology Protocols*
Edited by: D. Armstrong © Humana Press Inc., Totowa, NJ

The present chapter describes a microsphere system for release of two classes of lipid hydroperoxide (LHP), which may be helpful in determining their effect on tissue damage if high, or second-messenger functions if the concentration of LHP is low.

2. Materials

2.1. Equipment

1. Magnetic stirrer HM-19, Koike Precision Instruments (Tokyo, Japan).
2. Sonicator stirrer @-220, Heat System, Ultrasonics, Inc. (New York, NY).
3. Centrifuge.
4. Lyophilizer FDU839, EYELA (Tokyo, Japan).
5. LC-10A high performance liquid chromatograph system with dual pumps, SPD-M10A UV/Vis photodiode array detector, automatic sampler and chromatography data processing software (Shimadzu Inst. Corp, GA); 4.6 mm \times 25 cm Supelcosil C-18 column (5 μ particle size).
6. UV-Vis Spectrophotometer (Shimadzu).

2.2. Reagents

1. Poly(lactic acid) (PLA; molecular weight, 20,000).
2. Poly(lactic-glycolic acid) (PLGA; molecular weight, 5,000).
3. Poly(vinyl alcohol) (PVA; molecular weight, 66,000).

3. Methods

3.1. Preparation of LHP

1. Linoleic acid (18:2) and docosahexaenoic acid (22:6) are prepared from Type 1-B soybean lipoxidase as described in Protocols volume 108 (19).
2. Purity was determined by HPLC at >95% for the 13-isomer and <5% for the 9-isomer (20) using a mobile phase consisting of acetonitrile, tetrahydrofuran-0.025 parts acetic acid in water (41:41:18).
3. Concentration is calculated from UV absorbance at 234–236 nm using appropriate extinction coefficients (20).

3.2. Preparation of Microspheres

1. Polylactide microspheres of 5,000 MW containing 12–18 mg of 18:2 LHP, or 9 mg of 22:6 LHP are prepared by the solvent evaporation method (4).
2. Dissolve 10 mg of LHP and 90 mg of each polylactide polymer in 5 mL of methylene chloride at room temperature.
3. Pour the above solution rapidly into 10 mL of 2 wt% PVA aqueous solution, and then emulsify the mixture with a sonicator at 60 W for 2 min (see Note 1).
4. Add the emulsion to 290 mL of 2 wt% PVA aqueous solution and agitate using a magnetic stirrer for 8 h at 30°C until methylene chloride is completely evaporated (see Note 2).

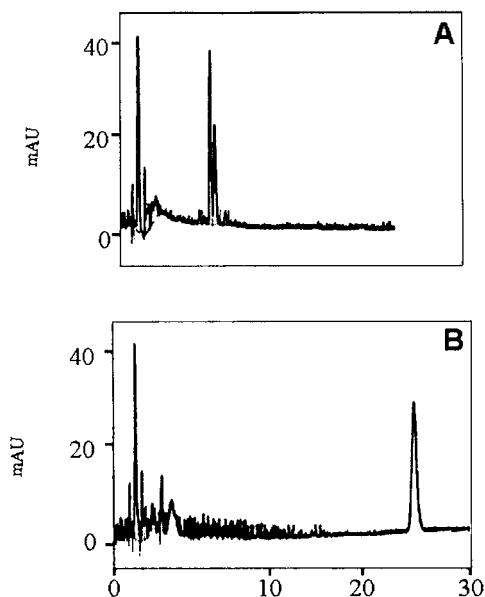


Fig. 1. Confirmation of 18:2 LHP (A) and 22:6 LHP (B) in microspheres. Elution times are 8 and 25 min, respectively.

5. Centrifuge the resulting microspheres at 10,000 rpm at 0°C for 15 min.
6. Discard the supernatant and wash the microspheres four times with cold distilled water.
7. Centrifuge the microspheres at 5,000 rpm at 0°C for 15 min, lyophilize, and store at -80°C until use.

3.3. Results

3.3.1. Linoleic Acid Hydroperoxide

1. One mg of microspheres is suspended in 1 mL of acetonitrile which dissolves the microsphere and releases LHP (*see Note 3*).
2. Ten μL is injected onto a LC-18 column and LHP identity is confirmed (**Fig. 1**). Isomeric species are determined to confirm that no transformations or hydrolysis have occurred during incorporation into the microspheres. This scan is identical to the original LHP. The amount recovered is calculated at 234–236 nm from peak area (x-axis) and standard curve (**Fig. 2**) of original LHP (**Subheading 3.1.**). Construct a plot for relationships of LHP concentration (y_1 -axis) to weight of microsphere (y_2 -axis) (**Fig. 2**).

3.3.2. Docosahexaenoic Acid Hydroperoxide

1. Follow same procedure as described in **Subheading 3.3.1.** and prepare plot of LHP concentration, to weight of microsphere (**Fig. 3**).

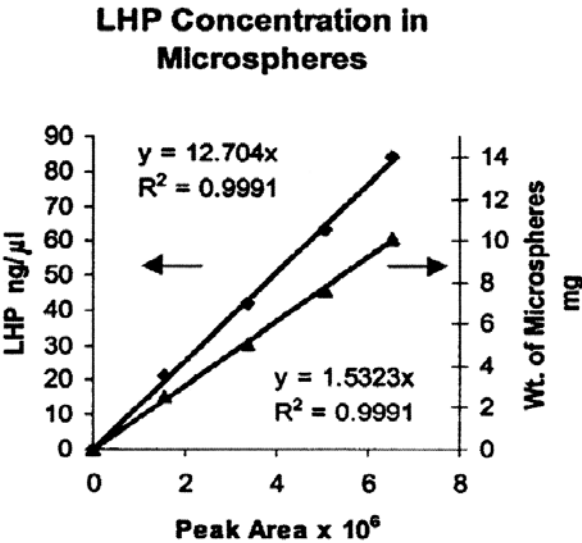


Fig. 2. Standard curve for 18:2 LHP in microspheres after complete extraction (■ = LHP concentration; ▲ = weight of microsomes).

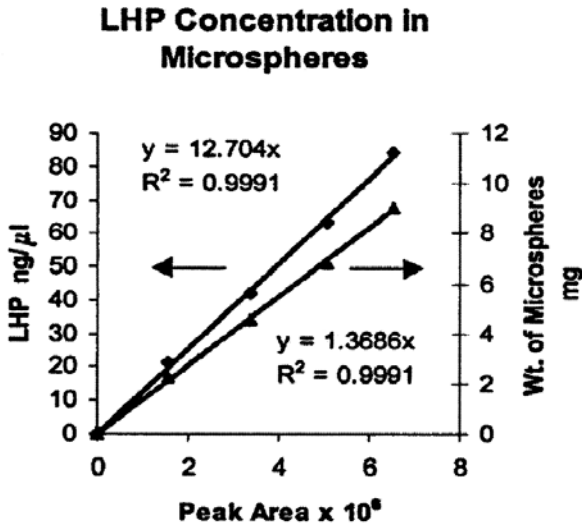


Fig. 3. Standard curve for 22:6 LHP in microspheres after complete extraction. (■ = LHP concentration; ▲ = weight of microsomes).

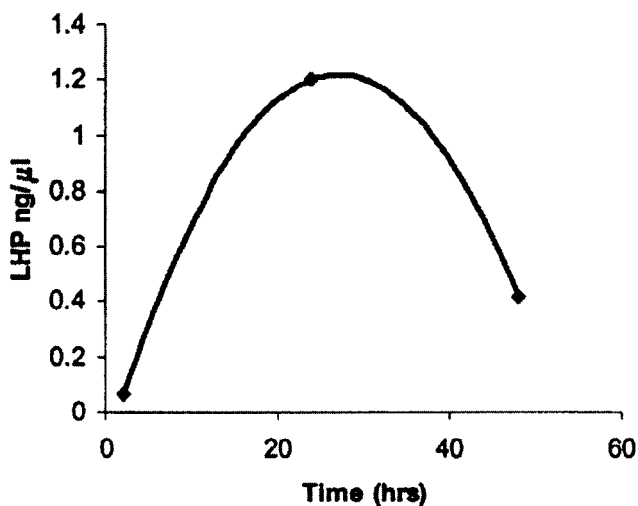


Fig. 4. Release profile of 18:2 LHP from microspheres as a function of time.

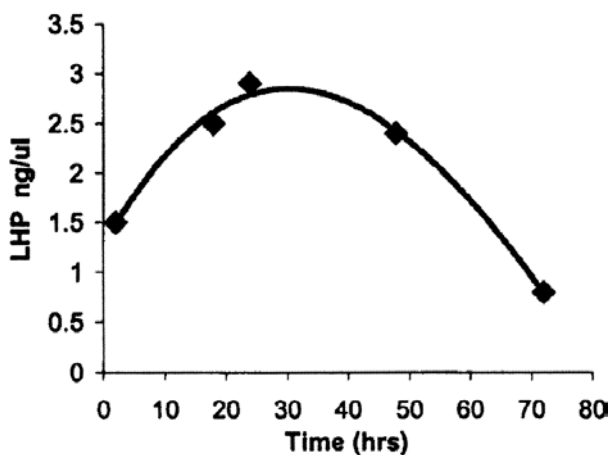


Fig. 5. Release profile for 22:6 LHP from microspheres as a function of time.

3.3.3. Kinetics

1. To determine rate of LHP release from microspheres, add 1 mL of HPLC-grade water containing 30% ethanol to 1 mg of microspheres (*see Note 4*).
2. Sample at daily intervals until there is no LHP remaining.
3. Plot concentration vs time (**Figs. 4 and 5**). The curve can be used as an estimate of biodegradation for in vivo/in vitro studies.

4. Remove 10 μL aliquot of appropriate LHP and inject onto LC-18 column to determine concentration. Replace with equal volume of water.

4. Notes

1. Low MW polymers used to prepare microspheres form aggregates that dissolve more slowly than high MW polymers. Addition of a surfactant such as Tween 80 may be helpful.
2. Other types of solvents may be used.
3. Caution should be taken not to contaminate the supernate with microsphere particles.
4. The release is dependent on type of polymers and type of LHP used in microsphere preparations.

References

1. Benita, F. (1996) Microencapsulation: methods and industrial applications, vol. 73, in *Biodegradable Microspheres: Advances in Production Technology* (Benita, S., ed.), Marcel Dekker, New York, NY, pp. 35–72.
2. Jain, R. A., Rhodes, C. T., Railkar, A. M., Malick, A. W., and Shah, N. H. (2000) Controlled release of drugs from injectable in situ formed biodegradable PLGA microspheres: effect of various formulation variables. *Eur. J. Pharm. Biopharm.* **50**, 257–262.
3. Witt, C. and Kissel, T. (2001) Morphological characterization of microspheres, films and implants prepared from poly(lactide-co-glycolide) and ABA triblock copolymers: is the erosion controlled by degradation swelling or diffusion? *Eur. J. Pharm. Biopharm.* **51**, 171–181.
4. Beck, L. R., Cowsar, D. R., Lewis, D. H., Cosgrove, R. J., Riddle, C. T., and Epperly, S. L. (1979) A new long-acting injectable microcapsule system for the administration of progesterone. *Fertil. Steril.* **31**, 545–554.
5. Kimura, H., Spee, C., Sakaoto, T., Hinton, D. R., Ogura, Y., Tabata, Y., Ikada, Y., and Ryan, S. J. (1999) Cellular response in subretinal neovascularization induced by bFGF-impregnated microspheres. *Invest. Ophthalmol. Vis. Sci.* **40**, 524–528.
6. Arras, M., Mollnau, H., Strasser, R., Wenz, R., Ito, W. D., and Schaper, S. J. (1998) The delivery of angiogenic factors to the heart by microsphere therapy. *Nat. Biotechnol.* **16**, 159–162.
7. Tabata, Y., Hijikata, S., Muniruzzaman, M., and Ikada, Y. (1999) Neovascularization effect of biodegradable gelatin microsphere incorporating basic fibroblast growth factor. *J. Biomater. Sci. Polym. Ed.* **10**, 79–94.
8. Yasukawa, T., Kimura, H., Tabata, T., Miyamoto, H., Honda, Y., and Ikada, Y. (1999) Targeted delivery of anti-angiogenic agent TNP-470 using water-soluble polymer in the treatment of choroidal neovascularization. *Invest. Ophthalmol. Vis. Sci.* **40**, 2690–2696.
9. Kimura, H., Ogura, Y., Moritera, T., Honda, Y., Wada, R., and Hyon, S. H. (1992) Injectable microspheres with controlled drug release for glaucoma filtering surgery. *Invest. Ophthalmol. Vis. Sci.* **33**, 3436–3441.

10. Ogura, Y. and Kimura, H. (1995) Biodegradable polymer microspheres for targeted drug delivery to the retinal pigment epithelium. *Surv. Ophthalmol.* **1**, S17–S24.
11. Dass, C. R., Walker, T. L., Kalle, W. H., and Burton, M. A. (2000) A microsphere-liposome (microplex) vector for targeted gene therapy of cancer. II. In vivo biodistribution study in a solid tumor model. *Drug Deliv.* **7**, 15–19.
12. Bassoe, C. F., Smith, I., Sornes, S., Halstensen, A., and Lehmann, A. K. (2000) Concurrent measurement of antigen- and antibody-dependent oxidative burst and phagocytosis in monocytes and neutrophils. *Methods* **21**, 203–220.
13. Torche, A. M., Jouan, H., Le Corre, P., Albina, E., Primault, R., Jestin, A., and Le, V. R. (2000) Ex vivo and in situ PLGA microspheres uptake by pig ileal Peyer's patch segment. *Int. J. Pharm.* **201**, 15–27.
14. Pettet, G. J., Please, C. P., Tindall, M. J., and McElwain, D. L. (2001) The migration of cells in multicell tumor spheroids. *Bull. Math. Biol.* **63**, 231–257.
15. Johnson, L. J., Hanley, D. F., and Thakor, N. V. (2000) Optical light scatter imaging of cellular and sub-cellular morphology changes in stressed rat hippocampal slices. *J. Neurosci. Methods* **98**, 21–31.
16. Armstrong, B., Stewart, M., and Mazumder, A. (2000) Suspension arrays for high throughput, multiplexed single nucleotide polymorphism genotyping. *Cytometry* **40**, 102–108.
17. Jackson, J. K., Springate, C. M., Hunter, W. L., and Burt, H. M. (2000) Neutrophil activation by plasma opsonized polymeric microspheres: inhibitory effect of pluronic F127. *Biomaterials* **21**, 1483–1491.
18. Carmona-Ribeiro, A. M. (2000) Interactions between cationic liposomes and drugs or biomolecules. *An. Acad. Bras. Cienc.* **72**, 39–43.
19. Armstrong, D. and Browne, R. (1998) Synthesis of lipid and cholesterol hydroperoxide standards, in *Free Radical and Antioxidant Protocols* (Armstrong, D., ed.), Humana Press, Inc., Totowa, NJ, pp. 139–145.
20. Browne, R. and Armstrong, D. (1998) Separation of hydroxy and hydroperoxy polyunsaturated fatty acids by high-pressure liquid chromatography, in *Free Radical and Antioxidant Protocols* (Armstrong, D., ed.), Humana Press, Inc., Totowa, NJ, pp. 147–155.

Measurement of Carotenoids in the Living Primate Eye Using Resonance Raman Spectroscopy

Paul S. Bernstein and Werner Gellermann

1. Introduction

The xanthophyll carotenoids lutein and zeaxanthin (*see Note 1*) are specifically concentrated in the macula of the primate eye, the region of the retina responsible for high-resolution visual acuity necessary for reading, driving, and recognizing faces. They are thought to protect the macula from light-induced oxidative damage by acting as light-screening filters for short wavelength visible light and by acting as *in situ* antioxidants to prevent oxidative damage to polyunsaturated membrane lipids (*1,2*). Since high dietary intakes and blood levels of lutein and zeaxanthin have been epidemiologically associated with a lower risk of visual loss from age-related macular degeneration (AMD) (*3,4*), there has been considerable interest in measuring carotenoid macular pigment levels in living human eyes as a possible early test to detect individuals at high risk for visual loss from AMD. The current most commonly used method, psychophysical heterochromatic flicker photometry, has significant drawbacks since it is a subjective test that requires an attentive observer with good visual acuity, and it has a high intrasubject variability that may exceed $\pm 50\%$ (*5,6*), which tends to limit its utility as a screening or diagnostic test. We have developed an alternative objective measurement method based on the principles of resonance Raman spectroscopy. This method is rapid, specific, sensitive, and highly reproducible, characteristics conducive to its use as a screening and diagnostic test on large populations with a wide range of visual acuities.

Raman spectra of molecules are generated from inelastically scattered laser light. Raman active molecules have a characteristic Raman scattering spectrum ("Raman signature"), originating from specific vibrational/rotational modes of

From: *Methods in Molecular Biology*, vol. 196: *Oxidants and Antioxidants: Ultrastructure and Molecular Biology Protocols*
Edited by: D. Armstrong © Humana Press Inc., Totowa, NJ

the molecule (*see* **Note 2**). Carotenoids exhibit strong Raman scattering signals at ~ 1160 and $\sim 1525\text{ cm}^{-1}$ associated with the vibrational modes of their long polyene backbone. When the excitation laser wavelength spectrally overlaps the carotenoids' absorption band in the blue/green wavelength range, the Raman signals are resonantly enhanced many orders of magnitude.

Initial studies in our laboratory demonstrated that carotenoid resonance Raman spectra could be recorded from the macula of excised human retina and from human eyecups (7). When the macula was illuminated with a large laser spot, we were able to demonstrate a linear correlation between Raman signal strength and carotenoid levels determined by high-performance liquid chromatography (HPLC) (7). We report here an extension of our Raman carotenoid detection technology to living primates. Our results are very promising and indicate that it will be possible to measure macular pigment levels in living human eyes using light illumination strengths that are well within American National Standards Institute (ANSI) safety standards for direct illumination of the retina (8).

2. Materials

2.1. Equipment

1. 50 mW air-cooled argon ion laser (model HN 61, National Laser, Inc., Salt Lake City, UT).
2. 10 mW He-Ne laser (model 05 LHR 991, Melles Griot, Inc., Irvine, CA).
3. Laser power meter (Laser Mate-Q, Coherent, Inc., Auburn, CA).
4. Raman spectrometer components (*see* **Subheadings 3.1.** and **3.2.** for details).
5. Personal computer with spectral analysis software (KestrelSpec for Windows, Catalina Scientific Corporation, Tucson, AZ).
6. Optical components (lenses, beam splitters, filters, slits, fiber optics) (Edmund Scientific, Inc., Barrington, NJ).
7. Fundus camera (model FF2, Carl Zeiss, Inc., Thornwood, NJ).
8. HPLC system (Waters, Inc., Milford, MA) consisting of two model 501 pumps, a model 486 variable wavelength detector, a Rheodyne 7725i injector, and a personal computer with data management and integration software.
9. HPLC column: Rainin Microsorb-MV cyano 100 Å, 5 μm , $250 \times 4.6\text{ mm}$ from Varian, Inc. (Walnut Creek, CA).

2.2. Reagents

1. Lutein and zeaxanthin standards were supplied by Kemin Foods (Des Moines, IA) and by Hoffmann-La Roche, Inc. (Basel, Switzerland), respectively.
2. HPLC solvents and other laboratory chemicals (hexane, dichloromethane, methanol, tetrahydrofuran, diisopropylethylamine, butylated hydroxytoluene) were obtained from Fisher Scientific (Pittsburgh, PA) or Sigma Chemicals (St. Louis, MO).

3. Eye drops (1% tropicamide, 2.5% neosynephrine, and normal saline) were purchased from a local pharmacy.

3. Methods

3.1. *In Vitro* Measurement of Carotenoids Using Resonance Raman Spectroscopy

1. In our initial experiments we used a research-grade Raman instrument to measure carotenoid standards in solution and dried onto filter paper. The same apparatus can be used without modification for measurements on human retinal eye-cup preparations and flat-mounted retinas. The experimental apparatus is sketched in **Fig. 1**.
2. As an excitation source, the vertically polarized 488 nm line of a 50 mW air-cooled argon ion laser was used. The laser power was reduced to several mW with neutral density filters, and the laser plasma lines were eliminated with a combination of a 600 lines/mm grating and a slit. The laser was directed through a beam splitter and weakly focused onto the sample with a 10 cm focal length lens.
3. The backscattered light was imaged onto the entrance slit of a 0.6 m focal length Spex TripleMate Raman spectrometer (model 1877C-AG, Instruments SA, Inc., Edison, NJ) with the beam splitter and an additional lens. The Raman spectrometer employed two stray light-rejection gratings with 300 lines/mm, a dispersion grating with 1200 lines/mm, and a liquid-nitrogen cooled silicon charge-coupled device (CCD) detector array with 25 μm pixel width (model CH 260, Photometrics, Ltd., Tucson, AZ).

3.2. *In Vivo* Measurement of Macular Carotenoids Using Resonance Raman Spectroscopy

1. For the measurement of carotenoids in the retina of living primates, the Raman instrument was interfaced with a Zeiss FF2 fundus camera to allow the operator to visually locate the macula of the animal and to document the size of the projected laser spot on the retina. The laser delivery and Raman detection optics, along with appropriate beam splitters and filters, were mounted as a custom-built module between the camera's objective lens and the subject's eye.
2. Light exposure of the retina has to be limited to a maximum permissible exposure (MPE), which according to ANSI Z136.1 standards is 2.7 J/cm² (equivalent to a laser power density at the retina of 2.7 mW/mm² for 10 s) (9). To accomplish these lower light levels, we added additional neutral density filters and replaced the Spex monochromator with a smaller monochromator having less spectral resolution but higher light throughput (Monospec 18, Thermovision Colorado, Inc., Grand Junction, CO). We were also able to simplify instrument operation by substituting a Peltier cooled CCD array (model ST-6, Santa Barbara Instruments Group, Inc., Santa Barbara, CA) for the original liquid-nitrogen cooled CCD array.

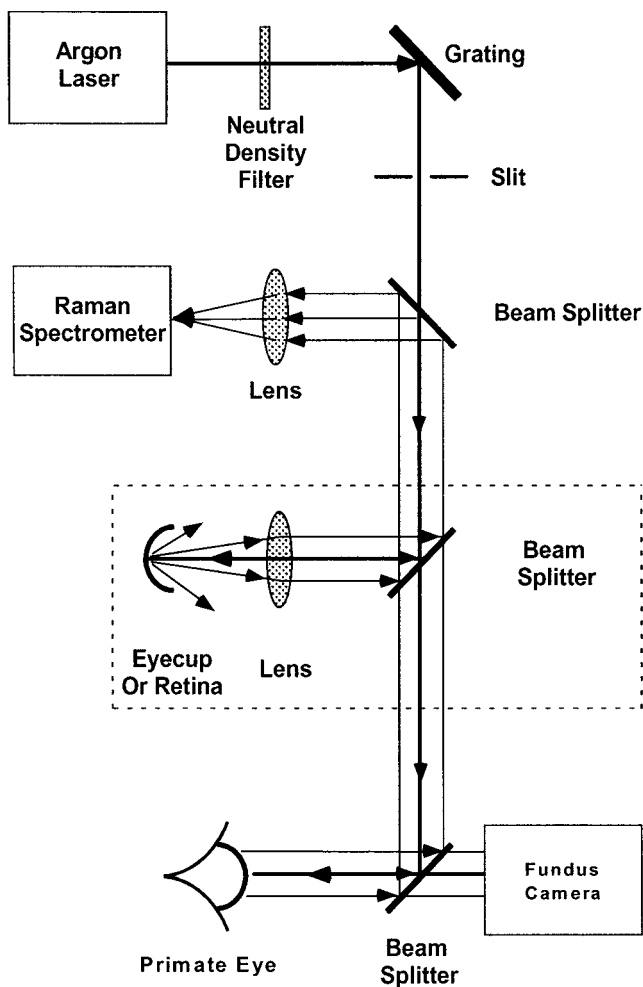


Fig. 1. Experimental setup of the laser Raman instrument for measurement of carotenoids, showing schematically the optical pathways of the laser-excitation beam and the Raman light backscattered into the Raman spectrometer. The dotted box shows the setup for in vitro measurements that required an external focusing lens. For in vivo measurements of primate eyes, the crystalline lens of the eye is used to focus the beam, and the optics are interfaced with a fundus camera permitting direct observation of the macula during measurements.

3. A laboratory cynomolgus monkey (*Macaca fascicularis*) was anesthetized, and its pupils were dilated with 1% tropicamide and 2.5% neosynephrine eye drops. The head was stabilized with a bite bar and head restraint, and a lid retractor was used to keep the eyelids open. Saline drops were administered periodically to

keep the cornea from drying. The 15 μ W He-Ne laser aiming beam was pointed at the center of the macula (the fovea) under direct visualization through the fundus camera. Typical measurements take 1–3 s and are repeated three to seven times.

3.3. HPLC Analysis of Macular Carotenoids

1. After completion of the Raman experiments, the monkey was sacrificed, and the eyes were enucleated. The macula of each eye was dissected out using a 4 mm trephine. The macular tissue was homogenized with sonication into 500 microliters of 50% methanol and extracted into an equal volume of hexane containing 0.5% butylated hydroxytoluene (BHT). 100 microliter portions were analyzed by HPLC using a silica-based cyano column eluted with 80% hexane, 19.4% dichloromethane, 0.5% methanol, and 0.1% diisopropylethylamine at 1 mL/min with monitoring at 450 nm.
2. The integrated peak areas of the lutein and zeaxanthin peaks were converted to nanograms by use of a standard curve generated by diluting solutions of pure lutein and zeaxanthin.

3.4. Results

3.4.1. In Vitro Measurements of Carotenoids Using Resonance Raman Spectroscopy

1. In **Fig. 2** we show the resonance Raman spectrum of lutein spotted on polyvinylidene difluoride (PVDF) filter paper. We observed strong and clearly resolved Raman signals superimposed on a weak fluorescence background. The Raman response is characterized by two prominent lines at 1159 and 1525 cm^{-1} (corresponding to wavelength shifts of 29.2 and 39.3 nm, respectively, for 488 nm excitation), with nearly identical relative intensities. These lines originate, respectively, from carbon-carbon single-bond and double-bond stretch vibrations of the conjugated backbone (**10**). In addition, a weaker but clearly distinguishable Stokes signal appears at 1008 cm^{-1} , which is attributed to rocking motions of the molecule's methyl components (**10**).
2. This experiment shows that strong Raman signals with excellent signal-to-noise ratios are readily obtainable from samples having a retina-like thin film structure. Furthermore it shows that a 180 degree backscattering geometry, as required for Raman measurements of intact human and laboratory primate eyes, poses no inherent problems. We were able to use this apparatus to measure the resonant Raman response from the macula of excised human retinas and human eyecups (**7**). The steep drop in signal strength as a focused laser beam was moved away from the fovea corresponded well with the known distribution of the macular carotenoids. When the macula was illuminated with a large laser spot, we were able to demonstrate a linear correlation between Raman signal strength and carotenoid levels determined by HPLC (**7**).

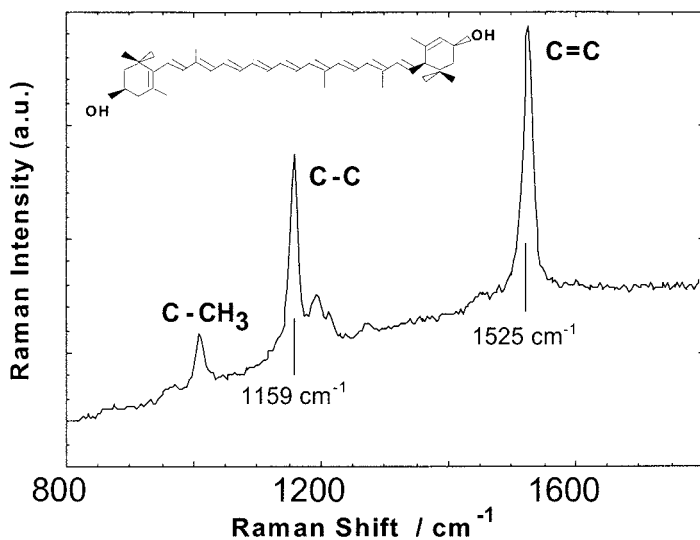


Fig. 2. Resonance Raman spectra of lutein spotted on filter paper, showing the Raman scattering signal intensity (in arbitrary units) as a function of the wavenumber shift (in cm^{-1}) from the 488 nm laser excitation line. Three characteristic strong carotenoid peaks are seen for this retina-like thin film sample at ~ 1004 , 1159, and 1525 cm^{-1} , corresponding to vibrations of the methyl side group, carbon-carbon single bonds, and carbon-carbon double-bonds, respectively. The molecular structure of lutein is also shown.

3.4.2. Resonance Raman Spectroscopy of Macular Carotenoids in the Living Primate Eye

1. A typical resonance Raman spectrum derived from a living primate eye is shown in **Fig. 3**. The spectra are plotted before and after subtraction of the weak fluorescence background. All three characteristic carotenoid Raman peaks are clearly distinguishable with an acceptable signal-to-noise ratio. As expected, nonmacular areas of the retina, where the carotenoid concentration is 100-fold lower, show only background fluorescence without discernable carotenoid Raman peaks.
2. After enucleation of this eye, the macular carotenoids were extracted and quantified by HPLC (**Fig. 4**). When the *in vivo* Raman apparatus is ultimately optimized and standardized, further resonance Raman measurements with HPLC correlation on additional monkeys could be used to generate a calibration curve of detector response vs macular carotenoid content suitable for use in human clinical studies.
3. Based on the experiments described here, we are confident that our resonance Raman technology will allow us to obtain data with good signal-to-noise ratio from living human eyes using light-exposure levels that are below the maximum

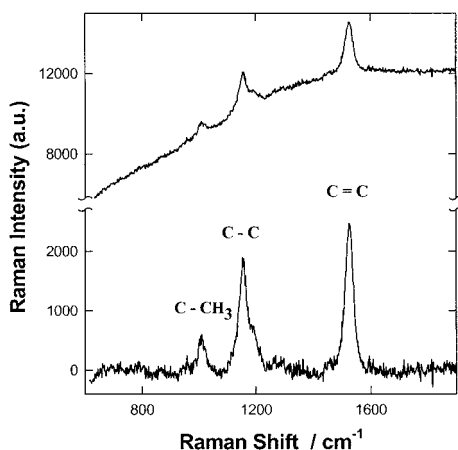


Fig. 3. Resonance Raman spectra of the macula of a living primate eye, showing Raman plots as measured before (upper curve) and after (lower curve) subtraction of the broad background signal originating from fluorescence. The three characteristic carotenoid Raman peaks are again clearly resolvable with good signal-to-noise ratios. Spectra were obtained with laser excitation at 488 nm, power level of 0.8 mW, time exposure of 3 s, and ~300 micrometer spot size on the retina, corresponding to an exposure level of 2.4 J/cm².

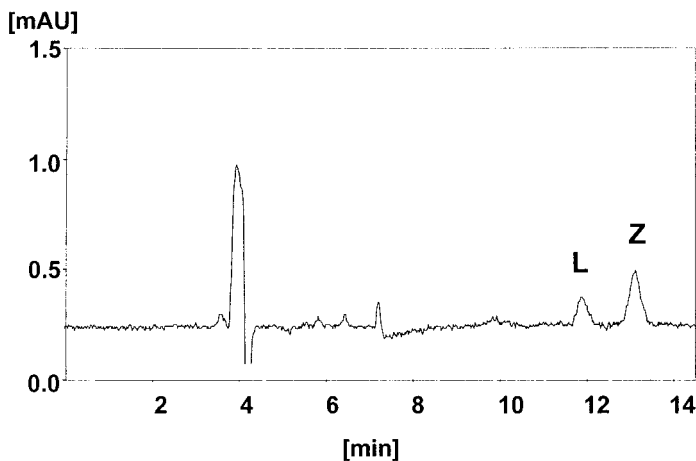


Fig. 4. HPLC chromatogram of extracted carotenoids from the macula of the monkey eye shown in **Fig. 3**. Macular lutein (L) and zeaxanthin (Z) levels were 1.5 ng and 3.6 ng, respectively. See **Subheading 3.3.** for a description of the HPLC methods.

permissible exposure level considered safe by ANSI standards (*see Note 3*) (8). These clinical studies will be invaluable for clarifying the roles of lutein and zeaxanthin in the prevention and treatment of AMD. Also, our apparatus is readily modifiable for Raman measurements of carotenoids and other substances in many other intact human tissues such as skin (11).

4. Notes

1. Lutein and zeaxanthin are members of a large family of $C_{40}H_{56}$ compounds known as the carotenoids. They are commonly synthesized by plants and micro-organisms, but higher animals are unable to synthesize them and therefore must ingest them in the diet. Carotenoids typically have a rigid polyene backbone consisting of nine alternating conjugated carbon-carbon double- and single-bonds. For lutein and zeaxanthin, each end of the conjugated chains is terminated by an ionone ring, and four methyl groups are attached along the polyene backbones. Since hydroxyl groups are attached to the 3- and 3'-positions of each of the ionone rings, these carotenoids are members of the xanthophyll subfamily. Zeaxanthin differs from lutein only in the location of one of the ionone ring double bonds.
2. The electronic absorptions of carotenoid solutions or thin films are strong in all cases and occur in broad bands (~ 100 nm width) in the blue/green wavelength region (~ 450 – 460 nm). They show clearly resolved vibronic substructure with a spacing of ~ 1400 cm^{-1} in the cases of lutein and zeaxanthin. The absorption transitions correspond to a fully allowed electric-dipole transition of the molecule's conjugated π -electron from its 1^1A_g singlet ground state to the 1^1B_u singlet excited state. The transition is strongly broadened by coupling of the electron to vibrational modes of the molecule. Laser excitation of the carotenoids in the long-wavelength shoulder of the absorption band results in a strikingly weak fluorescence band, which is shifted by ~ 70 nm to longer wavelengths. We estimate the quantum efficiency for fluorescence of carotenoids to be as low as $\sim 10^{-5}$. The reason for this very weak fluorescence is the existence of another excited singlet state, 2^1A_g , which lies *below* the 1^1B_u state in polyenes. This state is the energy state from which the fluorescence of the molecule occurs, and since this state has the same symmetry as the ground state, the fluorescence is forbidden. This fact allows us to explore the resonant Raman scattering response of the carotenoid molecules, which occurs in the same wavelength range as the fluorescence and which would be masked by the fluorescence if the latter would be electric-dipole allowed. Since the major Raman spectral lines are derived from the vibrations of the common polyene backbone, most carotenoids have virtually indistinguishable resonance Raman spectra unless very high-resolution instrumentation is used.
3. The monkey experiment in **Fig. 3** used light intensities just below the ANSI limit of 2.7 J/cm^2 . This monkey's 5 ng macular pigment level (**Fig. 4**) was approx one-sixth of the average macular pigment level determined in our laboratory on human autopsy specimens. We have successfully measured macular pigment resonance

Raman carotenoid spectra on living human volunteers with illumination levels as low as 38 mJ/cm².

Acknowledgments

This work was supported by NIH grants EY-11600 and EY-12324, by grants from Research to Prevent Blindness, Inc., New York, New York, and by internal funds of the Dixon Laser Institute. Dr. Nikita Katz, Dr. Igor Ermakov, Dr. Mihoko Yoshida, Dr. Da-You Zhao, Dr. Alexander Yemelyanov, and Robert McClane made substantial contributions toward the success of this project.

References

1. Schalch, W., Dayhaw-Barker, P., and Barker, F. M. (1999) The carotenoids of the human retina, in *Nutritional and Environmental Influences on the Eye* (Taylor, A., ed.), CRC Press, Boca Raton, FL, pp. 215–250.
2. Snodderly, D. M. (1995) Evidence for protection against age-related macular degeneration by carotenoids and antioxidant vitamins. *Am. J. Clin. Nutr.* **62** (suppl.), 1448S–1461S.
3. Eye Disease Case Control Study Group (1993) Antioxidant status and age related macular degeneration. *Arch. Ophthalmol.* **111**, 104–109.
4. Seddon, J. M., Ajani, U. A., Sperduto, R. D., Hiller, R., Blair, N., Burton, T. C., et al. (1994) Dietary carotenoids, vitamins A, C, E and advanced age-related macular degeneration: a multicenter study. *JAMA* **272**, 1413–1420.
5. Landrum, J. T., Bone, R. A., and Kilburn, M. D. (1997) The macular pigment: a possible role in protection from age-related macular degeneration. *Adv. Pharmacol.* **38**, 537–556.
6. Snodderly, D. M. and Hammond, B. R. (1999) *In vivo* psychophysical assessment of nutritional and environmental influences on human ocular tissues: lens and macular pigment, in *Nutritional and Environmental Influences on the Eye* (Taylor, A., ed.), CRC Press, Boca Raton, FL, pp. 251–273.
7. Bernstein, P. S., Yoshida, M. D., Katz, N. B., McClane, R. W., and Gellermann, W. (1998) Raman detection of macular carotenoid pigments in intact human retina. *Inv. Ophthalmol. Vis. Sci.* **39**, 2003–2011.
8. Bernstein, P. S., Gellermann, W., and McClane, R. W. (1999) Method and system for measurement of macular carotenoid levels. United States Patent 5,873,831.
9. ANSI Z136.1-1993. *American National Standards for Safe Use of Lasers*. American National Standards Institute, New York, NY, section 8.3.
10. Koyama, Y., Takatsuka, I., Nakata, M., and Tasumi, M. (1988) Raman and infrared spectra of the all-*trans*, 7-*cis*, 9-*cis*, 13-*cis*, and 15-*cis* isomers of β -carotene: key bands distinguishing stretched or terminal-bent configurations from central-bent configurations. *J. Raman Spectroscopy* **19**, 37–49.
11. Gellermann, W., McClane, R.W., Katz, N.B., and Bernstein, P.S. (2001) Method and apparatus for noninvasive measurement of carotenoids and related chemical substances in biological tissue. United States Patent 6,205,354.

Interstitial Photodynamic Therapy with Moving Exposure Fiber

Toru Hirano, Yasuo Hashimoto, Hideo Tanaka,
Ichirou Yamada, and Kenji Hashimoto

1. Introduction

Photodynamic therapy (PDT) is a cancer treatment modality, based on the synergistic photochemical reaction between tumor cells containing accumulated photosensitizer and laser light. The mechanisms of killing of malignant cells were studied by several researchers (1–3). Photosensitizers accumulate more in malignant cells than in normal cells, and this concentration difference contributes to the selective killing of the malignant cells. In general, the transmissivity of light in tissue seems to be low and a high light energy delivered for a long time causes the thermal change in tissue. Therefore, provided the malignant tumor is treated with a low light energy to avoid thermal effects, the use of a highly transmissible laser light should be favorable. Pulsed laser light is considered to be the best regimen in PDT (4), and an excimer laser-pumped dye laser (abbreviated as an excimer dye laser) seems to give better light transmission than a continuous-wave argon laser pumped dye laser (4). The effect of PDT with the photosensitizer Photofrin II and the excimer dye laser was investigated in Japan with mouse tumors (5) and human tumors clinically. PDT by means of Photofrin II and the excimer dye laser was officially approved by the Japanese government at October in 1994 for the treatment of superficial diseases such as lung cancer, esophagus cancer, stomach cancer, cervical cancer and its dysplasia. Cure rate of more than 80% was obtained in the official investigational clinical study (6–9). This success encouraged us to try the application of PDT to nonsuperficial cancers and we applied the interstitial PDT to treat these cancers.

From: *Methods in Molecular Biology*, vol. 196: *Oxidants and Antioxidants: Ultrastructure and Molecular Biology Protocols*
Edited by: D. Armstrong © Humana Press Inc., Totowa, NJ

The interstitial PDT has been already studied to treat nonsuperficial cancers by several researchers (10–12). They used plane cut fibers or cylindrical diffusing fibers to treat cancers interstitially. As these fibers were imbedded and fixed in the tissue to expose interstitially, the region that was affected by PDT was restricted and the thermal effect was not ignored. In order to overcome these problems of the interstitial PDT, we adopted the fiber movement method. The effectiveness of this new method was investigated by animal experiments and the clinical study has been conducted in a tongue cancer. We describe our interstitial PDT method in this article.

2. Materials

2.1. Photosensitizer

The photosensitizer Photofrin II (polyhematoporphyrin ether/ester, PHE) was developed by QLT PhotoTherapeutics (Vancouver, Canada) and it was supplied by Wyeth Lederle Japan, Ltd for our research studies. Photofrin II was dissolved in 5% glucose solution at a concentration of 2.5 mg/mL and it was administered intravenously.

2.2. Animal and Tumor Model

Five female beagle dogs, 12–16 wk old, bearing canine transmissible sarcoma (CTS) tumor model were supplied by the department of veterinary surgery, Tottori University (Tottori, Japan). CTS is of mesodermal origin, and it has been maintained as subcutaneous tumors in the inguinal region by injection of 10^7 cells of the CTS tumor (13). The mean body weight of the dogs was 6.2 kg, and they were anesthetized with an intramuscular administration of ketamine at a dose of 20 mg/kg during the experiments. The experiments were started when the diameter of the tumor reached about 35 mm, at about 4 wk after CTS cell transplantation, since a tumor of more than 35 mm in diameter frequently exhibited central necrosis.

2.3. Light Source

The excimer dye laser PDT EDL-1 (Hamamatsu Photonics, K.K., Hamamatsu, Japan) was used in our PDT experiment. The wavelength of the laser was tuned to 630 nm. The peak power of laser pulse was 500 kW, the pulse duration was 10 ns and pulses were delivered at a rate of 40 Hz or 80 Hz. A single quartz fiber was used to deliver the laser light. In order to expose laser light from the inside of the tumor, a laser-proof plastic tube (external and internal diameters, 1.5 mm and 1.2 mm, respectively) was inserted into the tumor, and then an optical fiber was guided into it. The external and core diameter of the optical fiber were 1.0 mm and 0.6 mm, respectively. The distal

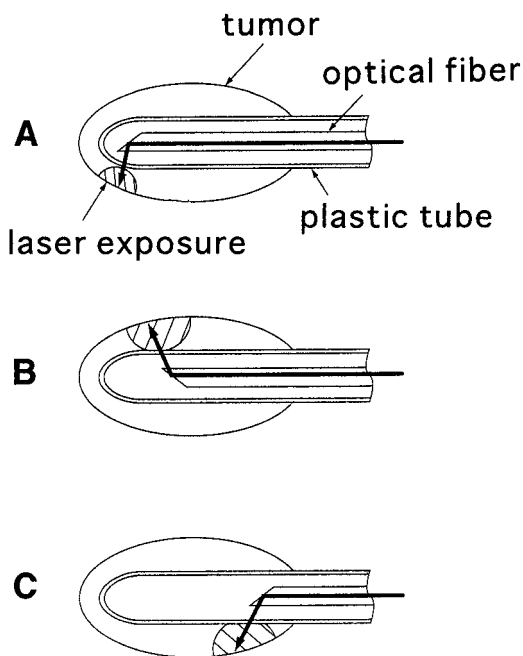


Fig.1. A schematic model of the interstitial PDT. A laser-proof plastic tube is implanted in tumor. An optical fiber, whose tip is cut and polished at an angle of about 45° , is inserted into it. Laser beam is delivered in a direction nearly perpendicular to the axis of the optical fiber. The fiber tip rotates at 12 rpm and performs a reciprocal motion at 18 mm/min. Laser beam rotation is observed in tumor when the fiber moves from (A) \rightarrow (B) \rightarrow (C).

tip of the fiber was cut and polished at an angle of about 45° , so that the laser beam was delivered nearly perpendicular to the optical axis of the fiber.

2.4. Fiber Movement Device

The fiber tip was rotated clockwise and anti-clockwise alternately at a speed of 12 rpm (rotations per min) and performed a reciprocal linear motion from one end to the other of the tumor at a speed of 18 mm per min (**Fig. 1**). The laser-irradiation dose was expressed as the integrated energy per unit cm along the tube during reciprocal motions of the fiber tip. The fiber movement device is shown in **Fig. 2**. It has two motors for the independent fiber movement, one is for the rotation and the other is for the reciprocal linear motion of the fiber. The range of the reciprocal linear motion could be set in the range of 0~100 mm according to the size of the tumor.

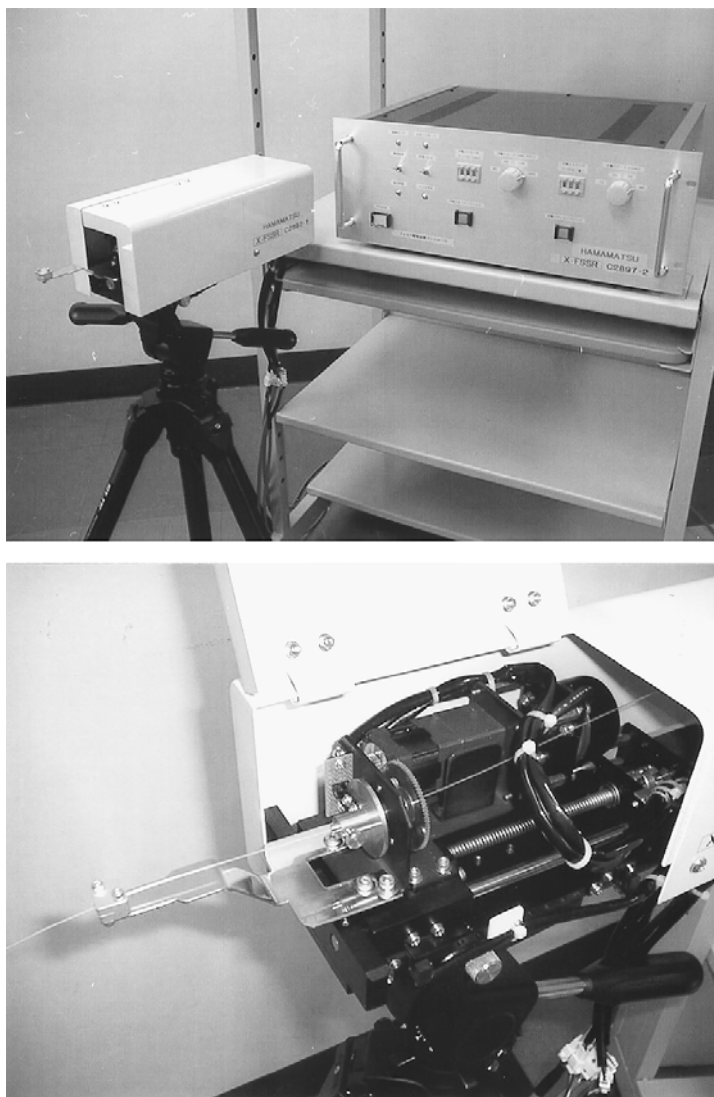


Fig. 2. A fiber movement device. The whole system (*upper*) and the driving mechanism (*lower*). Two motors are equipped for the rotation and the linear motion of the fiber.

3. Methods

3.1. Tumor Necrosis

1. An examination of tumor necrosis was used to evaluate the PDT response. Prior to the treatment, Photofrin II was administered intravenously at a concentration of 5 mg/Kg. At 48 h thereafter, PDT was performed.



Fig. 3. Interstitial PDT of the CTS tumor-bearing dog. A plastic tube is imbedded in the tumor and the irradiation optical fiber is inserted in the tube.

2. Irradiation power of 400 mW (5 mJ/pulse, 80 Hz) or 200 mW (5 mJ/pulse, 40 Hz) were adopted and irradiation doses were ranged from 0–1440 J/cm.
3. Tumors were excised 6 d after irradiations and fixed in the 20% formalin solution. The tumor was cut every 5 mm along the axis of the optical fiber, and the degree of tumor necrosis was calculated as the average diameter of round-shaped tumor necrosis in each cross-section. The diameter was measured eight times with the tube hole as the center by shifting by an angle of 22.5° and then the mean diameter was calculated.

4. Results and Conclusions

4.1. PDT Effect (Dog Experiments) (14,15)

The interstitial PDT experiments using CTS tumor-bearing dogs were conducted (**Fig. 3**) and the result is shown in **Fig. 4**. The mean diameter of tumor necrosis was correlated to the energy of laser light (irradiation dose). In the low-energy region below 120 J/cm, the tumor-necrosis diameter grew rapidly as the laser energy increased. But the increase of the tumor-necrosis diameter saturated as the laser energy increased above 120 J/cm. In the case of 80 Hz pulse rate, the maximum tumor necrosis diameter were 13.4 mm at 60 J/cm, 17.0 mm at 120 J/cm, 20.7 mm at 240 J/cm, 21.5 mm at 480 J/cm,

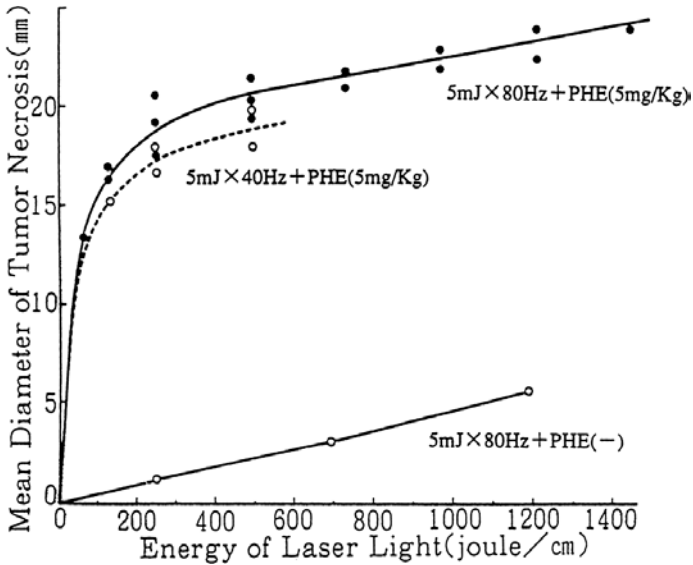


Fig. 4. Tumor necrosis diameter due to the interstitial PDT for CTS tumors.

23.0 mm at 960 J/cm, and 24.1 mm at 1440 J/cm. We observed the decrease of tumor necrosis by almost 10% in the case of 40 Hz pulse rate. We also observed the tumor necrosis in the irradiation without Photofrin II (PHE). This is due to the thermal effect of the irradiation, and diameters of necrosis were 1.5 mm at 240 J/cm, 3.0 mm at 680 J/cm, and 5.6 mm at 1200 J/cm. As the tumor-necrosis dependence on the energy of laser light without Photofrin II was similar to the dependence curve of the 80 Hz pulse rate, we supposed the tumor-necrosis saturation of 80 Hz might be due to the thermal effect by the irradiation.

From the aforementioned experiment, we confirmed the energy of the laser light (irradiation dose) of almost 100~150 J/cm would be adequate for interstitial PDT in respect of its effect and the thermal tissue damage. Clinical PDT for the animal (dog or cat) tumor is performed with 150 J/cm at present. **Figure 5** shows the interstitial PDT for a naturally occurred breast cancer of a dog. A long plastic tube is inserted along a row of breasts. As metastasis occurs from one breast to another along the row, it is necessary to treat all breasts simultaneously. Interstitial PDT by our method is adequate for the treatment of cancer of this kind. **Figure 6** shows the case of the large tumor that employs 2 plastic tubes. According to the tumor size, the number of the inserting plastic tube is chosen.



Fig. 5. Interstitial PDT for the breast cancer of a dog.



Fig. 6. Insertion of double tubes for a large tumor.

4.2. Clinical Study (16)

Three patients with squamous carcinoma of tongue were treated with the interstitial PDT (**Table 1**). They were all considered to be not affected by the ordinary surface irradiation PDT. Two patients with T₂ carcinoma had previously radiotherapy and chemotherapy, resulting in recurrence. One patient

Table 1
Interstitial PDT for Tongue Cancer (Patients and Results)

Case No.	Sex	Age	TNM classification	Tumor size (mm)	Numbr of tubes inserted	Total energy (J)	Response ^a	Duration of Follow-up period
1	M.	50	rT2N0M0	27 × 16 × 8	3	480	CR	14 mo
2	F.	53	T2N1M0	30 × 15 × 15	3	360	PR	Recurrence after 1 mo
3	F.	67	T1N0M0	8 × 8 × 3	1	80	CR	13 mo

^aCR, complete response; PR, partial response.



Fig. 7. Clinical interstitial PDT (case 2). Three plastic tubes were inserted for laser irradiation.

with T_1 was primary. Photofrin II was injected intravenously 48 h prior to laser irradiation. The tumor was penetrated with a 17G stainless-steel needle, then a plastic flexible tube was guided by the needle and inserted into the tumor. For patients of case 1 and 2, three plastic tubes were inserted at intervals of about 10 mm apart (**Fig. 7**). The optical fiber was passed into the tube and the laser irradiation was performed at a dose of 100 J/cm along the tube, with the pulse repetition of 80 Hz and the laser pulse energy of 4 mJ. The fiber tip was rotated at a speed of 20 rpm and performed a reciprocal motion from one end to the other of the tumor at a speed of 45 mm/min. The patient received block anesthesia for the mandibular nerve under intravenous sedation.

The patient with T_1 carcinoma (case 3, **Table 1**) and T_2 carcinoma (case 1) obtained complete responses and recurrence has not occurred within 13 and 14 mo follow-up, respectively. Edema at irradiated site rapidly occurred in the period of PDT procedure and lasted for about a week. Necrotic change of the tumor happened and desquamation of necrotic tissue was observed, and then it sloughed off within 2 wk. The damage of the surrounding tissue healed up within 3 wk and functional disability was not seen. One of T_2 carcinoma (case 2) recurred at the lingual back and the oral floor in a month after treatments. It seemed that it was because of the insufficient light distribution in tumor tissue.

From the animal experiment and the clinical study, we confirmed that the interstitial PDT is a powerful treatment modality. We found the tumor-necrosis diameter almost doubled in the interstitial PDT experiment using CTS tumor-

bearing dogs with the photosensitizer BPD-MA (QLT PhotoTherapeutics) and the 690nm excimer dye laser irradiation. Tumor-necrosis diameter of 35 mm was obtained at the irradiation dose of 300 J/cm (17). This was recognized mainly due to the increase of the light transmissivity in tissue when the laser wavelength changed from 630 nm to 690 nm.

The interstitial photodynamic therapy with the moving exposure fiber method would be useful for treatments of large solid or advanced cancers and its clinical applications are expected.

Acknowledgments

We thank Prof. S. Minami and Associate Prof. Y. Okamoto of the Department of Veterinary Surgery, Tottori University, for supplying CTS-bearing dogs.

References

1. Weishaupt, K. R., Gomer, C. J., and Dougherty, T. J. (1976) Identification of singlet oxygen as the cytotoxic agent in photoinactivation of a murine tumor. *Cancer Res.* **36**, 2326–2329.
2. Gibson, S. L. and Hilf, R. (1983) Photosensitization of mitochondrial cytochrome C oxidase by hematoporphyrin derivative and related porphyrins in vitro and in vivo. *Cancer Res.* **43**, 4191–4197.
3. Mitchel, J. B., McPherson, S., Degraff, W., Gamson, J., Zabell, A., and Russo, A. (1985) Oxygen dependence of hematoporphyrin derivative-induced photoactivation of Chinese hamster cells. *Cancer Res.* **45**, 2008–2011.
4. Okunaka, T., Kato, H., Konaka, C., Sakai, H., Kawabe, H., and Aizawa, K. (1992) A comparison between argon-dye and Excimer dye laser for photodynamic effect in transplanted mouse tumor. *Jpn. J. Cancer Res.* **83**, 226–231.
5. Tanaka, M., Uchibayashi, T., Obata, T., and Sasaki, T. (1995) Photodynamic therapy of Photofrin II and excimer dye laser on experimental tumors. *Cancer Lett.* **90**, 163–169.
6. Kato, H., Horai, T., Furuse, K., Fukuoka, M., Suzuki, S., Hiki, Y., et al. (1993) Photodynamic therapy for cancers: A clinical trial of porfimer sodium in Japan. *Jpn. J. Cancer Res.* **84**, 1209–1214.
7. Mimura, S., Ito, Y., Nagayo, T., Ichii, M., Kato, H., Sakai, H., et al. (1996) Cooperative clinical trial of photodynamic therapy with Photofrin II and excimer dye laser for early gastric cancer. *Lasers Surg. Med.* **19**, 168–172.
8. Kato, H. (1997) Photodynamic therapy for lung cancer. *J. Tokyo Med. Coll.* **55**, 387–393.
9. Muroya, T., Suehiro, Y., Kunugi, T., Umayahara, K., Akiya, T., Iwabuchi, H., et al. (1997) Photodynamic therapy (PDT) for early stage cervical cancer. *J. Tokyo Med. Coll.* **55**, 408–424.
10. Dougherty, T. J., Thoma, R. E., Boyle, D. G., and Weishaupt, K. R. (1981) Interstitial photoradiation therapy for primary solid tumors in pet cats and dogs. *Cancer Res.* **41**, 401–404.

11. Feather, J. W., Driver, I., King, P. R., Lowdell, C., and Dixon, B. (1990) Light delivery to tumour tissue through implanted optical fibers during photodynamic therapy. *Lasers Med. Sci.* **5**, 345–350.
12. Lowdell, C. P., Ash, D. V., Driver, I., and Brown, S. B. (1993) Interstitial photodynamic therapy. Clinical experience with diffusing fibres in the treatment of cutaneous and subcutaneous tumours. *Br. J. Cancer* **67**, 1398–1403.
13. Okamoto, Y., Fujinaga, T., Tajima, M., Hoshin, N., Otomo, K., and Koike, T. (1988) Isolation and cultivation of canine transmissible sarcoma cells. *Jpn. J. Vet. Sci.* **50**, 9–13.
14. Hashimoto, Y., Hirano, T., and Yamaguchi, N. (1995) Novel after-loading interstitial photodynamic therapy of canine transmissible sarcoma with Photofrin II and excimer dye laser. *Jpn. J. Cancer Res.* **86**, 239–244.
15. Hashimoto, Y., Hirano, T., and Yamaguchi, N. (1995) Effect of novel intra-tumor photodynamic therapy on canine transmissible sarcoma with Photofrin (PHE) and excimer dye laser. *Jpn. J. Laser Med. Assoc.* **16**, 1–10.
16. Tanaka, H., Hashimoto, K., Yamada, I., Masumoto, K., Ohsawa, T., Murai, M., and Hirano, T. (2001) Interstitial photodynamic therapy with rotating and reciprocating optical fibers. *Cancer* **91**, 1791–1796.
17. Hashimoto, Y., Hirano, T., Minami, S., and Okamoto, Y. (1997) Algorithm of novel after-loading interstitial photodynamic therapy with Benzoporphyrin derivative (BPD) Verteporfin and canine transmissible sarcoma. *Proc. JCIPA*, 49–51.

Statistical Analysis

Receiver Operating Characteristic (ROC) Curve and Lipid Peroxidation

Enrique F. Schisterman

1. Introduction

Laboratory diagnostic tests are central to the practice of modern medicine. Common indices include screening a specific population for evidence of disease and confirming a tentative diagnosis in an individual patient. The interpretation of a diagnostic test result depends on both the ability of the test to distinguish diseased from nondiseased subjects and the particular characteristics of the patient and setting in which the test is being used.

For convenience, a diagnostic test will be called continuous, dichotomous, or ordinal according to whether the test yields a continuous measurement (e.g., blood pressure) a dichotomous result (e.g., HIV-positive or HIV-negative), or an ordinal outcome (e.g., confidence rating for presence of disease: definitely, probably, possibly, probably not, definitely not). The main focus here is on continuous diagnostic tests, because the majority of laboratory diagnostic tests are of this type and because many of the oxidative stress markets are measured on a continuous scale.

Receiver operating characteristic (ROC) analysis was originally developed for use with radar to separate observer variability from the innate detectability of the signal (*I*). It has gained in popularity in laboratory medicine over the last 30 years as a tool for evaluating test performance. ROC curves simultaneously show the proportion of both abnormal and normal subjects correctly diagnosed at various test cutoff points. This graphical display not only facilitates the selection of an optimal threshold, but also enables easy comparison of different

From: *Methods in Molecular Biology*, vol. 196: *Oxidants and Antioxidants: Ultrastructure and Molecular Biology Protocols*
Edited by: D. Armstrong © Humana Press Inc., Totowa, NJ

tests. The use of this tool became popular in epidemiologic research as a statistical instrument to discriminate or identify the abnormal and normal individuals in a population based on variables or biomarkers, such as oxidative stress and antioxidants biomarkers.

Because tests described in this volume may be used in the future for design and management, the purpose of this chapter is to illustrate how the available discrimination indexes, including the area under the ROC curve, can be applied, and to summarize some recent statistical developments in this growing field applied to lipid peroxidation biomarkers.

2. Materials

Statistical software to perform ROC analysis is available upon request at eschisterman@iwon.com

3. Methods

3.1 Formulas and Terminology

1. In the general case, let N represent the normal and D the abnormal, with the upper case letters denoting the classification and the lower case the true condition. As shown in **Fig. 1**, if a cut point c_1 is selected, the dotted area represents the probability of the normal being classified as abnormal (false-positive), or $P(D|n)$, while the area with slant lines represents the probability of false-negative, or $P(N|d)$. The two other areas to the left and the right of c_1 under the two normal curves represent the probabilities of correct classification, $P(D|d)$ and $P(N|n)$. It plots the probability of the true-positive, $P(D|d)$ vs the probability of false-positive, $P(D|n)$, for various decision criteria. The y-axis is for $P(D|d)$ and the x-axis for $P(D|n)$. The ratio of these two probabilities at each point of the curve represents the slope of the curve at that point. This ratio is known as the Likelihood Ratio. A ROC curve is constructed by connecting these points.
2. In practice, the true $P(D|d)$ and $P(D|n)$ are unknown, the ROC curve is constructed by using estimated $P(D|d)$ and $P(D|n)$ and the likelihood is based on estimated conditional probabilities. The ROC curve summarizes the performance of various decision rules classifying individuals into one of the two groups by demonstrating the relationship of the two conditional probabilities. Since true-positive response, or sensitivity, is the complement of the false-negative response and the false-negative response the complement of the true-negative, each point of the curve represents the 2×2 decision matrix at one criterion. Thus, ROC curve can be described as summarizing the possible set of the 2×2 decision matrices that result when the cut-off is varied from the largest to the smallest possible value.
3. Since the x and y axes are identically scaled, every point on the diagonal line from (0,0) to (1,1) results from equal values of x and y. This is called the chance line since for every point the probability of true-positive response, $P(D|d)$,

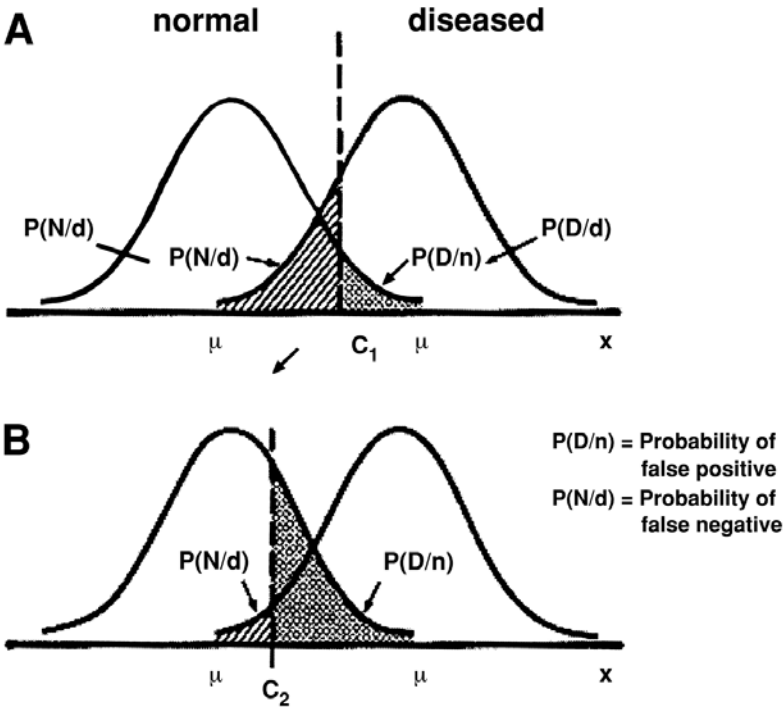


Fig. 1. Effect of criteria on error rates.

equals the probability of false-positive response, $P(D|n)$. The greater the height of the curve above this chance line, the better the discrimination between the two groups, and the better the detectability.

4. One index available from the ROC curve analysis, the area under the curve or the ROC criterion, measures the ability of a diagnostic test to discriminate between two patient states, often labeled abnormal and normal. Barber et al. (2) pointed out that this criterion is the $P(N>D)$, which is the probability that the normal population has higher values than the abnormal population for a specific marker. A large value of ROC criterion implies that the biomarker discriminates properly between the two groups being measured.

3.2. Application

1. Let TBARS be the biomarker based on which the decision rule is devised. The rule may be the selection of a criterion value c such that an individual is said to be abnormal if his observed value of TBARS is greater than c and normal if his observed value TBARS is less than c . Most of the statistical models assume that the abnormal and normal groups follow the normal distribution with equal variance (1). The ROC curve is constructed to show the result of classification of

Table 1
Simulated TBARS Values in Normal
and 5 Abnormal Individuals

TBARS values for normal	TBARS values for abnormal
0.1	0.2
0.3	0.4
0.5	0.6
0.7	0.8
0.9	1.0

Table 2
Definition of Values of TBARS as Abnormal Individuals and Normal;
Cut Point of the Marker at 0.1

Defined status	True normal	True abnormal	Total
Defined as normal	0	0	0
Defined as abnormal	5	5	10
Total	5	5	10

normal or abnormal individuals at various cut points criteria simultaneously. The graph will be based on the sensitivity and specificity of the biomarker at every possible value of the biomarker.

2. To demonstrate how to construct the ROC curve, assume that TBARS values are available on five abnormal people and five normal with the following values shown in **Table 1**.
3. If the cut-off point is set at 0.1, meaning every individual value below 0.1 will be defined as normal, and values greater or equal to 0.1 will be define as abnormal; the usual 2×2 table can constructed as shown in **Table 2**.
4. For the defined specific cut point of 0.1, estimates of sensitivity, specificity, positive predictive value, and negative predictive value of the test can be obtained as follows:

Sensitivity =1; Specificity = 0; Positive Predictive Value (PPV) = 0; and Negative Predictive Value (NPV) = 0.5. Now if the cut-off point is set to 0.2, and following the same procedure, the 2×2 table can be constructed as shown in **Table 3**.

5. For the defined specific cut point of 0.2, the Sensitivity = 1; Specificity = 1/5; PPV = 5/9 and NPV =1/1. Continuing in the same manner, the sensitivity, specificity, PPV, and NPV can be estimated. We present this data in **Table 4**.
6. To construct an empirical ROC curve, we have to plot the sensitivity vs 1-specificity and connect the points as explained in **Subheading 3**.

Table 3
Definition of Values of TBARS as Abnormal Individuals and Normal; Cut Point of the Marker at 0.2.

Defined status	True normal	True abnormal	Total
Defined as normal	1	0	1
Defined as abnormal	4	5	9
Total	5	5	10

Table 4
Sensitivity, Specificity, PPV, and NPV for all the Possible Cut Points of the Sample

Cut-off point	Specificity	Sensitivity	NPV	PPV
0.1	0	1	0	0.50
0.2	0.2	1	1.00	0.55
0.3	0.2	0.8	0.50	0.50
0.4	0.4	0.8	0.66	0.43
0.5	0.4	0.6	0.50	0.50
0.6	0.6	0.6	0.60	0.6
0.7	0.6	0.4	0.50	0.50
0.8	0.8	0.4	0.57	0.66
0.9	0.8	0.2	0.50	0.50
1.0	1.0	0.2	0.55	1
1.1	1.0	0.0	0.50	0

3.3. Statistical Background of the ROC Curve on the Parametric Case

1. We present the nonparametric case; however, normality assumptions are commonly made in laboratory medicine. Let $P = \text{Specificity} = \text{The probability of defining a normal individual as normal or in statistical terms } p = P(X \leq C) = F(C)$. $Q = \text{Sensitivity} = \text{The probability of defining a abnormal individual as abnormal or in statistical terms } p = P(Y > C) = 1 - G(C)$.
2. From the previous definitions, we can see that $X_p = F^{-1}(p)$ is the percentile of the normal population and $Y_{1-q} = G^{-1}(1-q)$ is the percentile of the abnormal population. The ROC curve is defined as $q = \phi(p)$ where:

$$\phi(p) = q = 1 - G(c) = 1 - G(F^{-1}(p)) = 1 - G(X_p)$$

3. In the case where the abnormal and normal population follows a Normal distribution, the ROC curve is defined as

$$\phi(p) = q = 1 - G(\mu_x + z_p \sigma_x) = 1 - \phi\left(\frac{\mu_x + z_p \sigma_x - \mu_y}{\sigma_y}\right)$$

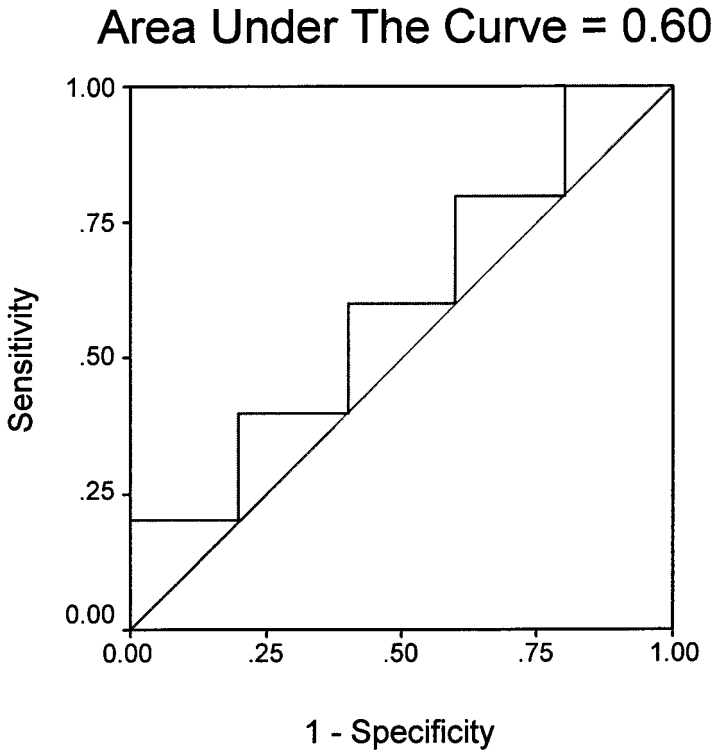


Fig. 2. ROC curve for TBARS.

4. Therefore, in the normal case $q = \Phi\left(\frac{\mu_y + z_p\sigma_x - \mu_x}{\sigma_y}\right)$ where Φ is the cumulative distribution function (cdf) of a normal distribution. A natural estimator of q is $\hat{q} = \Phi\left(\frac{\bar{y} - \bar{x} - z_p S_x}{S_y}\right)$, where \bar{x} is the sample mean of biomarker in the abnormal population, \bar{y} is the sample mean of biomarker in the normal population, S_x and S_y are the respective standard deviations, z_p is the percentile of the normal distribution, and Φ is the cdf of a normal distribution.

Going through approx all the possible values of sensitivity for a given specificity will yield infinity point, which can be plotted as a graph.

5. To understand the level of accuracy of the ROC point estimate, we need to calculate the confidence intervals (CI). Therefore, a lower bound CI proposed by Barkan (3) is presented as follows:

$$\Phi\left(\hat{K} \pm z_{1-\frac{\alpha}{2}} \sqrt{\hat{V}(\hat{K})}\right)$$

Where $\hat{K} = \Phi\left(\frac{\bar{y} - \bar{x} - z_p S_x}{S_y}\right)$ and $\hat{V} = \frac{1}{m} + \frac{S_x^2}{nS_y^2} + \frac{z_p^2 S_x^2}{2nS_y^2} + \frac{\hat{K}^2}{2m}$.

Table 5
Different Specificity Levels for Two Different Markers
for a Given Sensitivity Level

Sensitivity	Specificity when difference in means is one	Specificity when difference in means is ten
0	1	1
0.1	0.93	0.99
0.2	0.85	0.99
0.3	0.77	0.99
0.4	0.67	0.98
0.5	0.58	0.97
0.6	0.48	0.95
0.7	0.37	0.93
0.8	0.26	0.87
0.9	0.14	0.76
1.0	0	0

3.4. Application

1. To demonstrate the use of ROC analysis, two examples can be simulated. Suppose a sample from the biomarker TBARS is obtained on the abnormal population and is fitted to a normal distribution with sample mean = 20 and sample variance = 25; and another sample of the biomarker TBARS in the normal population is obtained and is also fitted to the normal distribution with sample mean = 10 and sample variance = 25. The differences in TBARS mean are 10 and they have the same variance. Applying the formula previously introduced in **Subheading 3.3.**, the ROC graph can be plotted.
2. In contrast with the previous example, suppose that the marker GSHPx is measured in the populations where the difference on means is 1 between the two populations. As previously described in **Subheading 3.3.**, the ROC graph using the formula described earlier can be plotted. Comparing the two graphs, we can see that the area under the curve of the graph with the larger difference in means (difference in means = 10) between the two populations is larger than the area under the curve of the graph with the smaller difference in means (difference in means = 1).
3. **Table 5** shows the different specificity levels for a given sensitivity level when the biomarkers discriminate very well between the two populations of TBARS, as is in the case where the difference in means is 10; and the different specificity levels for a given sensitivity level when the discrimination is not optimal (i.e., GSHPx), as in the case where the differences in means is 1.
4. **Table 5** demonstrates that when the discrimination is vague, any increase in sensitivity follows a drop in specificity, and vice versa. On the other hand, when the marker discriminates well, the changes of sensitivity do not affect the specificity of the marker.

5. The criterion to choose the optimal discriminating marker is the area under the ROC curve; however, before continuing with another application, more statistical background should be introduced.

3.5. Statistical Background to the ROC Criterion in the Normal Case

1. The area under the ROC curve is one of the existing criteria to compare biomarkers. In the normal case, Loyd (4) developed the estimator to the ROC criterion and Reiser and Guttman developed estimators for the variance (5). The area under the ROC curve in the normal case (6) is $A = \Phi\left(\frac{\mu_y - \mu_x}{\sqrt{\sigma_x^2 + \sigma_y^2}}\right)$ and the almost likelihood estimate is $\hat{A} = \Phi\left(\frac{\bar{y} - \bar{x}}{\sqrt{S_x^2 + S_y^2}}\right)$. To exemplify the use of the area under the ROC curve, the previous application will be utilized.

3.6. Application

1. In **Subheading 3.4.**, the difference in means in TBARS was $\bar{y} - \bar{x} = 10$ and the $S_x^2 = 25$ and the $S_y^2 = 25$. Applying the formula presented in **Subheading 3.5.** to calculate the ROC criterion yield $\hat{A} = \Phi\left(\frac{10}{\sqrt{25 + 25}}\right) = \Phi(1.41) = 0.921$.

TBARS discriminates very well between the two population (ROC criterion = 0.92).

2. On the other hand, looking at GSHPx as a discriminating marker, the difference in means was $\bar{y} - \bar{x} = 1$ and the $S_x^2 = 25$ and the $S_y^2 = 25$. Applying the formula presented in **Subheading 3.5.** to calculate the ROC criterion, we calculated the ROC criterion = $\hat{A} = \Phi\left(\frac{1}{\sqrt{25 + 25}}\right) = \Phi(0.141) = 0.55$. In this case, the

discrimination is not optimal. TBARS is a better discrimination marker than GSHPx, based on the ROC criterion. Now that we have reviewed how to compute the ROC graph and the ROC criterion, we will review more statistical background on how to combine biomarkers.

3.7. Statistical Background on the Linear Combination of Biomarker in the Normal Case

1. The method proposed by Su and Liu (7) will be the main tool to combine biomarkers and to achieve the best linear combination. This method maximizes the sensitivity over the entire specificity range uniformly under the multivariate normal distribution model with proportional covariance matrices and nonproportional covariance matrices.
2. The method proposed by Su and Liu (7) was based on in the linear discriminate analysis theory proposed by Fisher (8) for the proportional covariance matrices situation and on the theories of Anderson and Bahadur (9) for the classification

of two normal distribution with different covariance matrices. Their method provides the best linear combination that maximizes the ROC criterion (the area under the ROC curve).

Reiser and Faraggi (10) developed confidence intervals for the ROC criterion based on the noncentral Fisher distribution. To exemplify on the use of the linear combination of the biomarkers that maximized the area under the ROC curve, we will continue with the application described in **Subheading 3.6**.

3.8. Application

Suppose now that the combination of the information from the TBARS and GSHPx is of interest. To obtain the maximum discrimination between the abnormal and normal population, the application of the Su and Liu (7) method is necessary. Assuming that the covariance between the markers is zero, we obtained:

$$\text{Area} = \varphi \left(\sqrt{(\mu_x - \mu_y)'(\Sigma_x + \Sigma_y)^{-1}(\mu_x - \mu_y)} \right) = \varphi(2.02) = 0.98.$$

It is clear that the ROC criterion of the combined markers (0.98) is higher than each one separately (0.92 and 0.55).

4. Notes

1. If the area under the ROC curve is less than 0.5, the results should be turned over.
2. If the confidence intervals of the area under the ROC curve include the value 0.5, the marker does not discriminate between cases and controls.
3. Normality assumptions should be always evaluated using standard statistical procedure, such as the Q-Q plot.
4. If the minimum detectable levels of the marker of interest are high, this procedure might be biased.
5. The ROC criterion is defined between 0.5 to 1; where values close to 0.5 imply that the discrimination is undesirable and is due to chance, and values close to one imply that the discrimination is optimal or the biomarker discriminates well between the abnormal and the normal population

References

1. Erdreich, L. S. and Lee, E. T. (1981) Use of relative operating characteristic analysis in epidemiology. *Am. J. Epidemiol.* **114**, 649–662.
2. Barber, D. C. (1975) The area above the ordinal dominance graph and the area under the receiver operating characteristic graph. *J. Math. Psychol.* **12**, 387–415.
3. Barkan, N. (1998) Statistical Inference for the ROC. Dissertation Proposal. Haifa University.
4. Loyd, D. K. Estimating the life cycle of complex modeled systems, in *Institute of Environmental Science Proceedings*. Institute of Environmental Science Mount Prospect, IL, pp. 87–96.

5. Schisterman, E. F., Faraggi, D., Browne, R., Freudenheim, J., Dorn, J., Muti, P., et al. Minimal and best linear combination of oxidative stress and antioxidants biomarkers to discriminate cardiovascular disease. *J. Cardiovasc. Risk* (Submitted.)
6. Schisterman, E. F., Faraggi, D., Browne, R., Freudenheim, J., Dorn, J., Muti, P., et al. TBARS and cardiovascular disease in a population-based sample. (Submitted.)
7. Su, J. Q. and Liu, J. S. (1993) Linear combination of multiple diagnostic markers. *J. Am. Statist. Assoc.* **88**, 1350–1355.
8. Fisher, R. A. (1936) The use of multiple measurements in taxonomic problem. *Ann. Eugen.* **7**, 179–188.
9. Anderson, T. W., Bahadur, R. R. (1962) Classification into two multivariate normal distributions with different covariance matrices. *Ann. Math. Stat.* **33**, 420–431.
10. Reiser, B. and Faraggi, D. (1997) Confidence intervals for the generalized ROC criterion. *Biometrics* **53**, 194–202.